



Technische Universität München
Wissenschaftszentrum für Ernährung, Landnutzung und Umwelt
Lehrstuhl für Lebensmittelverpackungstechnik

High barrier materials for flexible and transparent encapsulation of organic electronics

Margot Marion Schmidt

Vollständiger Abdruck der von der Fakultät Wissenschaftszentrum für Ernährung, Landnutzung und Umwelt der Technischen Universität München zur Erlangung des akademischen Grades eines

Doktor-Ingenieurs

genehmigten Dissertation.

Vorsitzende: Univ.-Prof. Dr. P. Först

Prüfer der Dissertation: 1. Univ.-Prof. Dr. H.-C. Langowski
2. Univ.-Prof. Dr. H. Briesen
3. Univ.-Prof. Dr. J.-P. Majschak,
Technische Universität Dresden
(schriftliche Beurteilung)

Univ.-Prof. Dr. K. Sommer
(mündliche Prüfung)

Die Dissertation wurde am 16.05.2013 bei der Technischen Universität München eingereicht und durch die Fakultät Wissenschaftszentrum für Ernährung, Landnutzung und Umwelt am 11.11.2013 angenommen.

Contents

Abstract	15
Nomenclature	17
1 Motivation	25
2 Requirements for the encapsulation material	29
2.1 Protection from environmental gases	29
2.2 Further requirements	33
3 Existing encapsulation concepts	35
3.1 Permeation theory	35
3.1.1 Description of the permeation process	35
3.1.2 Transmission rate calculation for homogeneous monolayered materials	37
3.1.3 Time lag calculation for homogeneous monolayered materials	38
3.1.4 Transmission rate calculation for homogeneous multilayered encapsulation materials	39
3.1.5 Time lag calculation for homogeneous multilayered encapsulation materials	39
3.1.6 Transmission rate and time lag calculation for inhomogeneous monolayered encapsulation materials	40
3.1.7 Oxygen transmission rate calculation for inhomogeneous multilayered encapsulation materials	40
3.1.8 Water vapor transmission rate calculation for inhomogeneous multilayered encapsulation materials	43
3.1.9 Time lag calculation for inhomogeneous multilayered encapsulation materials	46
3.2 Experimental achievements	47
3.2.1 Existing experimental strategies	47
3.2.2 Potential high barrier effects I: Known from experiments	52
3.2.3 Potential high barrier effects II: Predicted theoretically	54
4 Experimental methodology	59
4.1 Materials	59
4.2 Coating techniques	62
4.3 Evaluation methods	66

4.4	Experimental methods developed during this work	79
4.4.1	Procedure of the “edge trials“	79
4.4.2	Characterization of the UV curing section of the pilot plant	80
4.4.3	Viscosity adjustment of Ormocer [®] coating materials	81
4.4.4	WVTR measurement by accumulating gas chromatography	83
5	Results and Discussion: Characterization of barrier materials	89
5.1	Processing and environmental stability of the base substrate	89
5.2	Process constraints for thin inorganic layers	95
5.3	Barrier performance of thin organic layers	101
6	Results and Discussion: Barrier effects resulting from the combination of different layers	107
6.1	Synergistic barrier effect	107
6.2	Tortuous path effect	117
6.3	Time lag effect	119
6.4	Multilayered versus laminated structures	124
7	Results and Discussion: Importance of the barrier effects within the entire layer stack	129
7.1	Influence of the barrier level of the inorganic layer	129
7.2	Influence of the barrier level of the organic layer	131
7.3	Structures with a high number of layers	135
8	Conclusions	137
9	Outlook	141
	Appendices	143
A	Additional experimental results	145
B	Additional calculated results	169
C	Cost assessment	177
D	Further explanation on the best barrier materials of this work	181
	Bibliography	187
	Affidavit	201
	Publications	203
	Acknowledgements	205

List of Figures

1.1	Conductivity of selected materials (adapted from [1]).	25
1.2	Selected examples for existing and planned OE products [2, 3, 4, 5, 6, 7, 8, 9, 10, 11].	26
2.1	Barrier targets for OE applications in comparison to those of other packing goods [12, 13, 14, 15, 16, 17].	29
3.1	Schematic of a membrane separating two compartments of different partial pressures, following [18].	35
3.2	The flux $-J_2$, that permeates out of the encapsulation material, as a function of time.	36
3.3	Transient and steady state aspects of the gas permeation process.	38
3.4	Schematics of the three theoretical approaches to gas permeation through multilayered encapsulation materials containing thin inhomogeneous inorganic barrier layers.	41
3.5	Schematics of the cross-sectional view of a two layer structure and three layer structure, respectively, containing one thin inorganic barrier layer with pores.	43
3.6	Schematic of the cross-sectional view of a two layer structure containing a thin inorganic barrier layer (with pores) on top of a polymer film.	44
3.7	Schematic of the cross-sectional view of a three layer structure containing one thin inorganic barrier layer (with pores).	45
3.8	Simplification of the FEA based calculations of the WVTR and time lag for a multilayered structure containing both organic and inorganic layers (a) by transforming the three dimensional flux (b) into a quasi one dimensional flux (c).	47
3.9	Scanning electron microscope (SEM) images of an anti-blocking particle that is integrated in a polymer film before (a) and after (b) the coating of the polymer film with a thin inorganic barrier layer [19, 20]. The thin inorganic barrier layer breaks at the periphery of the anti-blocking particle as a result from peak stress, to be seen in Fig.(b).	48

List of Figures

3.10	Pictures of pores of all sizes as they exist in thin transparent inorganic barrier layers taken by (a) light microscopy, (b) light microscopy after undercutting (i.e. the pore sizes are greatly increased now) and (c) scanning electron microscopy. Figures (a) and (c) are the result from samples that were prepared by the author, but measured at <i>Fraunhofer FEP</i> and <i>Fraunhofer IGB</i> , respectively, while figure (b) is taken from literature [21].	49
3.11	Intrinsic (effective) permeability coefficients of thin transparent inorganic barrier layers (as an average over literature data [22, 23, 24, 25, 26, 27, 21, 28, 29]) in comparison to the permeability coefficients of transparent organic barrier materials (own measurements, for details see Fig. 5.1).	50
3.12	WVTR and OTR of polyester films coated with thin inorganic barrier layers, as a function of the thickness of the thin inorganic barrier layer. The WVTRs and OTRs of the 12 μm PET film were measured by the author, all other data are from literature ((a,...,i) being [22, 23, 24, 25, 26, 27, 21, 28, 29]).	51
3.13	Transmission rates for Helium, Neon and Argon of polyester films coated with thin inorganic barrier layers, as a function of the thickness of the thin inorganic barrier layer. All results from literature ((i) being [29]).	51
3.14	Best reported WVTR over time for each encapsulation strategy until mid 2008 [26, 25, 14, 30, 31, 32, 33, 34, 35, 36, 37, 38, 39]. (Some WVTR results are included in this diagram despite the fact that they were no improvement over previous achievements, because they belong to important research groups in the research field of OE encapsulation.)	52
3.15	The synergistic barrier effect as found first in 1998 (figure taken from [40] and modified).	53
3.16	The lag time effect as described in 2004 (figure taken from [41]).	54
3.17	The filled pores effect as reported in 2008 (figure taken from [42] and modified).	55
3.18	The theory of how the permeation of the oxygen molecules happens along a tortuous path through the three-layer-structure (scheme).	56
3.19	The tortuous path effect as predicted originally (in 2003) (figure taken from [28]).	56
3.20	The tortuous path effect at the beginning of this work (in 2008) (figure taken from [42] and modified).	57
4.1	Schematic of the principle of the electron beam deposition process at <i>Alcan Packaging Services AG</i> (figure taken from [43]).	63
4.2	Schematics of the wet chemical pilot plant of <i>Fraunhofer IVV</i> without enclosure (figure taken from [44]).	64
4.3	Picture (a) and cross-sectional working principle (b) of the Erichsen K 303 Control Coater type 625 that was used for rod bench coating and lamination (figures (a) and (b) taken from [17]). The subsequent manual lamination is demonstrated in Fig.(c) (with two opaque sheets, for better visibility).	65
4.4	Schematic outline of the ACP unit.	67
4.5	Classification of the existing calcium tests, according to [45].	68

4.6	Cross-sectional schematic of the calcium test (a), exemplary recording of the optical transmission over time (b), top view of the calcium layer at the beginning of the measurement (c) and rear view of the cell during an exemplary measurement (d) (figures taken from [46, 47, 48]).	69
4.7	Principle of the electrolytical WVTR measurement (figure taken from [49]).	70
4.8	Gravimetric WVTR measurement: (a) principle, (b) wax method of <i>Fraunhofer IVV</i> and (c), (d) other types of closure: screwed cups, flanged cups (figures taken from [50, 51, 52, 53]).	70
4.9	Principle of the opto-chemical OTR measurement device of <i>Joanneum Research Forschungsgesellschaft mbH</i> (figure taken from [54]).	71
4.10	Layer thickness measurement by optical microscopy: exemplary cross-sections (a,b).	72
4.11	Layer thickness measurement by optical microscopy: exemplary failed cross-section.	73
4.12	Layer thickness measurement by scanning electron microscopy: exemplary pictures of samples prepared by cryo cutting (a,b) or cryo breaking (c,d).	73
4.13	Layer thickness measurement by transmission electron microscopy: exemplary cross-sections (a,b).	74
4.14	FTIR and Raman spectroscopy: exemplary combined spectrum.	75
4.15	Measurement of the surface roughness with atomic force microscopy: exemplary evaluation.	76
4.16	Surface energy measurement in (a) contact angle mode and (b) pendant drop mode (figures modified from [55, 56]).	76
4.17	Wettability check with test pens for two exemplary substrates: one with poor wettability (a), one with good wettability (b).	77
4.18	Two exemplary adhesive tape tests: one with bad result (a), one with good result (b).	78
4.19	Schematic view of the coating procedure of the "edge trials".	79
4.20	Results of the measurement of the UV-C dose emitted at the wet chemical coating plant and fit with a logarithmic regression line.	80
4.21	Ormocer [®] 09 (= C5.9) with different solids contents (a) and exemplary rheological measurement (b).	81
4.22	Ormocer [®] 09: Dynamic viscosity (a), layer thickness (b) as a function of solids content and layer thickness as a function of dynamic viscosity (c).	82
4.23	Side permeation: Cross-sectional scheme of the evaluated encapsulation material.	84
4.24	FEA calculation of the side permeation: meshing (a) and calculated permeation per finite element (b). In figure (b), one quarter of the sample in the measurement cell is shown, the 100% RH would be applied from the lower side. The lengths of the arrows indicate the amount of permeating water vapor and their tips the direction of permeation.	84
4.25	Exemplary measurement curve recorded during an ACP test.	85
4.26	Measured B(t) curve of structure 1.	86

List of Figures

4.27	According to the measured B(t) curves of structures 1 and 2 (4.26, 4.27a both water vapor permeation processes seem to have arrived in steady state, while this is actually true only for structure 1 (4.27b) and not for 3 (4.27c).	87
5.1	Permeability coefficients towards water vapor and oxygen of possible transparent polymer films (comprising 182 results from permeation measurements performed by the author and 91 results from literature [57, 58, 59, 60, 61, 62], the latter indicated with “[Lit]“ in the diagram). All diagram points contain error bars in x and y direction, but for many materials they are too small to be seen.	90
5.2	AFM pictures of a smooth substrate (a,b) coated with a 100 nm ZnSn _x O _y layer (c,d). These AFM measurements were performed by <i>Fraunhofer FEP</i>	95
5.3	AFM pictures of a rough substrate (a,b) coated with a 100 nm ZnSn _x O _y layer (c,d). These AFM measurements were performed by <i>Fraunhofer FEP</i>	96
5.4	AFM pictures of a rough but planarized substrate (a,b) coated with a 100 nm ZnSn _x O _y layer (c,d). These AFM measurements were performed by <i>Fraunhofer FEP</i>	96
5.5	Shrinkage of PET films with thin inorganic barrier coatings in dependancy of the substrate.	97
5.6	Shrinkage of PET films with thin inorganic barrier coatings in dependancy of the layer thickness.	98
5.7	Shrinkage of PET films with thin inorganic barrier coatings in dependancy of type of inorganic material.	99
5.8	Shrinkage of PET films with thin inorganic barrier coatings exposed to high temperatures in the pilot plant.	100
5.9	SEM evaluations of the shrunked samples (Fig. taken from [63]).	100
5.10	Lacquers and adhesives categories, following [64, 65, 66].	102
5.11	Average and standard deviation of permeability coefficients towards water vapor (a) and oxygen (b) of 49 possible transparent organic / hybrid coating materials (comprising 620 results from permeation measurements performed by the author and 2 results from literature [58]. The position of the data points in y direction is chosen arbitrarily for better visibility.)	104
5.12	Permeability coefficients towards water vapor and oxygen of 49 possible transparent organic coating materials (comprising 614 results from permeation measurements performed by the author and 2 results from literature [58]). Most diagram points contain error bars in x and y direction, but for some materials they are too small to be seen.	105
5.13	Water vapor transmission rate of the structure [thin inorganic barrier layer + organic top coat] ¹ for varying permeabilty coefficients of the organic top coat, in dependance of the permeability coefficient of the inorganic bulk (Fig. modified from [14]).	106

6.1	Average and standard deviation of oxygen (a) and water vapor (b) permeability coefficients of 46 organic coating materials. (The position of the data points in y direction is chosen arbitrarily for better visibility.) Important difference to Fig. 5.11: the three lacquers used for studying the synergistic barrier effect are marked in red.	108
6.2	Scheme of a thin inorganic barrier layer consisting of a bulk part with nano pores and a (micro) pores part (figure from [67]).	115
6.3	Calculated OTR (a), measured OTR (b) and measured WVTR (c) of the structure [PET substrate + SiO _x + Ormocer [®] 09 (= C5.9) + SiO _x], in dependancy of the thickness of the intermediate layer, and for two qualities of SiO _x . (Diagram (a) is reproduced from [42].)	118
6.4	Experimentally measured time lags as a function of the total number of layers of the encapsulation material. (In blue / red: the permeation process had / had not arrived in steady state, respectively.)	122
6.5	Cumulated flux of the 9 layer structure as a function of measurement time (the zeroing period is not shown here).	123
9.1	Best reported WVTR over time for each encapsulation strategy until now (2011) [26, 25, 14, 30, 31, 32, 33, 34, 35, 36, 37, 38, 39, 68, 69, 70, 71, 72, 73, 15, 74]. (Some WVTR results are included in this diagram despite the fact that they were no improvement over previous achievements, because they belong to important research groups in the research field of OE encapsulation.)	142
A.1	Light microscopic pictures of the surfaces of an intact silicon wafer (a), of one altered by a laser beam (c) and of one coated with Ormocer [®] and marked with a coloured pen (c).	146
A.2	Raman spectra of the silicon wafer used for calibration (a) and coated with Ormocer [®] (b).	147
A.3	Exemplary display of the curves of the standard deviations in comparison to the differences in the curves of the averages resulting from varying curing conditions.	150
A.4	Schematic picture of how organic and inorganic parts are chemically cross-linked within the the Ormocer [®] network.	151
A.5	Water vapor transmission rate of the two layer system for varying permeability coefficients of the organic top coat, in dependance of the permeability coefficient of the inorganic bulk (assuming pores with an average diameter of 170 nm and an average distance of 29 μm) (Fig. modified from [14]).	153
A.6	Transmission rates and Raman spectra of a thin Ormocer [®] 08 layer cured on top of a 200 μm ETFE film in a laboratory oven, as a function of drying period (b), (c) or drying temperature (d), (e), respectively.	155
A.7	Transmission rates and Raman spectra of a thin Ormocer [®] 08 layer cured on top of a 200 μm ETFE film in the pilot plant, as a function of drying period (b), (c) or drying temperature (d), (e), respectively.	156

List of Figures

A.8	Transmission rates and Raman spectra of a thin Ormocer [®] 04a layer cured on top of a 200 μm ETFE film in a laboratory oven, as a function of drying period (b), (c) or drying temperature (d), (e), respectively.	157
A.9	Transmission rates and Raman spectra of a thin Ormocer [®] 04a layer cured on top of a 200 μm ETFE film in a laboratory oven, as a function of drying period (b), (c) or drying temperature (d), (e), respectively.	158
A.10	Schematic pictures of failure types of laminated samples under peel stress.	161
A.11	Schematic pictures of the influence of the intrinsic flexibility of the adhesive on the effective bond area.	162
A.12	No quantitative bond strength value can be measured if the encapsulation material (i.e. mainly the PET substrate) breaks before bond failure: pictures of such a broken sample in the test machine (a) and after taking it out (b).	162
A.13	Simulation of climate stress by (a) damp heat test and (b) outdoor test. . .	165
A.14	Sample of the structure [PET + SiO _x + C5.6] after the climate test (1000 hours at 65°C and 09% RH). Figure (b) is a zoom into figure (a).	168
B.1	Both fluxes and cumulated fluxes as a function of time, schematic, following [18].	170
B.2	Schematic of (a) a two-port and (b) its equivalent circuit in terms of the short-circuit admittance parameters [75].	171
B.3	If the indicated number in the denominator would be deleted, all previously cited expressions for time lag calculations and the ones derived by the author would be in agreement with this expression, too (equation taken as a picture from [76] and modified).	176
C.1	Relationship of total costs of the encapsulation material versus its barrier performance: (a) as assumed in the community in 2008, (b) as found as a result of this work.	178

List of Tables

1.1	Funding for research in organic electronics for 2001-2013 [77, 78].	26
2.1	Structures of OE applications.	30
2.2	Environmental gases and their permeation-related properties (ordered according to increasing diffusion coefficient within the gas).	31
2.3	Molecular ratio of environmental gases after one year of permeation (in steady-state) through different barrier materials (at 25°C, 101,325 kPa, 100% RH).	32
2.4	Further requirements for OE encapsulation materials.	34
4.1	Organic materials: <u>A</u> dhesives.	59
4.2	Organic materials: <u>C</u> oatings.	60
4.3	Inorganic materials.	61
4.4	Polymer films (part 1).	61
4.5	Polymer films (part 2), other substrates.	62
4.6	Overview of coating methods and coating related methods.	62
4.7	Gravure roll sizes available for the wet chemical pilot coating plant. . . .	64
4.8	Rod size used for this work during rod bench coating and manual lamination.	65
4.9	Overview of evaluation methods.	66
4.10	Side permeation: FEA calculated and experimental results.	85
4.11	WVTR results of evaluations concerning the reproducibility of the ACP device.	86
5.1	Stability targets for the base substrate.	89
5.2	Mean surface roughness (RMS) of selected transparent polyester and fluoropolymer film grades. Marked in green are the polymer films that would fulfill the criterion of sufficiently smooth surface (for more details about this criterion see Chapter 5.2).	91
5.3	Mechanical stability of transparent polymer films, in the order of their tensile strength acc. to [79, 80, 81, 82] and own measurements. Marked in green are the polymer films that would fulfill the criterion of thermo-mechanical stability (tensile strength of either ≥ 60 N/mm ² at 120°C or ≥ 100 N/mm ² at 23 °C).	92

5.4	Thermal stability of transparent polymer films, in the order of their maximum long term temperatures acc. to [79, 80, 82, 83]. Marked in green are the polymer films that would fulfill the criterion of sufficient thermal stability (max. long term temperature at least 120°C and shrinkage after one hour at 130°C < 1%).	92
5.5	Climate stability of selected transparent polymer films. Marked in green are the polymers that would fulfill the criterion of sufficient climate stability (no material property changes significantly, i.e. more than ±10%).	93
5.6	UV stability of selected transparent polymer films. Marked in green are the polymers that would fulfill the criterion of sufficient UV stability (no material property changes significantly, i.e. more than ±10%).	94
5.7	Ranking of potential transparent polymer substrates with respect to the properties required for an OE encapsulation material.	94
5.8	Costs per kilogram transparent polymer pellets as an average over 2008-2011 according to [84]. Marked in green are the polymers that would fulfill the low cost criterion.	95
5.9	Lacquers and adhesives tested in this study.	103
6.1	Typical permeability coefficients of the three lacquers that were studied during “edge trials“ (permeability coefficients from Chapter 5.3).	107
6.2	Permeation results of the “edge trials“ samples consisting of a PET + SiO _x substrate with and without lacquer.	109
6.3	Expected transmission rates and synergistic effects for oxygen and water vapor permeation through the samples, consisting of PET + SiO _x + organic top coat.	111
6.4	Expected OTR and synergistic barrier effect S for two lacquers on PET + SiO _x substrate. As an example, all results (E,F,L,F+L) are shown for these two combinations of inorganic and organic barrier material. (To display all TR and S results for all samples would be too long and not add any further information or conclusion.)	113
6.5	Expected WVTR and synergistic barrier effect S for two lacquers on PET + SiO _x substrate. As an example, all results (E,F,L,F+L) are shown for these two combinations of inorganic and organic barrier material. (To display all TR and S results for all samples would be too long and not add any further information or conclusion.)	114
6.6	OTR of the structure [PET + SiO _x +Ormocer [®] 09 (= C5.9) + SiO _x], in dependancy of the thickness <i>d</i> of the intermediate layer and for two qualities of SiO _x	117
6.7	WVTR of the structure [PET + SiO _x +Ormocer [®] 09 (= C5.9) + SiO _x], in dependancy of the thickness <i>d</i> of the intermediate layer and for two qualities of SiO _x	118
6.8	Calculated versus measured WVTR at 38°C, 90% RH, all data cited from Graff et al. [41].	120
6.9	Calculated versus measured WVTR at 23°C, 50% RH.	121
6.10	Calculated versus measured time lags of the water vapor permeation process.	121
6.11	WVTR results: ACP test versus calcium tests.	125

6.12	Results regarding the transient barrier performance.	126
7.1	WVTR of encapsulation materials with varying inorganic qualities, measured by ACP test, at 23°C and 50% RH.	129
7.2	WVTR ^{Ca} of encapsulation materials with varying inorganic qualities, measured by calcium test at 23°C and 50% RH.	130
7.3	Barrier properties of the lacquers.	131
7.4	WVTR of encapsulation materials with varying organic qualities, at 23°C and 50% RH.	132
7.5	Barrier properties of the adhesives.	133
7.6	WVTR of encapsulation materials with varying adhesive qualities, measured with ACP test, at 23°C and 50% RH.	134
7.7	WVTR ^{Ca} of encapsulation materials with varying adhesive qualities, measured with calcium test, at 23°C and 50% RH.	134
7.8	Structures with a high number of layers, sorted according their number of thin inorganic barrier layers included. All WVTR values are given at 23°C and 50% RH.	136
A.1	Barrier related properties of the adhesives.	159
A.2	Mechanical properties of the adhesives.	159
A.3	WVTR and bond strength of laminates of the structure [PET + SiO _x + adhesive A + SiO _x + PET].	160
A.4	WVTR and bond strength of laminates of the structure [PET + ZnSn _x O _y + adhesive A + ZnSn _x O _y + PET] - all fabricated using bench lamination.	161
A.5	WVTR and bond strength of the structure [PET + SnO _x ^{HSE} + adhesive A + SiO _x ^{HSE} + PET] laminated with adhesive a2 by bench lamination.	163
A.6	Test conditions of the UV and climate stability tests used in this work.	164
A.7	Climate stability of three transparent polymer films suitable for climate stability tests (marked in green).	165
A.8	UV stability of one transparent polymer film suitable for UV stability tests (marked in green) and one unsuitable one.	166
A.9	Typical permeability coefficients of three organic coating materials (permeability coefficients from Chapter 5.3).	166
A.10	Climate stability of the three organic coating materials when applied as top coat on top of polymer films or inorganically coated polymer films.	167
A.11	UV stability of the three organic coating materials when applied as top coat on top of uncoated polymer films.	167
B.1	Overview of the equations for permeability and time lag for <i>n</i> layers.	175
C.1	Photovoltaics market: efficiencies and costs from 2010 [85].	177

Abstract

For more than 20 years the field of organic electronics (OE) has been a topic of interest for research and development. One important topic in this context is to develop an appropriate encapsulation material that would protect the OE application from environmental degradation for long periods, in order to ensure long product lifetimes, and which at the same time is flexible enough to profit from the possibilities of mass-production and bendability.

This work was aimed at collecting a general systematic understanding about high barrier encapsulation by means of experimental and theoretical evaluations. Experimental evaluation comprised the fabrication of approximately 1600 mono- and multilayered structures and their adequate characterization in about 4000 transmission rate measurements. Based on these data, known or expected barrier effects, like the synergistic barrier effect, the tortuous path effect or the time lag effect, as well as the optimum intrinsic barrier properties of a wide range of materials could be assessed in relation to their effectiveness in helping to decrease the water vapor transmission rate of the encapsulation material.

With respect to the encapsulation of organic photovoltaic (OPV) modules, these guidelines were used to produce flexible, transparent and environmentally stable high barrier material in a roll-to-roll process with a water vapor transmission rate of 5×10^{-4} g/(m² d). This is about three order of magnitudes lower than what was achieved for large scale, roll-to-roll produced material at the beginning of this work. OPV modules encapsulated with this material would have a lifetime of approximately 1.5 years at ambient conditions.

Nomenclature

Acronyms

ACP	accumulating gas chromatographic permeation
AFM	atomic force microscopy
ALD	atomic layer deposition
AlO _x	non stoichiometric aluminum oxide
DIN	Deutsches Institut für Normung (a German standardization org.)
EAA	ethyl acetoacetate
EC	electrochromic
ECTFE	ethylene chlorotrifluoroethylene
EPh	electrophoretic
ETFE	ethylene tetrafluoroethylene
EVOH	ethylene vinyl alcohol
FEA	finite elements analysis
FEP	fluorinated ethylene propylene
FTIR	Fourier transform infrared spectroscopy
GLYMO	3-glycidyloxypropyltrimethoxysilane
IEC	International Electrotechnical Commission
LCD	liquid crystal display

Nomenclature

LED	light emitting diode
MD	machine direction
MEMS	micro-electro-mechanical system
OE	organic electronics
OFET	organic field effect transistor
OLED	organic light emitting diode
OPD	organic photo detector
OPV	organic photovoltaic
PA	polyacetylene
PC	polycarbonate
PCB	polychlorinated biphenyl
PCTFE	polychlorotrifluoroethylene
PCL	polycaprolactone
PEEK	polyether ether ketone
PE-LD	polyethylene of low density
PEN	polyethylene naphthalate
PET	polyethylene terephthalate
PI	polyimide
PLA	polylactic acid
PMMA	poly(methyl methacrylate)
PP-c	polypropylene, fabricated by casting
PP-BO	polypropylene, biaxially oriented
PS	polystyrene

PS-BO	<u>p</u> ol <u>s</u> t <u>y</u> rene, <u>b</u> ia <u>x</u> ially <u>o</u> riented
PU	<u>p</u> ol <u>y</u> urethane
PVC	<u>p</u> ol <u>y</u> vinyl <u>cl</u> horide
PVdC	<u>p</u> ol <u>y</u> vinylidene <u>cl</u> horide
PVOH	<u>p</u> ol <u>y</u> vinyl alcohol
RH	<u>r</u> elative <u>h</u> umidity
SBS	<u>s</u> t <u>y</u> rene <u>b</u> utadiene <u>s</u> t <u>y</u> rene
SEM	<u>s</u> canning <u>e</u> lectron <u>m</u> icroscopy
SiO _x	non stoichiometric <u>s</u> ilicon <u>o</u> xide
SiO _x ^{HSE}	non stoichiometric <u>s</u> ilicon <u>o</u> xide of <u>h</u> igher <u>s</u> urface <u>e</u> nergy
STP	standard conditions for temperature and pressure, i.e. (acc. to DIN) at a temperature of 0°C and an absolute pressure of 1.01325 bar (for gases: at a molar volume of 22.413 968 l/mol)
sun	1 sun = 1367 W/m ² ≈ 1000W/m ²
(HR) TEM	(<u>h</u> igh <u>r</u> esolution) <u>t</u> ransmission <u>e</u> lectron <u>m</u> icroscopy
TD	<u>t</u> ransversal <u>d</u> irection
THV	<u>t</u> etrafluoroethylene <u>h</u> exafluoropropylene <u>v</u> inylidene
TMOS	<u>t</u> etramethyl <u>o</u> rthosilicate
UV	<u>u</u> ltraviolet light
UV-A	<u>u</u> ltraviolet light of type A (wave length range 315–380 nm)
UV-B	<u>u</u> ltraviolet light of type B (wave length range 280-315 nm)
UV-C	<u>u</u> ltraviolet light of type C (wave length range 100-280 nm)
UV-vis	all visible and UV light (wave length range 100-750 nm)
VIP	<u>v</u> acuum <u>i</u> nsulation <u>p</u> anel
ZnSn _x O _y	non stoichiometric zinc tin oxide

Symbols

<u>Symbol</u>	<u>Quantity</u>	<u>Unit</u>
a	area fraction covered with pores <i>or</i> coefficient of heat transfer	-
α	part of macro- and microscale pores per area	-
A	area perpendicular to the path of permeation	m ²
b^*	yellow part of the CIE colour system	-
Δb^*	relative increase of b^*	-
β	isobaric coefficient of volumetric expansion	-
B	normalized amount of permeating matter (\equiv accumulated transmission rate), for oxygen or water vapor transmission	mol/(m ² Pa) or mol/m ²
BIF	<u>B</u> arrier <u>I</u> mprovement <u>F</u> actor	-
BIF ^{local}	BIF referring to the area close to the pores	-
c	concentration of the permeating matter	mol/m ³
c_p	specific heat capacity	J/(kg K)
d	layer thickness	m
D	diffusion coefficient	m ² /s
E_{in}	energy that is introduced in the layer to be cured	J
F	improvement factor	-
g	gravimetric acceleration constant	m/s ²
j	flux density of the permeating matter	mol/(m ² s)
J	flux of permeating matter	mol/s
J_1	flux of permeating matter that permeates from the first compartment into the membrane	mol/s

<u>Symbol</u>	<u>Quantity</u>	<u>Unit</u>
J_2	flux of permeating matter that permeates out of the membrane into the second compartment	mol/s
$J_{2,\infty,n}$	flux of permeating matter that permeates at steady state out of a membrane consisting of n layers in total	mol/s
$J_{2,\text{meas},n}$	measured flux of permeating matter out of the a membrane consisting of n layers in total	mol/s
k	correction factor (for BIF calculations)	-
K_T	correction factor (for heat flow calculations)	-
L	characteristic dimension (for heat flow calculations)	m
λ	coefficient of thermal conduction	W/(m K)
n	number of macro- and microscale pores, number of layers or index number in derivation of a Taylor series	-
Nu	coefficient of Nusselt	-
ν	kinematic viscosity	m ² /s
$OTR \equiv T_{nL,O_2}$	experimentally gained (measured) <u>oxygen transmission rate</u> , for a membrane consisting of n layers	cm ³ (STP)/(m ² d bar)
OTR xx/yy e.g. OTR 23/50	OTR at $xx^\circ\text{C}$ and $xx\%$ relative humidity e.g. OTR at 23°C and 50% relative humidity	cm ³ (STP)/(m ² d bar)
p	partial pressure of the permeating matter	Pa
P	permeability coefficient	mol/(m ² s Pa)
Pr	coefficient of Prandtl	-
Q	amount of the permeating matter	mol
r	radius of the macro- and microscale pores	m

Nomenclature

<u>Symbol</u>	<u>Quantity</u>	<u>Unit</u>
Re	coefficient of Reynolds	-
Ra	coefficient of Rayleigh	-
R_a	average surface roughness, by arithmetic mean	nm
RMS	average surface roughness, by mean square	nm
ρ	density	kg/m ³
S	sorption coefficient <i>or</i> synergistic effect (percental “excess” of measured to the expected transmission rate)	mol/m ³ <i>or</i> -
t_{nL}	time lag of the permeation process through an encapsulation material consisting of n layers	min, h or d
t	time	s, min, h or d
t_{50}	time after which 50 % of the calcium test area has reacted	s, min, h or d
t_{fail}	time after which the <i>Konarka</i> OPV test cell is dead	s, min, h or d
T	transmission rate of the permeating matter	mol/(s m ² Pa)
T_{nL}	transmission rate of the permeating matter through a multilayered encapsulation material, consisting of n layers	mol/(s m ² Pa)
T	transmittance matrix	-
ϑ	temperature	°C
v	speed (e.g. web speed)	m/s

<u>Symbol</u>	<u>Quantity</u>	<u>Unit</u>
WVTR $\equiv j_{nL,H_2O}$	experimentally gained (measured) water vapor flux density, for a membrane consisting of n layers. WVTR is the abbreviation for <u>w</u> ater <u>v</u> apor <u>t</u> ransmission <u>r</u> ate and therefore incorrectly suggests to the reader that this would represent a transmission rate (i.e. a flux density normalized to the partial pressure difference). However, WVTR are not normalized, but, for historical reasons, nevertheless called water vapor <i>transmission rates</i> .	g/(m ² d)
WVTR ^{Ca}	WVTR derived from calcium test, with some remaining uncertainty whether the steady state is reached. The WVTR ^{Ca} might be an "unknown mixture" of transient and steady state barrier performance.	g/(m ² d)
ω	speed of heat flow	m/s
X	factor of reduction	-
$y(t)$	asymptote to the curve of $B(t)$ (i.e. the normalized amount of permeating matter), for water vapor transmission	mol/m ²
Y	admittance matrix	-

1 Motivation

'Organic Electronics'(OE) is the name commonly used in Europe for the field of electronics that deals with organic semiconductors. This field is called 'organic' electronics following the nomenclature of 'organic' chemistry, as it employs carbon-based materials (polymers or carbon-based molecules) - in contrast to traditional electronics which rely on inorganic conductors such as copper or silicon¹.

The field of OE research was launched from two sides during the last third of the 20th century: both the breakthroughs in the research on conductive molecules and in the research on conductive polymers contributed to the rising importance of this field.

The research on conductive molecules (molecular crystals) got a significant boost in 1960 with the demonstration of the first electroluminescent thin film structures by N.A. Vlasenko and Yuri A. Popkov [86] and, in 1987, with the demonstration of high-performance electroluminescent diodes when using vacuum evaporation as thin film deposition process [87].

In parallel, broad research on conductive polymers (conjugated polymers) was triggered by the demonstration of the first thin conductive polymeric films by Hideki Shirakawa in the 1970s and, in 1977, the discovery of the effect of "doping of a polymer" by Alan J. Heeger, Alan G. MacDiarmid and Hideki Shirakawa [1]. First "doped" polyacetylene films showed a conductivity of 10^5 S/m, which was higher than that of any previously known polymer (Fig. 1.1).

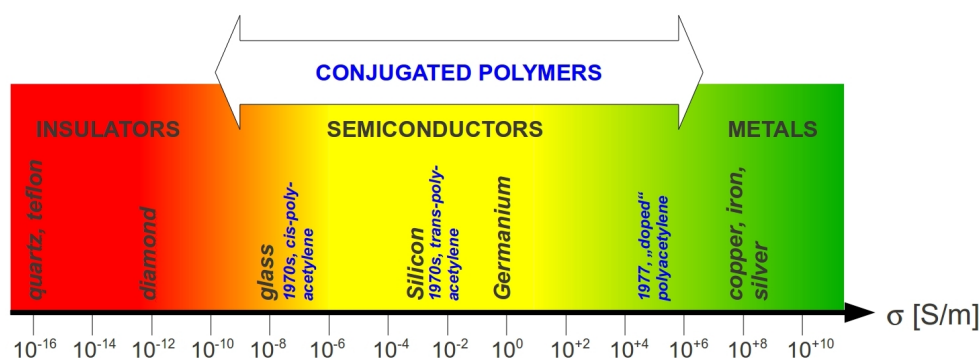


Figure 1.1: Conductivity of selected materials (adapted from [1]).

Further research on both classes of organic semiconductors lead, in 1997, to the first commercial OE product: Pioneer launched a monochrome 256 x 64 dot electrolumines-

¹Further common names are: *Plastic Electronics* (in UK), *Printed Electronics* (in primary printing platforms), *Large Area Electronics* or *Macro Electronics* (in military) or, more general, *Flexible Electronics* (in the USA) [77].

1 Motivation

cent (EL) display for automotive applications (Fig. 1.2) [88]. Until today, further products were commercialized that contained OE components like organic light emitting diode (OLED) displays, organic solar cells (OPV) or OLED lighting (Fig. 1.2).



Figure 1.2: Selected examples for existing and planned OE products [2, 3, 4, 5, 6, 7, 8, 9, 10, 11].

The interest in OE stems from their ability to be solution-processed, i.e. to be mass-produced by printing processes, their mechanical flexibility, their lightweight and their transparency. This would allow for a wide range of new applications: flat rigid products as well as 3-dimensional shaped or flexible products (Fig. 1.2), both low-cost and high-end.

The market for OE products is expected to have reached a size of 20 to 60 billion dollar by 2020 [77] - depending in which timeframe the main technological challenges will be solved. Global interest is high to be among the first to solve these challenges and profit from the potential economic success of the OE market - which is demonstrated by the impressive funding volumes that were spent by governments all over the world during the last decade (Table 1.1).

Table 1.1: Funding for research in organic electronics for 2001-2013 [77, 78].

Area	Total funding volume [\$]	Funding institution	Volume per institution [\$]	Initiatives
Europe	715,000,000	EC	369,000,000	FP 6 and 7
		Germany	265,000,000	OPV, OLED, smart labels
		UK	79,000,000	CPI, CENAMPS
USA	193,000,000	NIST-ATP	12,200,000	2 projects
		DARPA	15,000,000	MICE, FED
		Army	97,300,000	FDC, Phase I and II
		USDC	69,300,000	44 projects / centers
Taiwan	179,880,000	ITRI	156,700,000	-
		TPD	11,320,000	-
		NSC	11,860,000	-

There are three main technological challenges that OE research and development is currently facing on the way to broad commercialization [77]:

- An appropriate encapsulation has to be developed that enables a long protection from environmental degradation, and such a long product lifetime, and which is at the same time flexible enough to profit from the possibilities of mass-production and bendability.
- The compatibility of process temperatures and thermal stability of the substrate has to be improved: Either flexible substrates have to be developed that resist higher thermal impact and/or processes using lower temperatures have to be developed to accommodate the sensitive substrates.
- The brittleness of the device layers has to be reduced or to be protected to be able to exploit the full potential of flexibility in future applications.

From those three topics, the first one is often regarded to be the major hurdle to overcome, especially for OLED applications [89, 12].

In 2006, though considerable improvements were achieved for encapsulation materials (Chapter 3.2), there was still "no plastic [OE encapsulation] that is hermetic enough to make devices that will last a long period" [89]. The difficulties in developing flexible OE encapsulation result from the diversity of requirements that are imposed on such a material (Chapter 2). All requirements cannot be fulfilled by one single material type, but diverse material types have to be combined. This causes issues of interaction and converse optimization parameters. The more material types are included, the nearer one may come to the best possible implementation of all required properties, but the more complex and time-consuming the optimization process gets, too.

If there were general rules how to assemble barrier materials to create an effective encapsulation material at minimum costs, the (initial) experimental effort could be reduced and the development process could be accelerated. It was with this purpose that the experiments of this work were performed. The aim was to understand the dependencies between the material properties of the single layers of a multilayered encapsulation material and its overall barrier performance and thermal and mechanical stability.

This work presents the results of this broad experimental study that evaluated both the intrinsic properties of many potential barrier materials as well as their barrier and stability performance in combination with each other. Expectations for the transient and steady state barrier performance of roll-to-roll prepared encapsulation materials are clarified and put into realistic relation to financial effort spent on their production. The limits and benefits of fast theoretical calculation methods and new experimental evaluation methods, that were developed or extended to be able to assess the encapsulation materials, will be described.

The results show that there is no such thing as the "ultimate roll-to-roll encapsulation strategy" that fits all OE products. But it is possible to give general advice how to combine which materials to create the one roll-to-roll produced encapsulation material that best suits one certain OE product at minimum costs.

2 Requirements for the encapsulation material

2.1 Protection from environmental gases

The encapsulation material for OE devices should, first of all, provide a suitable gas barrier to prevent environmental gases from diffusing into it. However, the required performance of the gas barrier is not a strict value, but varies for each OE application. Furthermore, the sensitivity of one OE application varies with parameters like the type of its active layers, the layer thicknesses, the intrinsic sensitivity of the layers towards environmental gases and the type and time span of environmental exposure. Hence, the barrier requirement for the encapsulation material can only be roughly described per application and as a range of “orders of magnitude“ of transmission rates (Fig. 2.1).

Transparent, flexible barrier materials already exist nearly 20 years in the food industry [90, 91, 92]. Yet even sensitive food - which requires the highest gas barriers in the food industry - is sufficiently protected by using packaging materials that show water vapor transmission rates (WVTR) not lower than $10^{-1} \text{g}/(\text{m}^2 \text{d})$ - whereas WVTR that are orders of magnitude lower than this are required when transparent, flexible technical ap-

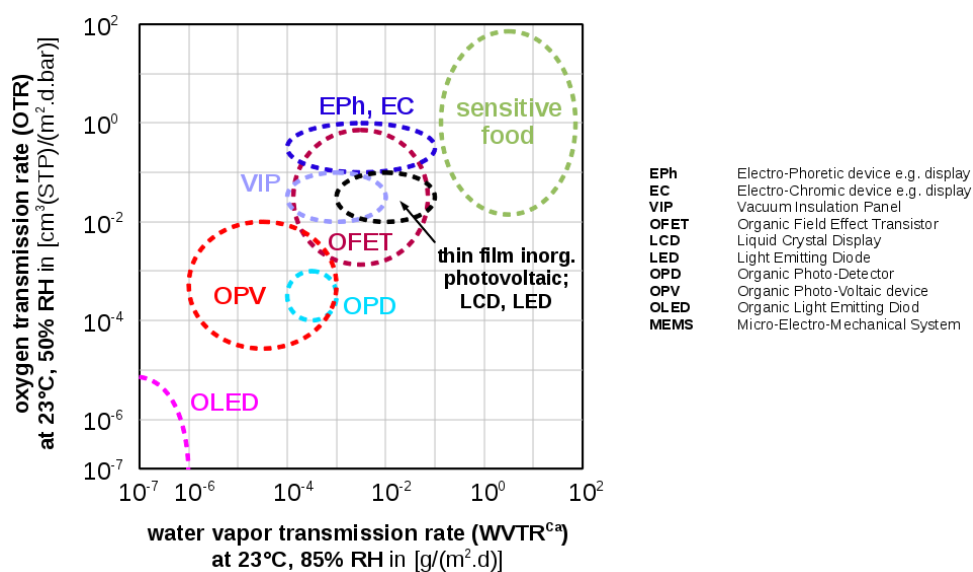


Figure 2.1: Barrier targets for OE applications in comparison to those of other packing goods [12, 13, 14, 15, 16, 17].

2 Requirements for the encapsulation material

plications are concerned (Fig. 2.1). Some organic electronics applications, like organic field effect transistors (OFET), require encapsulation materials similar to those necessary for the encapsulation of inorganic electronics: WVTR^{Ca} between 10^{-2} and 10^{-4} g/(m² d) (Fig. 2.1). Yet, the lowest WVTR^{Ca} - down to 10^{-7} g/(m² d) - are required for OE devices that have to use electrodes based on ignoble metals, like calcium or barium (Table 2.1).

Table 2.1: Structures of OE applications.

Electronic component	Most sensitive part	Required WVTR ^{Ca}
	part	level [g/(m ² d)]
	material	
organic diode	electrodes	$\sim 10^{-3}$ [14]
OFET	electronics	10^{-1} - 10^{-4} [13]
	acenes / thiophenes / phenylenes etc.	
organic memory	electronics	$\sim 10^{-2}$ [15]
OLED	electrodes	10^{-6} - 10^{-7} [14]
OPD	electrodes	$\sim 10^{-3}$ [14]
EPh display	electronics	10^{-1} - 10^{-2} [13, 12]
EC display	electronics	10^{-1} - 10^{-2} [15]
organic capacitor	electronics	$\sim 10^{-2}$ [15]
OPV	electrodes	10^{-3} - 10^{-6} [14]
organic battery	electronics	$\sim 10^{-2}$ [15]

Since charge transport through organic semiconductors uses less efficient transport mechanisms ("tunneling" and "hopping"), charge mobilities are low: some $10 \text{ cm}^2/(\text{Vs})$ for conductive organic molecules, compared to $1300 \text{ cm}^2/(\text{Vs})$ for crystalline silicon [93]. Efficient charge transport can nevertheless be ensured, when the distance between the electrodes is very small, i.e. the semiconductor layer is very thin, and the work function of the emitting electrode is very low, i.e. the electrode consists of, for example, ignoble metals. But ignoble metals oxidize vigorously when exposed to environmental gases, such as nitrogen, oxygen and water vapor, and therefore have to be encapsulated with materials with a high gas barrier.

Among all environmental gases that could degrade, i.e. oxidize, the electrodes, water vapor plays the major role. For this reason, the requirements for the barrier against water vapor are more severe than against other gases like oxygen (Fig. 2.1).

The dominant destructive role of water vapor results from two causes. First, the amount of water vapor available in the inner space of the encapsulated OE device due to permeation will always be much higher than that of any other environmental gas, because from all environmental gases, water vapor is the fastest permeant. This is not only a result from the size or mass of the water molecule. On the contrary, according to its size and mass, the water molecule should not permeate much faster than nitrogen or oxygen: the gas diffusion coefficient of water vapor is with $4.1 \times 10^{-5} \text{ m}^2/\text{s}$ not much higher than that of nitrogen or oxygen with $2.9 \times 10^{-5} \text{ m}^2/\text{s}$ and $3.0 \times 10^{-5} \text{ m}^2/\text{s}$, respectively (Fig. 2.1, Table 2.2).

But the potential of a gas to interact electro-chemically with other materials influences its permeation process. Gases with an elevated polarizability or dipole moment, such as

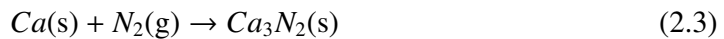
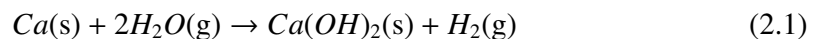
Table 2.2: Environmental gases and their permeation-related properties (ordered according to increasing diffusion coefficient within the gas).

Gas	Volume fraction in air [%] ^a	Gas kin. collision diameter at 20°C, 101,3 kPa [Å] ^f	Molec. mass [u] ^b	Diff. coeff. within gas [10 ⁻⁵ m ² /s] ^g	Polarizability [10 ⁻⁴⁰ C m ² /V] ^d	Dipole moment [debye] ^c	Permeability coeff. factors, compared to N ₂ for ^e	
							PE-LD (non-polar)	PET (polar)
CO ₂	0.032	4.8	44	1.6	3.0	0	13	22
Ar	0.93	3.8	40	2.6	1.8	0	2.9	2.0
NH ₄	<0.0005	4.6	17	2.7	2.5	1.47	29	324
CO	<0.0005	3.9	28	2.9	2.2	0.12	1.5	-
N ₂	78.1	4.0	28	2.9	1.0	0	1.0	1.0
O ₂	20.9	3.8	32	3.0	1.8	0	3.0	4.4
CH ₄	<0.0005	4.3	16	3.3	-	0	3.0	0.6
H₂O	-	3.7	18	4.1	1.6	1.85	93	29659
He	0.0005	2.3	4	23	0.2	0	5.1	4.4
H ₂	0.00005	2.8	2	21	0.9	0	10.1	118

^a[94]^b[95]^c[96, 97]^d[98, 99, 100, 101]^e[59, 102, 103]^f[104, 105]^gCalculated from collision diameter and molecular mass according Equ. (2.28) in [95]

carbon dioxide, ammonia or water vapor, show permeabilities that exceed many times the expectations based on their diffusion coefficient within gas (Table 2.2). The higher the potential to interact electro-chemically, the higher the additional increase in permeability. For this reason, from the main three gases that degrade the electrodes, water vapor permeates at least 100 times faster than the two others (Table 2.2). For polar multilayered barrier films, the relation of the permeated water molecules towards the permeated oxygen molecules can become up to 880 000 : 1 (Table 2.3). For OE encapsulation materials (which contain many more barrier layers than medium or high barrier films) this ratio will further increase towards the permeated water vapor.

Second, the reactions of the electrode material - most often calcium - are much faster with water vapor than with the other gases. From the three main reactions of the calcium with environmental gases:



reaction 2.1 is the fastest. For example, at 25°C, water vapor reacts about 350 times faster with unprotected calcium than oxygen [106]. Additionally, the reaction speed increases

2 Requirements for the encapsulation material

Table 2.3: Molecular ratio of environmental gases after one year of permeation (in steady-state) through different barrier materials (at 25°C, 101,325 kPa, 100% RH).

	Nitrogen [mol]	Oxygen [mol]	Water vapor [mol]	Molecular ratio
1m ³ air:	31,9	8,5	23,1	4 : 1 : 3
non-polar polymer film ^a :	0.0208	0.0627	3.47	1 : 3 : 170
polar polymer film ^b :	0.0001	0.0007	1.88	1 : 6 : 16000
non-polar barrier film, type 1 ^c :	-	0.000006	0.13	- : 1 : 22000
non-polar barrier film, type 2 ^d :	-	0.000003	0.10	- : 1 : 36000
polar barrier film, type 1 ^e :	-	0.000003	0.14	- : 1 : 46000
polar barrier film, type 2 ^f :	-	0.0000001	0.11	- : 1 : 880000

^aPE-LD of 50 µm thickness (own measurement).

^bPET of 50 µm thickness (own measurement).

^cPET+SiO_x+PE-LD-like lacquer (~51 µm in total), theoretical estimate acc. to Chapters 3.1.7, 3.1.8

^dPET+SiO_x+PCTFE-like lacquer (~51 µm in total), theoretical estimate acc. to Chapters 3.1.7, 3.1.8

^ePET+SiO_x+PET-like lacquer (~51 µm in total), theoretical estimate acc. to Chapters 3.1.7, 3.1.8

^fPET+SiO_x+PVdC-like lacquer (~51 µm in total), theoretical estimate acc. to Chapters 3.1.7, 3.1.8

quadratically with increasing water vapor partial pressure [106]. Hence, the development of encapsulation materials has to focus primarily on the the water vapor permeation process.

To reduce the water vapor permeation through a material, there are two possibilities. First, the spaces where water molecules could permeate through the so-called “free volume“ should be reduced. This includes both microscopic spaces, like defects in the layers, and nanoscale spaces, like open areas between widely bonded molecular chains.

Furthermore, the electro-chemical interaction of the water molecules should not easily move atoms, molecules or chain segments of the material ”out of the way“. In case this so-called ”molecular flexibility“ is high, this could, for example, induce swelling of the material and generate ”additional space“ for the passage of the water molecules.

Both the free volume and the molecular flexibility of an encapsulation material determine how many of the water molecules arriving on one side will be transmitted through the bulk to the other side - at given time, area and measuring conditions. This quantity is called ”water vapor transmission rate“ (WVTR) in steady state.

Additionally, before the permeation process corresponding to the steady state WVTR takes place, there is an ”adjustment period“. During this period, little of the arriving water molecules are transmitted, hence, this ”additional“ transient regime is convenient for the increase of the lifetime of the OE application. The transient regime can last very long, depending on the overall sorption capacity and diffusion behavior of the encapsulation material, and is therefore a useful second optimization parameter. To quantify the duration of this transient regime, the term “time lag” (t_{nL}) was introduced [107].

Both absolute barrier performance (in terms of WVTR) and time-dependant barrier performance (in terms of time lag) of a material need to be optimized to approach the target of an encapsulation material that ensures long OE product lifetimes. Hence, the focus of this work was to create an encapsulation material showing low steady state WVTR and

long time lag.

In addition to this, it was important to clarify to which extent each of the two parameters would (or should) contribute to the target of an encapsulation material ensuring a long product lifetime. At the beginning of this work, it was presumed that the WVTR requirements per OE application - when having been concluded from measurements including a calcium layer (i.e. calcium based WVTR tests or calcium including device tests) - were probably not requirements for the pure steady state WVTR, but an “unknown mixture“ of absolute and time-depending barrier performance [41] (like the requirements used for this work). Such measured WVTR or WVTR requirements will therefore be labeled ”WVTR^{Ca}” to separate them from pure steady state “WVTR“ (like applied in Fig. 2.1).

Besides the improvement of the encapsulation material, there is another possible strategy that would increase the lifetime of a packed product, that should at least be mentioned even though it is not subject of this work: One could also work on the decrease of the sensitivity of the packed good - in this case, focus on the desensitization of the electronic components. Research activities are ongoing on the desensitization of the electrodes - by replacing pure alkaline metals or alkaline earth metals by more stable alloys with, for example, silver or aluminum (e.g. Mg:Ag, Li/Al, Ca/Al or LiF/Al) [108] - as well as on the desensitization of the organic semiconductors. Even though progress has been made (e.g. red singlet OLED devices could survive in 2006 for 1 million hours at ambient conditions instead of 500 hours in 1987 [109]), long-lasting and full colour OE devices are still not possible without tight encapsulation.

2.2 Further requirements

To ensure the required barrier performance is the main purpose of OE encapsulation material. Yet there are additional requirements - summarized in Table 2.4 - that have to be kept in mind, because the need to fulfill them sometimes influences the choice of barrier materials. For this work the selection of barrier materials was strongly influenced by all additional requirements mentioned in Table 2.4. Of importance is not only the intrinsic performance of the pristine barrier layers towards these criteria, but also their performance in combination towards the same criteria - a major difference can occur between the two. In case the performance of some barrier materials (pristine or in combination) towards these criteria were not known, the corresponding tests were performed.

Since the main focus of this work lays in understanding and improving the barrier performance of roll-to-roll OE encapsulation materials, the results of these additional tests are reported in the main part of this work only if not omittable for the understanding. More information can be found in Appendices A2 and A3 or in the relevant publication [116].

Similarly, the cost targets for OE encapsulation materials influenced the selection of the barrier materials or fabrication processes, but were not in the main focus of this work. Some cost information can be found in Appendix C.

2 Requirements for the encapsulation material

Table 2.4: Further requirements for OE encapsulation materials.

Requirement	Criterion	Company [Ref.]
high UV and light transmission	for front sheets: > 85 %, UV cut at 380 nm	<i>heliatek</i> [110]
thermo-mechanical robustness	maximum elongation at 300 N of 0.5 %, both at room and elevated temperature,	<i>heliatek</i> [110]
	no major change up to 85 °C, better up to 120 °C	<i>Konarka</i> [14]
	no major change up to 100 °C, better up to 200 °C	<i>Siemens</i> [14]
low thermal shrinkage	CTE < 50 ppm/K, better up to < 5 ppm/K,	<i>Siemens</i> [14]
	dimensional change after storage at 130 °C for 1 hour < 0.25 %, better < 0.01 %	<i>Siemens</i> [14]
chemical robustness	t.b.d.	<i>Siemens</i> [14]
smooth and clean surface	no scratches or spikes > 50 nm	<i>heliatek</i> [110]
flexibility	no major loss of properties, especially barrier performance after 1,000 to 10,000 bending cycles with a bending radius of 5.5 cm at varying frequencies	working group of <i>NREL, Plextronics, Konarka, Mocon, Solarmer, ECN</i> [111]
UV and climate stability	outdoor testing acc. to IEC 61215 and IEC 61646 (from thin film PV, partially too harsh or too weak for OPV [112]),	initially for OPV [112]
	tests T1 to T6 for non-encapsulated OPV modules: up to 1 sun ^a , 85 °C and 85 % humidity	working group of <i>Plextronics, NREL, Konarka</i> [113, 114, 115]

^aThe expression "1 sun" is a casual term of the OPV community rooted in the solar constant E_0 which is the amount of incoming solar electromagnetic radiation per unit area at the mean distance from the sun to the earth. Yet, while $E_0 = 1367 \text{ W/m}^2$, "1 sun" = 1000 W/m^2 for simplification of the test procedures.

3 Existing encapsulation concepts

3.1 Permeation theory

3.1.1 Description of the permeation process

The process of gas permeation through plane homogeneous encapsulation materials is a three dimensional process, but due to the layered structure of the plane encapsulation material the physical system is a translation invariant and can be reduced to a one dimensional mathematical description. (Flux changes occur along the x axis only.)

The encapsulation material is regarded as a plane membrane and adjacent to that membrane are two compartments of different gas concentrations, i.e. different partial gas pressures, of the respective permeating matter ("M") (Fig. 3.1). The first compartment (at

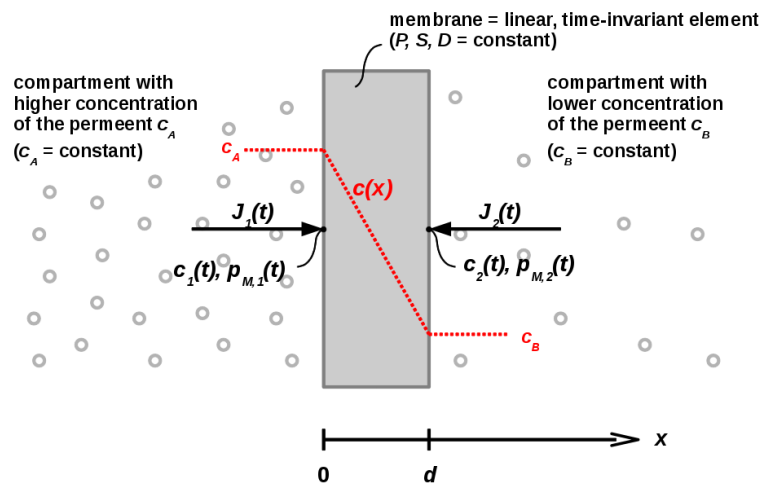


Figure 3.1: Schematic of a membrane separating two compartments of different partial pressures, following [18].

the $x < 0$ side) has a partial pressure $p_{M,1}$ that is higher than that of the second compartment $p_{M,2}$ at the $x > d$ side, while both are constant over time. Matter, e.g. water vapor, can only permeate starting from compartment one through the membrane to the second compartment - not from any other sources, for instance from the sides of the membrane. The flux entering the membrane from the first compartment is denoted J_1 , the flux leaving the membrane into the second compartment is denoted J_2 . Both fluxes are defined as incoming into the membrane to simplify future mathematical operations. Hence, it is the outgoing flux $-J_2$ that is of importance for the development of encapsulation ma-

terial, as it describes the amount of matter that would penetrate into the inner part of the package.

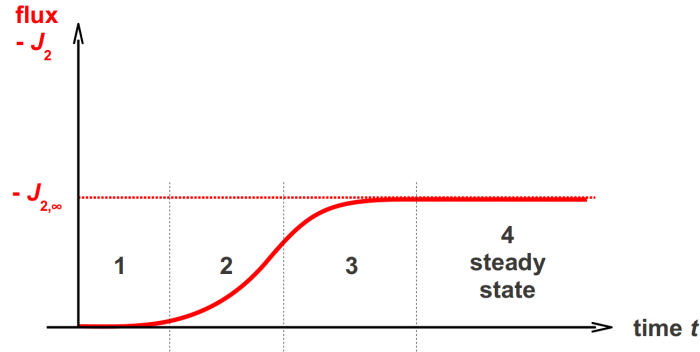


Figure 3.2: The flux $-J_2$, that permeates out of the encapsulation material, as a function of time.

Independent of the type of encapsulation material, the chronological development of the outgoing flux $-J_2(t)$ always follows the same four steps (Fig. 3.2). At time $t = 0$, the concentration of matter is zero within the whole membrane as it could be achieved by purging of the whole measurement system and of the sample before every barrier measurement. During the first period, more gas permeates into the encapsulation material than comes out of it, because a large part is absorbed in its inner. This results in a very small value of $-J_2(t)$ that barely increases. The more of the sorption capacity of the encapsulation material is consumed, the more and more of the permeating gas actually transits through the encapsulation material, which leads to a rapidly increasing value of $-J_2(t)$. During the third period, when the flux approaches its steady state value, the increase of the value of $-J_2(t)$ slows down and the curve converges towards the value of $-J_{2,\infty}$. At time $t \rightarrow \infty$, the gas permeation arrives in the steady state period, where exactly the same amount of gas Q_1 that arrives at the one side of the encapsulation material permeates entirely through it and comes out of its other side (as Q_2).

In opposite to theory, the experimentally measured flux is classified as “arrived in steady state” as soon as no further increase of $-J_2(t)$ can be observed - which depends greatly on the accuracy of the permeation test device (and for all test devices this naturally happens at a finite time t_{meas} instead of $t \rightarrow \infty$). For all future comparisons between mathematically calculated and experimentally measured results, it is assumed that the measured values as finally taken are (nearly) equal to the steady state values:

$$-J_{2,\infty} = \frac{\Delta Q_2}{\Delta t} \approx -J_{2,\text{meas}} \quad (3.1)$$

Normalization of the flux to the area of permeation A gives the flux density j_i :

$$j_i = \frac{-J_{i,\infty}}{A_i} \quad (3.2)$$

For some gases, e.g. for oxygen, the concentration of the gas is directly linked to its partial pressure:

$$c = S p \quad (3.3)$$

with S being the sorption coefficient of the gas in the encapsulation material. In case, Eq. (3.3) - the so-called Henry's law - is applicable, the flux density can further be normalized to the difference of partial pressure between the two compartments $\Delta p = (p_{M,A} - p_{M,B})$ which gives the transmission rate T [107]:

$$T = \frac{j}{\Delta p} = \frac{-J_{2,\infty}}{A(p_{M,A} - p_{M,B})} \quad (3.4)$$

expressed in SI units [$\text{mol}/(\text{m}^2 \text{ s Pa})$]. There are permeating matters, for example water vapor, that cause structural changes, like swelling or increase in flexibility, of the encapsulation material while passing through. In such cases, the sorption coefficient is not constant and Henry's law not applicable. Therefore, the flux density of such permeating matters is not normalized to the difference of partial pressure between the two compartments.

Yet, for historical reasons, experimental results of water vapor permeation measurements are nevertheless called water vapor *transmission rates*, despite they are actually water vapor *flux densities*. (Usually the reader receives the information of the difference of relative humidity along with it.) Additionally, again for historical reasons, the transmission rates for water vapor and oxygen are not measured in SI units in experimental environments, but in individual units: [$\text{g}/(\text{m}^2 \text{ d})$] for water vapor and [$\text{cm}^3(\text{STP})/(\text{m}^2 \text{ d.bar})$] for oxygen (or variations hereof).

In order to differentiate between the transmission rates in experimental units and SI units, the former will in the following be called WVTR and OTR, for water vapor transmission rate and oxygen transmission rate, respectively, in contrast to T for oxygen or j for water vapor. Hence, it is true that:

$$\text{WVTR} = j_{\text{water vapor, meas}} \approx j_{\text{water vapor, } \infty} \quad (3.5)$$

and:

$$\text{OTR} = T_{\text{oxygen, meas}} \approx T_{\text{oxygen, } \infty} \quad (3.6)$$

3.1.2 Transmission rate calculation for homogeneous monolayered materials

For homogeneous monolayer materials, normalization of the transmission rate to the thickness of the membrane d gives the permeability coefficient P of the membrane [117] which is at the same time the product of the diffusion coefficient D with the sorption coefficient S :

$$P = T d = D S \quad (3.7)$$

The diffusion coefficient is of the same dimension as the acceleration (units: [m²/s]) and therefore gives an information about the “speed” of the movement of the gas molecules through the encapsulation material. The sorption coefficient describes the amount of gas molecules that can be absorbed in the volume of the encapsulation material at a certain partial pressure (units: [mol/(m³ Pa)]). Both parameters are assumed to be constant over time, position and concentration of matter in the membrane, hence, P , D and S are used like material constants for the respective encapsulation material. With T or P and d or D , S and d , the steady state barrier performance of a homogeneous encapsulation material can be sufficiently characterized.

3.1.3 Time lag calculation for homogeneous monolayered materials

The transient barrier performance, i.e. the durations of steps one to three of the permeation process (Section 3.1.1) are not directly linked to the steady state data (transmission rate, sorption coefficient, diffusion coefficient or combinations). Therefore, they must be considered separately. To be able to quantify the duration of the transient regime of the permeation process, the “time lag” for a monolayered (1 Layer) membrane τ_{IL} was introduced as the time value that results when the asymptote $y_{IL}(t)$ to the permeated amount $B_{IL}(t)$ intersects with the x axis (the time axis) [107] (Fig. 3.3). This definition was cho-

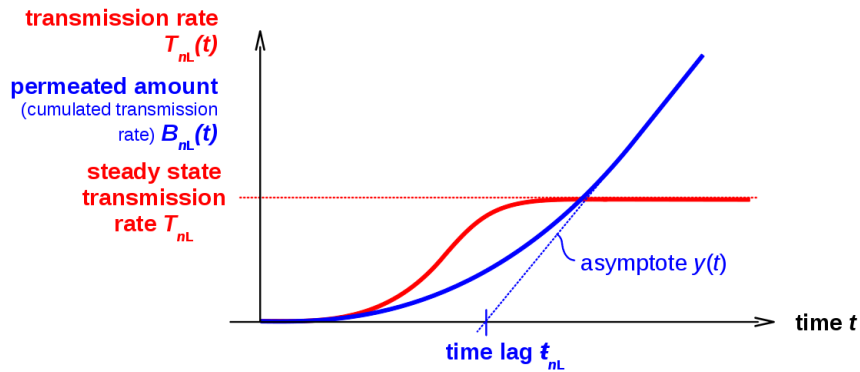


Figure 3.3: Transient and steady state aspects of the gas permeation process.

sen in such a way that the time lag would be easy to gain from permeation measurements on monolayered membranes [107] - the time lag is not a physical quantity that describes a specific moment of the permeation process (e.g. it is not the inflection point of the transmission rate curve).

It was demonstrated [118] that, for a monolayered material, the asymptote $y(t)$ could be calculated by using trigonometrical series development for the development of the concentration $c(x, t)$ in the membrane:

$$y(t) = \frac{D}{d}(c_A - c_B)t - \frac{d}{6}(c_A - 2c_B) \quad (3.8)$$

From this equation, for $c_B = 0$, the time lag τ_{IL} can be derived being:

$$\tau_{IL} = \frac{d^2}{6D} \quad (3.9)$$

For a monolayered material of known thickness d , the time lag can be determined from the measured transmission rate curve and, from it, the diffusion coefficient D of this material. From the diffusion coefficient and the steady state transmission rate, the sorption coefficient S can be calculated (using Eq. (3.7)). Therefore, both the transient and steady state barrier performance of a monolayer material can directly be evaluated from its permeation measurement.

3.1.4 Transmission rate calculation for homogeneous multilayered encapsulation materials

For a plane material consisting of n different, but in itself homogeneous layers, the analogy to the transport of current through a series of resistances can be used. The layers are assumed to be in full contact with each other, following the theory of the ideal laminate [25], and each layer of the membrane is characterized by its solubility coefficient S_i , its diffusion coefficient D_i and its layer thickness d_i . The overall transmission rate T_{nL} can be calculated as:

$$T_{nL} = \frac{1}{\sum_{i=1}^n \left[\frac{d_i}{D_i S_i} \right]} \quad (3.10)$$

This equation can be used to gain the permeability coefficient P_{organic} of an organic material that cannot be produced as freestanding film. It could be coated on top of a highly permeable polymer film, from which T_{polymer} is known (i.e. was measured before), and with the help of Eq. (3.10) P_{organic} can be derived:

$$P_{\text{organic}} = \frac{d_{\text{organic}}}{\frac{1}{T_{2L}} - \frac{1}{T_{\text{polymer}}}} \quad (3.11)$$

3.1.5 Time lag calculation for homogeneous multilayered encapsulation materials

The time lag of an encapsulation material consisting of two and three homogeneous layers, respectively, was derived independently via two different approaches. Both the first approach, based on the change of gas concentration [119], and the second approach, based on the analogy to the electrical current [18], yielded the same equations for the time lag for two layers (2L) and three layers (3L), respectively:

$$t_{2L} = \frac{1}{\frac{d_1}{S_1 D_1} + \frac{d_2}{S_2 D_2}} \left[\frac{d_1}{S_1 D_1} \left(\frac{d_1^2}{6D_1} + \frac{d_2^2}{2D_2} \right) + \frac{d_2}{S_2 D_2} \left(\frac{d_1^2}{2D_1} + \frac{d_2^2}{6D_2} \right) \right] \quad (3.12)$$

$$t_{3L} = \frac{1}{\frac{d_1}{S_1 D_1} + \frac{d_2}{S_2 D_2} + \frac{d_3}{S_3 D_3}} \left[\frac{d_1}{S_1 D_1} \left(\frac{d_1^2}{6D_1} + \frac{d_2^2}{2D_2} + \frac{d_3^2}{2D_3} \right) + \frac{d_2}{S_2 D_2} \left(\frac{d_1^2}{2D_1} + \frac{d_2^2}{6D_2} + \frac{d_3^2}{2D_3} \right) + \frac{d_3}{S_3 D_3} \left(\frac{d_1^2}{2D_1} + \frac{d_2^2}{2D_2} + \frac{d_3^2}{6D_3} \right) + \frac{d_1 d_2 d_3 S_2}{S_1 S_3 D_1 D_3} \right] \quad (3.13)$$

The second approach, based on the analogy of the gas permeation process to the electrical current [18], has the potential to be extended to many homogeneous layers. However, they were not essential for the main results of this work and are therefore not described here (Appendix B1).

3.1.6 Transmission rate and time lag calculation for inhomogeneous monolayered encapsulation materials

For this work, no inhomogeneous barrier materials other than thin inorganic barrier layers were used - and those are not producible freestanding. Therefore, the case of inhomogeneous monolayered encapsulation materials does not exist for this work and will therefore not be reported here.

3.1.7 Oxygen transmission rate calculation for inhomogeneous multilayered encapsulation materials

Every reasonably good encapsulation material has to contain at least one inorganic barrier layer (Chapter 2). For the development of OE encapsulation material, these thin inorganic barrier layers are deposited from an inorganic source during a vacuum process on top of a flexible polymer substrate which is or is not already precoated. The flexibility of the substrate and its sensitivity to energy absorption during the coating process leads to imperfect growth of the inorganic layer. Hence, all thin inorganic layers deposited under such constraints contain an intrinsic porosity in the form of randomly distributed nano- and microscaled pores and defects, and they cannot be regarded as homogeneous layers.

For the theoretical prediction of gas permeation through stacks containing such inorganic layers, there are three different approaches:

- The easiest model treats the inorganic barrier layers as a homogeneous layer with effective materials properties derived from both the pores and the inorganic bulk. Gas permeation is regarded as occurring through the whole area of the effective material (Fig. 3.4a).
- A second approach models these layers as a combination of a homogeneous inorganic bulk material and simple cylindrical pores that penetrate completely the inorganic layer (Fig. 3.4b). The permeation through the pores occurs without resistance while the inorganic bulk puts different resistance to gas permeation in dependency of the gas type. Water vapor is allowed to permeate through the inorganic bulk, while oxygen is blocked completely. The bulk parts of the inorganic layer are performing a geometrical shadowing of the gas permeation, like a sieve.
- The third approach uses the same concept of a homogeneous inorganic bulk containing cylindrical pores, but assumes a three-dimensional gas permeation which takes into account certain situations where the flux through the pores is much higher than expected from pure geometrical shadowing [120] (Fig. 3.4c).

The first approach is the easiest of the three to model geometrically, because it remains with the one dimensional mathematical description described earlier (chapter 3.1.1). This

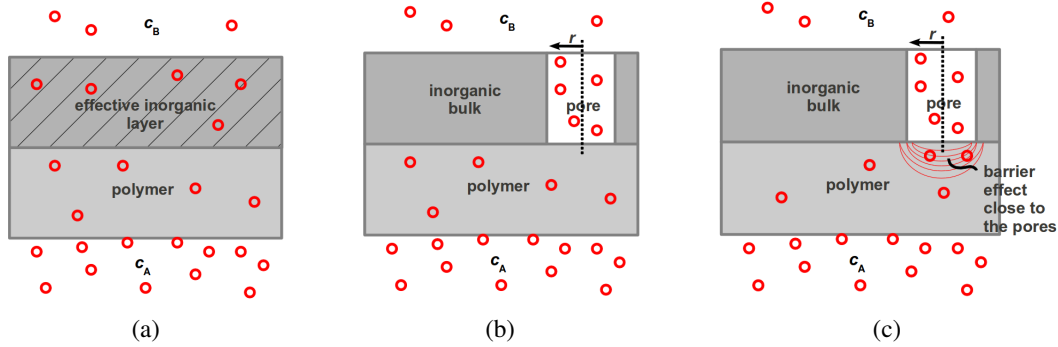


Figure 3.4: Schematics of the three theoretical approaches to gas permeation through multilayered encapsulation materials containing thin inhomogeneous inorganic barrier layers.

reduction of calculation effort could help to compute results, e.g. time lag results, with calculation tools that would be too weak to do so if the two other approaches were used. Yet it has to be kept in mind that the results will have an intrinsic error that increases with increasing number of thin inorganic barrier layers, so that only the tendencies between different samples could be evaluated. For WVTR calculations of better accuracy, the inhomogeneous nature of the permeation through thin inorganic barrier layers can no further be neglected and the second or the third approach have to be used. The second approach can be used when the layer thickness of the organic layers is much smaller than the radius(es) of the pores of the thin inorganic layers [120]. Otherwise, the third approach has to be used [120]. The time lag results still deviate from experimental reality even by using these two approaches, but the steady state WVTR of inhomogeneous multilayered materials can be calculated with such a high accuracy that it could be used for prediction of experimental WVTR results.

For this work thin inorganic barrier layers will be used that are deposited on a polymer substrate by electron beam deposition or by magnetron sputtering. For thin inorganic barrier layers produced by electron beam deposition, defect distributions are typical that correspond to radii in the order of some 100 nm, depending on the thickness of the thin inorganic barrier layer [29, 121]. For the thin inorganic barrier layers of this work, having layer thicknesses of maximum 100 nm, the typical defect size would be 60 to 330 nm [21, 27, 29, 121]. The polymer substrates that are used in this work have thicknesses between 50 to 150 μm . The thin organic intermediate layers of this work have typical layer thicknesses between 1 to 3 μm . Hence, the third approach has to be used for predictions of gas permeation through the multilayered encapsulation material of this work.

According to this model, the transmission rate T through a two layer structure consisting of one organic layer (e.g. the polymer substrate) and one thin inorganic barrier layer can be described with Equ. (3.14), under the condition that the gas can permeate through the pores only [120] (as it is the case for oxygen):

$$T_{\text{organic+inorganic}}^{\text{pores only}} = \frac{D_{\text{organic}}}{d_{\text{organic}}} (c_A - c_B) \pi r^2 n \left(1 + 1.18 \frac{d_{\text{organic}}}{r}\right) \quad (3.14)$$

3 Existing encapsulation concepts

with D_{organic} and d_{organic} being the diffusion coefficient and the thickness of the polymer substrate, c_A and c_B being the concentrations on the two sides of the encapsulation material and r and n being the the radius and the number of the pores, respectively.

The barrier improvement factor ($\text{BIF}^{\text{local}}$) achieved with an inorganic coating on top of an organic layer is quantified in comparison to the uncoated organic layer with respect to a gas that permeates only through the pores, i.e. the barrier improvement is achieved locally, in the close surrounding of the pores:

$$\text{BIF}^{\text{local}} = \frac{T_{\text{organic}}}{T_{\text{organic+inorg}}} = \frac{\text{cm}^2}{\pi r^2 n (1 + 1.18 \frac{d_{\text{organic}}}{r})} \quad (3.15)$$

From Eq. (3.15) it becomes clear that the local barrier improvement factor of a thin inorganic coating is independent of the barrier performance of the adjacent organic layers, i.e. independent of the type of organic materials adjacent to the inorganic layer. Only the layer thickness of the organic material has an influence.

However, the main barrier effect of the thin inorganic barrier layer is created close to its pores, within a distance of approximately 2.5 times the radius of the pore [122]. There, the drop of gas concentration is highest - whereas in distances above this critical adjacent layer thickness the concentration gradient is marginal compared to the areas near the pores. Therefore, none of the organic barrier material that is coated more than the critical adjacent layer thickness, i.e. more than 1 μm for this work, is of any relevance for the barrier performance of the complete layer stack. Hence, for the barrier performance of the encapsulation material towards pores-only-permeating gases, it is of no use to integrate organic intermediate layers thicker than 1 μm .

Furthermore, this phenomenon of the critical adjacent layer thickness enables - under the condition that the organic layer is thicker than 1 μm - to calculate the $\text{BIF}^{\text{local}}$ for the same thin inorganic coating deposited on top of a differently thick organic layer [122]:

$$\text{BIF}_2^{\text{local}} \approx \text{BIF}_1^{\text{local}} \frac{d_1}{d_2} \quad (3.16)$$

with d_1 and d_2 being the different thicknesses of the organic layer.

It is because of Eq. (3.16) that the prediction of the barrier performance of multilayered encapsulation materials containing thin inorganic barrier layers becomes possible. Even when trying to use as few different layer materials as possible, at least two different organic materials are contained: the polymer substrate with at least 50 μm thickness and the organic coating which is much thinner.

For example, the oxygen transmission rate of a three layer (3L) structure consisting of a polymer coated with one thin inorganic barrier layer and one thin organic top coat $T_{3\text{L}}$ can be calculated if the permeation related data of the two layer (2L) structure and the organic material are known (i.e. T_{polymer} , $T_{2\text{L}}$, d_{organic} and P_{organic}) (Fig. 3.5a). By integrating the barrier phenomenon of the pores (in form of the $\text{BIF}^{\text{local}}$) the overall transmission rate $T_{2\text{L},\text{O}_2}$ becomes:

$$T_{2\text{L},\text{O}_2} = \frac{T_{\text{polymer},\text{O}_2}}{\text{BIF}_{\text{O}_2}^{\text{local}}} \quad (3.17)$$

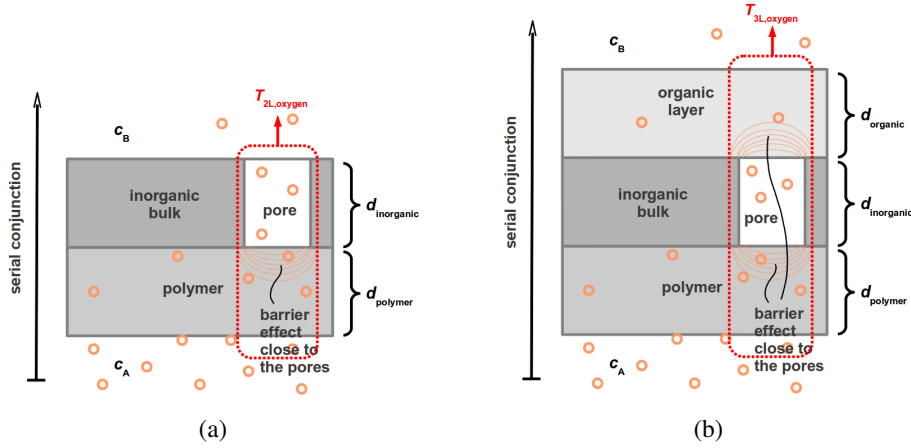


Figure 3.5: Schematics of the cross-sectional view of a two layer structure and three layer structure, respectively, containing one thin inorganic barrier layer with pores.

and so, for known (i.e. measured) $T_{\text{polymer},\text{O}_2}$ and $T_{2\text{L},\text{O}_2}$, the $\text{BIF}_{\text{O}_2}^{\text{local}}$ can be derived.

Using the analogy to electrical current, the oxygen permeation through the three layer structure can be calculated combining the two parts of the oxygen permeation process, i.e. the barrier effects close to the pores at the polymer side and the organically coated side of the pores, via serial conjunction (Fig. 3.5b), including Eq. (3.16):

$$T_{3\text{L},\text{O}_2} = \frac{1}{\text{BIF}_{\text{O}_2}^{\text{local}} \left(\frac{1}{T_{\text{polymer},\text{O}_2}} + \frac{d_{\text{polymer}}}{P_{\text{organic},\text{O}_2}} \right)} \quad (3.18)$$

3.1.8 Water vapor transmission rate calculation for inhomogeneous multilayered encapsulation materials

For water vapor, permeation occurs through the inorganic bulk, too. Therefore, to be able to calculate the water vapor transmission of a three layer structure containing a thin (inhomogeneous) inorganic barrier layer the method reported in the previous chapter was extended by the author. (For the benefit of the reader this mathematical extension is reported here and not in the methodology chapter 4 where it would normally belong.)

Assuming water vapor permeates through the inorganic bulk, two paths of water vapor permeation exist: (1) through the polymer substrate solely and (2) through both the polymer substrate and the inorganic bulk (Fig. 3.6). These two paths cause $T_{\text{organic+inorganic}}$ to be higher than $T_{\text{organic+inorganic}}^{\text{pores only}}$. Therefore, the overall $\text{BIF}_{\text{H}_2\text{O}}$ is smaller than $\text{BIF}_{\text{H}_2\text{O}}^{\text{local}}$.

$$\text{BIF}_{\text{H}_2\text{O}} = \frac{T_{\text{organic},\text{H}_2\text{O}}}{T_{\text{organic+inorganic},\text{H}_2\text{O}}} \ll \text{BIF}_{\text{H}_2\text{O}}^{\text{local}} \quad (3.19)$$

while they are identical for oxygen:

$$\text{BIF}_{\text{O}_2} = \frac{T_{\text{organic},\text{O}_2}}{T_{\text{organic+inorganic},\text{O}_2}} \equiv \text{BIF}_{\text{O}_2}^{\text{local}} \quad (3.20)$$

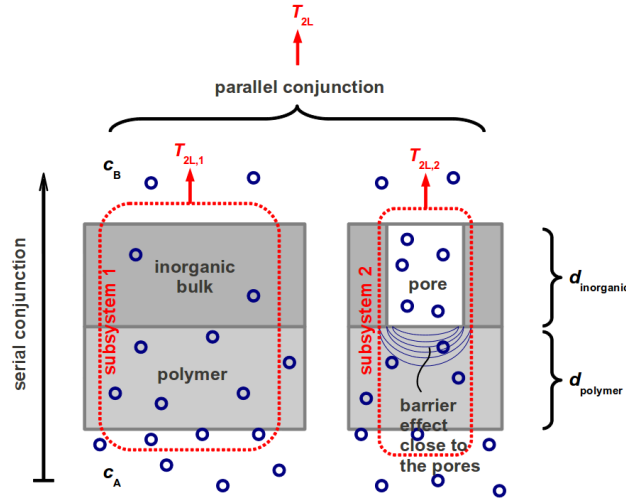


Figure 3.6: Schematic of the cross-sectional view of a two layer structure containing a thin inorganic barrier layer (with pores) on top of a polymer film.

This assumption is supported by the experimentally gained BIF_{O_2} and BIF_{H_2O} : the BIF for oxygen permeation through a thin inorganic barrier layer on top of a polymer substrate is always higher than for water vapor.

The transmission rate of subsystem 1 can be calculated using a serial conjunction of the polymer substrate and the inorganic bulk with respect to the area of subsystem 1:

$$\frac{1}{T_{2L,1,H_2O}} = \frac{1}{(1-\alpha)} \left(\frac{1}{T_{polymer,H_2O}} + \frac{1}{T_{bulk,H_2O}} \right) \quad (3.21)$$

with α being the fraction of the whole area that is covered with pores. For thin inorganic barrier layers of the type that will be used in this work, α is usually below 0.03% [29, 121]. Hence,

$$(1-\alpha) \approx 1 \quad (3.22)$$

The part of the water vapor permeation that is occurring through subsystem 2 is - in analogy to the oxygen permeation through pores - described by:

$$\frac{1}{T_{2L,2,H_2O}} = \frac{T_{polymer,H_2O}}{BIF_{H_2O}^{local}} \quad (3.23)$$

Yet, as opposed to oxygen permeation, $BIF_{H_2O}^{local}$ cannot be experimentally measured independent of the global BIF_{H_2O} . The local BIF of water vapor may be lower than the local BIF of oxygen, because a permeable inorganic bulk adjacent to the pores may lead to lower permeation through the pores themselves. This decrease is not quantifiable, but can be expressed with the help of a parameter k defined as:

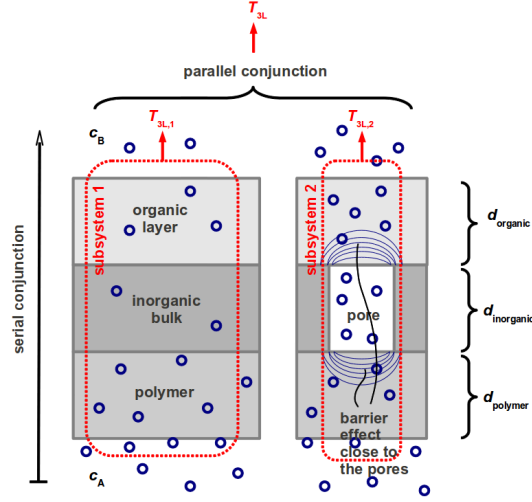


Figure 3.7: Schematic of the cross-sectional view of a three layer structure containing one thin inorganic barrier layer (with pores).

$$\text{BIF}_{\text{H}_2\text{O}}^{\text{local}} = k \text{BIF}_{\text{O}_2}^{\text{local}} \quad (3.24)$$

k is unknown, but can be limited to a small range, which will be demonstrated later. First, the permeation through both subsystems have to be combined with parallel conjunction to get the transmission rate of the two layer system:

$$T_{2\text{L},\text{H}_2\text{O}} = \frac{1}{\frac{1}{T_{\text{polymer},\text{H}_2\text{O}}} + \frac{d_{\text{inorg}}}{P_{\text{bulk},\text{H}_2\text{O}}}} + \frac{T_{\text{polymer},\text{H}_2\text{O}}}{k \text{BIF}_{\text{O}_2}^{\text{local}}} \quad (3.25)$$

which gives for the permeability coefficient of the inorganic bulk:

$$P_{\text{bulk},\text{H}_2\text{O}} = \frac{d_{\text{inorganic}}}{\frac{1}{T_{2\text{L},\text{H}_2\text{O}} - \frac{T_{\text{polymer},\text{H}_2\text{O}}}{k \text{BIF}_{\text{O}_2}^{\text{local}}}} - \frac{1}{T_{\text{polymer},\text{H}_2\text{O}}}} \quad (3.26)$$

Using the same principle of calculation now for the three layer system (Fig. 3.7), together with Eq. (3.16), (3.22), (3.24) and (3.26), the theoretical gas transmission through the three layer structure can be calculated for oxygen:

$$T_{3\text{L},\text{O}_2} = \frac{1}{\text{BIF}_{\text{O}_2}^{\text{local}} \left(\frac{1}{T_{\text{polymer},\text{O}_2}} + \frac{d_{\text{polymer}}}{P_{\text{organic},\text{O}_2}} \right) + \frac{d_{\text{inorganic}}}{\alpha P_{\text{organic},\text{O}_2}}} \quad (3.27)$$

and for water vapor:

$$T_{3\text{L},\text{H}_2\text{O}} = \frac{1}{\frac{1}{T_{2\text{L},\text{H}_2\text{O}} - \frac{T_{\text{polymer},\text{H}_2\text{O}}}{k \text{BIF}_{\text{O}_2}^{\text{local}}}} + \frac{d_{\text{organic}}}{P_{\text{organic},\text{H}_2\text{O}}}} + \frac{1}{k \text{BIF}_{\text{O}_2}^{\text{local}} \left(\frac{1}{T_{\text{polymer},\text{H}_2\text{O}}} + \frac{d_{\text{polymer}}}{P_{\text{organic},\text{H}_2\text{O}}} \right) + \frac{d_{\text{inorganic}}}{\alpha P_{\text{organic},\text{H}_2\text{O}}}} \quad (3.28)$$

In case the pores of the inorganic layer are completely filled with the same organic material as coated on top, Eq. (3.27) and (3.28) have to be applied as they are. For empty (unfilled) pores, the filled pores parts of these two equations have to be omitted, which gives Eq. (3.29) for oxygen and Eq. (3.30) for water vapor:

$$T_{3L,O_2} = \frac{1}{\text{BIF}_{O_2}^{\text{local}} \left(\frac{1}{T_{\text{polymer},O_2}} + \frac{d_{\text{polymer}}}{P_{\text{organic},O_2}} \right)} \quad (3.29)$$

$$T_{3L,H_2O} = \frac{1}{\frac{1}{T_{2L,H_2O} - \frac{T_{\text{polymer},H_2O}}{k \text{BIF}_{O_2}^{\text{local}}}} + \frac{d_{\text{organic}}}{P_{\text{organic},H_2O}}} + \frac{1}{k \text{BIF}_{O_2}^{\text{local}} \left(\frac{1}{T_{\text{polymer},H_2O}} + \frac{d_{\text{polymer}}}{P_{\text{organic},H_2O}} \right)} \quad (3.30)$$

Two constraints help to limit the possible interval of k : both P_{bulk,H_2O} and T_{3L,H_2O} have to be positive and greater than zero. This gives:

$$0 < k < \frac{\text{BIF}_{H_2O}}{\text{BIF}_{O_2}^{\text{local}}} \quad (3.31)$$

For the permeability properties of the materials used in this work, variation of k influences the calculated WVTR and can therefore not be neglected. In calculations using Eq. (3.25) and (3.28) the results will be a range - derived according the range of k .

3.1.9 Time lag calculation for inhomogeneous multilayered encapsulation materials

The time lags of multilayered stacks containing inhomogeneous layers cannot be calculated explicitly, iterative methods have to be used. Solving the diffusion equation by using Finite Elements Analysis (FEA) to gain WVTR data of such structures was demonstrated before ([41]). For this work, this approach is used to gain simultaneously WVTR and time lag data. (The calculation of time lags of inhomogeneous multilayered encapsulation materials by doing FEA of the diffusion equation was not done before and would therefore not belong to the state of the art. However, it will be reported here, for the benefit of the reader.)

The original structure is a stack of thin organic and thin inorganic barrier layers. The thin inorganic layers would show a random combination of bulk parts and pores parts (Fig. 3.8a) and thus lead to a three dimensional flux through the multilayered material (Fig. 3.8b). In order to decrease the calculation effort, the thin inorganic layers were simplified to be homogenous “effective” layers. This leads to a two dimensional model (Fig. 3.8c). The properties of the effective inorganic layers (the effective permeability, sorption and diffusion coefficients) were designed to have the same water vapor transmission and time lag in the two layer structure [organic layer + inorganic layer] as the original two layer structure (with pores) would have had. In doing so, the flux through the multilayered, plane structure becomes translation invariant and can be treated mathematically as a one dimensional system (as already explained in Chapter 3.1.1).

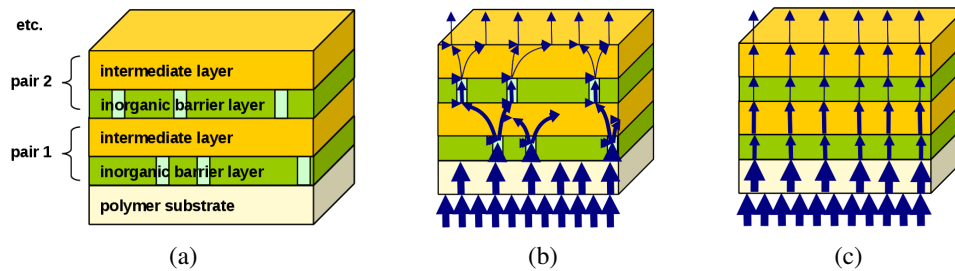


Figure 3.8: Simplification of the FEA based calculations of the WVTR and time lag for a multilayered structure containing both organic and inorganic layers (a) by transforming the three dimensional flux (b) into a quasi one dimensional flux (c).

3.2 Experimental achievements

3.2.1 Existing experimental strategies

The very high barrier requirements, especially against water vapor barrier, can - with one single material - only be fulfilled by using inorganic bulky solid state materials. These materials have a much denser network structure (compared to, for example, organic coating materials) and, therefore, are - with respect to the existing permeation test devices - quasi impermeable to gases. For solid OE applications, glass is in fact used as the front encapsulation material.

For flexible OE applications, too, attempts exist to manufacture glass or stainless steel [12] in such low thicknesses that the materials are roll-to-roll processable (i.e. windable) and flexible to a small extent. However, for the exploitation of the full potential of flexibility, glass and stainless steel are not suitable, since they cannot be produced thinly enough without running into severe problems of mechanical stability leading to frequent breakage during roll-to-roll usage (for thin glass) or are lacking high transparency (for stainless steel).

Therefore, inorganic materials coated by vacuum coating processes became the materials of interest. With these coating processes, very thin layers of solid state materials can be produced. Depending on the type of vacuum coating process, closed inorganic layers of thicknesses down to some nm are possible. Due to such low thicknesses, these inorganic solid state layers are much more flexible, but they are also mechanically unstable and need to be produced on a carrier substrate.

The requirements of optical transparency and mechanical flexibility suggest using transparent polymer films as carrier substrates. Yet polymer films do not provide perfect conditions for the inorganic coating step: the position of the web perpendicular to the coating source is constantly moving (within some tens of nanometers which is small for the polymer film but a lot for the inorganic coating step) and the surface contains artefacts, like anti blocking particles (Fig. 3.9a). Both reasons trigger defect growth in the thin inorganic layer (Fig. 3.9, 3.10) (which is already assumed or known since 1971 [123]).

The largest pores or defects of transparent layers are visible in reflected-light mi-

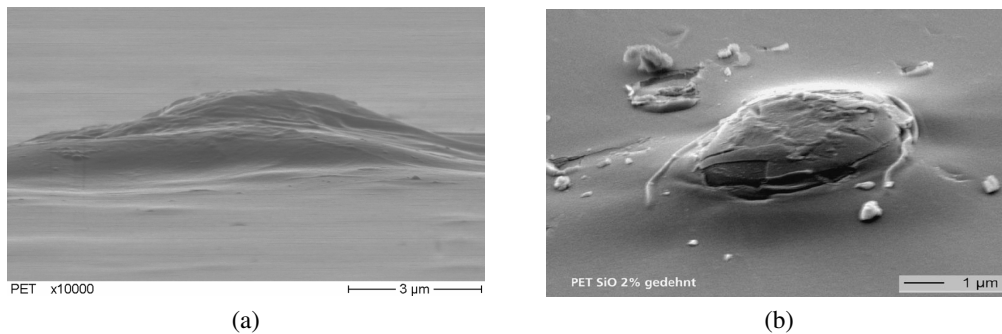


Figure 3.9: Scanning electron microscope (SEM) images of an anti-blocking particle that is integrated in a polymer film before (a) and after (b) the coating of the polymer film with a thin inorganic barrier layer [19, 20]. The thin inorganic barrier layer breaks at the periphery of the anti-blocking particle as a result from peak stress, to be seen in Fig.(b).

scopy when using differential interference contrast mode (Fig. 3.10a). Their size goes up to 15 μm in diameter, but they are not the ones most important for water vapor transmission, as there are usually only a few of them within the thin inorganic barrier layers and because they can be avoided by improving the technological process, e.g. reducing the number of dust particles in the deposition chamber [27] or improving the pre-treatment procedures [28]. The pores or defects of medium size of a thin transparent layer can be made detectable by using light microscopy in combination with an undercutting¹ preparation (Fig. 3.10b). They have a mean diameter of 1.2 μm (ranging from 0.2 to 2.8 μm) [21, 23, 28]. The most important pores for water vapor permeation, the smallest (nanoscale) ones, cannot be quantified [27], neither in size nor in number, but they are assumed to exist, because they can be seen qualitatively in SEM images (Fig. 3.10c). Because of these defects, thin inorganic barrier layers on top of polymer substrates are not as (nearly) impermeable as their bulky equivalent. Still, their intrinsic barrier properties are orders of magnitude better than that of any organic barrier material (Fig. 3.11). Hence, its the thin inorganic barrier layers that have to be improved and piled up on top of a polymer substrate in order to achieve the gas barrier targets.

One parameter that is known to influence the barrier quality of a thin inorganic layer is its layer thickness [22, 23, 24, 25, 26, 27, 21, 28, 29]. Figure 3.12 summarizes various WVTR and OTR of polyester substrates that were coated with thin inorganic barrier layers by various processes and in various layer thicknesses. Figure 3.13 gives the same kind of overview for inert gases. To be able to compare all data, they are displayed in the units of $[\text{mol}/(\text{m}^2 \text{ s Pa})]$. Additionally, the corresponding transmission rates of a 12 μm PET film (which was the polyester film of lowest thickness that was coated) are marked with a dotted line in both figures.

¹Undercutting is a technique that uses reactive ion etching in low pressure oxygen plasma to enlarge microscale pores so that they would become visible for light microscopy. During the preparation, atomic oxygen passes through defects in the thin inorganic barrier layer and destroys the polymer underneath. The radius of the spot of destroyed polymer around the defect grows as a function of the exposure time. Therefore, the original pore radius can be calculated from the final radius after the preparation and the exposure time [21].

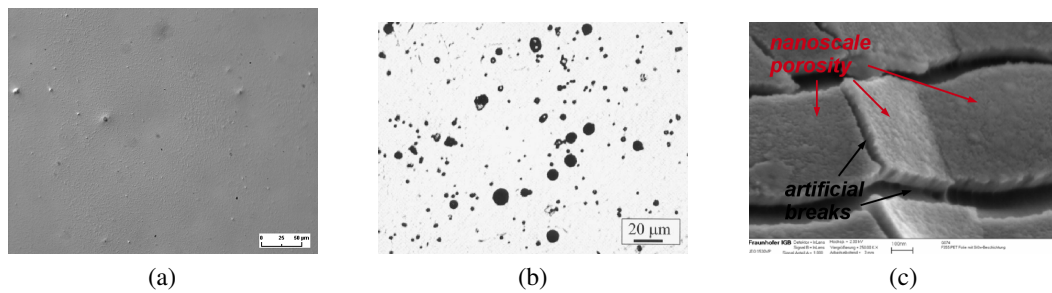


Figure 3.10: Pictures of pores of all sizes as they exist in thin transparent inorganic barrier layers taken by (a) light microscopy, (b) light microscopy after undercutting (i.e. the pore sizes are greatly increased now) and (c) scanning electron microscopy. Figures (a) and (c) are the result from samples that were prepared by the author, but measured at *Fraunhofer FEP* and *Fraunhofer IGB*, respectively, while figure (b) is taken from literature [21].

From the diagrams, it can be seen that - despite individual fluctuations between the individual measurement series - all transmission rates decrease with increasing layer thickness. The greatest reduction of the transmission rates happens during the first 50 nm which can be seen in the fact that there is a linear correlation in both double logarithmic diagrams. One explanation could be the inhomogeneous growth of the thin inorganic barrier layers. This could result in layers that are not perfectly closed at low layer thicknesses. According to Fig. 3.12 and 3.13, the thickness of approximately 50 nm could be the range where the thin inorganic barrier layers are becoming progressively closed and should therefore be applied as minimum thickness.

Above 100 nm, there are clear differences between the individual measurement series: some level out at the optimum transmission rate while in others the transmission rates decrease further or even increase again. In general, the more inorganic material is deposited the better the layer gets closed and the transmission rates should get lower and lower. Yet the thicker an inorganic coating gets, the more brittle it becomes and the higher the risks of cracks resulting in increased transmission rates. It depends on the individual flexibility of the inorganic layer at which layer thickness these defects starts to influence the barrier performance.

Furthermore, the diagrams show a different permeation behavior of water vapor and helium compared to oxygen, neon and argon: the reduction of the transmission by a thin inorganic barrier layer compared to the original substrate is much less pronounced for water vapor and helium than for oxygen, neon and argon. This indicates that helium permeates through both pores and inorganic bulk, like water vapor, while neon and argon permeate through the pores only, like oxygen.

Therefore, to improve the barrier performance of a thin inorganic layer against water vapor, it is necessary to both improve bulk and reduce the porosity. However, to just use thin inorganic barrier layers and coat subsequently one inorganic barrier layer on top of the previous one would - even for thickness optimized thin inorganic layers - not lead to the encapsulation material of high water vapor barrier. This is not possible for two reasons: first, each layer would copy the quality of the previous one, i.e. existing defective areas would be continued due to mechanisms like shadowing, island growth etc.

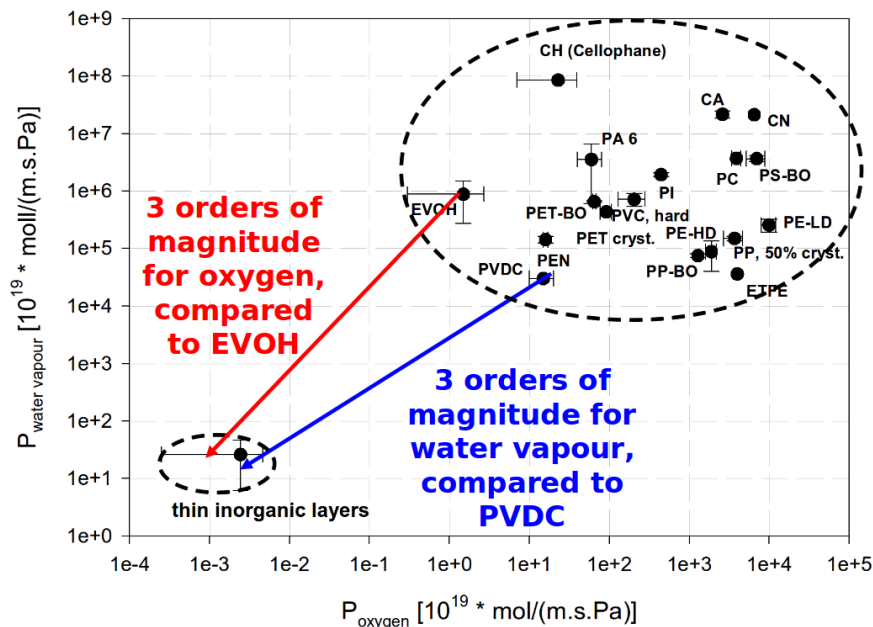


Figure 3.11: Intrinsic (effective) permeability coefficients of thin transparent inorganic barrier layers (as an average over literature data [22, 23, 24, 25, 26, 27, 21, 28, 29]) in comparison to the permeability coefficients of transparent organic barrier materials (own measurements, for details see Fig. 5.1).

[124, 125, 126]. Second, the flexibility resulting from the small thickness of the inorganic layers, would be lost.

For this reason, intermediate more flexible layers have to be coated inbetween. This could be either organic layers [127, 128, 129, 38], hybrid layers [14] or highly flexible (but also more permeable) inorganic layers [39]. Intermediate layers that can be vacuum deposited would - for roll-to-roll processing - have the advantage that all layers could be produced in the same machine. Intermediate layers that need a different coating process would still be advantageous if the additional coating step is a very low cost one (compared to the vacuum deposition process) and could reduce the number of necessary inorganic barrier layers [14].

Another approach is to renounce completely from intermediate layers and instead improve the one inorganic barrier layer to such an extent that one layer itself could fulfill the gas barrier requirements. This single layer approach has the advantage of no negative interaction between several barrier layers and less parameters have to be controlled on the way towards very high gas barrier.

Both approaches, either single layer or multilayer, can be applied to three main strategies: “thin film encapsulation”, sheet encapsulation and encapsulation with roll-to-roll material. The first strategy aims to deposit the barrier layer(s) directly on top of the OE device layers, while the two others produce a stand-alone encapsulation material that is later wrapped around the OE device. Thin film encapsulation has the advantage of covering the OE device three-dimensionally, while the two other strategies could provide constant substrate conditions to the deposition of the barrier layers (and therefore achieve device-independent barrier performances) and protect the sensitive barrier layers under

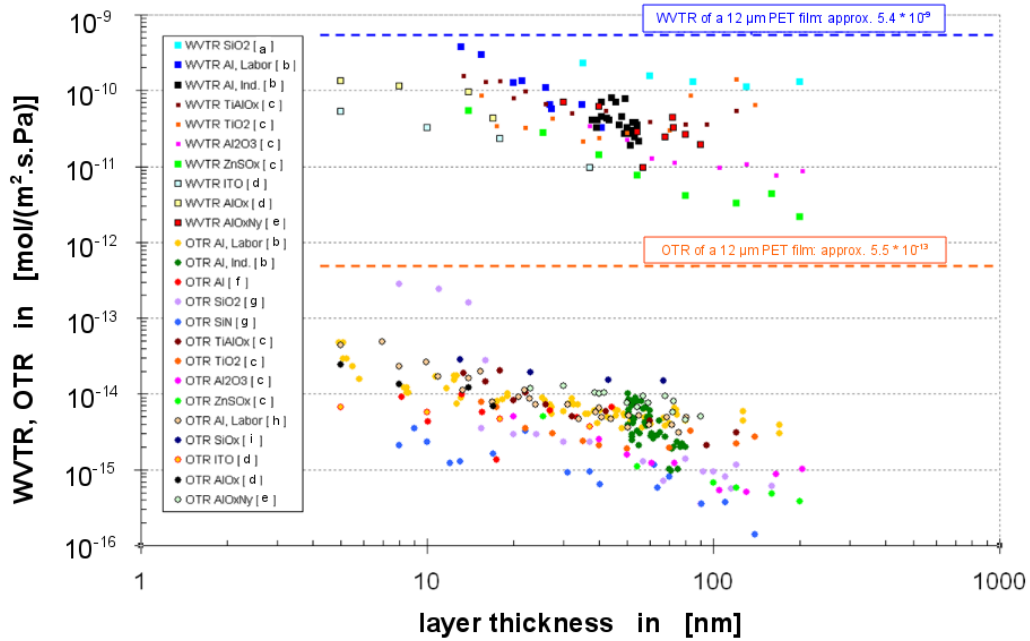


Figure 3.12: WVTR and OTR of polyester films coated with thin inorganic barrier layers, as a function of the thickness of the thin inorganic barrier layer. The WVTRs and OTRs of the $12 \mu\text{m}$ PET film were measured by the author, all other data are from literature ((a,...,i) being [22, 23, 24, 25, 26, 27, 21, 28, 29]).

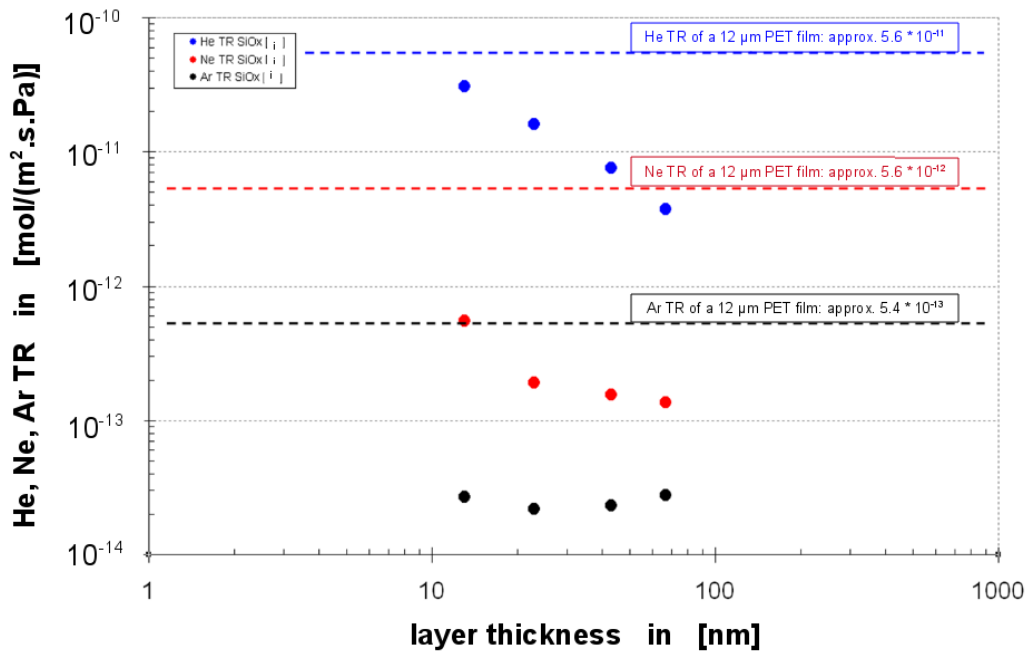


Figure 3.13: Transmission rates for Helium, Neon and Argon of polyester films coated with thin inorganic barrier layers, as a function of the thickness of the thin inorganic barrier layer. All results from literature ((i) being [29]).

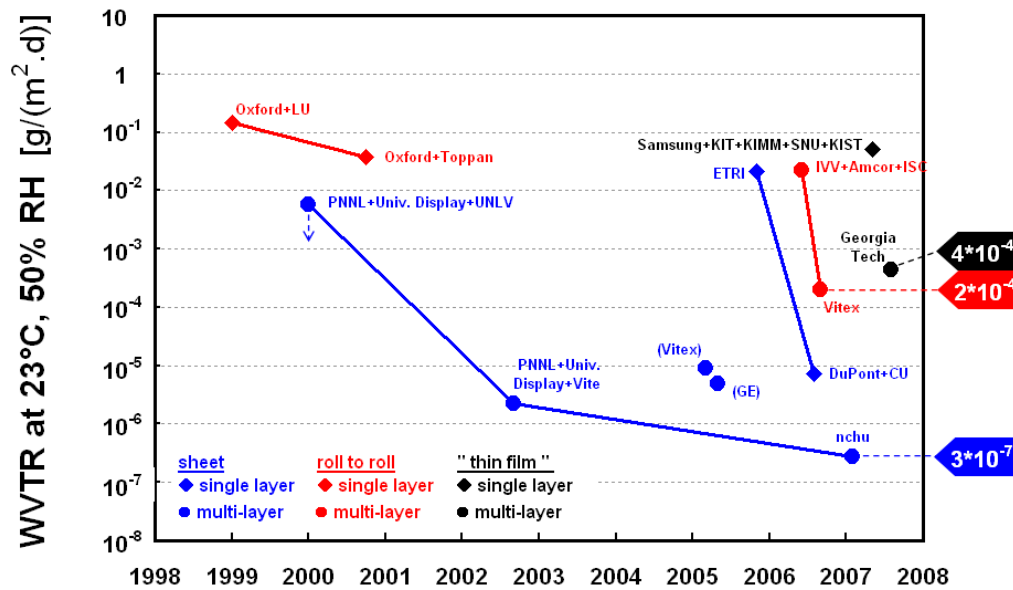


Figure 3.14: Best reported WVTR over time for each encapsulation strategy until mid 2008 [26, 25, 14, 30, 31, 32, 33, 34, 35, 36, 37, 38, 39]. (Some WVTR results are included in this diagram despite the fact that they were no improvement over previous achievements, because they belong to important research groups in the research field of OE encapsulation.)

a protective top coat before coming into contact with further handling procedures. The sheet encapsulation strategy is in fact not an independent approach, but a first step of the respective research group towards roll-to-roll produced encapsulation materials.

In total - still counting the sheet strategies individually - six strategies exist. Their best reported WVTR are displayed in Fig. 3.14 - except for the thin film encapsulation strategy. Even though work was done in this field much earlier, WVTR data for thin film encapsulation only appear in this diagram starting in 2007. The reason is that the barrier performance of thin film encapsulation is mostly evaluated indirectly, by studying the performance of the respective encapsulated OE device - scarcely by permeation tests on the pure barrier layer(s) alone (where a WVTR value would be gained).

From this diagram, it becomes obvious that the barrier performances achieved on top of single sheets of polymer film have already progressed very much. The lowest achieved WVTR of $3 \times 10^{-7} \text{ g}/(\text{m}^2 \text{ d})$ would largely fulfill the barrier requirements. Yet to upscale these achievements to a continuous roll-to-roll production is a great technological challenge. At the beginning of this work, only the company *Vitex* had succeeded in the development of roll-to-roll encapsulation material better than $10^{-2} \text{ g}/(\text{m}^2 \text{ d})$ - and only with a trick: the web was very short and as such in fact a large sheet [38].

3.2.2 Potential high barrier effects I: Known from experiments

At the beginning of this work, there were two experimentally known barrier effects that were supposed to supply high barrier performance to an encapsulation material if integrated wisely: the synergistic barrier effect [40] and the time lag effect [41].

Synergistic barrier effect

When coating a thin inorganic barrier layer with a thin organic top coat, the improvement of the barrier performance of the three layer structure [polymer + thin inorganic barrier layer + organic top coat] should not be very impressive compared to the barrier performance of the original two layer structure, because the barrier performance of the inorganic layer should dominate the overall barrier performance.

Yet it was found that the transmission rates of the three-layer-structure is reduced significantly, compared to the expected transmission rates of the three-layer-structure (calculated from the known permeability coefficients of each of the layers); especially for oxygen transmission [40]. Even though the effect could not be explained, it occurred repeatedly, with an improvement factor of over 400 (Fig. 3.15). Hence, this effect will be studied during this work with respect to its usefulness for the development of OE encapsulation materials.

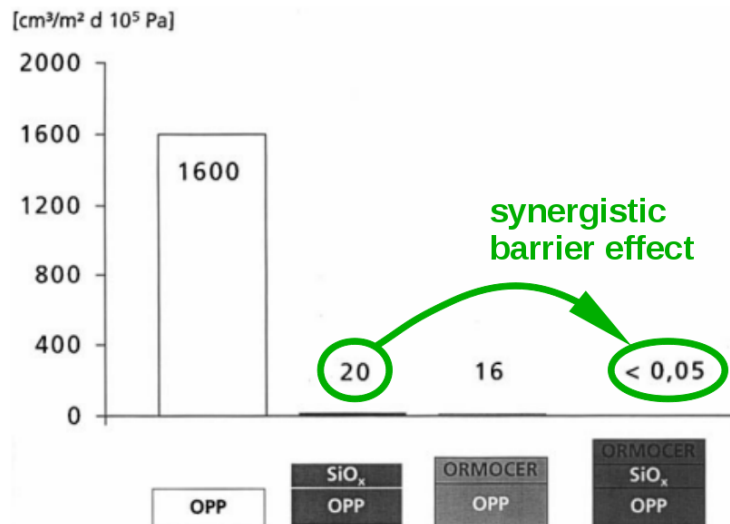


Figure 3.15: The synergistic barrier effect as found first in 1998 (figure taken from [40] and modified).

Time lag effect

For the creation of an OE encapsulation material that contains many barrier layers, the following approach is used very often: first, a polymer film is used as mechanical substrate, then a thin inorganic barrier layer is coated on top and protected by a thin organic top coat. The pair of one thin inorganic barrier and one thin organic barrier layer is called a “dyad”. As the thin organic barrier layer can also act as a mechanical decoupling of the thin inorganic barrier layers (see Chapter 3.2), the easiest way is now to repeat coating dyads. The materials produced with the greatest number of dyads so far reported comprise five or six of them.

For these multi-dyad materials, it was found that the reported transmission rates were much smaller than what was expected from the first dyad [41]. This effect was mathe-

matically explained by the extreme increase of the instationary period of the permeation process: the reported transmission rates were, in fact, no “final data“, but transmission rates derived somewhere in the instationary period. This can happen when the increase of the transmission rate takes so much time that it looks to the operator as if the system was in equilibrium.

As the instationary period is described quantitatively by the time lag (see Chapter 3.1), the time lag would increase the longer the instationary period is. As an example, it was found by FEA based calculations based on experimental data that the time lag of a structure whose dyads are based on thin AlO_x and acrylate layers increases from 22 hours to approximately 1.5 years when the number of dyads is increased from one to five (Fig. 3.16). Since the increase of the instationary period of the permeation process is one possible option for the development of OE encapsulation material (see Chapter 2.1), this effect will be studied during this work.

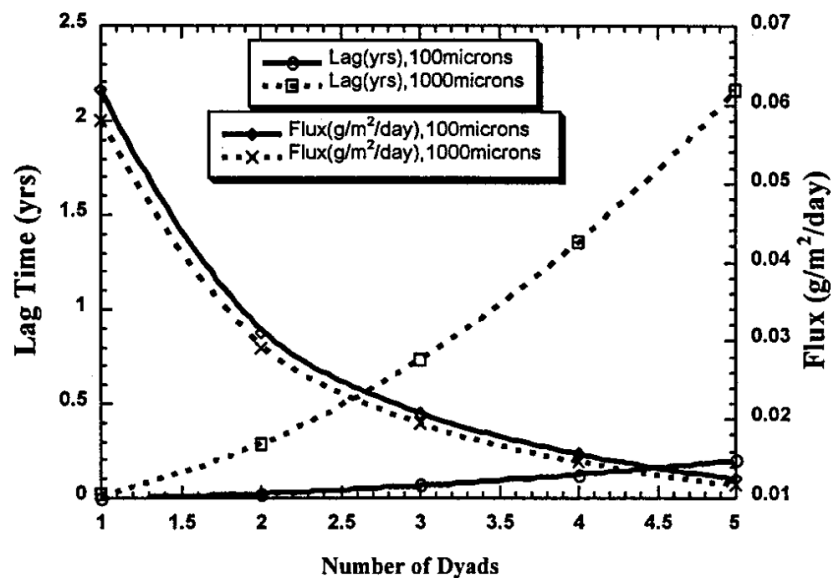


Figure 3.16: The lag time effect as described in 2004 (figure taken from [41]).

3.2.3 Potential high barrier effects II: Predicted theoretically

Additionally, two further barrier effects - even though they were not experimentally tested so far - were predicted by theoretical calculations to be of great use for the development of encapsulation material: the filled pores effect [42] and the tortuous path effect [28, 42].

Filled pores effect

The organic coating material applied on top of a thin inorganic barrier layer might be able - due to appropriate chemical match and low viscosity - to penetrate into the pores of the inorganic layer and not just stay on the surface. The question to which extent this influences the overall barrier performance of the two layer structure [polymer substrate + thin inorganic barrier layer + organic top coat] lead to theoretical FEA based calculations

in 2008. It was found that the complete filling of the pores of a typical thin inorganic barrier layer could lead to an improvement of the overall barrier performance of up to a factor of two (Fig. 3.17). Even though this is only a small potential barrier effect, it was taken into account during this work.

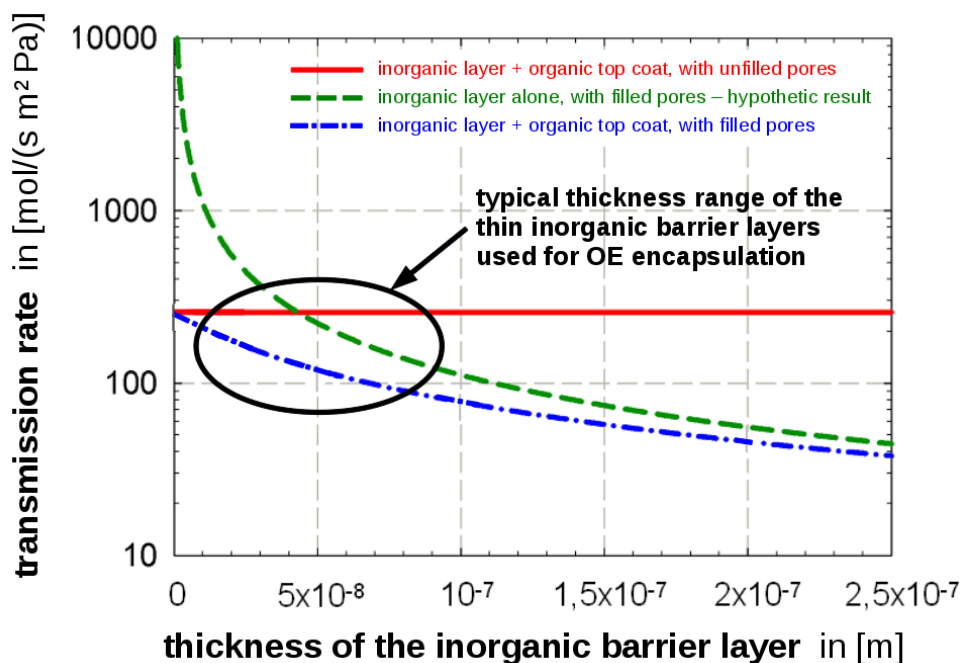


Figure 3.17: The filled pores effect as reported in 2008 (figure taken from [42] and modified).

Tortuous path effect

The so-called “tortuous path effect” describes the over-proportional barrier improvement that occurs when reducing (mathematically) the thickness of an intermediate organic layer that is enclosed between two thin inorganic barrier layers. This effect results when modelling the two thin inorganic barrier layers as two homogeneous layers with cylindrical pores that penetrate completely through the entire layer and that are equally distributed over the area - and assuming the two layers shifted relative to each other in such a way that the pores would be situated at maximum distance (Fig. 3.18). Thus, the oxygen molecules - that are assumed to not to be able to permeate through the bulk² but through the pores² only - have to follow a tortuous path: they have to pass vertically through one pore, then horizontally through the organic layer and finally vertically through the next pore of the second inorganic layer (Fig. 3.18).

²During this work, the terms “inorganic bulk” and “pores” will be used to distinguish between the parts of the thin inorganic barrier layer that are not / are permeable for gases like oxygen, argon or nitrogen. This way, the inorganic bulk is not free of pores (it should not be imagined like a solid, intact piece of metal or metal oxide), just its porosity is of much smaller scale than the size of the larger “pores”.

3 Existing encapsulation concepts

The resulting tortuous path would be much longer than the one directly perpendicular through all layers - which would decelerate and as such reduce the permeation of oxygen through such a “sandwich structure”³.

In 2003, the reduction of the oxygen transmission rates by the tortuous path effect was calculated to be exponential and to be able to reduce the oxygen permeation through such a sandwich structure by several orders of magnitude (Fig. 3.19) [28].

In 2008, these calculations were revised [42]. They had been repeated and it was found that the calculations of 2003 must have been stopped too early, i.e. at a non-stationary state of calculation, which adds a great error to the transmission data. When waiting until the stationary state of calculation (even though this takes extremely long) fewer reduced oxygen transmission data are derived: the improvement factor was now predicted to be at maximum 15 (Fig. 3.20) instead of several orders of magnitude as believed before.

Still, even to this extent, this is a barrier effect worth to be included in a multilayered encapsulation material and will therefore be studied during this work.

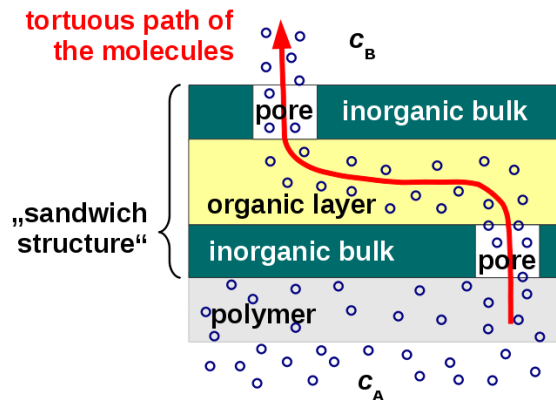


Figure 3.18: The theory of how the permeation of the oxygen molecules happens along a tortuous path through the three-layer-structure (scheme).

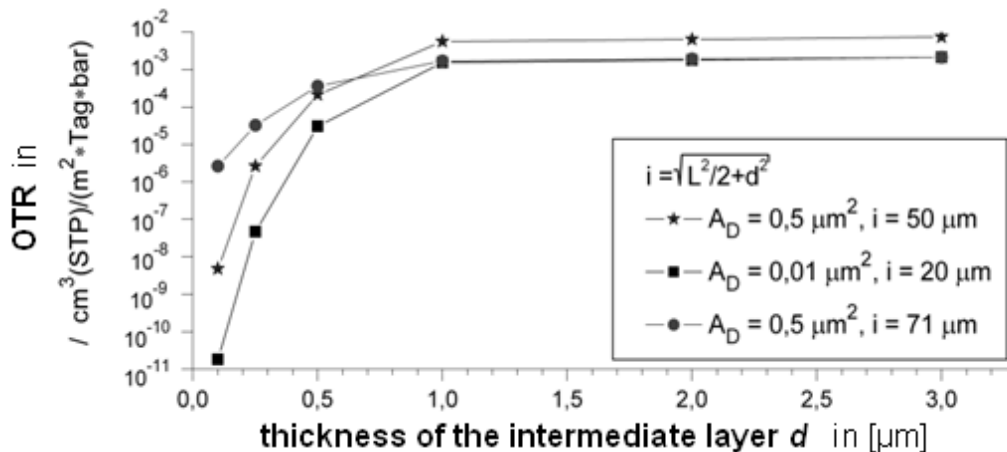


Figure 3.19: The tortuous path effect as predicted originally (in 2003) (figure taken from [28]).

³The idea of tortuous permeation mechanisms was introduced already 1967 for particle filled polymers [130].

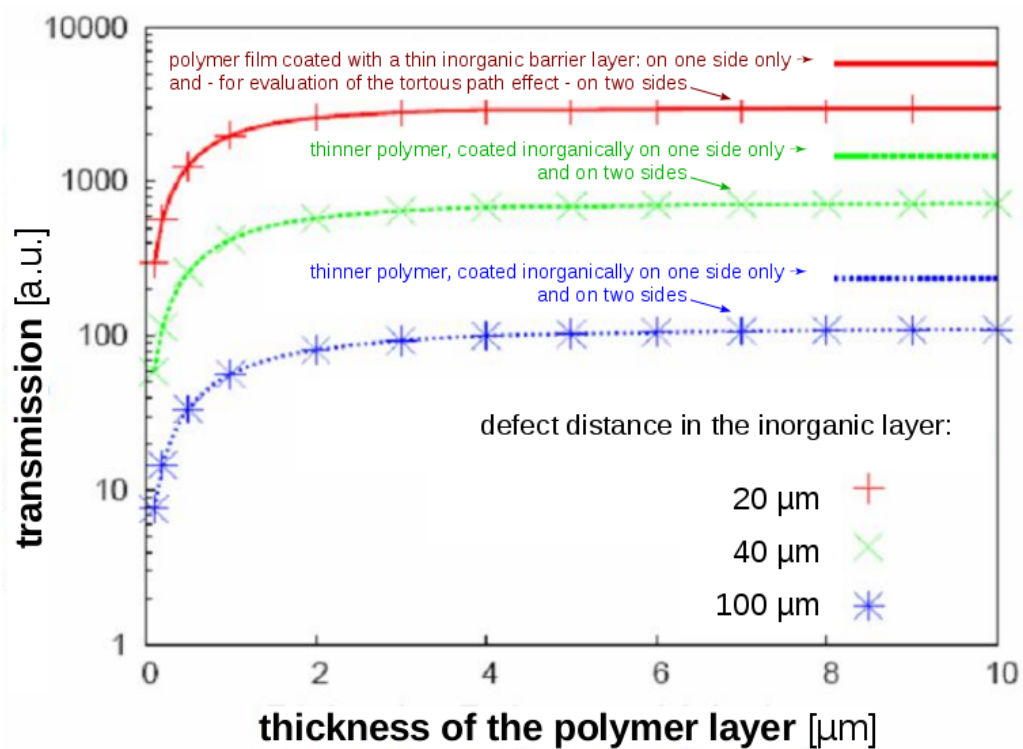


Figure 3.20: The tortuous path effect at the beginning of this work (in 2008) (figure taken from [42] and modified).

4 Experimental methodology

The focus of this work was the evaluation of water vapor permeation through encapsulation materials. Therefore a range of encapsulation materials was prepared by the author, using the materials and the coating techniques summarized in sections 4.1 and 4.2.

The encapsulation materials and the single layers were analyzed not only by means of permeability measurement techniques, but many additional evaluation methods. Why these evaluations were necessary and a description of the corresponding evaluation methods will be given in section 4.3.

Additionally, experimental methods that were developed by the author during this work are described in section 4.4.

4.1 Materials

All materials used for this work are listed in Tables 4.1 to 4.5.

Table 4.1: Organic materials: Adhesives.

code ^a	grade	supplier
A3.1	JG 08.08	tesa
A5.1	Rengolux DVD 3203-094	Mäder
A5.2	DVD XD 4861	Huntsman
A5.3	KATIOBOND LP VE 18190	DELO Industrie Klebstoffe
A5.4	KATIOBOND LP 655	DELO Industrie Klebstoffe
A5.5	KATIOBOND LP VE 19781	DELO Industrie Klebstoffe
A5.6	KATIOBOND LP VE 19405	DELO Industrie Klebstoffe
A5.7	KATIOBOND LP VE 19418	DELO Industrie Klebstoffe
A5.8	PHOTOBOND LP VE 512600	DELO Industrie Klebstoffe
A5.9	PHOTOBOND LP VE 512057	DELO Industrie Klebstoffe
A5.10	PHOTOBOND LP VE 512642	DELO Industrie Klebstoffe
A6.1	Herberts EPS 74-1 / 7711	Bostik
A6.2	Liofol UK 3640 / UK 6800	Henkel

^aMissing consecutive code numbers result from adhesives that were tested but could not - with the technological possibilities at hand - be brought to optimized coating qualities suitable for barrier evaluation.

Table 4.2: Organic materials: Coatings.

code ^a	grade	supplier
C1.1	VaporCoat [®] 2200	Michelman
C1.2	Terraflex-F Barrierelack G 11/128 MVTR	Actega Terralacke
C1.3	Genius Pro Metall Klarlack	J.W.Ostendorf
C1.4	Genius Pro 2 in 1 Klarlack	J.W.Ostendorf
C1.5	Yachtlack	Clou
C1.6	2 in 1 Klarlack	Alpina
C1.7	Genius Pro Treppen- und Parkettversiegelung	J.W.Ostendorf
C1.8	Fußbodenlack	PNZ
C1.9	SolVin Diofan [®] A736/193D	Solvay SolVin
C1.12	oxidized, hydroxypropylated (OHP) potato starch, original	Lyckeby
C1.13	hydroxypropylated (HP starch), optimized	Emsland
C1.14	G-Polymer	Nichigo
C1.15	Mowiol 4-98	Kuraray
C1.16	Aquasil	Paramelt
C2.2	Lack B	Landshuter Lackfabrik
C2.3	Lack C	Landshuter Lackfabrik
C3.1	PE-LD extrusion coat	Borouge
C3.2	PP extrusion coat	Borouge
C3.5	Ecoflex 7011	BASF
C3.6	PLA HM 2	Hycail
C3.7	Bioflex 219	FKuR
C3.8	Mater Bi	Novamont
C5.1	UV-Lack farblos glänzend Lab.-Nr. 01-130	Dreisol
C5.2	industrial grade 75-711	Mankiewicz
C5.3	Ormocer [®] 01	Fraunhofer ISC
C5.4	Ormocer [®] 04	Fraunhofer ISC
C5.5	Ormocer [®] 04a	Fraunhofer ISC
C5.6	Ormocer [®] 08	Fraunhofer ISC
C5.7	development grade 1	Mankiewicz
C5.8	development grade 2	Mankiewicz
C5.9	Ormocer [®] 09	Fraunhofer ISC
C5.10	EK-PUR Reaktionsgrund UV PD-000090-UV	Dr.Conrads Lacke
C6.1	EPO Klarlack glänzend 2:1 ED-000090-PG mit WE-7500-PG	Dr.Conrads Lacke
C6.2	Bucopur Anti-Graffiti	Bucolin
C6.3	2K-PUR Decklack	Dr.Conrads Lacke
C6.4	Bucopur Lack	Bucolin

^aMissing consecutive code numbers result from organic coating materials that were tested but could not - with the technological possibilities at hand - be brought to optimized coating qualities suitable for barrier evaluation.

Table 4.3: Inorganic materials.

inorganic material	process	supplier
SiO _x	electron beam	Alcan, later AMCOR
AlO _x	electron beam	Applied Materials
AlO _x	magnetron sputtering	Fraunhofer FEP
AlO _x	ALD	MPI Halle
ZnSn _x O _y	magnetron sputtering	Fraunhofer FEP

Table 4.4: Polymer films (part 1).

polymer	film grade	film thickness [μm]	supplier
ECTFE	Aclar Flex 380	38	Honeywell
ETFE	Nowoflon ET 6235	100	Nowofol
	Hiproloco grade	150	Nowofol
	Nowoflon ET 6235	200	Nowofol
FEP	FEP 6307	1000	3M Dyneon Fluoropolymers
	Teflon 500 C	130	DuPont Teijin Films
	Teflon 500 LZ	130	DuPont Teijin Films
PA	PA 6	15	Wipak Walsrode
PC	Macrofol	250	Bayer Material Science
PCTFE	Aclar UltRx 4000	102	Honeywell
	P 8000 TR	200	Honeywell
PE-LD	PE-LD	30	defa-folien
	PE-LD	70	defa-folien
PET	Melinex 813	12	Petroplast
	RHB Y	12	Mitsubishi Polyester Film
	Melinex 807	12	DuPont Teijin Films
	RNK	12	Mitsubishi Polyester Film
	Mylar PT03-01600	36	DuPont Teijin Films
	Mylar A	50	DuPont Teijin Films
	Melinex 401	50	DuPont Teijin Films
	Melinex 400 CW (\approx M 401 ^a)	50	DuPont Teijin Films
	Melinex 400 CW (\approx M 401) ^a	75	DuPont Teijin Films
	Melinex ST 504	125	DuPont Teijin Films
	Melinex ST 506	125	DuPont Teijin Films
	Melinex ST 504 7ML	175	DuPont Teijin Films
	RD O	50	Mitsubishi Polyester Film
	GN 4600	50	Mitsubishi Polyester Film
	Hostaphan RN	50	Mitsubishi Polyester Film

^aMelinex 400 CW and Melinex 401 are the same materials with same surfaces with just one difference not relevant for this work: the edges of Melinex 401 are creased while the edges of Melinex CW 400 are not.

Table 4.5: Polymer films (part 2), other substrates.

polymer	film grade	film thickness [μm]	supplier
PEN	Teonex Q 51	38	DuPont Teijin Films
	Teonex Q 51	75	DuPont Teijin Films
	Teonex Q 51	85	DuPont Teijin Films
	Teonex Q 65 FA	125	DuPont Teijin Films
	Kaladex S1020	125	DuPont Teijin Films
PLA	Bio-Flex [®]	25	FKuR
PP-BO	BOPP	20	Sigdopack
PP-c	PP-c	30	Fraunhofer IVV
PVC	PVC	200	Pütz
THV	THV 500	80	3M Dyneon Fluoropolymers
	THV 815 G	100	3M Dyneon Fluoropolymers
board	Performa Natura 255	350	Stora Enso
paper	UPM Unique 60	50	Walki Wisa
	Gerbier HDS	55	Ahlström

4.2 Coating techniques

In total ten techniques were used to prepare the barrier layers of the encapsulation materials of this work (Table 4.6).

Table 4.6: Overview of coating methods and coating related methods.

purpose	technique	process type	scale of production
pre-treatment	plasma pre-treatment	roll-to-roll	pilot
	corona pre-treatment	roll-to-roll	pilot
inorganic coating	electron beam deposition	roll-to-roll	pilot + industrial
	magnetron sputtering	roll-to-roll	pilot
	atomic layer deposition	batch	pilot
organic coating	reverse gravure coating	roll-to-roll	pilot
	rod coating	batch	lab (bench)
lamination	reverse gravure lamination	roll-to-roll	pilot
	rod lamination	batch	lab (bench)

Plasma pre-treatment was done by the author using a Leybold machine of type “Labor-Bandbeschichtungsanlage A 120 B1 EB / A 260 E1 EB“. This electron beam coating machine is an individual fabrication of *Leybold AG - Werk Alzenau* for *Fraunhofer IVV* for the roll-to-roll coating of small and short webs (maximum length ~ 200 m, maximum web width of 200 mm). Additionally, it can be switched from the default electron beam coating mode to the plasma pre-treatment. Plasma pre-treatment was done with Argon (plasma ignition with 2.8 kW micro wave power, working power at ~ 2 kW) at a vacuum level of $< 5 \cdot 10^{-5}$. During the pre-treatment, the drum transporting the web

close to the magnetron was kept at $-15\text{ }^{\circ}\text{C}$ so that the polymer film is cooled from the rear side. For this work, plasma pre-treatment was used to enable or enhance the adhesion of thin barrier layers on top of a polymer substrate or on top of the previous barrier layer. Yet, compared to corona pre-treatment, it was used less often due to its much more time consuming handling effort.

Corona pre-treatment was done using a SOFTAL 7015 of *SOFTAL electronic Erik Blumenfeld GmbH & Co. KG*. This commercial type of corona station is integrated in the pilot wet chemical coating machine of *Fraunhofer IVV*. The power of the corona station can be adjusted in steps of 1 W from zero to 1500 W. For this work, corona pre-treatment was done on the majority of the films to enable or enhance the adhesion of thin barrier layers on top of a polymer substrate or on top of the previous barrier layer. In all cases, a power of 300 W at a web speed of 3 m/min was applied. (The rear part of the coating machine contains a second corona station of *TIGRES Dr. Gerstenberg GmbH* for the potential pre-treatment of the second polymer film during lamination trials - yet, the lamination trials of this work did not require to use it.)

Electron beam deposition of thin SiO_x barrier layers in roll-to-roll was done by *Alcan Packaging Services AG*, later *Amtor Flexibles*, at Neuhausen, Switzerland.

All initial SiO_x coated polyester films were fabricated using the Ceramis[®] industrial line with a web speed of approximately 300 m/min and a web width of 4 m. Deposited thickness is for all samples 100 ± 10 nm. To be able to handle the material at the machines of *Fraunhofer IVV*, the rolls were always afterwards cut down to a web width of 400 mm. The deposition of SiO_x barrier layers on top of all materials of web widths smaller than 4 m, i.e. on all rolls fabricated at *Fraunhofer IVV*, was done using the Ceramis[®] pilot line of *Alcan Packaging Services AG* (both working with the same principle, to be seen in Fig. 4.1).

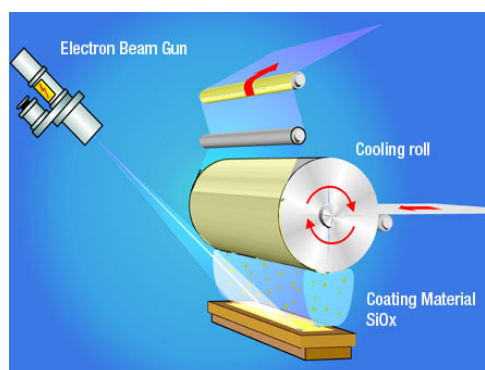


Figure 4.1: Schematic of the principle of the electron beam deposition process at *Alcan Packaging Services AG* (figure taken from [43]).

Magnetron sputtering of thin AlO_x or ZnSn_xO_y barrier layers in roll-to-roll was done either by *Applied Materials Inc.* in Alzenau, Germany, or by *Fraunhofer FEP* in Dresden, Germany. The AlO_x barrier layers used for Chapter 7 were fabricated on the Smartweb[®] coating machine of *Applied Materials Inc.* at a web speed of approximately 0.6 m/min and a web width of 400 mm. Deposited thickness was 40 ± 5 nm. The AlO_x barrier layers used for Chapter 5 and the ZnSn_xO_y barrier layers used for Chapters 5,6 and 7 were fabricated on the CoFlex[®]600 coating machine of *Fraunhofer FEP* with a web speed of approximately 0.5 m/min and an effective web width of 200 mm. Deposited thicknesses were 67 ± 5 nm and 200 ± 10 nm, respectively. For this work, all magnetron sputtered barrier layers were fabricated using cylindrical material sources.

Reverse gravure roll-to-roll coating and lamination was done by the author using the pilot plant developed by *Fraunhofer IVV*. All parts of this machine are completely enclosed in a clean room compatible chamber with particle filters and controlled (laminar) air flow. The first part of the machine is the unwinding unit, followed by the corona pre-treatment unit, the web cleaning unit, the wet chemical application unit, the drying unit, the lamination unit and the upwinding unit (Fig. 4.2). If not indicated elsewhere, the web speed was 3 m/min, the rotation speed of the gravure roll was 5 to 6 m/min and the drying used circulated air of a volume of 8000 m³/h (2000 m³/h of it was constantly exchanged with fresh air) at temperatures between 60 and 120°C (depending on the organic material). For lamination, the pressure at assembly was 1 bar. The coated thicknesses can be adapted in three steps by changing the gravure roll (Table 4.7). If not indicated otherwise, gravure roll 1 was always used for wet chemical coating (which gave, as an example, a dry coating thickness of $1.1 \pm 0.1 \mu\text{m}$ for the organic coating material C5.9 = Ormocer[®]09) and gravure roll 3 was always used for lamination. For this work, this machine was the preferred tool for the coating and lamination of organic lacquers and adhesives due to its very constant and homogeneous coating and curing quality (see Chapter 4.4.1).

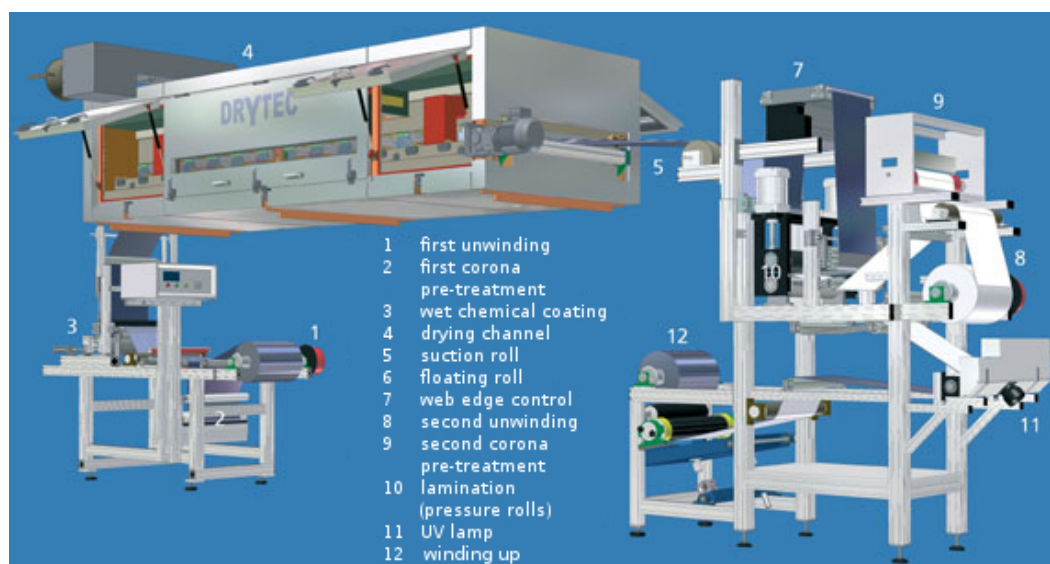


Figure 4.2: Schematics of the wet chemical pilot plant of *Fraunhofer IVV* without enclosure (figure taken from [44]).

Table 4.7: Gravure roll sizes available for the wet chemical pilot coating plant.

gravure roll	wet coated thickness calculated from roll geometry [g/m ²]	as an example: wet coated thickness for C5.9 = Ormocer [®] 09, calculated from its solids content [g/m ²]
1	6.5	2-3
2	8	3-4
3	25	8

Rod bench coating and lamination was done by the author using a “K 303 Control Coater type 625“ of *Erichsen GmbH & Co. KG* (Fig. 4.3a) for organic materials that could not be used on the wet chemical pilot plant. In most cases, the reason for using this tool instead of the pilot plant was a lack of a sufficient amount of organic material to fill the basin of the wet chemical application unit of the pilot plant. Such very small amounts of organic material can be coated and evaluated with the help of this device. To do so, the material is applied manually next to a wired rod on top of sheets in the size of A3 or smaller. The dispersion of the material is done by automatic (motorized) motion of the rod along the sheet (Fig. 4.3b). The choice of the rod roughly determines the level of coated thickness. For this work, always the yellow rod was used to achieve low thicknesses similar to the coating conditions at the pilot plant (Table 4.8) and because higher rods would in fact not be helpful to fabricate thicker organic layers for low viscous materials (since the coating material in wet state typically spreads and the surplus flows astray). After being coated, the sheets are taken away from the rod bench coater and

Table 4.8: Rod size used for this work during rod bench coating and manual lamination.

stem colour of the rod	wet coated thickness, information from rod supplier [μm]	as an example: dry coated thickness for C5.9 = Ormocer [®] 09, average from experiments [μm]
yellow	6	~ 2

either - for the fabrication of coatings - dried in a climatized chamber or oven or - for the fabrication of laminates - laminated manually against another sheet by using a hand-held pressure roll (Fig. 4.3c). However, in terms of layer thickness homogeneity, the rod bench coating or lamination is not at all comparable to the pilot plant. To gain reliable barrier results from samples fabricated with rod bench coating or lamination, the fabrication and evaluation of the barrier layers has to be repeated many times and samples have to be analyzed at several areas of the sample (to derive a reliable average from many individual values) which increased the experimental effort tremendously.

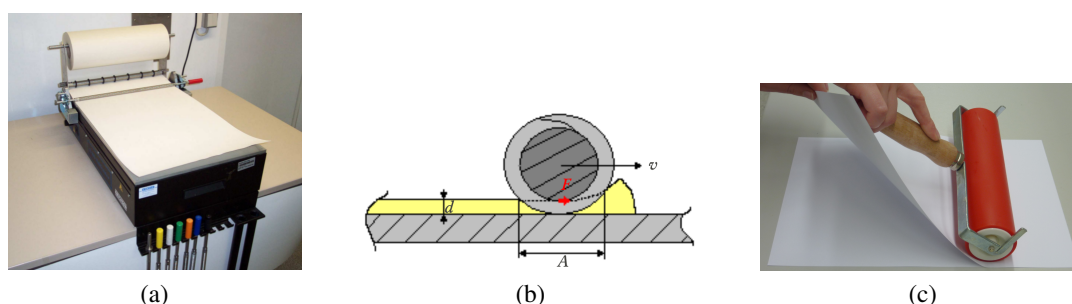


Figure 4.3: Picture (a) and cross-sectional working principle (b) of the Erichsen K 303 Control Coater type 625 that was used for rod bench coating and lamination (figures (a) and (b) taken from [17]). The subsequent manual lamination is demonstrated in Fig.(c) (with two opaque sheets, for better visibility).

4.3 Evaluation methods

All evaluations methods used for this work are listed in Table 4.9 and described in more detail in the following.

Table 4.9: Overview of evaluation methods.

field	classification	method
barrier performance	water vapor transmission	ACP optical calcium test electrolytical: Aquatran [®] / WDDG gravimetical
	water vapor sorption oxygen transmission	gravimetical: SPS11-10 μ electrochem.: Oxtran 2/20 opto-chemical
layer thickness	several μm	digital dial gauge
	mm to μm	visible light microscopy
	μm to nm	SEM
	< 50 nm	TEM
chemical composition	asymmetric bonds	FTIR
	symetric bonds	polarized Raman
surface evaluation	surface (qualitatively)	SEM
	surface roughness	AFM
	surface energy	contact angle
		pendant drop
		test pens
stability tests	mechanical	tensile strength
		laminate bond strength
		tape test
	thermo-mechanical	heated tensile test
		shrinkage test
	climate	damp heat test
outdoor climate test		
UV test: Suntest		
other evaluations	viscosity	rheometer
		flow cup (DIN 4mm)
	colour	spectrophotometer
	UV dose	dosimeter

Water vapor transmission was measured using five different methods. The two most important methods for this work are the accumulating gas chromatographic permeation (ACP) test and the calcium test, because of their very high sensitivity and accuracy: their lower detection limit and their accuracy are at low 10^{-6} g/(m² d) (Chapter 4.4.4). While the calcium test cannot measure samples showing a WVTR > 10^{-3} g/(m² d), the upper

detection limit of the ACP test is at approximately $3 \text{ g}/(\text{m}^2 \text{ d})$. As such, the ACP test would be able to cope with the WVTR evaluation of all samples fabricated for this work except the base substrates. Some of the samples with an expected WVTR between $> 10^{-3}$ and $> 10^{-1} \text{ g}/(\text{m}^2 \text{ d})$ were measured electrolytically with an Aquatran® Model 1 of *Mocon Inc.* (few only, due to low measurement capacity, too). Samples of an expected WVTR between $> 10^{-1}$ and $5 \text{ g}/(\text{m}^2 \text{ d})$, e.g. polymer films with one single inorganic coating or uncoated or organically coated polymer films of good water vapor barrier, were measured electrolytically with an WDDG of *Brugger Feinmechanik GmbH*. The samples with the highest WVTR ($> 5 \text{ g}/(\text{m}^2 \text{ d})$), i.e. uncoated or organically coated polymer films of low water vapor barrier, were measured using the gravimetric method.

The accumulating gas chromatographic permeation (ACP) test has its name from the two principles that are combined: the accumulation of the water vapor that has permeated through the encapsulation material and the detection of this amount of accumulated water vapor via a thermal conductivity sensor like used in gas chromatographic devices. This concept enables gaining WVTR as well as time lag data, even for very low WVTR and very long time lags. The sample is put like a membrane in between the two cups of the measurement cell, the measurement area being approximately 200 cm^2 (Fig. 4.4). The lower cup is filled with water to ensure a constant relative humidity of 100%. The upper cup is constantly flushed with dry nitrogen, setting the upper cell at constant relative humidity (RH) of 0%. A nitrogen flux takes the permeated water vapor away to the accumulation step of the ACP device. All measurement cells are placed in a climate chamber that keeps the temperature at constant level, i.e. at 40°C during zeroing period and at 23°C during measurement. Since the ACP test was not used for WVTR measurement before this work [131], characterization for WVTR measurement with respect to reproducibility, accuracy, trustable lower detection limit etc. had to be performed by the author (Chapter 4.4.4).

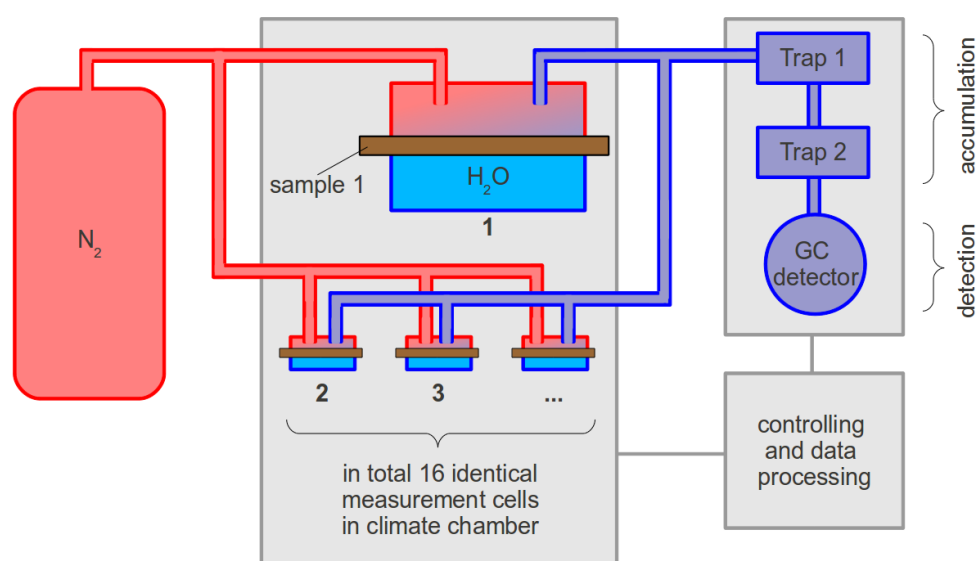


Figure 4.4: Schematic outline of the ACP unit.

4 Experimental methodology

The term "calcium test" refers to a group of test methods that all use the degradation of a thin calcium layer by water vapor as the indicator for the WVTR of an encapsulation. Many techniques were derived from the original measurement method [132]. They differ in how they detect the degradation of the calcium layer (sensor type + evaluation procedure), in the geometry of the measurement cell, in the measurement conditions and in the "translation" of the calcium degradation into a WVTR (Fig. 4.5). As this makes the comparability of the results of the calcium test quite difficult, attempts are ongoing to develop a standard [45].

The calcium test of this work was done by *Fraunhofer IAP* in Golm, Germany, using the optical transmission as quantity to be measured and an optical sensor as detector. For the sample preparation, approximately 90 nm of calcium are deposited on top of the encapsulation material and, with the help of an adhesive, a glass sheet was put on the very top (Fig. 4.6a). The adhesive was put largely around the edges of the calcium area, too, to avoid water vapor degradation from the sides. Compared to other calcium tests, the measurement area of this test is rather large with approximately 5 cm². The complete procedure was performed in dry nitrogen atmosphere in a glove box. Before the measurement, the so prepared cell is stored in a climate chamber with 23 °C and 50% relative humidity. The change of the calcium layer from reflecting and opaque (Fig. 4.6c) to transparent (Fig. 4.6d) is captured by recording the increasing optical transmission over time. This curve is correlated to the decrease of the calcium thickness (Fig. 4.6b). Defects that are obviously not related to the intrinsic barrier performance of the sample, like the scratches (as in Fig. 4.6d), are excluded from the interpretation of the results. It is subject of discussion in the community whether a bimodal evaluation of the calcium test

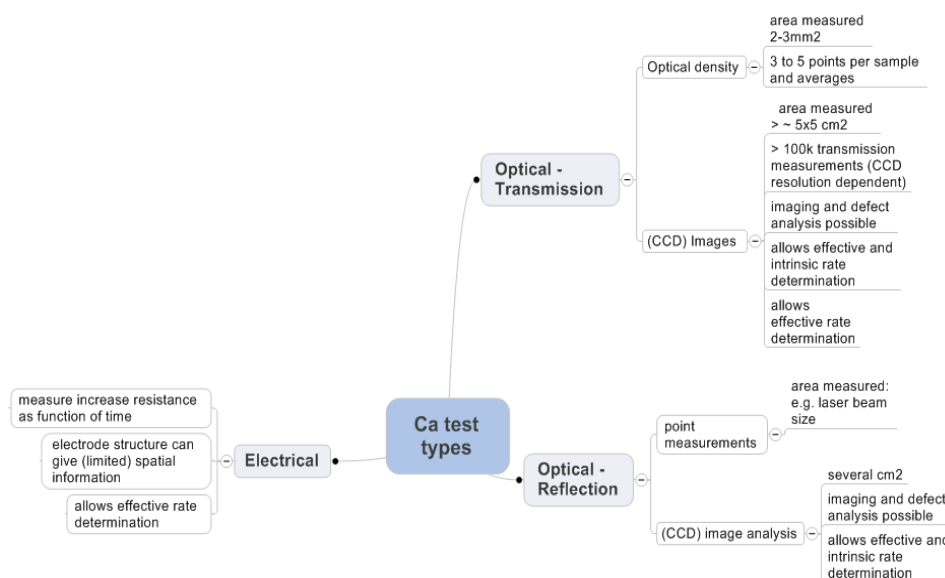


Figure 4.5: Classification of the existing calcium tests, according to [45].

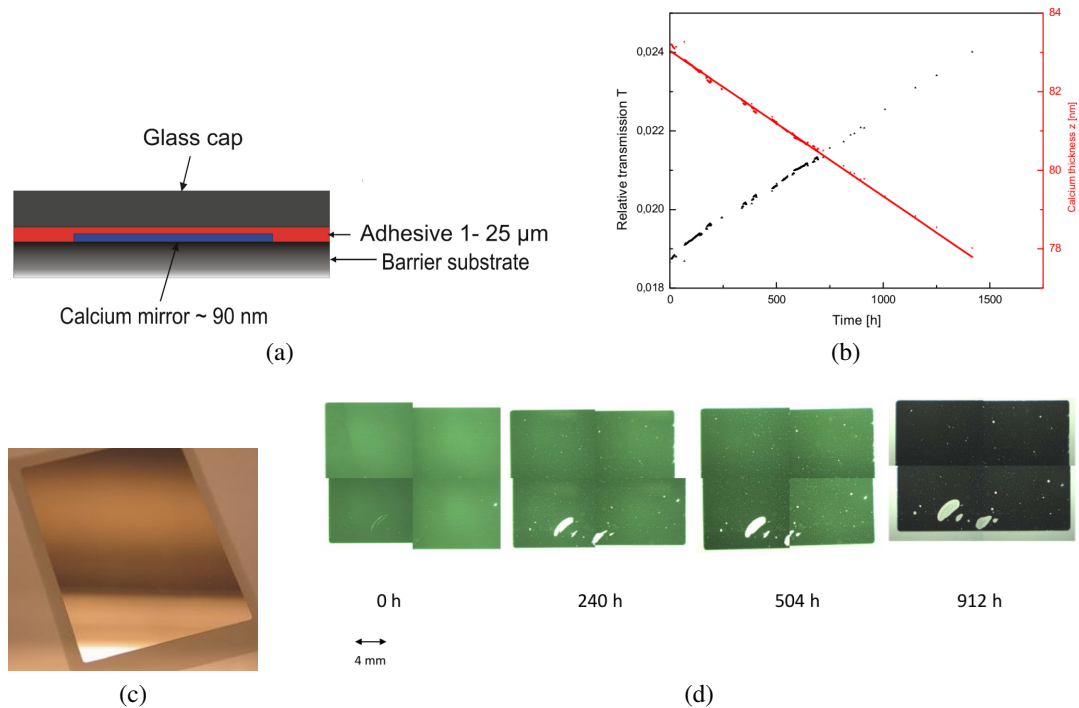


Figure 4.6: Cross-sectional schematic of the calcium test (a), exemplary recording of the optical transmission over time (b), top view of the calcium layer at the beginning of the measurement (c) and rear view of the cell during an exemplary measurement (d) (figures taken from [46, 47, 48]).

would be more adequate: assuming a first period during which one mol of calcium reacts with only one mol of water until approximately 1 nm of the calcium layer is transformed into calcium oxide (CaO), and then a second period during which two mol of water react with one mol of calcium to form calcium hydroxide ($\text{Ca}(\text{OH})_2$) [133]. For this work, the standard calculation using only Eq. (2.1) (Chapter 2.1) is used to calculate the cumulated amount of water vapor arriving at the calcium layer. From the slope of this curve, the WVTR can be derived.

Both the Aquatran[®] Model 1 of *Mocon Inc.* and the WDDG of *Brugger Feinmechanik GmbH* are using the principle of electrolytical measurement of water vapor (Fig. 4.7). The sample material is put into a cylindrical measurement cell as a membrane between the two chambers. In one chamber, a relative humidity of 85% is adjusted by either moisturized nitrogen or aqueous solutions of salts or acids, for Aquatran and WDDG, respectively. The second chamber is constantly flushed with dry nitrogen which transports the permeated water vapor to an electrolysis cell containing platinum wires coated with phosphorous pentoxide. The water vapor is absorbed in the phosphorous pentoxide, where an electrical current applied on the platinum wires leads to electrolytical splitting of the water molecules into hydrogen and oxygen. The lower detection limit of the Aquatran[®] Model 1 is $5 \times 10^{-4} \text{ g}/(\text{m}^2 \text{ d})$, its accuracy 1 to $2 \times 10^{-4} \text{ g}/(\text{m}^2 \text{ d})$ and its measurement area approximately 50 cm^2 . The effective lower detection limit of the WDDG is approximately

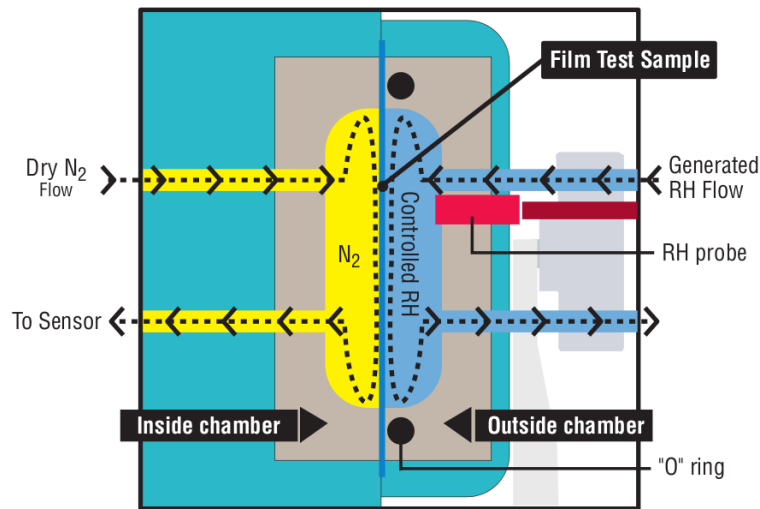


Figure 4.7: Principle of the electrolytical WVTR measurement (figure taken from [49]).

$1 \times 10^{-1} \text{ g}/(\text{m}^2 \text{ d})$, its accuracy $1 \times 10^{-1} \text{ g}/(\text{m}^2 \text{ d})$ and its measurement area 80.6 cm^2 .

The gravimetical WVTR measurements were done using permeability cups. The barrier films are cut into circular pieces with a measurement area of 50 cm^2 and put flat on top of glass cups filled with dry silica gel as desiccant. The distance between the surface of the silica gel and the barrier film should be approximately 10 mm. The edges are closed by casting liquid wax of good gas barrier, e.g. type "Compound RD 914 H" from *Schröder Prüfmittel Weinheim* (having a temperature of 90 to 100°C) in a circle along the rim of the cup and the sample (Fig. 4.8a, 4.8b). The closed cup is stored in a climate chamber at 23°C and 85% relative humidity. Water vapor that permeates through the sample is absorbed in the silica gel and this increase of weight is measured with a balance. Using wax as closure mechanism (Fig. 4.8b) instead of screwed caps (Fig. 4.8c) or flanges (Fig. 4.8d) improves the accuracy and lower detection limit of this method (accuracy of $\pm 0.05 \text{ g}/(\text{m}^2 \text{ d})$ and lower detection limit of $\pm 0.3 \text{ g}/(\text{m}^2 \text{ d})$ possible), but also increases the effort to be spend on preparation. For this work, for each sample an average value was gained by preparing and measuring four cups each time.

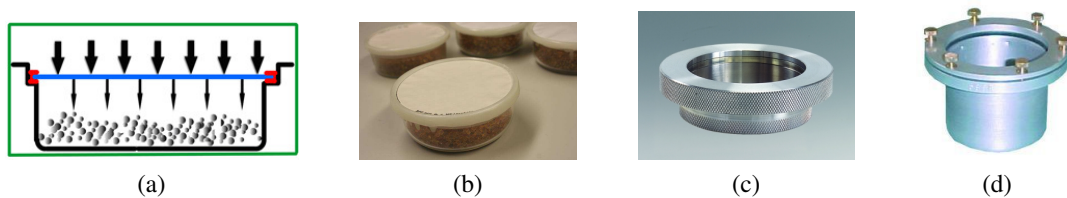


Figure 4.8: Gravimetical WVTR measurement: (a) principle, (b) wax method of *Fraunhofer IVV* and (c), (d) other types of closure: screwed cups, flanged cups (figures taken from [50, 51, 52, 53]).

Water vapor sorption was measured by the author using an SPS11-10 μ from *Projekt Messtechnik*. The samples are put into cups of 20 cm^2 area and 12 ml volume at 23°C .

The moisture uptake is measured automatically with a micro balance of $\pm 20 \mu\text{g}$ accuracy until steady state was attained. For this work, this method was used to determine the solubility coefficient for water vapor of barrier materials.

Oxygen transmission was measured using two different methods. The first method was performed by the author, using an Oxtran 2/20 of *Mocon Inc.*. The principle is similar to the Aquatran[®] Model 1 of the same company (Fig. 4.7), just having a different measurement gas (oxygen instead of moisturized nitrogen) and a different sensor. The sensor consists of a graphite cathode and a porous cadmium anode. The permeated oxygen is transported by the carrier nitrogen gas to the sensor and absorbed in the Cadmium anode, where it reacts with the Cadmium. The oxidation of the Cadmium anode creates electrical current which can directly be calculated into the oxygen transmission rate (OTR). Both the lower measuring limit and the accuracy of this method is $0.001 \text{ cm}^3(\text{STP})/(\text{m}^2 \text{ d bar})$, the upper detection limit is at $10,000 \text{ cm}^3(\text{STP})/(\text{m}^2 \text{ d bar})$. For this work, it was used to measure the OTR at $23 \text{ }^\circ\text{C}$ and 50% RH of polymer films that were either uncoated, coated with organic barrier layers or coated with maximum one thin inorganic barrier layer.

For encapsulation materials with better barrier performance against oxygen, i.e. containing more thin inorganic barrier layers, a more sensitive oxygen transmission measurement was done at *Joanneum Research Forschungsgesellschaft mbH* in Graz, Austria, using their opto-chemical method. Again, the encapsulation material is used as the membrane separating two chambers. One chamber is flushed with oxygen which permeates through the sample into the second chamber. The second chamber contains an oxygen sensitive luminescent dye immobilized in a matrix material (Fig. 4.9). This dye is brought into an excited state with LED light and emits light when relaxing to ground state. Oxygen permeating across the encapsulation material accumulates in the second chamber and progressively quenches the luminescence of the irradiated sensor dye. The luminescent response of the sensor is permanently monitored by an opto-electronic instrument through a glass window. After 60 min, the second chamber is flushed with oxygen free nitrogen

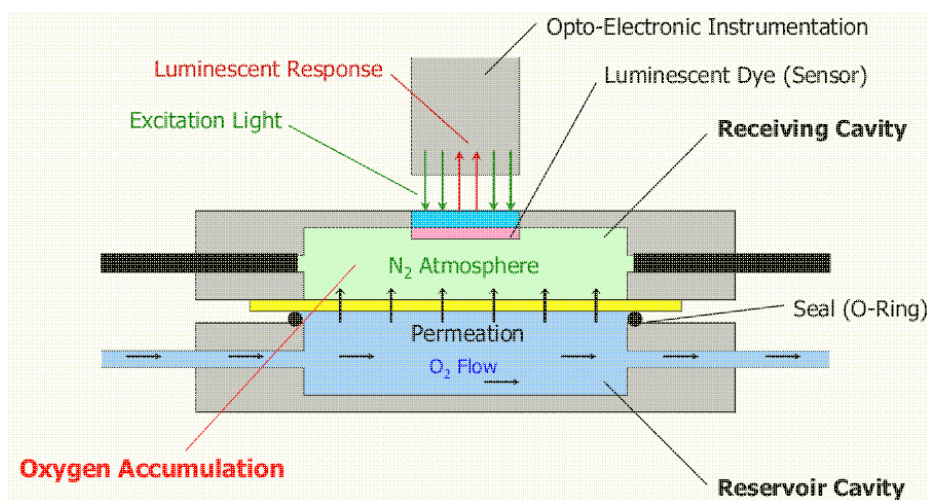


Figure 4.9: Principle of the opto-chemical OTR measurement device of *Joanneum Research Forschungsgesellschaft mbH* (figure taken from [54]).

4 Experimental methodology

and the accumulation and recording step restarted. The whole procedure happens at 23 °C and 0% RH and is repeated until steady state is attained. Both the lower detection limit and the accuracy of this method are in the $10^{-5} \text{ cm}^3(\text{STP})/(\text{m}^2 \text{ d bar})$ regime [54].

Layer thicknesses were measured using three different methods, depending on the thickness of the respective layer.

Freestanding materials - like polymer films or organic coatings that could be fabricated as free-standing plates (possible only for very few of the screened adhesives) - were measured by the author using a digital dial gauge type Millimar C 1216 from *Mahr*. The sample is put inbetween the base plate and the bolt and the displacement of the bolt is recorded. The accuracy of this device is approximately $\pm 1 \mu\text{m}$. For each sample, an average out of ten measurements is calculated.

The thicknesses of non-free-standing layers thicker than 2 to 3 μm were measured by the author using visible light microscopy with a Leitz diaplan from *Leica Microsystems GmbH*. During this work, such layers were fabricated mainly during the screening of potential organic barrier materials. To be able to evaluate these organic materials, they were coated on top of a highly permeable polymer film or, for adhesives, as layer between two highly permeable polymer films. From these samples, thin cross-sectional slices were cut using a microtome cutting device type Jung Autocut 2055 from *Leica Instruments GmbH*. The thicknesses of the carrier polymer films were either 12, 15 or 23 μm which is a compromise between trying to take substrates of high transmission (i.e. low thickness required) and sufficient geometrical stability during coating and drying (i.e. higher thickness required). Samples based on polymer films of such low thicknesses are relatively flexible and have to be prepared before being sliceable with a microtome cutting device. Therefore, they were put inbetween two small pieces of thick plastic plates made of PVC or PE (e.g. PE plates type "Sandwichhalter" from *MicroKern*) and fixed vertically in the clamp of the microtome cut device with some excess end of approximately 5 mm protruding out of the clamp. On top of this excess end, so much of transparent adhesive of medium viscosity ("UHU Plus schnellfest 5 min transparent mit Mischwanne und Spatel (2K)") is trickled that the whole material stack is enclosed by adhesive. Slices are cut from the glued stack with the microtome cutting device. The first

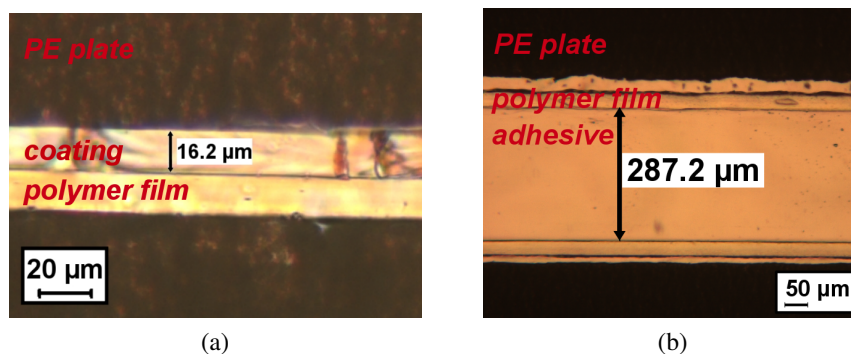


Figure 4.10: Layer thickness measurement by optical microscopy: exemplary cross-sections (a,b).

slices are removed until the surface of the cross-section is sufficiently plane. The next slice is layed on top of an object holder and fixed at the ends with tesa adhesive tape. In the light microscope, differential interference contrast imaging at magnifications between 200 x and 400 x was used to visualize the layers. At least 10 measurements were made to determine the average thickness of a coating layer (Fig. 4.10a) or an adhesive layer (Fig. 4.10b), respectively. The resolution of this method is approximately 0.2 μm .

Thicknesses below 2 μm down to 50 nm were measured by the author using field emission scanning electron microscopy (SEM) with a Hitachi S-4000 of *Hitachi High-Technologies Europe GmbH* (in cooperation with the *Chair of Experimental Physics of Technische Universität München*). Additionally, thicker layers (up to 130 μm) were analyzed by SEM, too, if they were not able to be analyzed by light microscopy, because of cohesive breaks or delaminations from the polymer film during microtome cutting (like in Fig. 4.11).

For this work, for the evaluation with SEM, two preparation techniques were applied. Samples consisting of polymer films coated with flexible materials were cooled in liquid nitrogen, cut into cross-sectional slices with the microtome cutting device, fixed with

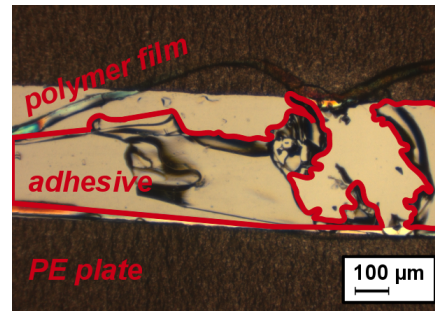


Figure 4.11: Layer thickness measurement by optical microscopy: exemplary failed cross-section.

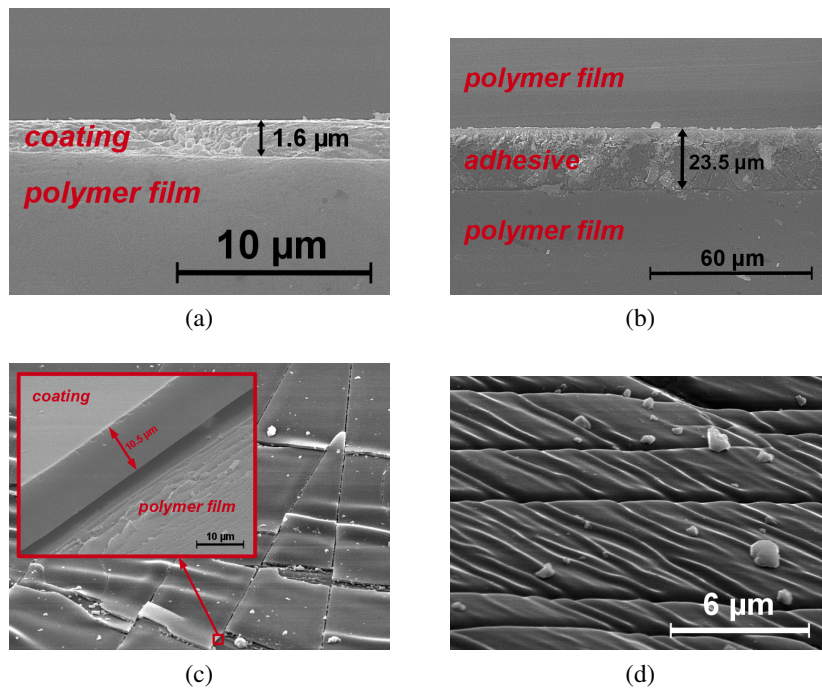


Figure 4.12: Layer thickness measurement by scanning electron microscopy: exemplary pictures of samples prepared by cryo cutting (a,b) or cryo breaking (c,d).

4 Experimental methodology

conductive pads on top of a metallic holder and coated with a thin layer of gold (approximately 10 nm). As such, the layers remain intact and SEM is done on the cross-section (Fig. 4.12a, 4.12b). Samples consisting of polymer films coated with stiff materials, like thin inorganic barrier layers or stiff organic coatings, were cooled in liquid nitrogen, rumpled manually to break the layers and again fixed with conductive pads on a metallic holder and coated with gold. Here, with the help of SEM, pieces of the layers that are standing up from the substrate are used to evaluate the layer thickness by measuring the edge of the pieces (Fig. 4.12c). The first preparation does not work for stiff coatings which would delaminate and fall off the sample, while the second preparation does not work for flexible coatings which would not break, but only wrinkle and therefore not expose free edges (as in Fig. 4.12d). With the Hitachi S-4000, magnifications between 50 x and 100,000 x (effectively approximately 60,000 x) are possible and the effective resolution is approximately 1 nm.

Thicknesses below 50 nm were measured at the *FELMI-FZE* of *Technische Universität Graz* in Graz, Austria, using their scanning transmission electron microscope type Tecnai 12 from *FEI*. The samples were embedded in Epofix before cutting ultra thin cross-sectional slices using a 35° diamond knife. Magnifications between 35 x and 700,000 x are possible at a resolution of down to 0.34 nm. The pictures were taken using a CCD camera type Bioscan Camera from *Gatan* (like in Fig. 4.13a and 4.13b).

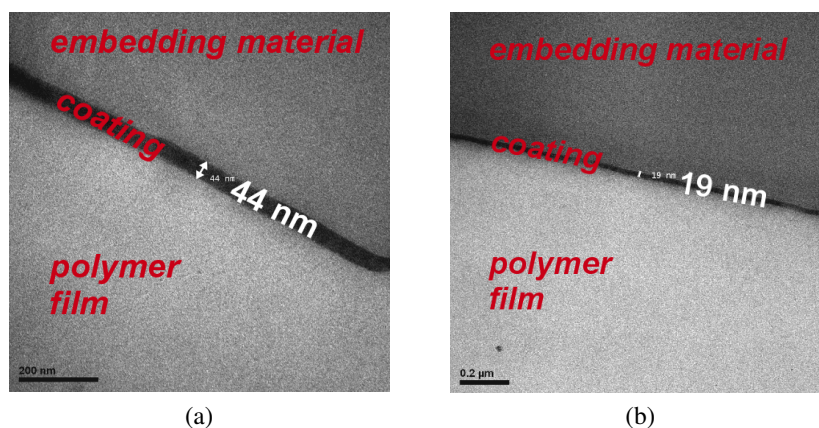


Figure 4.13: Layer thickness measurement by transmission electron microscopy: exemplary cross-sections (a,b).

Chemical composition was analyzed by the author using two different methods: Raman spectroscopy and Fourier transform infrared spectroscopy (FTIR). Both methods are non-destructive and use basically the same principle: they measure the frequencies in which atoms swing relatively to each other. For FTIR, a PerkinElmer Spectrum One from *PerkinElmer Inc.* was used. For Raman spectroscopy, an alpha500 from *Witec GmbH* was used, having an external Nd-YAG laser from *Andor Technology plc.* which emits green light of a wavelength of 532 nm. Since both methods are complementary in their content of information (FTIR being sensitive to asymmetric oscillations as found in functional groups, Raman being sensitive to symmetric oscillations as found in the carbon skeleton of polymers or in inorganic lattice), always both methods were used, if possible, for this work to characterize barrier layers. The spectra are displayed in combination (as in Fig.

4.14). Inner layers of a multilayered material could only be evaluated by Raman, because the alpha500 can measure confocally, while the SpectrumOne measures in ATR (attenuated total reflectance) mode with a maximum depth of measurement of 3 μm into the sample. With the alpha500 the intensities for all wave numbers (from zero to 4000 /cm) can be evaluated, while with the Spectrum One only the intensities of wave number beyond 400 /cm are measurable. In this work, both methods showed to be unable to detect layers of thicknesses below 150 nm.

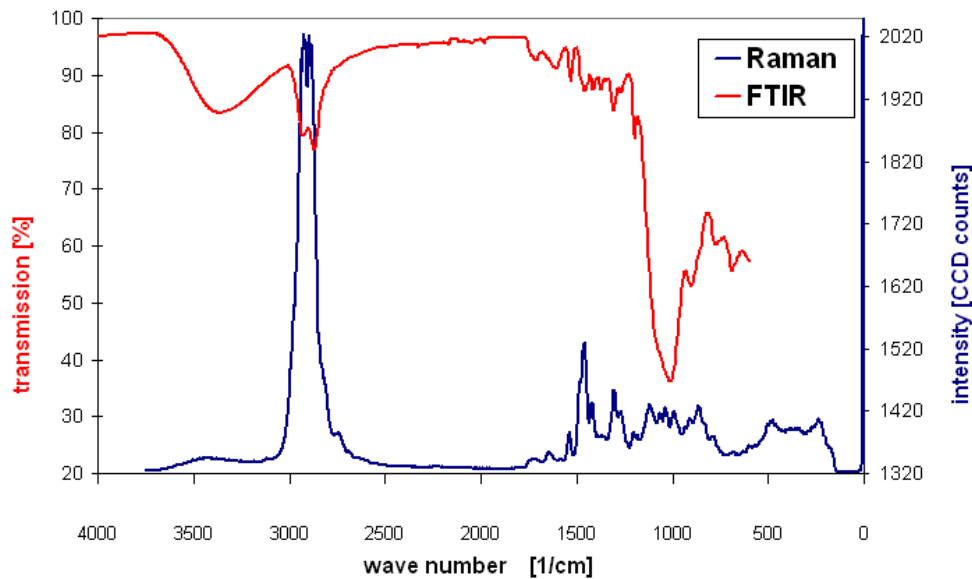


Figure 4.14: FTIR and Raman spectroscopy: exemplary combined spectrum.

Qualitative surface evaluation was by the author using SEM with the same Hitachi S-4000 mentioned above. For this work, qualitative surface evaluation was used to understand failure mechanisms, for example the breakage of the thin inorganic barrier layers after shrinkage of the polymer substrate or the reason for delamination of the layers after laminate bond strength tests or climate tests performed on the sample.

Surface roughness was measured at the *Brno University of Technology* in Brno, Czech Republic, using atomic force microscopy (AFM) with an Atomic Force Microscope Explorer from *ThermoMicroscopes*. In this work, this method was used to characterize the surface roughness of polymeric substrates and the thin inorganic and organic barrier layers coated on top of them. From each sample, at least three areas of a size between 1 and 9 μm at different positions on the sample were measured to derive an average, resulting in average values of the average height, the maximum range, the average surface roughness in form of the arithmetic mean (R_a) and the average surface roughness in form of the root mean square (RMS) (see Fig. 4.15 as an example). The resolution was approximately 0.1 nm.

Surface energy was measured by the author using three different methods. The contact angle method was done using a G2 from *Krüß GmbH* to apply drops of 3 μl of four increasingly polar liquids (dimethyl phthalate, diiodomethane, ethylene glycol and water)

4 Experimental methodology

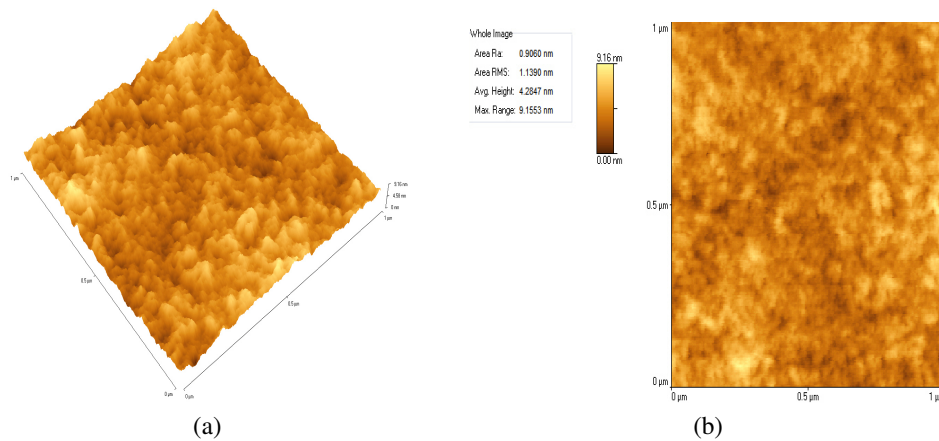


Figure 4.15: Measurement of the surface roughness with atomic force microscopy: exemplary evaluation.

on the surface of the sample of interest. The surface tension of the respective sample was calculated using the Owens-Wendt-Rabel&Kaelble equation [134, 135]. For this work, this method was used to understand adhesion problems between coatings or adhesives and uncoated or coated polymer films.

The second method, the pendant drop method (Fig. 4.16b), was done using the same G2 from *Krüiss GmbH*. The surface energy of the liquid was calculated using the Young-Laplace equation [136, 137]. For this work, this method was used to measure the surface energies of potential barrier adhesives. Both methods have an accuracy of approximately 0.5 mN/m.

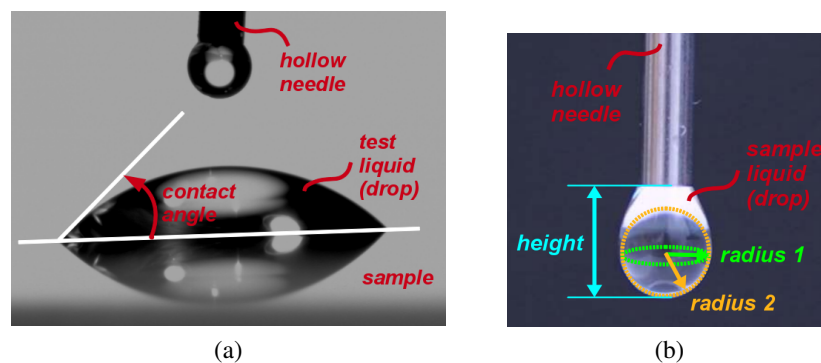


Figure 4.16: Surface energy measurement in (a) contact angle mode and (b) pendant drop mode (figures modified from [55, 56]).

A third method was used by the author when - before coating trials - fast proof of sufficient surface tension was required: wettability check with test pens from *Arcotec GmbH*, ranging from 30 to 44 mN/m of surface energy in steps of 2 mN/m. As a rule of thumb, most coating materials are going to wet appropriately if the surface tension of the substrate, using these test pens, is approximately 40 mN/m or higher, i.e. if the streaks applied with the 40 nN/m pen are not rolling off into drops 3 seconds after application but

stay streaks (Fig. 4.17a, 4.17b). This method does not differentiate between dispersion and polar force and its effective accuracy is approximately 2 mN/m.

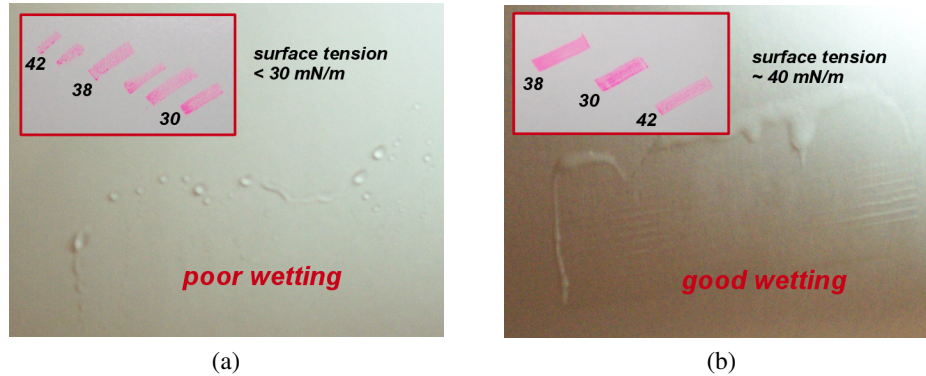


Figure 4.17: Wettability check with test pens for two exemplary substrates: one with poor wettability (a), one with good wettability (b).

Mechanical and thermo-mechanical stability was evaluated by the author measuring five different properties: tensile strength, tensile strength under heating, laminate bond strength, shrinkage and resistivity in the tape test. The last test just gives out a “yes“ or “no“, while the other tests deliver quantitative results.

For this work, tensile strength measurements were used to evaluate polymer films before and after specific treatments. From the films, stripes of 200 mm by 15 mm were cut and conditioned for 24 hours at 23°C and 50% RH. Per sample, 10 stripes were measured to derive an average, using a “Universalprüfmaschine Schenck-Trebel Typ RM 50“ from *Bischoff Prüftechnik GmbH*. Test length (between the clamps) at start was 50 mm, starting speed was 5 mm/min and test speed was 100 mm/min.

Shrinkage was measured storing rectangular squares of the respective sample, with an area of approximately 250 times 300 mm², for one hour in an oven at 130 °C. After the treatment, the change in length of the sample was measured in both directions, i.e. machine direction (MD) and transversal direction (TD), using a sliding calliper with a resolution of 50 µm.

The adhesive tape test was used to do a fast test to check whether a coating adheres to a substrate or not. For this, a stripe of transparent adhesive tape is applied to the surface of the coating and afterwards manually pulled off. For non-transparent coatings, a (partial) change of colour of the adhesive tape would indicate that parts of the layers have come off (like in Fig. 4.18a) which would easily indicate adhesion problems - while for transparent coatings, an FTIR or Raman spectroscopy analysis (plus optionally an SEM investigation of the surface) of the sticking side of the adhesive tape has to be made to know whether parts of the coating came off or not. If the originally sticking side of the adhesive tape would not be sticky any more at all, this would also indicate that much of the coating was transferred to the adhesive tape (i.e. adhesion problems). As the adhesive tape is pulled off manually, the pulling force and speed are not controllable to be equal each time. Hence, comparisons between results from different operators are to be taken with caution.

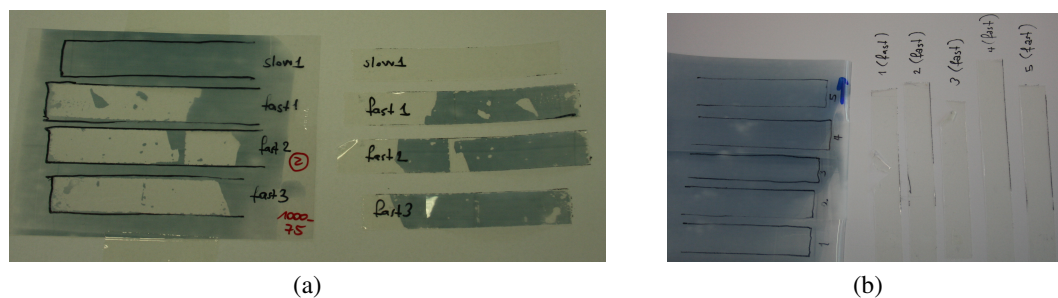


Figure 4.18: Two exemplary adhesive tape tests: one with bad result (a), one with good result (b).

Viscosity was measured by the author using two different devices: a rheometer type Bohlin CVO from *Malvern Instruments GmbH* and a flow cup type DIN 4 mm. For this work, the rheometer was used for the characterization and adjustment of the viscosity of organic coating materials during the studying of the potential synergistic barrier effect. The flow cup was used much more - as a routine income control of the organic coating materials before each coating trial.

For the measurement with the rheometer, the cylinder-bob method was used: a metallic cylinder ("bob") with a diameter of 25 mm was used to rotate in a cylindrical cup, filled with approximately 5 ml of the sample material. Temperature was kept constant at 23°C. This method was used to quantify the viscosity as a function of shear rate. Viscosities between 1 and 10^7 mPas can be measured. The accuracy of holding the gap is $< 1 \mu\text{m}$, the accuracy of holding the torsional moment is 3×10^{-9} Nm.

The flow cup has the form of a cone with a small opening of 4 mm diameter at the narrow end. The sample material is filled into the cup manually up to the spill rim, closing the small opening with one finger. The time from taking away the finger until the flow cup is completely emptied is measured in seconds. This number is used for income control. The flow cup test has many undefined parameters and is not applicable for liquids with higher viscosities (above approximately 10,000 mPas).

Colour was measured by the author using a spectrophotometer type VTLCM-700 from *Konica Minolta Holdings, Inc.*. Within one measurement, light at different wavelengths is sent to the sample and the intensity of the reflected light is detected. Calibration of zero intensity is done taking a measurement while the detection spot is completely covered from light, and calibration of 100% intensity is done measuring a very bright and reflective white standard. For this work, a white tile was used as white standard. To ensure a constant white standard even though tiles are aging, several tiles of the same batch were organized and, while one was in use, the others were stored in a cool dark place. Within this work, this evaluation method was used to quantify the colour change, mainly the yellowing, of samples that were exposed to climate or UV stress.

UV dosage was measured by the author using a dosimeter type UV Power Puck from *EIT Inc.*. When fixing the device in such a way that its detector spot would pass the same way as the sample, the UV dosage is measured (by an optical sensing system) simul-

taneously for UV-A (320-390nm), UV-B (280-320nm), UV-C (250-260nm) and UV-vis (395-445nm). For this work, this method was used to characterize the UV curing section at the wet chemical pilot plant.

4.4 Experimental methods developed during this work

4.4.1 Procedure of the “edge trials“

This procedure was developed to be independent of the variations of the thin inorganic barrier layer along the length of one roll, in order to be able to study the synergistic barrier effect (Chapter 6.1) of roll-to-roll prepared samples.

During the edge trials, the organic barrier material is coated in short repeating lengths on top of the thin inorganic barrier layer (Fig 4.19). Each short organically coated length begins and ends with an edge. To do so, the application unit of the pilot plant is repeatedly (sharply) moved up and down, between the coating and the non-coating mode of operation. The two samples, i.e. the two layer and the three layer structure, will be extracted adjacent to both sides of one “edge“ of the organic coating material (see “sample 1” and “sample 2” in Fig. 4.19). Therefore, the variations of the original transmission rates of the two layer structure between the two samples become lower than $1 \times 10^{-3} \text{ g}/(\text{m}^2 \text{ d})$ or $\text{cm}^3(\text{STP})/(\text{m}^2 \text{ d bar})$ and deviations of the transmission rates of the three layer structure compared to the theoretically expected ones above these values can confidently be allocated to other effects - for example to the synergistic barrier effect.

Variations of the barrier performance of the thin inorganic barrier layer along the width of the roll were eliminated by using rolls with small roll width (below 400 mm) and cutting the samples only from the middle of the web (within an actual width of below 200 mm).

Otherwise, the barrier performances of the thin inorganic barrier layers of this work would vary too much along the length (of several hundred meters) of the roll and evalua-

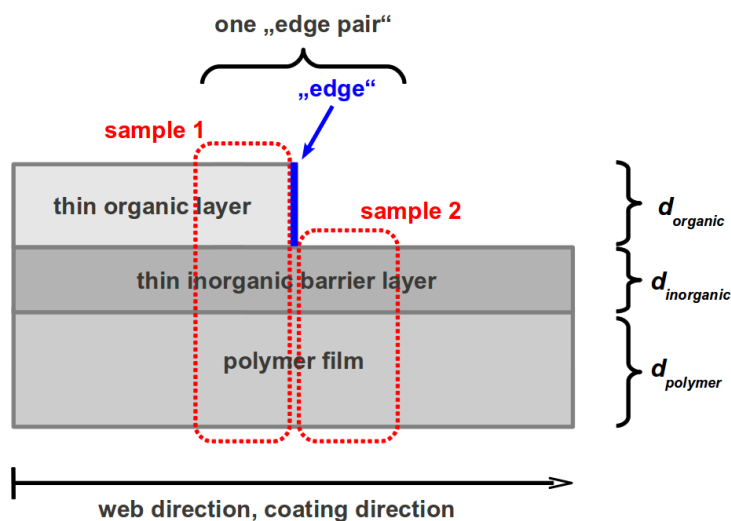


Figure 4.19: Schematic view of the coating procedure of the “edge trials“.

tions of barrier effects would not be possible. For example, the WVTR of the PET+SiO_x film used for this work varies between 0.08 and 0.27 g/(m²) and its OTR between 0.13 and 0.65 cm³(STP)/(m² d bar). The edge trials are using the fact that, within small distances, i.e. below approximately 200 mm, the change of the transmission rates of the two layer structure is below 1×10^{-3} g/(m²) or cm³(STP)/(m² d bar) and would therefore be negligible compared to the accuracy required for the investigation of the synergistic barrier effect.

When using the wet chemical coating plant, the variation of the barrier performance of the organic layers is so low that it can be neglected for further evaluation: transmission rate changes over several hundred meters are below 1×10^{-3} g/(m² d) or cm³(STP)/(m² d bar).

4.4.2 Characterization of the UV curing section of the pilot plant

The wet chemical coating plant contains a UV lamp type “UVAprint SLF-H“ from *Dr. Hönle AG*. In this lamp, a mercury vapor (in argon) is used to produce the UV light, emitting all wavelengths (UV-A, UV-B and UV-C). At the control unit, the power of the lamp is adjustable between 0 and 100% in steps of 1%, but, at the beginning of this work, there was no idea which dosage of each emitted wavelength this would be equal to. Because, in this work, coating materials or adhesives were going to be studied that would require a precise UV-C dose for optimum curing, the UV lamp of the pilot plant had to be characterized first.

A dosimeter was fixed on a carrier substrate in such a way that the sensor of the dosimeter was at the same distance to the lamp where an organic coating would be. The carrier substrate, together with the dosimeter, was then moved at different web speeds through the pilot plant, passing the UV lamp, too. Therefore, the dosimeter would measure the doses of visible light, UV-A, UV-B and UV-C a coating material would be exposed to when being cured in the wet chemical coating plant. This measurement procedure was repeated three times. From the experimental results for UV-C dose a regression

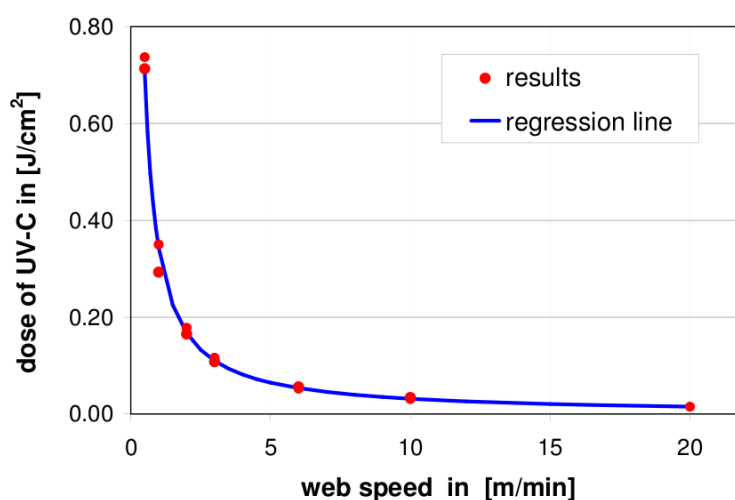


Figure 4.20: Results of the measurement of the UV-C dose emitted at the wet chemical coating plant and fit with a logarithmic regression line.

line was calculated (Fig. 4.20), using the method of least squares. The logarithmic law of this regression line was used in the following for all trials to adjust the UV-C dose to the requirements of the individual coatings by adapting the web speed. It is:

$$\lg(D_{UV-C}) = -1.03714 \lg(v_{web}) - 0.46463 \quad (4.1)$$

with D_{UV-C} being the dose of UV-C the surface of the coating would be exposed to in the wet chemical coating plant and v_{web} being the web speed.

4.4.3 Viscosity adjustment of Ormocer[®] coating materials

For this work, Ormocer[®] coating materials were supplied by Fraunhofer ISC as a ready to use gel, with just the solvent having to be dried out during the coating procedure and the cross-linking reactions having to be started by high temperature and optionally UV radiation. In the supplied state, the solvents of the Ormocer[®] coating materials (mainly water and ethanol, plus smaller parts of methanol, propanol and butanol) sum up to at least 50% of the mass. As the easiest way to adjust the layer thickness during reverse gravure coating is to adjust the viscosity of the liquid, it was important to understand the relationship between the solids content of an Ormocer[®] coating material, its viscosity and the layer thickness after being coated with the wet chemical coating plant.

To quantify this relationship, Ormocer[®] coating materials of different solids contents were prepared by the author (Fig. 4.21a) and their dynamic viscosities were measured as a function of shear rate using a rheometer.

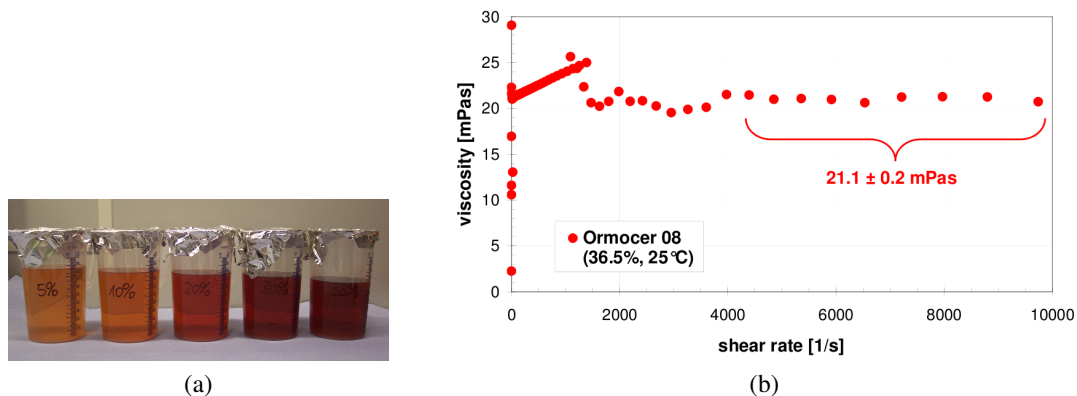
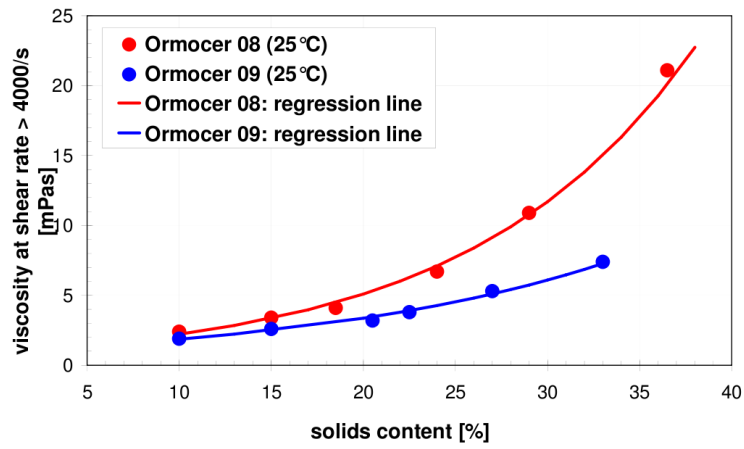


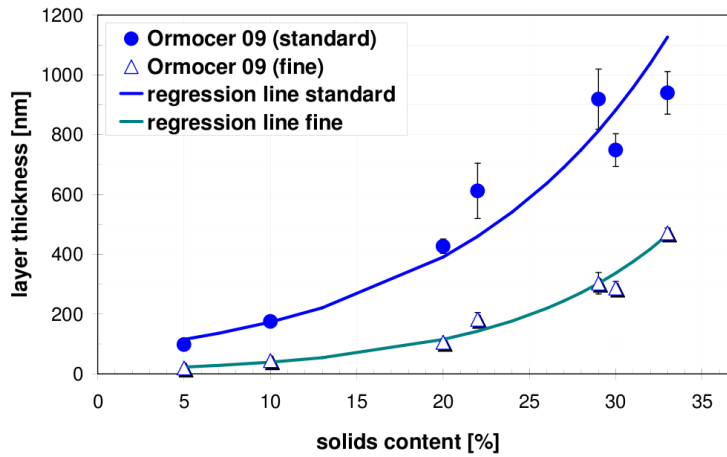
Figure 4.21: Ormocer[®] 09 (= C5.9) with different solids contents (a) and exemplary rheological measurement (b).

For Ormocer[®] coating materials, the dynamic viscosity stabilizes at a constant level for shear rates above 4000/s (see Fig. 4.21b as an example). This last part of the curve was used to calculate the average dynamic viscosity. This way, for two Ormocer[®] types, 08 and 09, the dynamic viscosity at a shear rate of > 4000/s was measured as a function of solids content (Fig. 4.22a). For Ormocer[®] 09, the same prepared liquids were roll-to-roll coated on top of a PET film of 50 μm , using two types of gravure rolls: the standard one and a finer one. From these coated samples, the thicknesses of the Ormocer[®] layers were

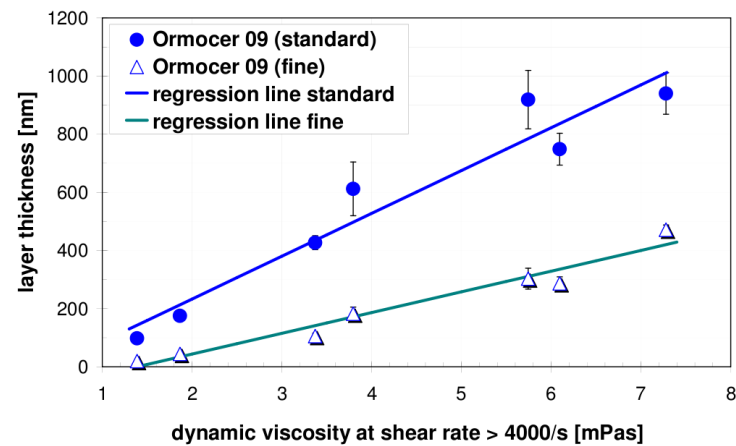
4 Experimental methodology



(a)



(b)



(c)

Figure 4.22: Ormocer[®] 09: Dynamic viscosity (a), layer thickness (b) as a function of solids content and layer thickness as a function of dynamic viscosity (c).

measured (using TEM and SEM) as a function of solids content of the liquid material (Fig. 4.22b).

Both graphs in Fig. 4.22 show exponential behavior: with increasing solids content, both the viscosity of the Ormocer[®] and the corresponding layer thicknesses are increasing exponentially in a similar way. This suggests to check whether the relationship between layer thickness and viscosity would be linear - which is in fact the case (Fig. 4.22c). This proportionality implies that the layer thickness is determined only by the spreading of the coating material, which itself is proportional to the dynamic viscosity. Comparison of the coating trials with the two different gravure rolls (standard and fine) leads to the result that with the standard roll approximately twice as much is coated as with the fine gravure roll (the ratio of the slopes of the regression lines is 147 nm/mPas to 71 nm/mPas, i.e. approximately 2). The derived relationships were used during the coating trials of this work to adjust very specific Ormocer[®] thicknesses.

4.4.4 WVTR measurement by accumulating gas chromatography

Since the ACP test was not used for WVTR measurement before this work [131], characterization for WVTR measurement with respect to reproducibility, accuracy and trustable lower detection limit had to be performed.

With the background of the development of OE encapsulation material, the lowest trustable detection limit is the most important criterion. The ACP device uses a gas chromatographic sensor that could detect WVTR in the 10^{-9} g/m² regime. Yet the tightness of the whole ACP device, the water release from the walls and the leakages through the test samples themselves (via side diffusion) do influence the lowest level of WVTR that can be measured correctly and that should be regarded as the official detection limit of the ACP device.

At current design and best zeroing conditions, the tightness of the ACP device would enable measurement of WVTR lowest at the level of 10^{-7} g/(m² d). What is more complex, is to assess the amount of water vapor that comes in or gets lost via side diffusion through the samples themselves. The part of water vapor that permeates via side diffusion depends on the structure of the test sample. Two constraints would amplify side diffusion: (1) In the multilayered sample, there are contained layers of very high water vapor barrier that decelerate the water vapor permeation perpendicular through the sample (the higher the barrier, the more pronounced) - like thin inorganic barrier layers, or (2) In the multilayered sample, there are contained layers of low barrier and very high thickness (the thicker and the lower the barrier the more pronounced) - like the polymer substrate. In the extreme case, this would lead to a situation where the water vapor permeates easily in all directions through the low barrier layer, also sideways, but is blocked at the interfaces to the high barrier layer (Fig. 4.23).

Diffusion through an example of the two layer structure [polymer substrate + thin inorganic barrier layer] was calculated (via FEA) to understand how much of the water vapor would permeate sideways for one of the extreme cases (Fig. 4.23). The structure was chosen to consist of layers that are typically used in encapsulation materials: the polymer substrate being PET film of 75 μ m thickness, and the inorganic barrier layer being of a good barrier quality like typical for a ZnSn_xO_y layer of 60 nm thickness. Thus, the intrinsic permeability of the substrate was at least 175,000 times higher than the effective

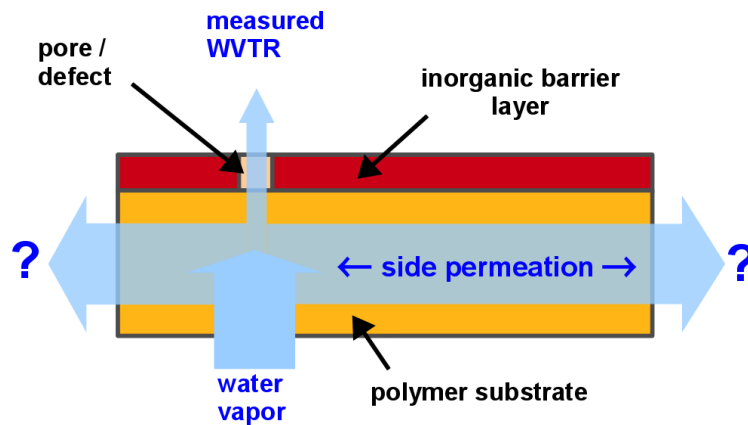


Figure 4.23: Side permeation: Cross-sectional scheme of the evaluated encapsulation material.

intrinsic permeability of the inorganic layer, and its thickness was more than 1,200 times larger than the one of the inorganic layer - which shows why this structure is in fact an extreme case concerning side permeation. The geometry for the calculation was adapted to the size of one measurement cell of the ACP unit, i.e. having an inner diameter (of the measurement area) of 16 cm, followed by a rim of approximately 1 cm (Fig. 4.24). The simulations were repeated twice: once for open and once for closed sides of the sample, i.e., in the second case, permeation was only allowed to occur through all the layers of the sample. From the difference of the two cases the amount of water vapor permeating sideways was calculated.

For this example, side permeation was calculated to be in the high 10^{-7} g/(m² d) (Table

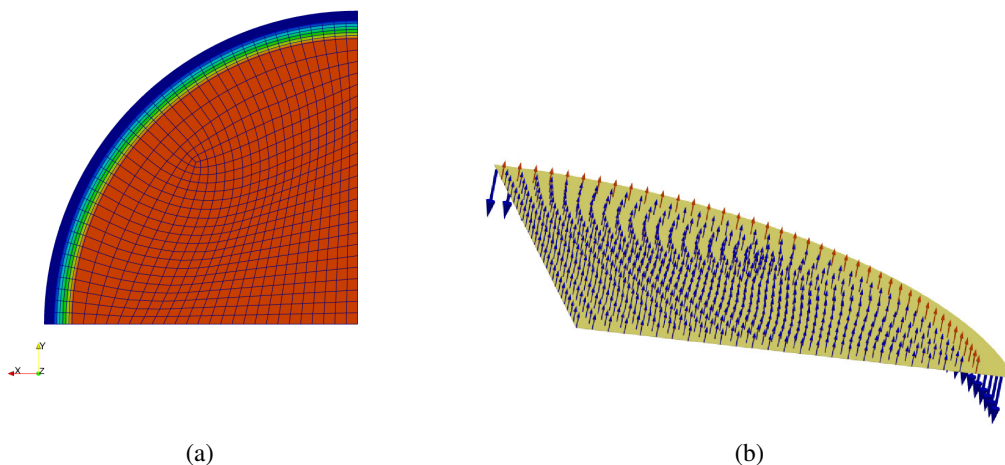


Figure 4.24: FEA calculation of the side permeation: meshing (a) and calculated permeation per finite element (b). In figure (b), one quarter of the sample in the measurement cell is shown, the 100% RH would be applied from the lower side. The lengths of the arrows indicate the amount of permeating water vapor and their tips the direction of permeation.

Table 4.10: Side permeation: FEA calculated and experimental results.

	permeation through all layers	side permeation
FEA calculated WVTR	$5.04 \times 10^{-2} \text{g/m}^2$	$7 \times 10^{-7} \text{g/m}^2$
ACP measured WVTR	$5.01 \times 10^{-2} \text{g/m}^2$	-

4.10). As it is an extreme case, it should be sufficient to subtract this "amount of leakage" from the technical detection limit. Hence, the lowest correctly measurable WVTR, i.e. the lower detection limit of the ACP device, is at approximately $1 \times 10^{-6} \text{g}/(\text{m}^2 \text{d})$.

This lower detection limit is valuable as long as the zeroing (Fig. 4.25) was completed, i.e. the emptying of the ACP device and - mainly - of the samples themselves from absorbed water was finished within the tolerance of the detection limit of approximately $1 \times 10^{-6} \text{g}/(\text{m}^2 \text{d})$. For the sample materials for which such a low detection limit was not necessary (because they were expected to be of medium to low barrier level only), the ACP test was run with shortened zeroing period, and such, with an artificially increased lower detection limit. For example: For samples that were expected to show a WVTR around $10^{-3} \text{g}/(\text{m}^2 \text{d})$, it was sufficient to have a lower detection limit of approximately $1 \times 10^{-4} \text{g}/(\text{m}^2 \text{d})$ and, in exchange, to save time.

Regarding reproducibility evaluation, eleven samples were zeroed and measured twice without any handling of the sample between the two measurements. The deviation between the results of the two measurements, and hence the reproducibility of the ACP device, was found to be on average 15% of the WVTR value (Table 4.11). Similar deviations were found when doing such tests on other permeation test devices (e.g. Mocon, Brugger), which leads to the conclusion, that - once the resolution of the permeation test device is fine enough (e.g. one order of magnitude below the expected transmission rate), one has to be aware of 10 to 15% of fluctuations when measuring the same sample.

Besides the technical constraints that lead to the lower detection limit and resolution

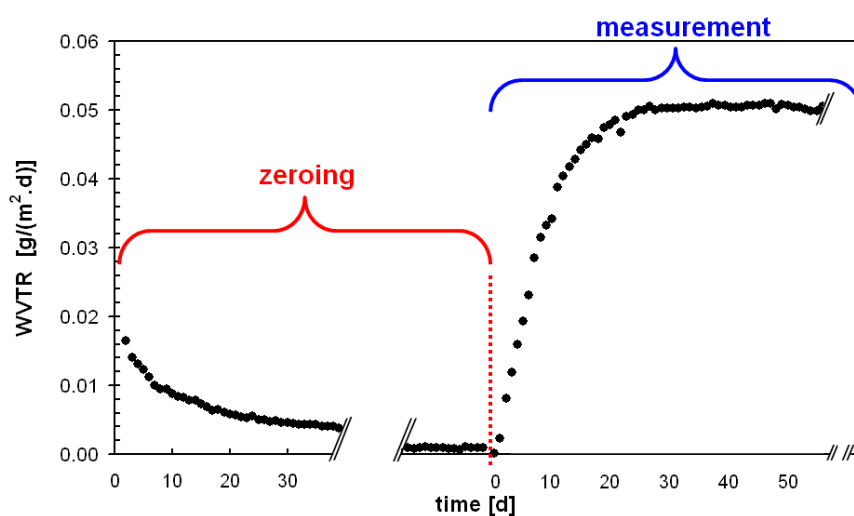


Figure 4.25: Exemplary measurement curve recorded during an ACP test.

4 Experimental methodology

Table 4.11: WVTR results of evaluations concerning the reproducibility of the ACP device.

sample	measurement 1 [g/(m ² d)]	measurement 2 [g/(m ² d)]	deviation from the mean [%]
1	0.1937	0.2387	21
2	0.0613	0.0768	22
3	0.0647	0.0891	32
4	0.0515	0.0772	40
5	0.0124	0.0133	7
6	0.0086	0.0078	10
7	0.0502	0.0472	6
8	0.0527	0.0490	7
9	0.0305	0.0275	10
10	0.0274	0.0257	7
11	0.0302	0.0279	8
			average: ~15%

of a permeation test device, there is another aspect that may introduce an additional error if not handled correctly: the choice of the abortion criterion. For this work, a permeation measurement was stopped when the WVTR value did not change any more - within the chosen accuracy - over a period of 10 days. If the chosen accuracy was $1 \times 10^{-4} \text{g}/(\text{m}^2 \text{d})$, the measurement was stopped when the WVTR increased less than $1 \times 10^{-4} \text{g}/(\text{m}^2 \text{d})$ during the last 10 days of measurement. It is important for the accuracy of the measured WVTR data that the abortion criterion is connected to the WVTR, not to the cumulated amount of permeated water vapor $B(t)$ - and that it is quantitative. Very common in the community are abortion decisions taken by the operator based on visual inspection of the $B(t)$ measurement curve. Yet the $B(t)$ data points represent, mathematically seen, the integrated form of the of the $WVTR(t)$ data points. As integration smoothens data sets, there is a risk to assume a permeation process to be in steady state while it is actually not (Fig. 4.27).

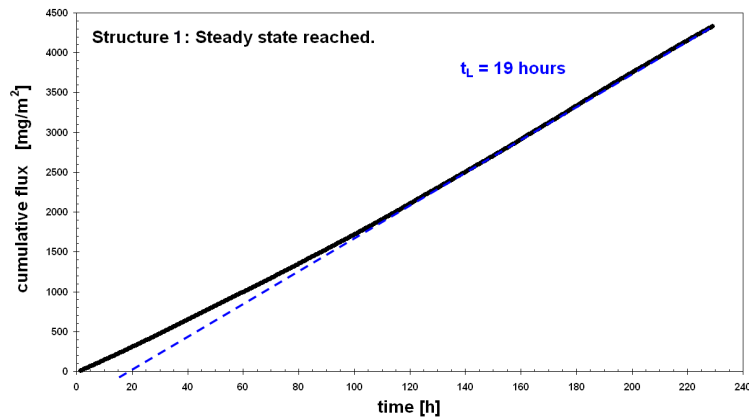


Figure 4.26: Measured $B(t)$ curve of structure 1.

4.4 Experimental methods developed during this work

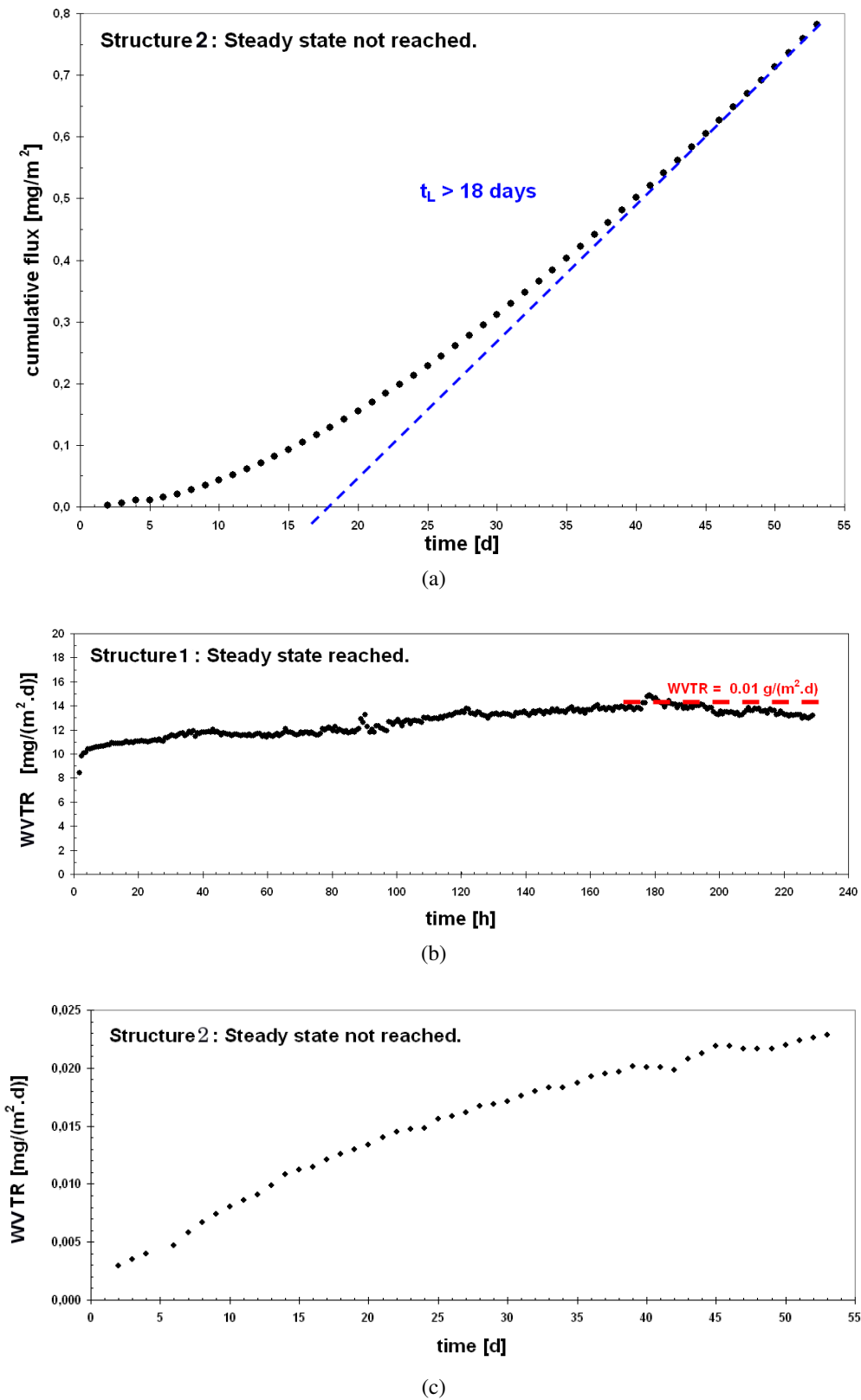


Figure 4.27: According to the measured $B(t)$ curves of structures 1 and 2 (4.26, 4.27a) both water vapor permeation processes seem to have arrived in steady state, while this is actually true only for structure 1 (4.27b) and not for 3 (4.27c).

5 Results and Discussion:

Characterization of barrier materials

For the understanding and improvement of the barrier performance of multilayered encapsulation materials the intrinsic properties of each of the barrier materials were necessary. As few of the required data existed in literature, they were either completed or measured for the first time or derived from combined theoretical-experimental evaluations (all by the author). The results are reported in this chapter.

5.1 Processing and environmental stability of the base substrate

The stability targets that were identified for the base substrate are summarized in Table 5.1:

Table 5.1: Stability targets for the base substrate.

Property	requirement
maximum long term temperature	$\geq \vartheta_{\text{process,max}}$ i.e. ≥ 120 °C
shrinkage after long term temperature	$< 1\%$
tensile strength at high temperature	no dimension change at r2r transport at $\vartheta_{\text{process,max}}$, i.e. ≥ 60 N/(mm ²) at 120 °C or ≥ 100 N/(mm ²) at 23 °C
P_{wv}	$< 4 \times 10^{-13}$ g/(m ² d)
P_{O_2}	$< 6 \times 10^{-17}$ cm ³ (STP)/(m ² d bar)
costs	low cost (cost of entire encapsulation material < 13 €/m ²)
climate stability (1000 h, 65 °C, 90 % RH)	properties changes $\leq \pm 10\%$ ^a
UV stability (750 W/m ² , 35 °C, 0 % RH, 381 h)	properties changes $\leq \pm 10\%$ ^a
mean surface roughness	low, approximately RMS ≤ 1.5 nm

^aImportant properties that should not change more than 10% are in this context: barrier performance, tensile strength at break and elongation at break.

While most targets are of quantitative nature, one criterion was of qualitative nature at the beginning of this work: the requirement for sufficient tensile strength at high temperatures, i.e. for sufficient stability at combined thermal and mechanical stress. For efficient accomplishment of the stability evaluation of the polymer films, i.e. without testing each polymer film in roll-to-roll trials, it is favorable to translate this requirement into a "data sheet number". With this purpose, several polymer films were transported at the lowest possible web tension through the heating section of the pilot plant, applying 120 °C to the web. The results of these trials showed that only polymer films with a tensile strength of at least 60 N/mm² at 120 °C can withstand this treatment without damage. Furthermore, it was found that this correlates to a minimum tensile strength at room temperature of approximately 100 N/mm². (The data of these trials are included in Table 5.3.) Hence, the appropriate substrate should show a tensile strength of either ≥ 60 N/(mm²) at 120 °C or ≥ 100 N/(mm²) at 23 °C.

Now that all requirements were quantified, all typical transparent polymer films were compared to all targets and are summarized in Tables 5.2 to 5.4. The conclusions will now be reported one by one.

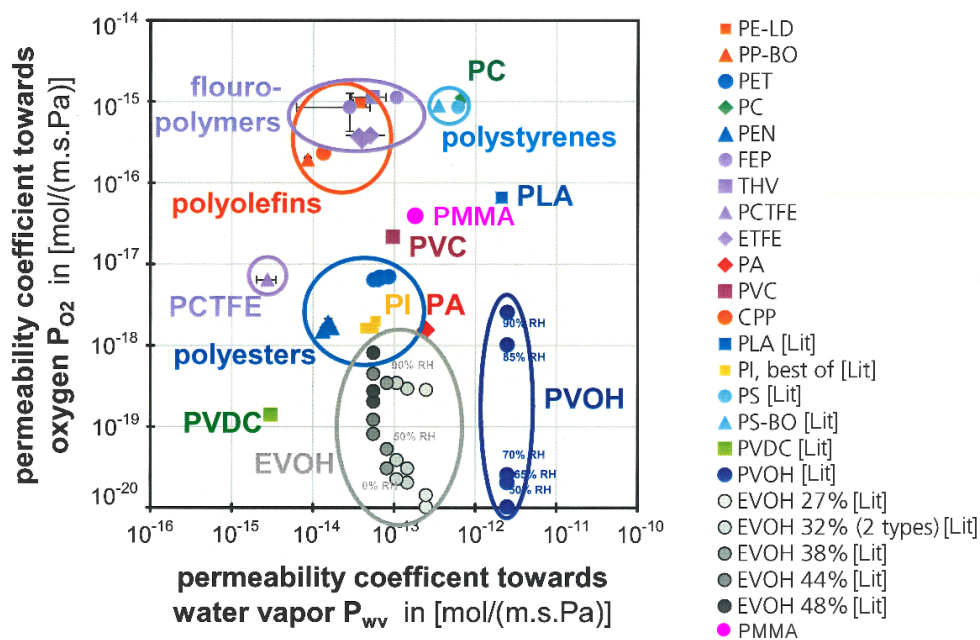


Figure 5.1: Permeability coefficients towards water vapor and oxygen of possible transparent polymer films (comprising 182 results from permeation measurements performed by the author and 91 results from literature [57, 58, 59, 60, 61, 62], the latter indicated with "[Lit]" in the diagram). All diagram points contain error bars in x and y direction, but for many materials they are too small to be seen.

In a multilayered OE encapsulation material so many thin inorganic barrier layers will be contained that the intrinsic barrier performance of the polymer substrate will be negligible. Still, the substrate should have at least medium barrier properties against water vapor ($< 4 \times 10^{-13}$ g/(m² d)) to avoid water vapor permeating into the interface between the

5.1 Processing and environmental stability of the base substrate

Table 5.2: Mean surface roughness (RMS) of selected transparent polyester and fluoropolymer film grades. Marked in green are the polymer films that would fulfill the criterion of sufficiently smooth surface (for more details about this criterion see Chapter 5.2).

Polymer	Film	Film thickness [μm]	Film Producer	RMS [nm]
PET	Melinex 401	50	DuPont Teijin Films	0.5
	RD O	50	DuPont Teijin Films	0.5
	Melinex 400 CW	50	DuPont Teijin Films	0.7-1.3
	Mylar A	50	DuPont Teijin Films	0.9
	GN 4600	50	DuPont Teijin Films	1.1
	Melinex ST 504	125	DuPont Teijin Films	1.3
	Melinex ST 504 7ML	175	DuPont Teijin Films	1.5
	Hostaphan RN	50	DuPont Teijin Films	1.5
	RHB Y	12	DuPont Teijin Films	1.8
PEN	Melinex 807	12	DuPont Teijin Films	4.2
	Teonex Q 51	38	DuPont Teijin Films	2.1
	Teonex Q 51	75	DuPont Teijin Films	2.1
PC	Teonex Q 65 FA	125	DuPont Teijin Films	2.2
	Makrofol	250	Bayer Material Science	2.8
ETFE	Teflon 500 C	130	DuPont Teijin Films	3.2
	Teflon 500 LZ	130	DuPont Teijin Films	4.5
THV	THV 815 G	100	Nowofol	4.3

polymer substrate and the first inorganic layer and degrading the adhesion or the inorganic layer itself. This criterion was fulfilled for PVdC, the polyester films (PEN and PET), PI, PA, PVC, PMMA, the fluoropolymers (PCTFE, ETFE, THV, FEP), the polyolefines (PP and PE), some polystyrenes (Fig. 5.1) and maybe PC. EVOH was not chosen as it has to be protected from water vapor itself in order not to lose its good barrier properties (due to swelling of the network). In this work, the first layer on top of the polymer substrate was never a material sensitive to oxidation, therefore, the criterion of (at least) medium oxygen barrier could be ignored.

Most of these films do not exist with a surface sufficiently smooth for subsequent coating with thin inorganic barrier layers (Table 5.2). In fact, the mean surface roughness (RMS) measurements showed that only some of the PET grades could ensure a good inorganic coating step without taking further measures. Yet the RMS of a substrate could be adapted by adding a planarization coating step, i.e. by coating an organic planarization layer right on top of the polymer substrate before coating it with the thin inorganic barrier layer (see the results of according experiments in Chapter 5.2). So, in case a polymer substrate would otherwise be outstanding in its properties, the RMS should not be a failure criterion.

Some organic barrier materials of this work require drying at 120 °C. It was shown above that sufficient dimensional stability of a polymer substrate would be given if its tensile strength is still 60 N/mm² or higher at this temperature. Only the polyesters (PET,

5 Results and Discussion: Characterization of barrier materials

Table 5.3: Mechanical stability of transparent polymer films, in the order of their tensile strength acc. to [79, 80, 81, 82] and own measurements. Marked in green are the polymer films that would fulfill the criterion of thermo-mechanical stability (tensile strength of either ≥ 60 N/mm² at 120°C or ≥ 100 N/mm² at 23 °C).

Polymer	tensile strength at breakage (in MD) at 25 °C [N/mm ²]	tensile strength at breakage (in MD) at 120 ^a or 150 °C [N/mm ²]
PEN	280	-
PI	72-280	-
PET	60-108 ^a -230	62 ^a
PET ST	183 ^a	102 ^a
PMMA	72-80	-
PC	65-80	approx. 39
PA	approx. 70	16
PS	40-62	-
PVC hard	45-55	-
ETFE	49 ^a	8 ^a
	43-53	-
PP	35	approx. 5
PVC weak	22-35	-
PE-HD	25	0
PE-LD	9	0

^aOwn measurement.

Table 5.4: Thermal stability of transparent polymer films, in the order of their maximum long term temperatures acc. to [79, 80, 82, 83]. Marked in green are the polymer films that would fulfill the criterion of sufficient thermal stability (max. long term temperature at least 120°C and shrinkage after one hour at 130°C < 1%).

Polymer	maximum short term temperature [°C]	maximum long term temperature [°C]	shrinkage after one hour at 130 °C [%]
PI	480	290 to 400	
PEN	-	160-180	-0.11 to +0.37
ETFE	-	150	-3.21 to +3.80
PET	170 to 200	100 to 150	-0.05 to +0.65
PC	135 to 150	100 to 130	
PP	140	100 to 110	
PA	-	71-93	
PE-HD	100	90	
PE-LD	95 to 100	60 to 80	
PMMA	70 to 95	70 to 85	
PS	80 to 90	80	
PVC	70	50 to 60	

5.1 Processing and environmental stability of the base substrate

PEN) and PI were found to fulfill this requirement (Table 5.3). In case only barrier materials (or later: functional layers) would be used that are deposited under less pronounced thermal impact on the substrate, some of the other polymer substrates could be used as well: PA, PMMA and PC could be options. Similar conclusions were drawn with respect to the maximum long term temperature and the shrinkage after long term temperature (Table 5.4).

Yet PA or PC are neither sufficiently stable against high temperature and humidity nor against UV light: Table 5.5 shows the results of the climate test on PA film: it was found to become brittle, accompanied by the entire loss of its good barrier performance. Transparent polymers that are known to be very resistive are all fluoropolymers, PI and PEEK - according to experiments they showed no loss of barrier performance for ETFE (within the tolerance of the measurement, Table 5.6). The polyester films (PEN and PET) show a fair stability, accompanied by only a small loss of intrinsic barrier properties (Tables 5.5, 5.6). Depending on the targeted lifetime of the OE product (i.e. on the time span of exposure), this performance can either be accepted or has to be improved. There are several ways of improving UV degradation in plastics: by using stabilizers, absorbers or blockers. Yet, it has to be kept in mind that the most common (because low cost) carbon or titanium dioxide absorbers cannot be used as they would decrease transparency. Furthermore, so far, there are no polyester films commercially available that are stabilized enough for targeted lifetimes longer than two to three years. Hence, additional UV protective layers would have to be coated on top when using PET as a substrate.

From the technological point of view, four types of polymer films were identified to be potential substrates for OE encapsulation materials: PEEK, PI, polyesters and PMMA (Table 5.7) - PMMA only under the constraint that all process steps (of the entire process chain of the OE product, not only of the fabrication of the OE encapsulation material) would take place at moderate temperatures. From the remaining three, the polyester ma-

Table 5.5: Climate stability of selected transparent polymer films. Marked in green are the polymers that would fulfill the criterion of sufficient climate stability (no material property changes significantly, i.e. more than $\pm 10\%$).

Polymer film		tensile strength at break [N/mm ²]	elongation at break [%]	OTR 23/50 [cm ³ (STP)/(m ² d bar)]	WVTR 23/85 [g/(m ² d)]
ETFE (200 μ m)	O ^a	46 \pm 1	544 \pm 9	329 \pm 22	0.74 \pm 0.04
	T ^b	45 \pm 2	541 \pm 30	359; 337	0.98; 0.71
PEN (85 μ m)	O	183 \pm 10	93 \pm 17	3.8 \pm 0.1	0.74
	T	188 \pm 8	90 \pm 11	3.9; 4.0	0.74; 0.68
PET (50 μ m)	O	252 \pm 7	132 \pm 8	26 \pm 2	4.8 \pm 0.9
	T	253 \pm 8	122 \pm 9	27.5; 20.0	4.3
R ^c PA 6 (15 μ m)	O	251 \pm 26	103 \pm 18	20.1	60.3 \pm 0.5
	T	112 \pm 17	17 \pm 5	692	87.7; 72.6

^aO ... Original film.

^bT ... Treated for 1000 hours at 65 °C, 90 % RH.

^cR ... Reference material known to be not stable, measured in parallel to quantify "bad climate stability".

5 Results and Discussion: Characterization of barrier materials

Table 5.6: UV stability of selected transparent polymer films. Marked in green are the polymers that would fulfill the criterion of sufficient UV stability (no material property changes significantly, i.e. more than $\pm 10\%$).

Polymer film		tensile strength at break [N/mm ²]	elongation at break [%]	OTR 23/50 [cm ³ (STP)/(m ² d bar)]	WVTR 23/85 [g/(m ² d)]
PCTFE (102 μ m)	O ^a	46 \pm 3	337 \pm 31	17.8	0.07
	T ^b	46 \pm 5	338 \pm 68	18.3	0.01
ETFE (200 μ m)	O	52 \pm 2	613 \pm 33	329 \pm 22	0.74 \pm 0.04
	T	52 \pm 2	602 \pm 31	314; 316	0.79
PEN (85 μ m)	O	232 \pm 9	142 \pm 9	3.8 \pm 0.1	0.74
	T	179 \pm 6	74 \pm 9	-	0.83
PET (50 μ m)	O	252 \pm 7	132 \pm 8	26 \pm 2	4.8 \pm 0.9
	T	99 \pm 5	6 \pm 1	17.7 18.9 16.5 ^c	3.8 ^c
R^d PE-LD (70 μ m)	O	18 \pm 3	492 \pm 77	2647 \pm 160	2.0 \pm 0.4
	T	9 \pm 1	9 \pm 2	234 1750 ^c	1.7 1.4 ^c

^aO ... Original film.

^bT ... Treated for 381 hours at 100% UV, 35 °C, 0 % RH.

^cImproving barrier performance despite mechanical degradation could be the result of recrystallization processes within the polymer - as reported for PET or PE [138].

^d**R** ... Reference material known to be not stable, measured in parallel to quantify "bad UV stability".

Table 5.7: Ranking of potential transparent polymer substrates with respect to the properties required for an OE encapsulation material.

Polymer type	Process stability	Mean surface roughness	Climate / UV stability	Gas barrier	Costs	$\sqrt{\text{in total}}$
polyesters	$\sqrt{\sqrt{}}$	$\sqrt{}$	$\sqrt{(\sqrt{)}}$	$\sqrt{}$	$\sqrt{}$	6-7
PI	$\sqrt{\sqrt{}}$	-	$\sqrt{\sqrt{}}$	$\sqrt{}$	-	5
PEEK	$\sqrt{\sqrt{}}$	-	$\sqrt{\sqrt{}}$	$\sqrt{}$	-	5
PMMA	$(\sqrt{\sqrt{)})}$	-	$\sqrt{\sqrt{}}$	$\sqrt{}$	$(\sqrt{)}$	3-6
PA	$\sqrt{\sqrt{}}$	-	-	$\sqrt{}$	$\sqrt{}$	4
fluoropolymers	- $(\sqrt{)}$	-	$\sqrt{\sqrt{}}$	$\sqrt{}$	-	3-4
PC	$\sqrt{(\sqrt{)}}$	-	-	$\sqrt{}$	$(\sqrt{)}$	3-4
PVdC	-	-	$\sqrt{(\sqrt{)}}$	$\sqrt{}$	-	2-3
polyolefins	-	-	-	$\sqrt{}$	$\sqrt{}$	2
PVC	-	-	-	$\sqrt{}$	$\sqrt{}$	2
PS	-	-	-	$\sqrt{}$	$\sqrt{}$	2

materials, especially the PET films, are the best compromise between performance and costs (Table 5.8). It cannot be ignored that one of the main drivers for the rising interest in OE products is their ability to be roll-to-roll processed, i.e. to be fabricated at (comparatively) low processing costs. As the selection of the polymer substrate should not counteract or erase this benefit, polyester films were preferred towards PI or PEEK films. Concerning

Table 5.8: Costs per kilogram transparent polymer pellets as an average over 2008-2011 according to [84]. Marked in green are the polymers that would fulfill the low cost criterion.

Cost range	Transparent polymer
< 1.50 €/kg	PVC, PET, PP, PE-LD, PE-HD, PS
< 3.00 €/kg	PA 6, POM, PMMA, PC, PBT
< 7.00 €/kg	EVOH, PEN (approx. 5 times PET)
>> 7.00 €/kg	PI (approx. 15*PET), PEEK (approx. 600*PET)

the choice between PEN and PET, PET would be more suited for short living outdoor OE products while PEN films would resist somewhat longer. For this work, PET was used for all test fabrications of OE encapsulation materials.

5.2 Process constraints for thin inorganic layers

Is the surface of the polymer substrate too rough, undesired effects (like shadowing) occur during the inorganic coating step that decrease the intrinsic barrier performance of the inorganic layer. It was necessary for this work to clarify to which extent a thin Ormocer[®] layer could work as planarization.

For this study, a thin inorganic barrier layer which would not require a plasma pre-

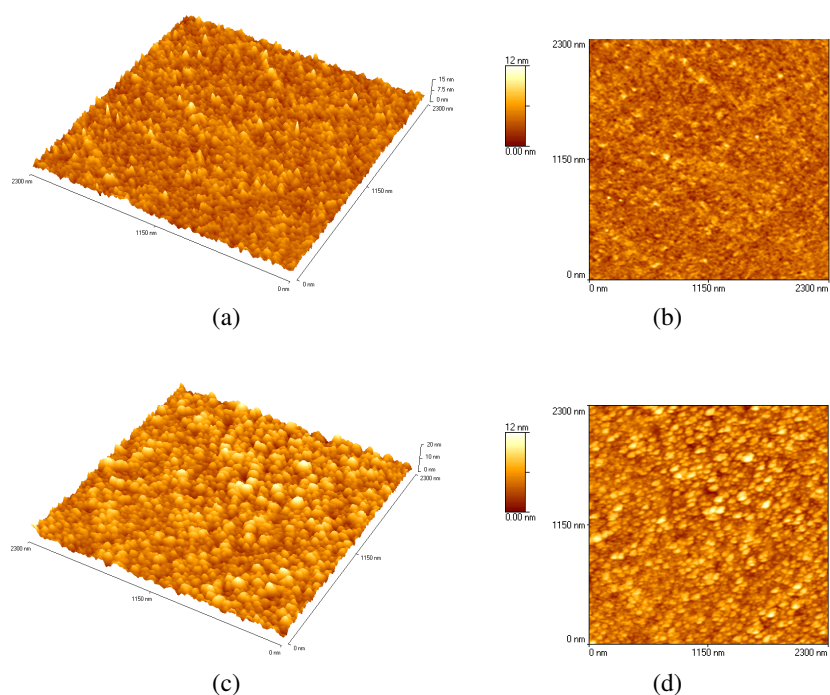


Figure 5.2: AFM pictures of a smooth substrate (a,b) coated with a 100 nm $ZnSn_xO_y$ layer (c,d). These AFM measurements were performed by *Fraunhofer FEP*.

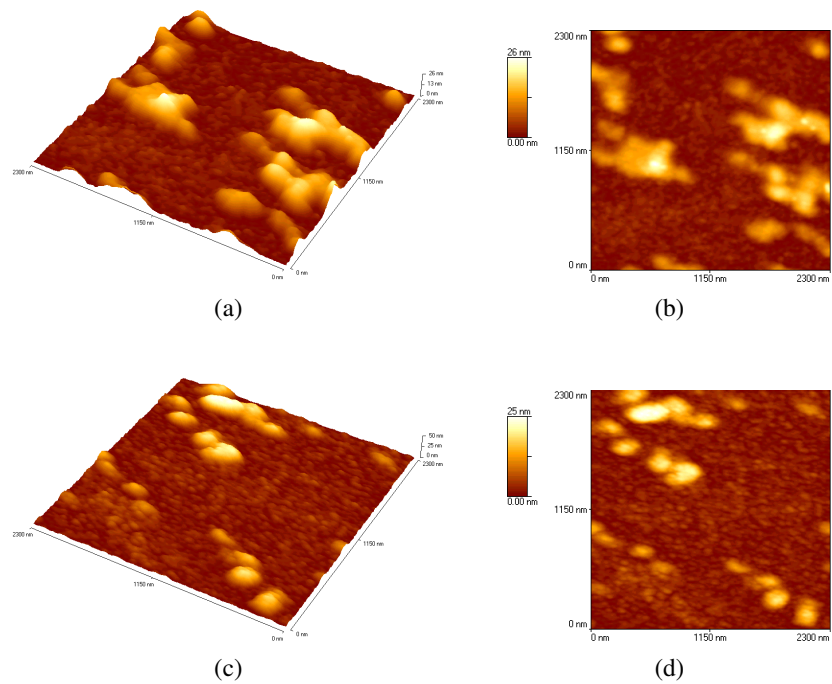


Figure 5.3: AFM pictures of a rough substrate (a,b) coated with a 100 nm ZnSn_xO_y layer (c,d). These AFM measurements were performed by *Fraunhofer FEP*.

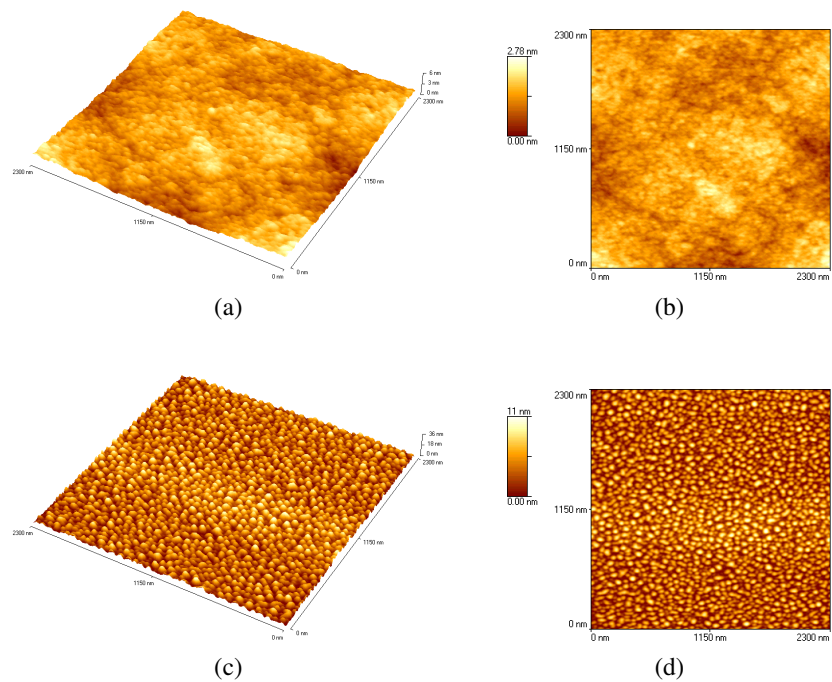


Figure 5.4: AFM pictures of a rough but planarized substrate (a,b) coated with a 100 nm ZnSn_xO_y layer (c,d). These AFM measurements were performed by *Fraunhofer FEP*.

treatment of the substrate (in order not to change the surface roughness and the AFM results), namely a 100nm ZnSn_xO_y layer, was deposited on top of three different substrates: on a smooth one with an average surface roughness R_a of approximately 0.8 nm (Fig. 5.2a, 5.2b), on a rough one with an average surface roughness R_a of 1.7 to 3.8 nm (Fig. 5.3a, 5.3b) and on the same rough substrate planarized with a thin Ormocer[®] top coat having an average surface roughness R_a of approximately 0.3 nm (Fig. 5.4a, 5.4b).

The AFM measurements show clearly that the thin inorganic barrier layer is almost exactly a copy of the underlying surface: the average surface roughness R_a of the ZnSn_xO_y layer on top of the smooth substrate is 0.2 to 0.7 nm (Fig. 5.2c, 5.2d), on the rough substrate 1.4 to 4.5 nm (Fig. 5.3c, 5.3d) and on the planarized substrate 1.1 to 1.6 nm (Fig. 5.4c, 5.4d). They furthermore show that it was very effectful to use a thin Ormocer[®] layer for planarization: in this case, the surface roughness of the rough, but planarized substrate was even a littler bit smoother than the one of the smooth substrate.

Another important aspect of thin inorganic barrier layers is their brittleness, leading to cracks in the layers if too much mechanical (tensile) stress is applied. Previous studies identified a critical strain of 0.9% for standard polyester substrates (1.4% for heat stabilized polyester substrates) at which cracks would start to be visible in light microscopy [139, 140]. For this work, it was necessary to clarify at which process parameters shrinkage above the critical strains could be avoided. With this purpose, the shrinkages of various thin inorganic barrier layers on top of polyester films were measured that had been exposed for 5 minutes to temperatures between 60 and 140 °C.

According to the results of these measurements, the two most important parameters that influence the shrinkage are the thickness of the substrate and of the thin inorganic barrier layer. Here, with increasing substrate thickness, the shrinkage increases (Fig. 5.5)

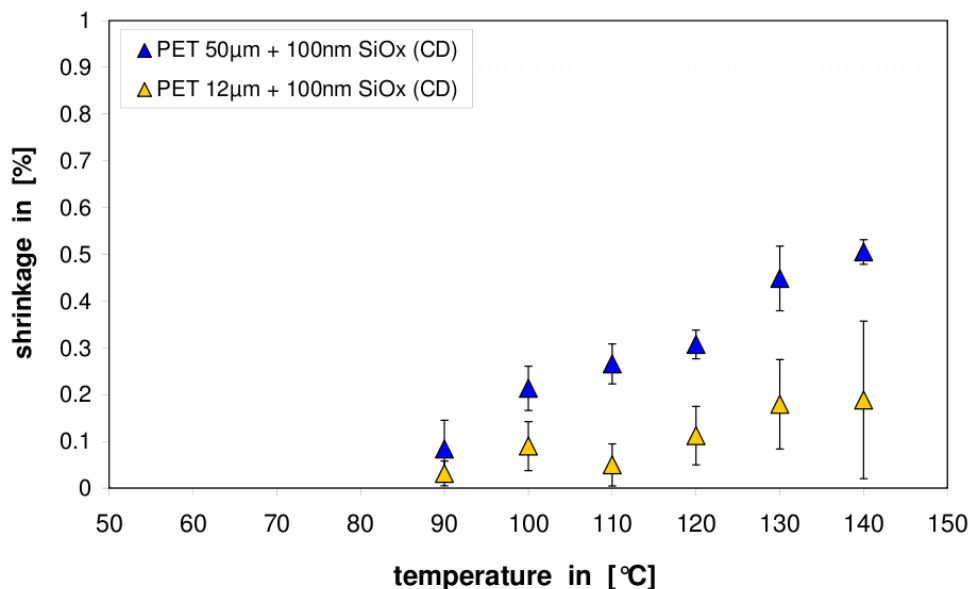


Figure 5.5: Shrinkage of PET films with thin inorganic barrier coatings in dependency of the substrate.

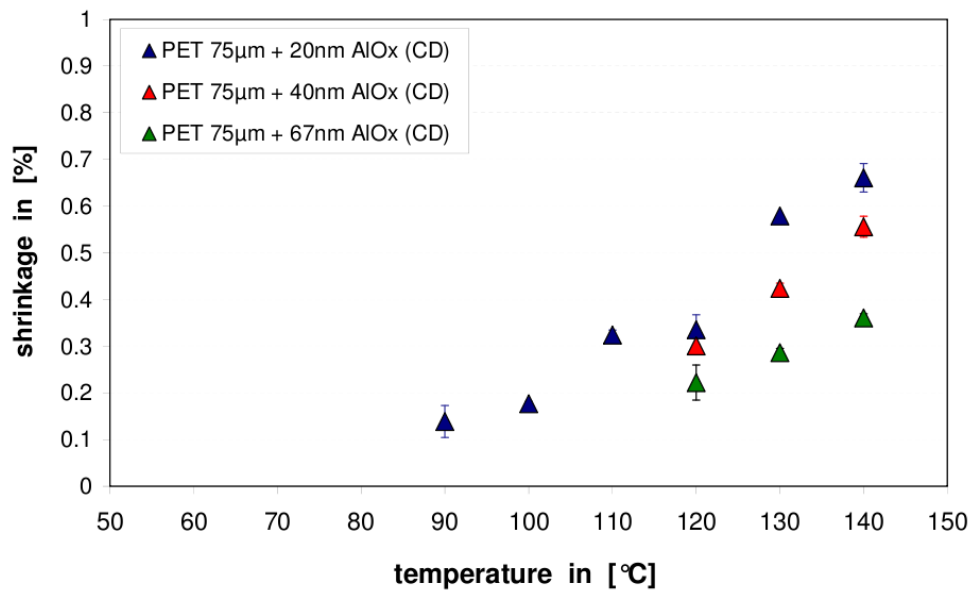


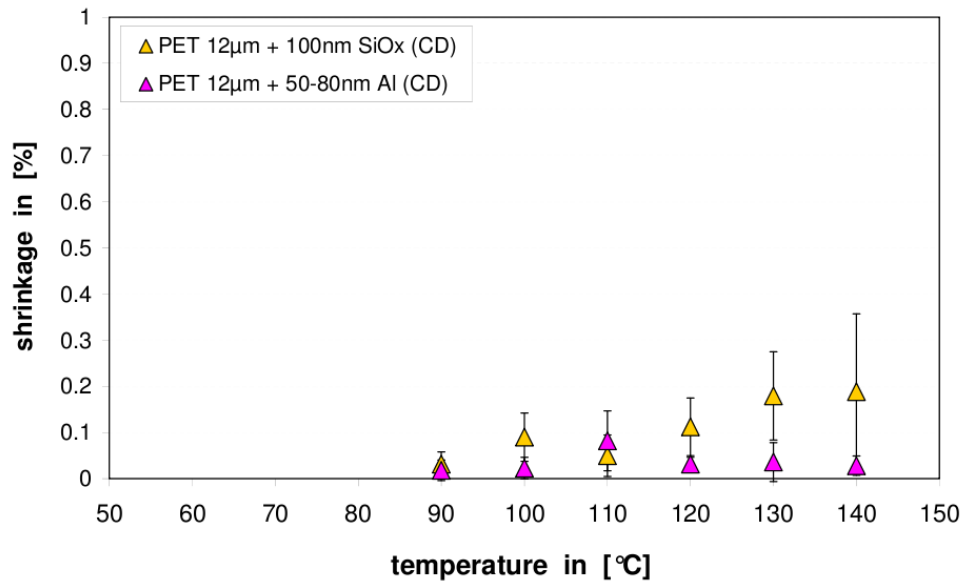
Figure 5.6: Shrinkage of PET films with thin inorganic barrier coatings in dependency of the layer thickness.

which seems to be the contrary to what should be expected [141]. In fact, the rule that increased substrate thickness leads to lower shrinkage only applies for films produced in the same machine [142], i.e. produced under the same conditions at the film supplier. Obviously, this was not the case for the two films tested here, the 50 µm PET film did undergo more stretch during the film production [142].

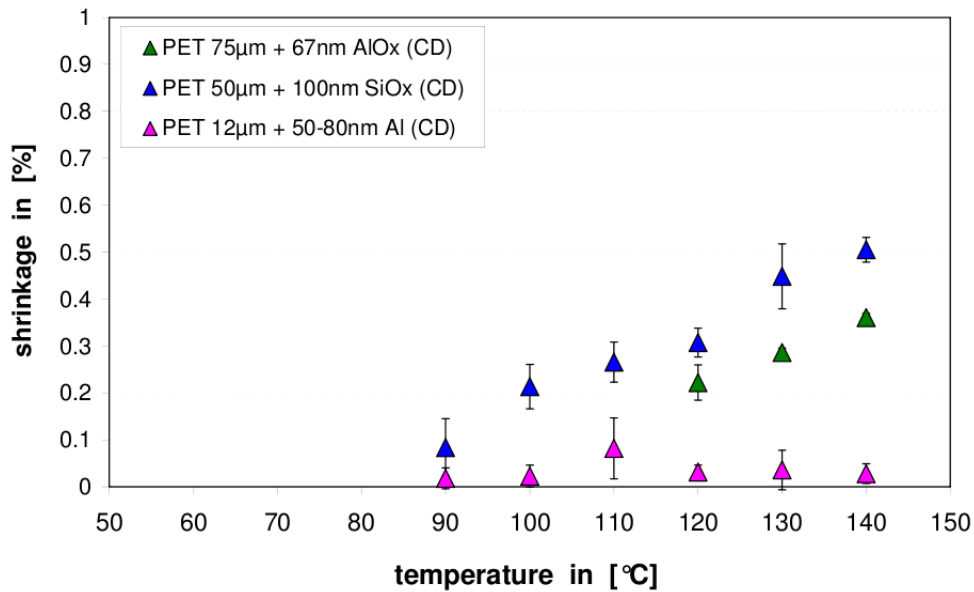
Increasing thickness of the thin inorganic barrier layer leads to a decrease in shrinkage (Fig. 5.6) which is consistent with previous studies [143]. The reason is the transfer of a part of the deformation energy to the inorganic material. The thicker the inorganic layer, the more deformation energy it can absorb.

Comparing different inorganic materials, thin SiO_x coatings are less resistive to shrinkage than thin aluminum coatings (Fig. 5.7a) and thin AlO_x coatings (Fig. 5.7b), despite even thicker layer thickness. Hence, the nanoscale hardnesses of these three inorganic coating materials are increasing in the order SiO_x , AlO_x , aluminum. This is consistent with the results of the nanoscale hardness measurements of thin SiO_x and AlO_x coatings being 5 and 10 GPa, respectively [144].

Finally, the film that had shown the highest shrinkage in lab scale, i.e. the 75 µm PET film with 20 nm AlO_x coating, was exposed during roll-to-roll trials in the drying section of the the pilot plant to the same temperatures. The rolls fabricated this way in the pilot plant showed a higher shrinkage than the samples fabricated at lab scale (Fig. 5.8), because the heat transfer is higher in the pilot plant (heat convection from the turbulent flow of heated air) than in the laboratory oven (thermal radiation from the oven walls and heat conduction in the steady air in the oven). No difference in the shrinkage can be seen between the roll-to-roll samples fabricated at web speeds of 3 and 6 m/min, respectively (Fig. 5.8) which is the result of an only marginal difference between the according drying periods of 1.3 min and 1.5 min, respectively.



(a)



(b)

Figure 5.7: Shrinkage of PET films with thin inorganic barrier coatings in dependency of type of inorganic material.

Up to the highest potential drying temperature of 140 °C the shrinkage of this film remained below the recommended 0.9%, where no crack was visible in light microscopy. However, in scanning electron microscopy, finer cracks can be seen and they occur already at 0.3 % shrinkage (Fig. 5.9, second picture).

Previous studies showed at 1 % shrinkage already an increase of transmission rate of +11 % on average for thin SiO_x layers and of +70 % on average for thin AlO_x layers

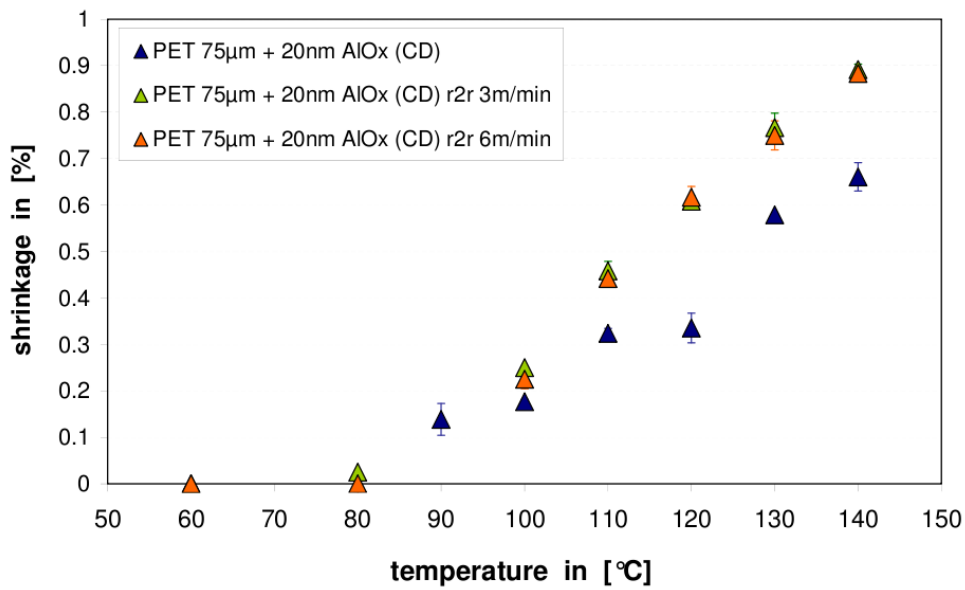


Figure 5.8: Shrinkage of PET films with thin inorganic barrier coatings exposed to high temperatures in the pilot plant.

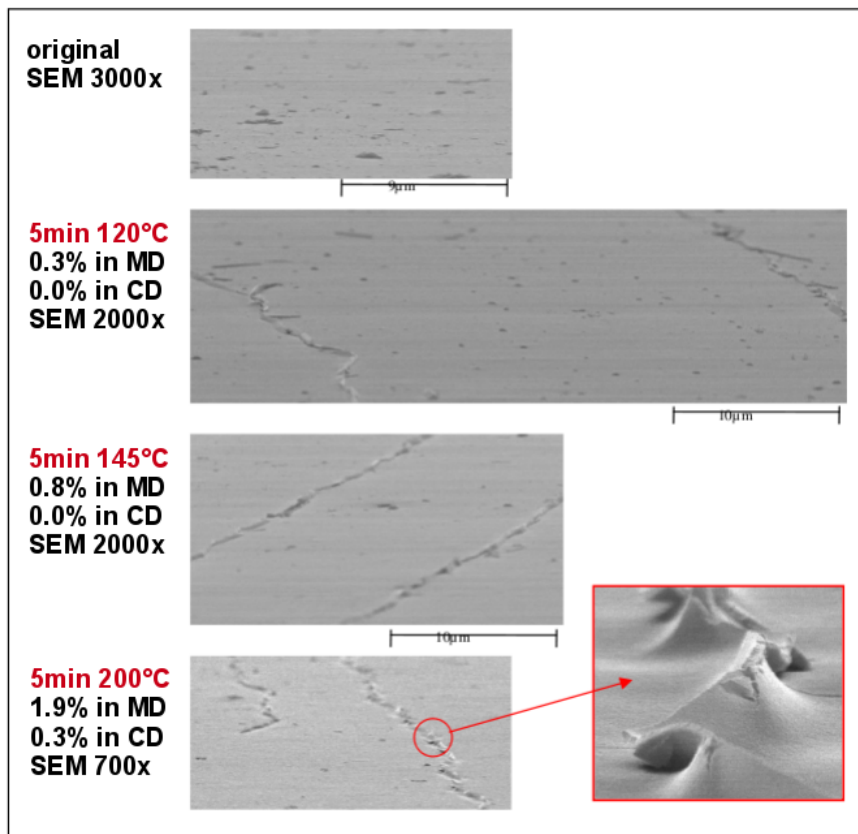


Figure 5.9: SEM evaluations of the shranked samples (Fig. taken from [63]).

[145]. This high barrier loss implies revising the recommendations given on maximum shrinkage of thin inorganic layers: 0.9 % shrinkage is already too much when trying to keep the original barrier level of thin inorganic barrier layers; and it is not clear whether 0.3 % or a higher value should be taken as critical limit instead. In future, with respect to avoiding barrier relevant defects, deformation checks have compulsorily to be made by SEM (not light microscopy alone).

In general, four strategies to avoid damage of the thin inorganic barrier layers by shrinkage can be derived from these trials: reduction of the temperatures applied during the encapsulation and OE production processes (and reduction of the time spans during which these temperatures are applied), increase of the thickness of the polymer substrate (but check different film types and suppliers in order to avoid opposed effects), increase of the thickness of the inorganic coating and selection of a thin inorganic barrier coating showing low nanoscale hardness.

5.3 Barrier performance of thin organic layers

At the beginning of this work, permeation data of organic coatings were scarce (one single source only: [58]) and the knowledge about which type of organic coatings could possibly be a potential barrier material was not existing. Therefore, a screening of organic coating materials was performed that tried to represent all categories of lacquers and adhesives.

For this work, categorization was done according to the hardening process (Fig. 5.10), because the hardening process was expected to have a great influence on the intrinsic barrier performance of the coatings. There are two main classes:

- **Physically hardening lacquers** and adhesives are on application already present in their final chemical state. They are either liquefied polymers that have to be dried from the solvents or they are poorly cross-linked elastomers with a high ability to swell that are solidified by either heating or cooling after application. Physically hardening lacquers or adhesives typically show good bond flexibility [64, 65, 66].
- **Chemically hardening lacquers** and adhesives are applied in a preliminary chemical state, either liquid or thermoplastic, and transform via chemical reaction into a solid. They typically ensure a high bond strength and good resistance against high temperatures and humidity or chemicals [64, 65, 66].

Based on these two main classes six chemical sub-classes exist: water based, organic solvent based, hot melt, one component chemical hardening (1C), two component (2C) chemical hardening and hybrid-type lacquers or adhesives (Fig. 5.10). Plastics were not included (and not tested), because their processing temperatures of 160 to 180 °C would anyway be too high compared to the thermal stability of polymer substrates (Table 5.4). Pressure sensitive adhesives are included according to their hardening process during first preparation (not according to their final adhesion due to pressure). In total, 49 lacquers and adhesives were tested (Table 5.9). The attribution of these 49 materials to the categories was done according to their chemical structure identified from IR-/Raman-spectroscopy.

It was found that the water vapor permeability coefficients of organic coatings range from 10^{-15} to 10^{-11} mol/(m s Pa) and that the oxygen permeability coefficients of organic

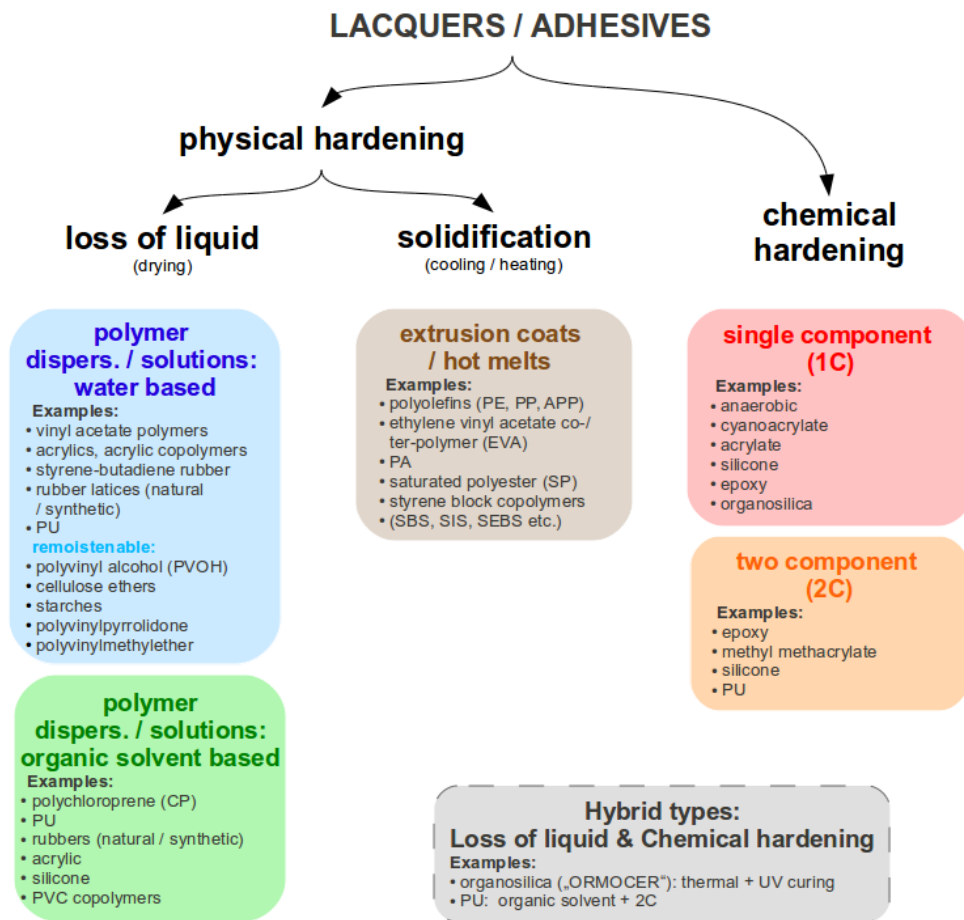


Figure 5.10: Lacquers and adhesives categories, following [64, 65, 66].

coatings range from 10^{-19} to 10^{-15} mol/(m s Pa) (Fig. 5.11). As these are exactly the same ranges that are covered by the permeability coefficients of polymer films [59], the notation regarding “very good barrier“, “good barrier“ etc. is adopted (and included in Fig. 5.11). Staying with this notation, in the following, an organic “barrier“ material will be called an organic “barrier“ material if its intrinsic permeability coefficient is good or very good, i.e. if its oxygen permeability coefficient is $< 6 \times 10^{-18}$ mol/(m s Pa) and its water vapor permeability coefficient is $< 6 \times 10^{-14}$ mol/(m s Pa).

Furthermore, it turned out that the distribution of permeability coefficients of organic coating materials over the whole scale is different for water vapor and oxygen. For water vapor, the majority of materials have a permeability coefficient between 2×10^{-14} and 2×10^{-13} mol/(m s Pa), i.e. they show medium to good intrinsic water vapor barrier (Fig. 5.11a). The barrier performance against water vapor of low-cost adhesives and lacquers, as to be found in do-it-yourself-stores, and of more industrial, high-end formulations are not laying far apart. The best intrinsic water vapor barriers are shown by PVdC dispersions, the poorest intrinsic water vapor barriers are shown by biopolymer-based coating materials. For oxygen, the permeability coefficients of the same 49 organic materials are distributed more equally over the whole scale (Fig. 5.11b). However, for all levels of intrinsic oxygen barrier, from “poor“ to “very good“, examples for organic coating mate-

Table 5.9: Lacquers and adhesives tested in this study.

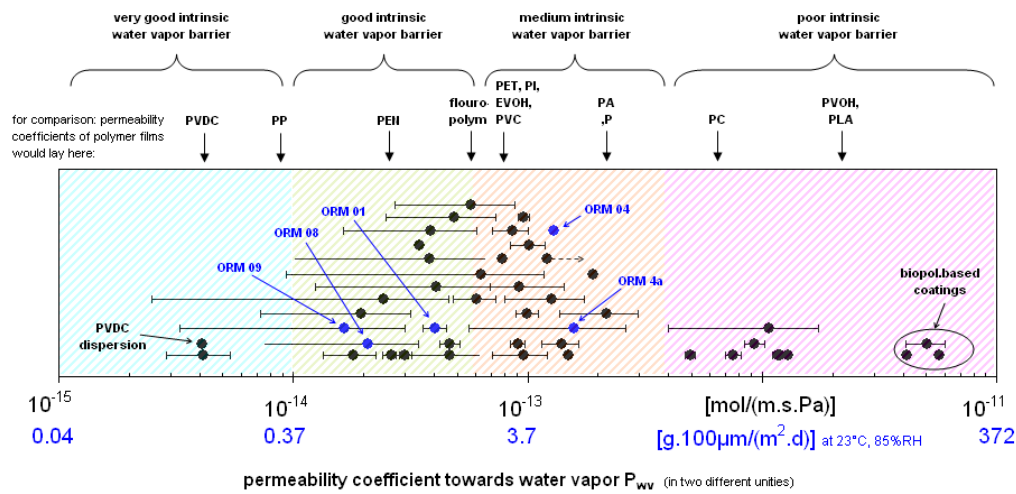
Category		Coating material
Physical hardening		
polymer dispersion / emulsion	acrylate	C1.2, C1.3, C1.4, C1.5
	acrylate-wax	C1.1
	PU-acrylate	C1.6, C1.7, C1.8
	PVdC	C1.9
	polyolefin: PE	C1.16
	PVOH	C1.14, C1.15
	modified starch	C1.12, C1.13
organic solvent based	acrylate	C2.2, C2.3
extrusion coatings	polyolefin: PE	C3.1
	polyolefin: PP	C3.2
	PLA blend	C3.5
	PLA blend	C3.6
	styrene block copolymer	A3.1
	starch-PCL-copolymer	C3.7
	starch-PCB-copolymer	C3.8
Chemical hardening		
1C	acrylate	C5.1, A5.1, A5.2, A5.8, A5.9, A5.10
	epoxy-acrylate	C5.2
	epoxy	A5.3, A5.4, A5.5, A5.6, A5.7
	organosilica ^a	C5.3, C5.4, C5.5, C5.6, C5.7, C5.9
	PU-acrylate-silica ^a	C5.8
	PU	C5.10
2C	epoxy-PU	C6.1
	PU	C6.2, C6.3, C6.4, A6.1, A6.2

^aThe names “organosilica“ or “xxx-silica“, respectively, are used as abbreviations for members of a group of organic coating materials that consist of a hybrid network that includes both inorganic network parts (resulting from silanol condensation) and organic (especially “xxx”) network parts.

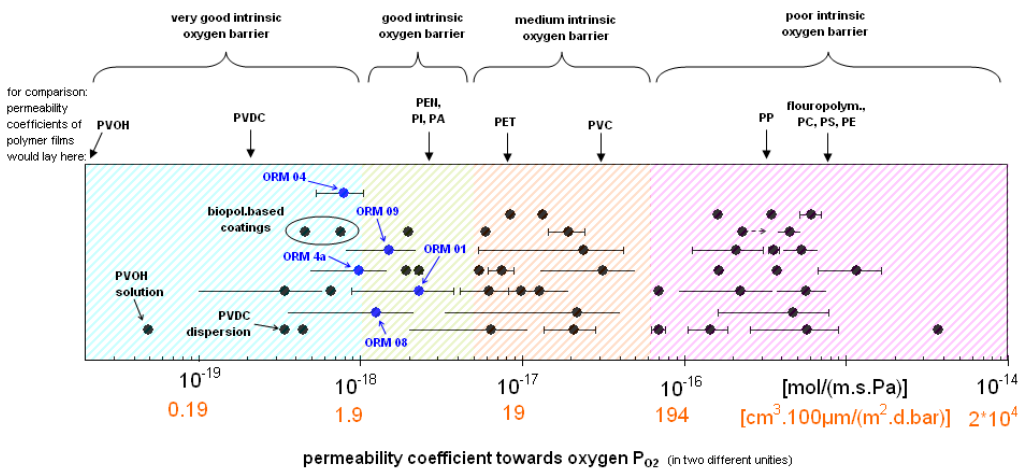
rials exist, and it is no longer unimportant whether it was a low-cost mass product of a do-it-yourself-store or an industrial, high-end product: the industrial products show much better intrinsic oxygen barrier. The best intrinsic oxygen barriers are shown by PVOH, PVdC or biopolymer-based coating materials, the poorest intrinsic oxygen barriers are shown by polyolefin-based coating materials. The Fraunhofer Ormocer[®] lacquers - while having only some intrinsic water vapor barrier for certain types - show throughout good to very good intrinsic oxygen barrier (marked in blue in Fig. 5.11).

If the transmission rate data both for oxygen and water vapor are combined in one diagram (Fig. 5.12), three clusters appear: one (roughly) along the diagonal, one in the upper left corner and one in the lower right corner. Most organic coating materials were found

5 Results and Discussion: Characterization of barrier materials



(a)



(b)

Figure 5.11: Average and standard deviation of permeability coefficients towards water vapor (a) and oxygen (b) of 49 possible transparent organic / hybrid coating materials (comprising 620 results from permeation measurements performed by the author and 2 results from literature [58]. The position of the data points in y direction is chosen arbitrarily for better visibility.)

to belong to the largest cluster along the diagonal, showing a typical ratio of water vapor permeation to oxygen permeation of approximately 10000 : 1. Hence, this difference of four orders of magnitude is concluded to be typical for organic coating materials, at whatever intrinsic barrier level (along the diagonal) they are (for explanation see Section 2.1 about the extraordinary permeation properties of water vapor). To shift an organic coating material (roughly) along this diagonal, it is necessary to improve its structural, network-density-dependant barrier properties.

The cluster above the diagonal contains organic coating materials that show an improved water vapor barrier towards oxygen barrier compared to the typical ratio. Highly

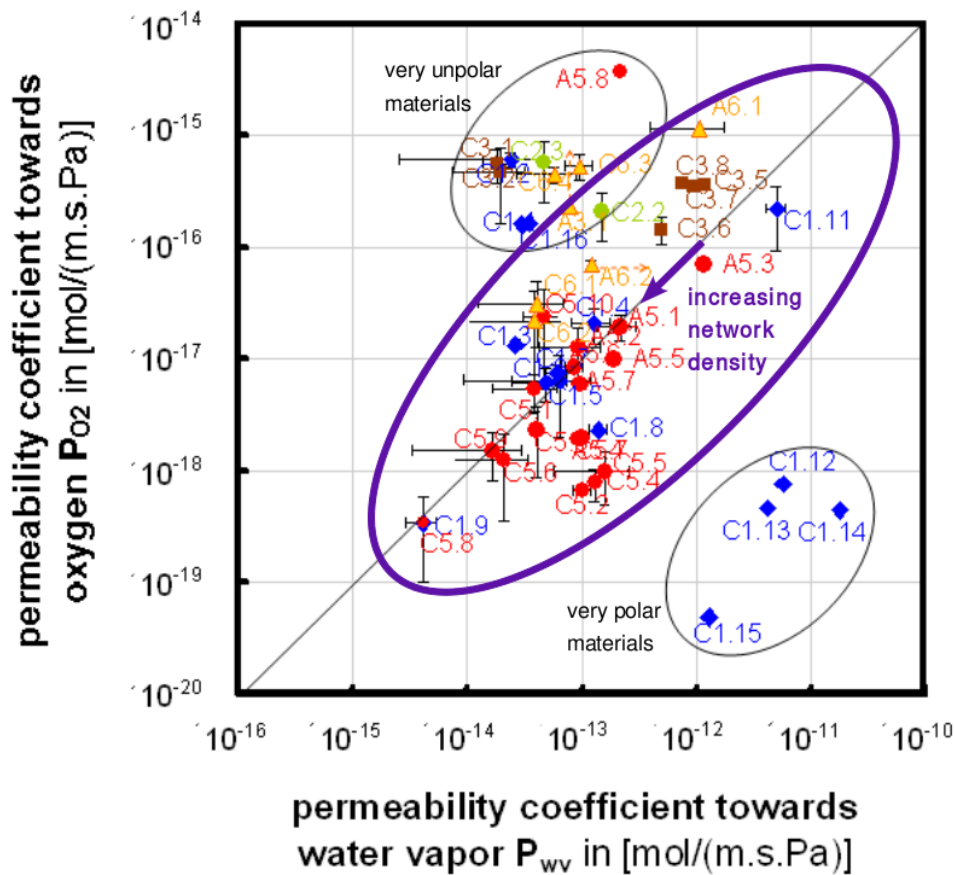


Figure 5.12: Permeability coefficients towards water vapor and oxygen of 49 possible transparent organic coating materials (comprising 614 results from permeation measurements performed by the author and 2 results from literature [58]). Most diagram points contain error bars in x and y direction, but for some materials they are too small to be seen.

non-polar materials, like polyolefin based coating materials (C1.16, C3.1, C3.2), belong to it. The cluster below the diagonal contains organic coating materials with improved oxygen barrier towards water vapor barrier compared to the typical ratio. Highly polar materials, like starch-based biopolymer coatings (C1.12, C1.13) or PVOH-based coating materials (C1.14, C1.15), belong to it.

The colors of the data points in Fig. 5.12 refer to the colors in Fig. 5.10, i.e. to the classification of the organic material. From the random distribution of all classes over the whole diagram, it can only be concluded that either there is no relationship between classification of the organic coating materials and their intrinsic barrier performance or (more likely) the base of information about the chemical structure of the organic coating materials was just too sparse (resulting from the fact that FTIR and Raman analyses on "black box" organics can just deliver very rough information).

From the worst to the best organic material along the diagonal in Fig. 5.12 the permeability coefficient improves by approximately a factor of 1000 (3 orders of magnitude). However, as the thin inorganic barrier layer dominates the overall barrier performance, it

depends on its barrier quality how much of the barrier improvements on the organic layers will eventually improve the overall barrier performance.

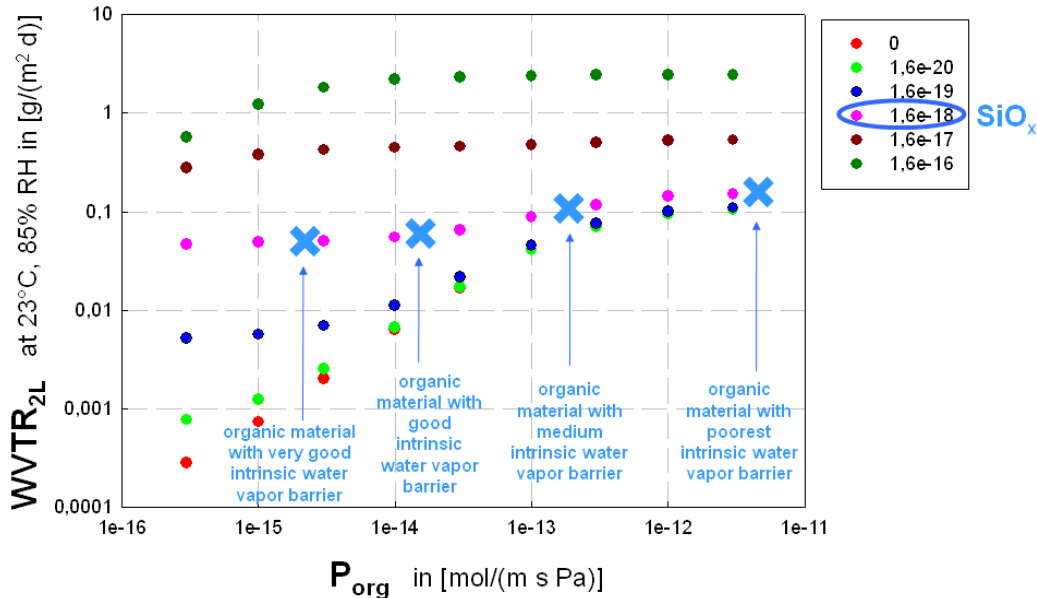


Figure 5.13: Water vapor transmission rate of the structure [thin inorganic barrier layer + organic top coat]¹ for varying permeability coefficients of the organic top coat, in dependence of the permeability coefficient of the inorganic bulk (Fig. modified from [14]).

For example, even the use of a 1000 times improved organic coating material would still improve the overall water vapor transmission rate of the structure [thin inorganic barrier layer + organic top coat]¹ only by a factor of four to five, if the typical SiO_x layer of this work was used as inorganic layer (see blue crosses in Fig. 5.13). The same is true for intrinsic barrier improvements one could gain for the organic layer by bringing the curing process to perfection (for more details see Appendix A1).

Besides, it has to be kept in mind that the intrinsic steady-state barrier performance of organic coating materials is not the only important criterion for their suitability for the assembly of multilayered encapsulation materials. Further criteria are their time-dependant barrier (time lag), additional barrier effects when combined with inorganic layers, their wetting, their adhesion and their long-term mechanical, thermal and chemical stability. These issues are not secondary. In many cases they become so important that an organic coating material has to be used which has a lower intrinsic barrier performance, but fits these other criteria much better. Hence, it is not sufficient to study the intrinsic barrier performance alone, but also the performance of inorganic / organic barrier materials with respect to these criteria (details in Chapters 6, 7 and Appendices A1, A2, A3).

¹The polymer substrate, which would anyway have only negligible influence on the WVTR of the structure [polymer substrate + thin inorganic barrier layer + organic top coat] was omitted to reduce the calculation effort.

6 Results and Discussion: Barrier effects resulting from the combination of different layers

6.1 Synergistic barrier effect

After coating a thin inorganic barrier layer with an organic or hybrid top coat, the barrier performance of this combination may exceed the expectations based on the intrinsic barrier performances of its layers (Chapter 3). For the evaluation of the occurrence and quantity of this synergistic barrier effect ¹, three from the 49 organic coating materials were selected to be coated on inorganic barrier layers. Their data points are highlighted in red in Fig. 6.1.

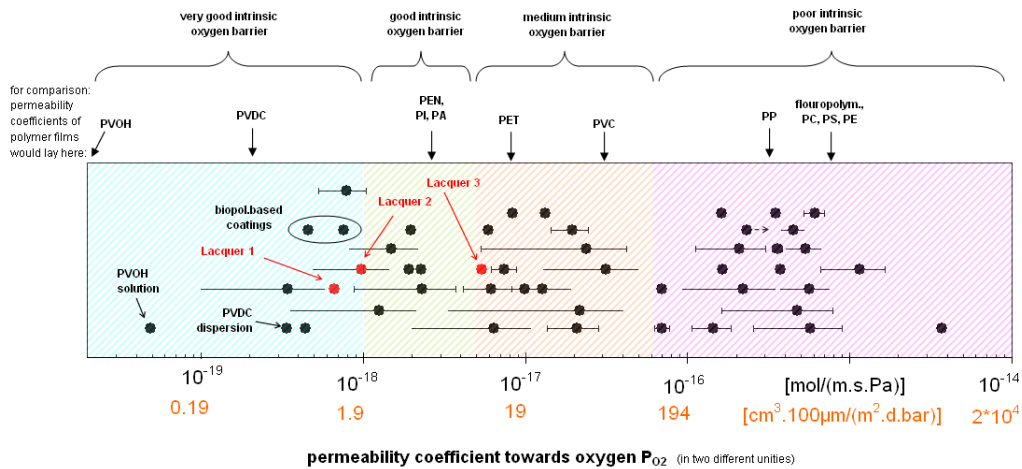
Lacquer 2 was studied as reference material, because its synergistic barrier effect to thin inorganic (SiO_x) coatings was reported previously [40]. Lacquer 1 was studied additionally, because its intrinsic oxygen barrier is better than Lacquer 2. Lacquer 3 was studied additionally, because its intrinsic water vapor barrier is better than Lacquer 2. Both lacquers fulfilled another important, practical criterion: they were processable on the pilot machine (in contrary to PVdC dispersions, for example). With respect to their intrinsic oxygen barrier, the three lacquers are in the order Lacquer 1 / Lacquer 2 (similarly better) - Lacquer 3 (worst). With respect to their intrinsic water vapor barrier, the three lacquers are in the reverse order: Lacquer 3 (best) - Lacquer 1 / Lacquer 2 (similarly worse) (Table 6.1).

Table 6.1: Typical permeability coefficients of the three lacquers that were studied during “edge trials“ (permeability coefficients from Chapter 5.3).

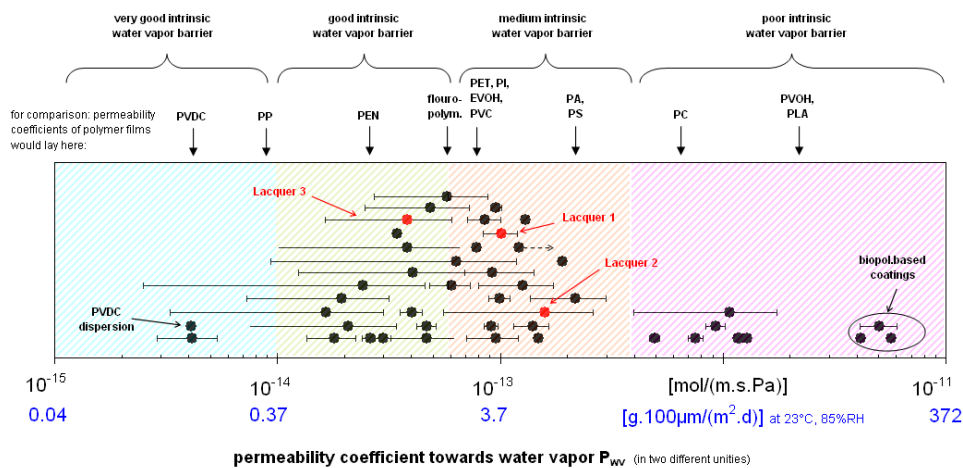
Coating	P_{O_2} [mol/(m s Pa)]	P_{H_2O} [mol/(m s Pa)]
Lacquer 1 (= C5.2)	6.6×10^{-19}	1.4×10^{-13}
Lacquer 2 (= C5.5)	9.8×10^{-19}	1.6×10^{-13}
Lacquer 3 (= C5.1)	5.4×10^{-18}	3.8×10^{-14}

¹In this work, the term “synergistic barrier effect shall represent all ”excess of barrier improvement“, i.e. all barrier performance better than what is expected and that cannot be explained - independent of possible mechanisms behind. In this work, this term is not connected exclusively to any of the possible explanation mechanisms, but represents a sum of all ”unexplained surplus“.

6 Results and Discussion: Barrier effects resulting from the combination of different layers



(a)



(b)

Figure 6.1: Average and standard deviation of oxygen (a) and water vapor (b) permeability coefficients of 46 organic coating materials. (The position of the data points in y direction is chosen arbitrarily for better visibility.) Important difference to Fig. 5.11: the three lacquers used for studying the synergistic barrier effect are marked in red.

All three lacquers were coated during "edge trials" (see description above) on top of SiO_x coated PET substrates. The results are summarized in Table 6.2. Comparing first the oxygen transmission rates (OTR) of the PET+ SiO_x samples with and without organic coating between the three different lacquers, an increase can be observed from Lacquer 1 to Lacquer 3. The best results, i.e. the lowest OTR, were achieved for the samples with Lacquer 1 as top coat. This becomes even clearer when not the absolute OTR, but the relative improvements are compared. For this purpose, the factor F is defined (by the author) as the ratio between the transmission rate of the original material to the coated one:

Table 6.2: Permeation results of the “edge trials“ samples consisting of a PET + SiO_x substrate with and without lacquer.

Coating	number of edge trial	OTR 23/0 [m ³ (STP)/(m ² d bar)]			WVTR 23/85 [g/(m ² d)]		
		uncoated	coated	F	uncoated	coated	F
Lacquer 1	1	0.186	0.008	23	0.216	0.026	8
	2	0.269	0.019	14	0.204	0.068	3
	3				0.198	0.098	2
Lacquer 2	1	0.160	0.015	11	0.189	0.050	4
	2	0.161	0.053	3	0.201	0.070	3
	3				0.123	0.061	2
Lacquer 3 ^a	(1) ^a	0.22-0.46	0.066	3-7	0.1-0.3	0.093	1-3
	(2) ^a		0.168	1-3			1-3
	(3) ^a		0.217	1-2			

^aThe trials with Lacquer 3 on top of PET + SiO_x substrate were performed before the procedure of the “edge trials” was developed. Therefore, no clear allocation of uncoated and coated samples is possible for this set of results. Hence, only ranges of F can be calculated.

$$F = \frac{TR_{\text{PET+SiO}_x}}{TR_{\text{PET+SiO}_x+\text{Lacquer}}} \quad (6.1)$$

so that it takes into account the fluctuations of the OTR and WVTR, respectively, of the original substrate of the structure PET + inorganic layer.

For oxygen, F shows even clearer the same tendency: Best improvements are achieved for Lacquer 1 (F of 14 to 23), followed by Lacquer 2 (F of 3 to 11) and Lacquer 3 (F of 1 to 7), similiary good. This tendency fits the order of the oxygen permeability coefficients of the three lacquers: Lacquer 1 having the best and Lacquer 2 and 3 having similiary worse intrinsic oxygen barrier.

One theory about the permeation mechanism through thin inorganic barrier layers, the pore modell [120], describes the inorganic layer as an inhomogeneous material containing randomly distributed pores. It is stated that oxygen permeation would occur only through these pores, but not through the impermeable bulk of the thin inorganic layer [120]. According to this theory, the next organic layer on top should reduce the oxygen permeation through the pores to a value proportional to its intrinsic oxygen barrier. The results seen in this study for oxygen permeation confirm this part of this theory: the better the intrinsic oxygen barrier of the lacquer the higher the improvement factor F.

For water vapor transmission, the improvement factors are generally not as high as for oxygen transmission and they lay closer together. The highest F, for the combination with Lacquer 1, was calculated to be 8, but the rest of the samples all showed F between 1 and 4. This explains why it is not possible to derive a tendency from the comparison of the absolute WVTR of the coated samples alone. Even comparing F between the three lacquers only shows a slight tendency: F increases slightly from Lacquer 3 and Lacquer 2 to Lacquer 1.

6 Results and Discussion: Barrier effects resulting from the combination of different layers

In one point, the pore model fits here again: It states that water vapor, different from oxygen, is permeating not only through the pores alone, but through the bulk, too [120]. Therefore, improvements after organic coating would always be lower for water vapor than for oxygen - which is matching with the results of this study. However, the improvements regarding water vapor barrier by coating the inorganic layer with Lacquers 1 to 3 should, according to the pore model, follow their intrinsic water vapor barrier. But here, on the contrary, the improvement factors increase with increasing permeability coefficient of the lacquers for water vapor. This tendency leads to a first conclusion that the barrier performance of the combination substrate + inorganic coating + organic coating is influenced by more than just the intrinsic barrier properties of the organic top coat.

So far, the absolute and relative improvements of the overall OTR and WVTR of the three layered structure were compared between different combinations of inorganic and organic coating materials. Additionally will now be evaluated whether the synergistic barrier effect exists and how much of “excess of barrier improvement” is possible.

For the quantification of the synergistic barrier effect, S is introduced as the percentage “excess” of transmission rate reduction compared to the expected transmission rate:

$$S = \frac{TR_{\text{expected}} - TR_{\text{measured}}}{TR_{\text{expected}}} 100\% \quad (6.2)$$

For a three layer system with unfilled (empty = E) pores, the expected transmission rates can be calculated using equations (3.27) and (3.28) omitting the blue (pore filling) part, which is:

$$T_{3L,O_2} = \frac{1}{BIF_{O_2}^{\text{local}} \left(\frac{1}{T_{\text{polymer},O_2}} + \frac{d_{\text{polymer}}}{P_{\text{organic},O_2}} \right)} \quad (6.3)$$

and:

$$T_{3L,H_2O} = \frac{1}{\frac{1}{\frac{1}{T_{2L,H_2O} - \frac{T_{\text{polymer},H_2O}}{k BIF_{O_2}^{\text{local}}}} + \frac{d_{\text{organic}}}{P_{\text{organic},H_2O}}} + \frac{1}{k BIF_{O_2}^{\text{local}} \left(\frac{1}{T_{\text{polymer},H_2O}} + \frac{d_{\text{polymer}}}{P_{\text{organic},H_2O}} \right)}} \quad (6.4)$$

Table 6.3 summarizes the so calculated expected transmission rates TR_{expected}^E and synergistic effects S^E for a three layer system with unfilled (empty = E) pores. From these results, it can be concluded that the synergistic barrier effect does, first, exist for all three organic coating materials, second, for both oxygen permeation and water vapor permeation, third, in significant dimension and, fourth, in larger size for water vapor permeation than for oxygen. Furthermore, comparing the synergistic effects between the different lacquers for oxygen and water vapor transmission rates, respectively, the same tendency as for the improvement factors F can be seen:

The synergistic effect S increases for both oxygen and water vapor transmission with decreasing permeability coefficient of the lacquers for oxygen and increasing permeability coefficient of the lacquers for water vapor, i.e. the synergistic effect S are more pronounced for Lacquer 1 and Lacquer 2 (which are close) compared to Lacquer 3. Lacquer 1 is only slightly better than Lacquer 2.

Table 6.3: Expected transmission rates and synergistic effects for oxygen and water vapor permeation through the samples, consisting of PET + SiO_x + organic top coat.

Coating	number of edge trial	OTR [m ³ (STP)/(m ² d bar)]		S _{O₂} ^E	WVTR [g/(m ² d)]			S _{H₂O} ^E
		measured	expected ^{Ea}		measured	expected ^E		
						k = 1	k = 0.5	
Lacquer 1	1	0.008	0.017	52%	0.026	0.203	0.190	86-87%
	2	0.019	0.024	21%	0.068	0.191	0.178	62-64%
	3				0.098	0.185	0.172	43-47%
Lacquer 2	1	0.015	0.020	26%	0.050	0.213	0.205	71-72%
	2	0.053	0.020	none	0.070	0.192	0.184	62-64%
	3				0.061	0.114	0.106	42-47%
Lacquer 3 ^b	(1) ^b	0.066	0.098 to 0.204	32-68% none-18% none	0.093 0.116	0.047 to 0.273	none-66% none-58%	
	(2) ^b	0.168						
	(3) ^b	0.217						

^aE ... Empty (unfilled) pores assumed for calculation.

^bThe trials with Lacquer 3 on top of PET + SiO_x substrate were performed before the procedure of the "edge trials" was developed. Therefore, no clear allocation of uncoated and coated samples is possible for this set of results. Hence, only ranges of expected TR and S can be calculated.

These observations confirm the conclusion drawn above: The barrier performance of the combination substrate + inorganic coating + organic coating is influenced more by another mechanism resulting from the organic coating material on top of a thin inorganic barrier coating than by the intrinsic barrier performance of the organic coating material towards oxygen or water vapor. The considerable values for S, i.e. the significant difference between the expected and the measured transmission rates, show that this additional mechanism is in fact even dominating the overall barrier performance. Hence, the existing pore model theory has to be extended by one additional mechanism. The resulting question is: What exactly is this additional mechanism?

The most obvious interpretation would start with a closer look at the interface between the inorganic and the organic layer. An organic coating material never changes only one material property if its chemistry is modified. It is possible that a chemical modification not only decreases the intrinsic water vapor barrier, but at the same time improves the situation at the interface between inorganic and organic layer. If this improved situation at the inorganic - organic interface is dominant towards the intrinsic barrier performance of the organic top coat, the overall WVTR could be reduced with an organic coating material of worse intrinsic water vapor barrier but good "interface building properties". The results of Tables 6.2 and 6.3 indicate that the improvement of the intrinsic oxygen barrier from Lacquer 3 and 2 to Lacquer 1 goes along with the decrease of the intrinsic water vapor barrier, but at the same time with an increase of the "interface building properties".

As possible explanations for these good "interface building properties" were already suggested:

- The viscosity and wettability of the organic coating material is suited to fill (at least partially) the pores of the inorganic coating [42].

6 Results and Discussion: Barrier effects resulting from the combination of different layers

- A matching chemistry between the organic coating material and the inorganic barrier layer leads to covalent bonding at the interface of the organic layer and the inorganic one, which is initiating a zone of increased network density in the organic layer [146].

In the following, both theories will be compared to the experimental results.

First, to understand whether the theory of the filled pores could explain the synergistic effect, the calculations from above are repeated assuming the pores to be completely filled (F) with organic coating material, using equations (3.27) and (3.28) (which are repeated here for the benefit of the reader):

$$T_{3L,O_2}^F = \frac{1}{\text{BIF}_{O_2}^{\text{local}} \left(\frac{1}{T_{\text{polymer},O_2}} + \frac{d_{\text{polymer}}}{P_{\text{organic},O_2}} \right) + \frac{d_{\text{inorganic}}}{\alpha P_{\text{organic},O_2}}} \quad (6.5)$$

and:

$$T_{3L,H_2O} = \frac{1}{\frac{1}{T_{2L,H_2O} - \frac{T_{\text{polymer},H_2O}}{k \text{BIF}_{O_2}^{\text{local}}}} + \frac{d_{\text{organic}}}{P_{\text{organic},H_2O}}} + \frac{1}{k \text{BIF}_{O_2}^{\text{local}} \left(\frac{1}{T_{\text{polymer},H_2O}} + \frac{d_{\text{polymer}}}{P_{\text{organic},H_2O}} \right) + \frac{d_{\text{inorganic}}}{\alpha P_{\text{organic},H_2O}}} \quad (6.6)$$

with α representing the fraction of the surface area that is covered with pores.

In doing so, for oxygen, the expected transmission rates get significantly reduced, and such get the synergistic barrier effects S (Table 6.4). Assuming the inorganic pores are filled with the organic top coat, the expected OTR would already be at the level of the measured ones - which means that the synergistic barrier effect for oxygen permeation could completely be explained with the filled pores theory. For water vapor permeation, assuming filled inorganic pores leads only to a small reduction of the expected transmission rates and synergistic barrier effects (6.5).

The second theory explains the synergistic barrier effect with an increased network density of the organic top coat. A denser network within the organic barrier layer is a structural change that increases the intrinsic barrier performance of the organic coating material. Therefore, the permeability coefficients for both oxygen and water vapor would decrease equally and, to integrate the increased network density of the lacquers (L) into the expected transmission rates, re-calculations were performed using new, reduced permeability coefficients for oxygen and water vapor for the organic coating materials:

$$P_{\text{organic},O_2}^L = \frac{P_{\text{organic},O_2}}{X} \quad (6.7)$$

and

$$P_{\text{organic},H_2O}^L = \frac{P_{\text{organic},H_2O}}{X} \quad (6.8)$$

that are both reduced by the same factor of reduction X.

Table 6.4: Expected OTR and synergistic barrier effect S for two lacquers on PET + SiO_x substrate. As an example, all results (E,F,L,F+L) are shown for these two combinations of inorganic and organic barrier material. (To display all TR and S results for all samples would be too long and not add any further information or conclusion.)

index	OTR [m ³ (STP)/(m ² d bar)]			OTR [m ³ (STP)/(m ² d bar)]		
	expec.	meas.	S_{O_2}	expec.	meas.	S_{O_2}
	Lacquer 1			Lacquer 2		
E ^a	0.017	0.008	52%	0.020	0.015	26%
F ^b	0.011		25%	0.014		none
L (:5) ^c	0.004		none	0.005		none
F + L (:5) ^d	0.002		none	0.003		none
L (:10)	0.002		none	0.002		none
F + L (:10)	0.001		none	0.001		none
E	0.024	0.019	21%	0.020	0.053	none
F	0.013		none	0.014		none
L (:5)	0.005		none	0.005		none
F + L (:5)	0.003		none	0.003		none
L (:10)	0.003		none	0.002		none
F + L (:10)	0.001		none	0.002		none

^aE ... Empty (unfilled) pores assumed for calculation.

^bF ... Filled pores assumed for calculation.

^cL (:X) ... Lacquer with increased network density assumed for calculation, having an X times better intrinsic barrier performance.

^dF + L (:X) ... Both filled pores and a lacquer with X times better intrinsic barrier performance assumed for calculation.

The theory of the higher network density is based on the idea that the first atomic monolayer of the organic material at the interface towards the inorganic layer is a mirror image of the the inorganic structure due to symmetric covalent bonding. It is assumed that then the network is becoming gradually “looser“, i.e. more and more like the organic material on the very top. However, in this theory, there is no clear idea of how thick the part of the organic layer could be that resembles more the inorganic network than the organic one, and there is no idea of how much the permeability coefficients of the organic material could be reduced (i.e. there is no idea about the size of X).

Therefore, the re-calculations of the expected transmission rates for increased lacquer (L) density were performed for two different X: 5 and 10, respectively. As the difference of permeability coefficients between the inorganic bulk and the organic layer is five to six orders of magnitude (for the samples of this study), these reduction factors would correspond to an organic layer whose network density is 0.005% and 0.01%, respectively, as dense as an inorganic barrier layer (while the rest is as dense as the original organic layer).

With this, the expected water vapor transmission rates get further reduced, and such

6 Results and Discussion: Barrier effects resulting from the combination of different layers

Table 6.5: Expected WVTR and synergistic barrier effect S for two lacquers on PET + SiO_x substrate. As an example, all results (E,F,L,F+L) are shown for these two combinations of inorganic and organic barrier material. (To display all TR and S results for all samples would be too long and not add any further information or conclusion.)

index	WVTR [g/(m ² d)]			WVTR [g/(m ² d)]		
	expec.	meas.	S _{H₂O}	expec.	meas.	S _{H₂O}
	Lacquer 1			Lacquer 2		
E ^a	0.190-0.203	0.026	86-87%	0.205-0.213	0.050	71-72%
F ^b	0.173-0.197		85-87%	0.195-0.210		70-72%
L (:5) ^c	0.158-0.185		83-86%	0.181-0.200		67-71%
F,L (:5) ^d	0.146-0.180		82-85%	0.173-0.198		66-70%
L (:10)	0.146-0.176		82-85%	0.172-0.194		66-70%
F,L (:10)	0.138-0.174		81-85%	0.167-0.193		65-69%
E	0.178-0.191	0.068	62-64%	0.184-0.192	0.070	62-64%
F	0.161-0.186		58-63%	0.174-0.189		60-63%
L (:5)	0.146-0.173		54-61%	0.161-0.180		56-61%
F,L (:5)	0.134-0.169		49-60%	0.152-0.177		54-60%
L (:10)	0.135-0.165		50-59%	0.152-0.174		54-60%
F,L (:10)	0.127-0.163		46-58%	0.146-0.172		52-59%
E	0.172-0.185	0.098	43-47%	0.106-0.114	0.061	42-47%
F	0.155-0.180		37-46%	0.096-0.112		37-45%
L (:5)	0.140-0.167		30-41%	0.084-0.103		27-41%
F,L (:5)	0.128-0.163		24-40%	0.075-0.100		19-39%
L (:10)	0.129-0.160		24-39%	0.075-0.098		19-38%
F,L (:10)	0.121-0.157		19-38%	0.070-0.097		13-37%

^aE ... Empty (unfilled) pores assumed for calculation.

^bF ... Filled pores assumed for calculation.

^cL (:X) ... Lacquer with increased network density assumed for calculation, having an X times better intrinsic barrier performance.

^dF + L (:X) ... Both filled pores and a lacquer with X times better intrinsic barrier performance assumed for calculation.

get the synergistic barrier effects S (Table 6.5), but still, a significant part of synergistic barrier effect remains unexplained. Adding the theory of pore filling to the theory of increase organic network density (F + L:X) leads to the lowest expected water vapor transmission rates, but still not as low as the measured ones. Even both theories together are not able to explain the synergistic effect of water vapor barrier.

As a summary, the theory of pore filling does completely explain the significant synergistic barrier effects for oxygen permeation, but there is a large remaining synergistic barrier effect for water vapor permeation that even would not be explained by summing up the barrier effects resulting from filled pores and increased organic network density at the inorganic-organic interface. Yet such an improved inorganic-organic interface should

lead to even lower oxygen transmission rates for the three layer structure than what was measured. Hence, assuming the same "interface building" effect for oxygen and water vapor permeation is not going to explain both the high synergistic barrier effects for water vapor and the lower synergistic effects for oxygen at the same time.

Therefore, this theory alone is already useful, but not sufficient. The "interface building properties" of organic barrier lacquers on top of inorganic barrier layers have to be explained by two types of mechanisms: those of the type referring to both gases (like the filled pores and theory of increased network density at the inorganic-organic interface) and (at least) one type of mechanism referring to water vapor only.

One idea is to introduce "nano pores" (or "nano defects") into the model of the thin inorganic barrier layer [67]. The thin inorganic barrier layer would no longer consist of an impermeable bulk and permeable pores only. The "impermeable bulk" would then consist of an impermeable inorganic lattice with many nanoscale pores - like a "solid sponge" (Fig. 6.2). These nano pores are on the one hand too small or too tortuous to allow unhindered permeation for any gaseous permeant, but allow the condensation of water vapor. Thus, water vapor could penetrate, but no oxygen. On the other hand, the nano pores have to be big enough to be filled with liquid (uncured) organic coating material - e.g. in the range between 0.4 and 4 nm [67]. When coating such an inorganic layer with an organic top coat, the organic material would (partially) fill the pores as well as the nano pores and as such enhance the barrier, not only of the macro pores part, but also of the bulk part of the layer. Hence, water vapor permeation, which happens through the bulk, too, would get an extra barrier improvement compared to oxygen permeation, which happens through the pores only.

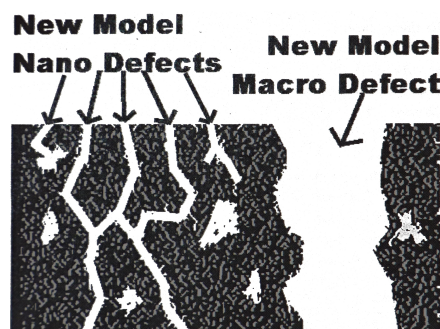


Figure 6.2: Scheme of a thin inorganic barrier layer consisting of a bulk part with nano pores and a (micro) pores part (figure from [67]).

It could not be evaluated during this work whether this approach would be correct, because a suitable detection method for such nano pores was missing. More difficult even would be the proof of the filled pores.

What could be done to clarify this additional mechanism, is to perform further studies and conclude from them indirectly (as was done above): New edge trials should preferably be performed on three types of inorganic barrier layers in parallel, i.e. amorph network (e.g. SiO_x), ionic lattice (e.g. AlO_x) and metallic lattice (e.g. Al). Additionally to the permeability measurements, properties related to the fluidity of the lacquers (e.g. rheology, surface tension of the organic material and of the inorganic surface, wettability) and properties related to the chemical match of lacquer and inorganic layer (e.g. chemical characterization of the organic material, of the inorganic surface and of the interface zone) should be varied systematically. In this context, it would be favorable, too, to be able to coat PVdC based coating materials (supplying the highest possible intrinsic oxygen barrier as well as very good intrinsic water vapor barrier) as one of the tested lacquers. Studies with that purpose have already started.

6 Results and Discussion: Barrier effects resulting from the combination of different layers

As a summary, it was understood from these trials that:

1. Pure transmission rate data are not sufficient to conclude about the dimension of the synergistic barrier effect.
2. Calculating the improvement factor F is useful as a first indication: if F is ≥ 2 for water vapor and ≥ 5 for oxygen, a synergistic effect greater than predicted with the existing theories is probable. (However, to ensure that high factors F are not resulting from side effects, e.g. an especially thick organic coating, the synergistic barrier effect S has to be calculated quantitatively.)
3. The calculation of S takes into account that water vapor permeates in a different way than oxygen (not only through the pores, but also through the bulk of the inorganic barrier layer) and therefore shows, in contrary to the improvement factor F , that synergistic barrier effects are even more pronounced for water vapor than for oxygen.
4. The synergistic barrier effect is not exclusively related to one single group of organic barrier coating material, but does generally exist for the combination of an inorganic barrier layer with an organic top coat.
5. The gain in barrier performance by synergistic effect can out-perform the gain resulting from high intrinsic barrier of the organic material. This is especially the case for water vapor permeation.
6. High synergistic effects are not linked to a high intrinsic barrier of the organic material alone, but are more influenced by the chemical situation at the inorganic-organic interface. This interface situation seems to be related to the same structural chemical reasons that lead to a high intrinsic oxygen barrier of the organic coating material.
7. Organic barrier coating materials with unspectacular intrinsic water vapor barrier, but high intrinsic oxygen barrier can therefore show high synergistic barrier effects against water vapor.
8. One reason behind the synergistic barrier effects is probably the filling of the porosity of the inorganic barrier layer with organic coating material. The synergistic barrier effects for oxygen transmission could be completely explained with that theory. The theory of the increased network density within the organic barrier layer close to the inorganic-organic interface, that leads to higher gas barrier within the organic layer, is probably no or a minor reason for the occurring synergistic effects.
9. An additional (proven) theory is missing that explains the (large) remaining synergistic barrier effect for water vapor. One way to evaluate is the idea of the bulk being penetrated by many very small nano pores.

As a general conclusion for the development of high performing encapsulation materials, it is not sufficient to search for the ultimate organic coating material of lowest possible intrinsic water vapor barrier. As synergistic barrier effects play an important role

in defining the overall barrier performance, multilayered encapsulation materials have to be optimized towards the best combination of the selected inorganic barrier layer with an organic barrier coating that supplies both an appropriate intrinsic water vapor barrier, but also good “interface building properties” which seem to be linked to high intrinsic oxygen barrier.

6.2 Tortuous path effect

As the tortuous path effect is assumed to be a permeation mechanism related to the porosity of the thin inorganic barrier layer, two qualities of SiO_x were tested. One SiO_x quality shows TR values that are better than the typical average of this work (Table 6.6), which will therefore be called “good”. The other SiO_x quality shows TR values that lay below the typical average of this work (Tables 6.6, 6.7), which will therefore be called “bad” (despite this is actually no bad material at all). Due to different proprietary recipes of the oxidic evaporation material, it is assumed that different area densities were generated during the deposition process. The “bad“ quality is assumed to have more and larger intrinsic pores, i.e. a higher area defect density, than the “good” quality. The less and the smaller the pores and the greater the distances between them, the more pronounced the tortuous path effect should be. Hence, the structures including the “good” SiO_x should show greater improvements of the oxygen barrier when reducing the thickness of the intermediate layer.

However, the experimental evaluation shows the contrary: The transmission rates of samples of the structure [PET + SiO_x + Ormocer[®] 09 (= C5.9) + SiO_x] rise, both for oxygen and water vapor, when decreasing the thickness of the intermediate Ormocer[®] 09 (= C5.9) layer. At the intermediate thickness of 50 nanometers, when the OTR should

Table 6.6: OTR of the structure [PET + SiO_x + Ormocer[®] 09 (= C5.9) + SiO_x], in dependancy of the thickness d of the intermediate layer and for two qualities of SiO_x .

	OTR in [$\text{cm}^3(\text{STP})/(\text{m}^2 \text{ d.bar})$] for d being:			
	1.1 μm	500 nm	200 nm	50 nm
PET (base substrate)	26.3 ± 1.7			
PET + “bad“ SiO_x	$0.65 0.75$			
PET + ”bad” SiO_x + C5.9	0.009	-	-	-
	0.026			
PET + ”bad” SiO_x + C5.9 + SiO_x	0.012	0.022	0.052	0.22
	0.029	0.041	0.110	0.32
PET + “good“ SiO_x	0.29 ± 0.08			
PET + ”good” SiO_x + C5.9	0.026	-	-	-
	0.029			
PET + ”good” SiO_x + C5.9 + SiO_x	0.007	-	0.027	-
	0.021		0.050	

6 Results and Discussion: Barrier effects resulting from the combination of different layers

Table 6.7: WVTR of the structure [PET + SiO_x + Ormocer[®] 09 (= C5.9) + SiO_x], in dependency of the thickness d of the intermediate layer and for two qualities of SiO_x.

	WVTR in [g/(m ² d)] for d being:			
	1.1 μm	500 nm	200 nm	50 nm
PET (base substrate)	4.8 ± 1.0			
PET + “bad“ SiO _x	0.66			
PET + ”bad” SiO _x + C5.9	0.0322	-	-	-
PET + ”bad” SiO _x + C5.9 + SiO _x	0.0314	0.0343	0.0358	0.0841
PET + “good“ SiO _x	0.19 ± 0.07			
PET + ”good” SiO _x + C5.9	0.0336	-	-	-
PET + ”good” SiO _x + C5.9 + SiO _x	0.0339	-	0.0484	-

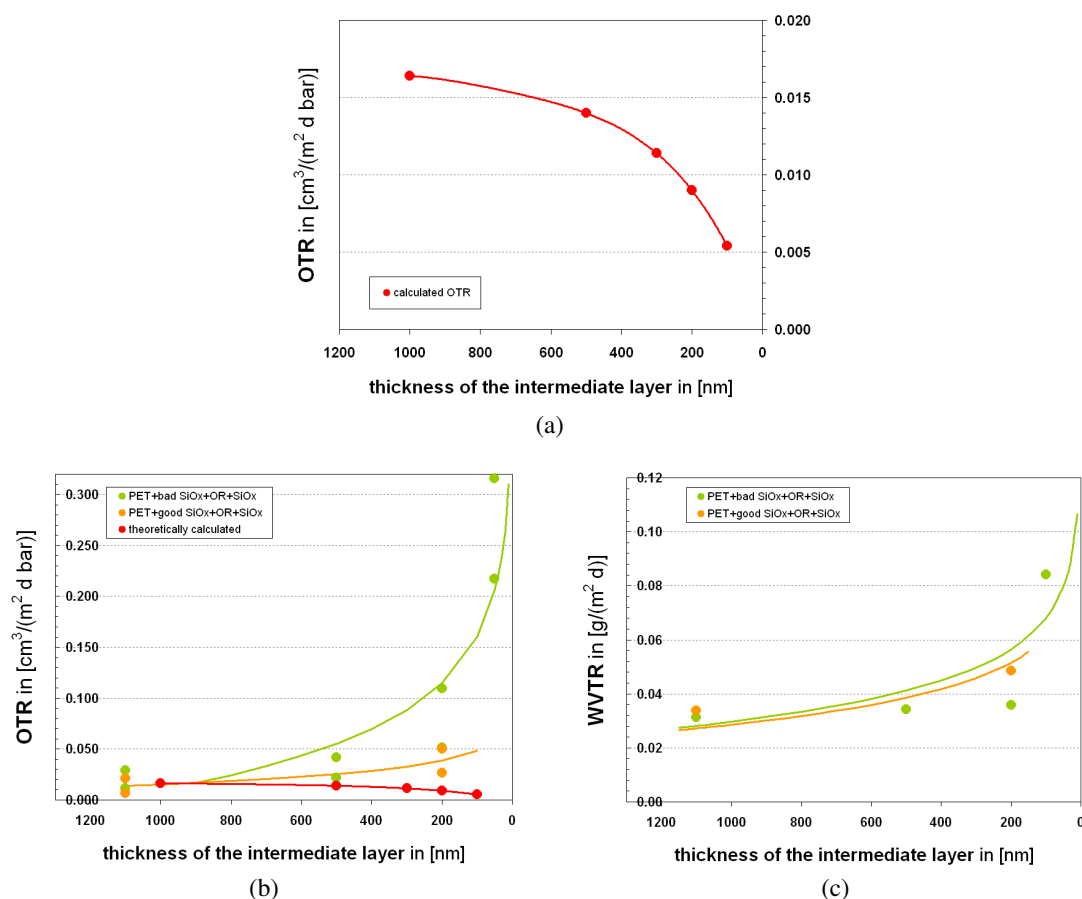


Figure 6.3: Calculated OTR (a), measured OTR (b) and measured WVTR (c) of the structure [PET substrate + SiO_x + Ormocer[®] 09 (= C5.9) + SiO_x], in dependency of the thickness of the intermediate layer, and for two qualities of SiO_x. (Diagram (a) is reproduced from [42].)

decrease by a factor of 6 according to theory (Fig. 6.3a), they actually increase in this experiment by a factor of 3 to 13 - depending on the SiO_x type (Fig. 6.3b).

According to the theory of the tortuous path effect, the water vapor transmission rates should stay unaffected by the reduction of the thickness of the intermediate layer. Yet, in this experimental study, the WVTR are increasing, too (Fig. 6.3c). These WVTR results suggest that the thin inorganic barrier layers have suffered (partial) damage during the roll-to-roll preparation of the samples. It seems that the thinner the intermediate layer, the more damage has been done to the thin inorganic barrier layers.

These results do not allow a more detailed conclusion about the existence of the tortuous path effect. Either, it could be that the tortuous path effect is completely suppressed by the mechanical damage of the thin inorganic barrier layers that increases with decreasing thickness of the intermediate layer. Or, it could be that the increasing transmission rates resulting from the mechanical damage of the thin inorganic barrier layers suppress the fact that the tortuous path effect would not exist anyway in “roll-to-roll reality”.

In any case, for this procedure of preparation, the thickness of the intermediate layer should not go below 1 μm. Taking into account that the pilot plant at *Fraunhofer IVV* was constructed to be able to handle the web in a very soft way (e.g. coated side never touching a winding roll etc.), this intermediate thickness of 1 μm marks a lower limit. For less soft plants (more towards high speeds and mass production), the minimum thickness of the intermediate layer to prevent damage of the thin inorganic barrier layer, should be several micrometers - or the barrier loss will be even more pronounced.

Hence, in practice, the tortuous path effect is no option for further improvement of the barrier performance of OE encapsulation material that is targeted to be produced by roll-to-roll methods.

6.3 Time lag effect

By the measurement of the WVTR of OE encapsulation materials with increasing time lag, Graff et al. [41] had found that the increase of the length of the instationary period of the water vapor permeation mechanism - while in fact decreasing the absolute WVTR only marginally - could be a very effective strategy for the development of OE encapsulation material (see Chapter 3.2.2). These conclusions result from the comparison of calculated with measured WVTR. It was found that the WVTR predicted by FEA calculations were much higher than the ones measured by calcium test (Table 6.8) and it was suggested that this may come from a much increased time lag [41].

In order to understand this “time lag effect” better, encapsulation materials of different expected time lags were prepared and evaluated both theoretically and experimentally. For the theoretical calculation of the WVTR and the time lags, the finite elements analysis (FEA) was used to solve the diffusion equation for water vapor permeation (see Chapter 3.1.9). In addition to what Graff et al. [41] had done, the WVTR were measured using not only the calcium test, but also the ACP test. The use of the ACP test enables to gain experimental data not only about the WVTR, but about the time lags as well, which had not been possible for Graff et al. [41].

To prepare encapsulation materials with increasing time lag, seven encapsulation materials were produced that had a similar structure (i.e. using the same polymer substrate

6 Results and Discussion: Barrier effects resulting from the combination of different layers

Table 6.8: Calculated versus measured WVTR at 38°C, 90% RH, all data cited from Graff et al. [41].

total number of layers	sample structure	calculated WVTR (FEA) ^a [g/(m ² d)]	measured WVTR	
			Mocon [g/(m ² d)]	calcium test [g/(m ² d)]
1	P ^b	-	-	-
2	P+L ^c	6.8	4.58	-
4	P+L+1 (A + L) ^d	0.036	0.058	-
6	P+L+2 (A + L) ^e	0.018	< 0.005	-
8	P+L+3 (A + L) ^f	0.012	< 0.005	-
10	P+L+4 (A + L) ^g	0.009	< 0.005	-
12	P+L+5 (A + L) ^h	0.007	-	~ 10 ⁻⁶

^aA simplified model with effective thin inorganic barrier layers was used, similar to the one used by the author.

^bPET

^cPET + acrylic lacquer

^dPET + acrylic lacquer + 1 dyad of AlO_x and acrylic lacquer

^ePET + acrylic lacquer + 2 dyads of AlO_x and acrylic lacquer

^fPET + acrylic lacquer + 3 dyads of AlO_x and acrylic lacquer

^gPET + acrylic lacquer + 4 dyads of AlO_x and acrylic lacquer

^hPET + acrylic lacquer + 5 dyads of AlO_x and acrylic lacquer

and the same thin organic and inorganic barrier layers), but differed in the total number of layers: from 1 to 9 (Table 6.9).

A trend can be seen comparing the calculated WVTR and the WVTR^{Ca} measured with calcium test to the results of the existing study (Table 6.9): the theoretically predicted WVTR decrease much slower than those actually measured by calcium test. For an encapsulation material consisting of seven layers, the difference between the calculated and the measured WVTR^{Ca} is one order of magnitude (Table 6.9), for nine layers it is nearly two orders of magnitude (Table 6.9) and for 12 layers it is nearly three orders of magnitude (Table 6.8).

But when looking at the results of the ACP test, there is indeed a very good match of the calculated and the measured WVTR - at least, as long as the ACP measurement was finished (for the materials with one, two and three layers). Due to an electrical problem with the ACP device the other measurements had to be stopped before having arrived in steady state permeation. For these samples (with four to nine layers) there is a difference between the calculated and measured WVTR, with the same trend again: the higher the total number of layers, the greater the difference. This circumstance suggests to take a too early abort of measurement as the reason behind that huge deviation of experimentally measured WVTR^{Ca} results towards theoretically predicted ones. This theory is sustained by the experimentally measured time lags that get, for a high number of layers, into the level of several months (Table 6.10), while typical calcium test measurements are running for much shorter periods.

Yet the reason for the calcium tests running much shorter is not a mistake of the operator to stop the test too early. On the contrary, the calcium tests were stopped when

Table 6.9: Calculated versus measured WVTR at 23°C, 50% RH.

total number of layers	sample structure	calculated WVTR (FEA) ^a [g/(m ² d)]	measured WVTR Aqu. ^b / ACP [g/(m ² d)]	calcium test [g/(m ² d)]
1	P ^c	1.89	1.89 (Aqu.)	-
2	P+Z ^d	0.03	0.01 - 0.03	≫ 10 ⁻³
3	P+Z+O ^e	0.012	0.011	5 × 10 ⁻³
4	P+Z+O+Z ^f	0.0080	0.0018 ^g	2 × 10 ⁻³
5	P+Z//a ^h	0.0075	0.001 ^g	1 × 10 ⁻³
7	P+Z+O//a ⁱ	0.0060	0.0004 ^g	5 × 10 ⁻⁴
9	P+Z+O+Z//a ^j	0.0030	0.0003 ^g	~ 7 × 10 ⁻⁵

^aA simplified model with effective thin inorganic barrier layers was used (Chapter 3.1.9).

^bThe WVTR of the PET film had to be measured using the Aquatran device, since the ACP device is not able to measure WVTR above 3 g/(m² d).

^cPET

^dPET + ZnSn_xO_y

^ePET + ZnSn_xO_y + Ormocer[®]04a (= C5.5)

^fPET + ZnSn_xO_y + C5.5 + ZnSn_xO_y

^gMeasurement had to be stopped too early (before arriving in steady state) due to failure in ACP device.

^hPET + ZnSn_xO_y + adhesive A6.1 + ZnSn_xO_y + PET

ⁱPET + ZnSn_xO_y + C5.5 + adhesive A6.1 + C5.5 + ZnSn_xO_y + PET

^jPET + ZnSn_xO_y + C5.5 + ZnSn_xO_y + adhesive A6.1 + ZnSn_xO_y + C5.5 + ZnSn_xO_y + PET

Table 6.10: Calculated versus measured time lags of the water vapor permeation process.

total number of layers	sample structure	calculated with FEA	measured with Aqu. ^a / ACP
1	P ^b	-	16 min (Aqu.)
2	P+Z ^c	8.8 h	19 - 34 h (Aqu.)
3	P+Z+O ^d	17 h	18 d
4	P+Z+O+Z ^e	4 d	≫ 13 d ^f
5	P+Z//a ^g	17 d	≫ 15 d ^f
7	P+Z+O//a ^h	37 d	≫ 30 d ^f
9	P+Z+O+Z//a ⁱ	56 d	≫ 60 d ^f

^aThe time lags of the PET film and the PET film coated with one single layer had to be measured using the Aquatran device, since the accuracy of the ACP device towards time lag measurement ± 1 day.

^bPET

^cPET + ZnSn_xO_y

^dPET + ZnSn_xO_y + Ormocer[®]04a (= C5.5)

^ePET + ZnSn_xO_y + C5.5 + Sn_xO_y

^fMeasurement had to be stopped too early (before arriving in steady state) due to failure in ACP device.

^gPET + ZnSn_xO_y + adhesive A6.1 + ZnSn_xO_y + PET

^hPET + ZnSn_xO_y + C5.5 + adhesive A6.1 + C5.5 + ZnSn_xO_y + PET

ⁱPET + ZnSn_xO_y + C5.5 + ZnSn_xO_y + adhesive A6.1 + ZnSn_xO_y + C5.5 + ZnSn_xO_y + PET

6 Results and Discussion: Barrier effects resulting from the combination of different layers

either all calcium is degraded and turned completely transparent or no further change of the calcium is detectable by microscope or CCD camera. It is in fact the design of the calcium test that leads to "absolute WVTR" data that are concluded while the water vapor permeation has not yet arrived in steady state. The reason is that the calcium test combines two mechanisms: first, the permeation of water vapor through the encapsulation material to the surface of the sensor which is the calcium layer and, second, the chemical reaction of the sensor with the water molecules, which is the degradation of the mirroring calcium into black or transparent derivatives. These two processes are not happening sequentially and not at the same speed. The chemical reaction of the calcium is much faster than the permeation of the water molecules through the encapsulation material. Hence, it can happen that the calcium is already completely used up while the water vapor permeation process has not yet arrived in steady state. The calcium test would then put out as result one arbitrary, current "speed" of permeation before steady state, i.e. one arbitrarily too low WVTR. In addition to that, the chemical products of calcium with water molecules were proven to "reinforce" the calcium layer [106]. (If the calcium layer was not inbetween other layers, but had one open surface, one would call this process "passivation"). This mechanism leads to reduced reaction speed of the calcium layer with the water molecules and to hindered permeation of water molecules through the calcium hydroxide and oxide parts to unreacted parts of the calcium layer [106] further away from the side where the water molecules come from. Therefore, it may happen that for structures of low WVTR the reinforcement of the calcium layer is fast enough to block the complete degradation of the calcium layer already at a point when the water vapor permeation has not yet reached steady state. Even though the calcium test would then look like it has finished (because of no further optical change of the calcium layer) the process of water vapor permeation did not arrive in steady state regime and is not going to do so. As a conclusion, the $WVTR^{Ca}$ results gained from calcium tests are not reflecting in a physically correct way the absolute, steady state WVTR of the encapsulation material.

Furthermore, from Table 6.10, a conclusion regarding the theoretical time lag calculations can be drawn - when comparing the experimentally measured to the theoretically predicted time lags: the calculated time lags are much too short compared to the measured ones. Obviously, there must be additional mechanisms happening during the permeation process of water molecules through OE encapsulation materials that are not known and therefore not included in the FEA algorithms. These mechanisms seem not to have much influence

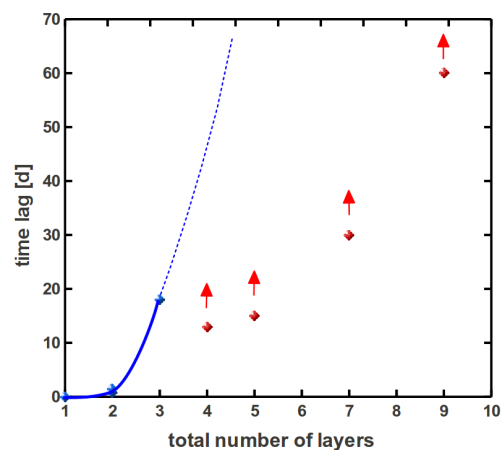


Figure 6.4: Experimentally measured time lags as a function of the total number of layers of the encapsulation material. (In blue / red: the permeation process had / had not arrived in steady state, respectively.)

on the steady state WVTR, because the theoretical prediction of these values fit very well to the experiments. But they seem to extend extremely the instationary period of the water permeation process. The electrical problem with the ACP device occurred after 110 days of measurement - still, at this time, even the permeation measurement of the four layer structure was not finished. Hence, the hopeful conclusion made by Graff et al. [41], that the time lag of encapsulation materials with a high number of layers might be in the order of "several years" [41], was not that far from reality (illustrated in Fig. 6.4).

During the long ACP measurement of the encapsulation materials with a high number of layers, one phenomenon was observed additionally that had not been that noticeable with encapsulation materials having SiO_x as thin inorganic barrier layers: there are "steps" occurring repeatedly in the curve of the cumulated flux, indicating a kind of repeated "intermediate equilibrium" before the permeation process continues. The first of these pseudo equilibriums could be seen after approximately two days (the time lag of this first part would be less than one day), the second pseudo equilibrium is observed after approximately 30 to 35 days (the time lag of this second part is approximately 20 days) and so on (Fig. 6.5).

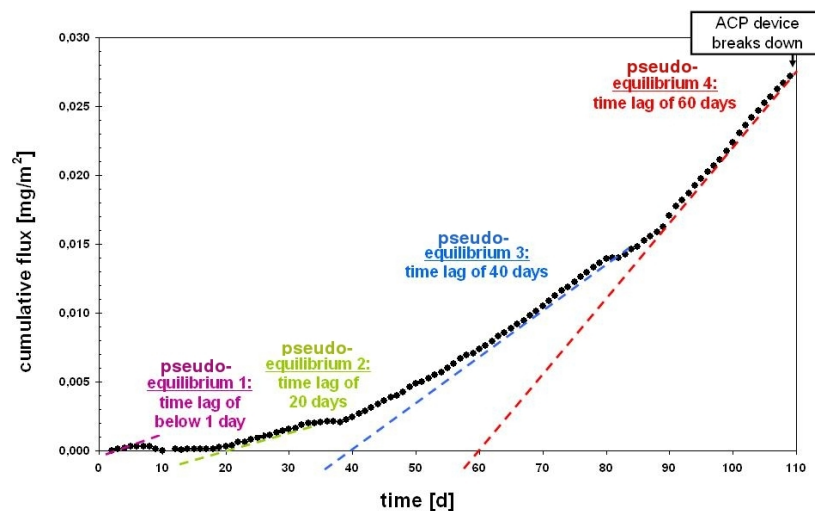


Figure 6.5: Cumulated flux of the 9 layer structure as a function of measurement time (the zeroing period is not shown here).

One possible explanation might be that the water molecules only progress along their permeation paths into the next layer to such an extent that would be detectable for the ACP device once a certain minimum amount of water molecules is arrived in the previous layer. This "filling up" of the previous layer, until this critical minimum amount of water molecules is reached, happens at pseudo steady state (steady state for the permeation into this one layer, not the entire structure). Assuming this effect occurs layer by layer again, the majority of the water molecules were just "filling up" the fifth layer of the 9 layer structure shown in Fig. 6.5 (taking into account that the ACP device is not able to measure more accurate than 1 d and this would mean having missed the breakthrough of the water vapor permeation through the first layer which would have happened during the first 30 minutes). It is probably not unrealistic to say that at least one year of measurement is required until the entire structure of the encapsulation material would arrive in steady

state permeation.

Since the time lag effect was not visible that strongly for the SiO_x-based structures, it may be the case that this effect of “delayed permeation“ becomes more pronounced with further improvement of the intrinsic barrier properties of the thin inorganic (and maybe organic) layers, and that this leads to highly extended time lags useful for ensuring long lifetimes of OE devices.

As a summary, it seems that the time lag effect is not only indeed existing detectably, but that it contributes very importantly to the actual protection performance of OE encapsulation materials against environmental gases.

6.4 Multilayered versus laminated structures

In the previous chapter, the time lag effect was proven to play an important role for calcium test results. Because of the similarities between the aging of calcium tests and of real OE devices, this promises great time lag effects for real devices. First, to evaluate whether this is actually true and, second, to understand the time lag effect better, further experiments were performed.

For this, encapsulation materials of different time lags were prepared (see Table 6.11) and evaluated. The WVTR evaluation was done using the ACP test and two different calcium tests: the one that is used as standard during this work, and a second one from *Konarka* which runs at higher temperature and humidity (at 65°C and 85% RH instead of 23°C and 50% RH) and uses thinner calcium layers (40 nm instead of 100 nm). *Konarka* has experience with its type of calcium test and how to correlate the results of this calcium test to the lifetime of OPV devices that would be encapsulated into the same sample material. Hence, this calcium test is used by *Konarka* to pre-screen potential OE encapsulation materials before doing actual device tests. Finally, one OE encapsulation material of choice was used to encapsulate a real OPV device of *Konarka*.

In order to prepare encapsulation materials of increasing time lag, barrier materials of increasing intrinsic barrier properties as well as a high number of barrier layers were used. There are two possibilities to prepare an encapsulation material with many barrier layers: Either more and more layers are stacked on top of a polymer substrate to create a ”multilayer stack“. Or one uses a small multilayer stack with few layers only and doubles them by laminating this material against itself. Each strategy has its advantages and disadvantages: In case the organic and inorganic layers can be coated within the same machine, the multilayer stack approach allows coating all layers in one run, i.e. without changing the machine. On the other hand, the sensitive thin barrier layers remain unprotected. Face-to-face lamination of small multilayer stacks would result in the same amount of barrier layer, i.e. in the same absolute barrier performance, but have the advantage of enclosing the sensitive barrier layers in the middle of the laminated structure. The polymer substrate on both sides would protect them from mechanical, chemical or environmental impact. Additionally, the layers are situated on the neutral axis of the encapsulation material and would as such be protected from tension or compression strains that would occur during bending (Chapter 3.2). One focus of the evaluation of these trials will be to compare both strategies.

The WVTR results (Table 6.11) show that the use of barrier materials with increas-

Table 6.11: WVTR results: ACP test versus calcium tests.

	ACP WVTR 23/50 [g/(m ² d)]	Ca test (with precond.) WVTR 23/50 [g/(m ² d)]	Ca test (without preconditioning) WVTR 65/85 ⇒ 23/50 ^a [g/(m ² d)]
Multilayer stacks			
A P+S+O+S ^b	3.5×10^{-2}	2.0×10^{-3}	-
B P+Z+O+Z ^c	3.3×10^{-3}	6.0×10^{-5} 8.0×10^{-4}	$4.7 \times 10^{-2} \Rightarrow 1.9 \times 10^{-3}$ $1.2 \times 10^{-2} \Rightarrow 5.0 \times 10^{-4}$
Laminates			
C P+S+O+S//a2 ^d	2.9×10^{-3}	8.0×10^{-4}	$2.9 \times 10^{-2} \Rightarrow 1.2 \times 10^{-3}$
D P+Z+O+Z//a1 ^e	7.5×10^{-4}	4.5×10^{-4}	$9.0 \times 10^{-3} \Rightarrow 3.8 \times 10^{-4}$
E P+Z+O+Z//a2 ^f	3.5×10^{-4}	2.0×10^{-4}	$5.4 \times 10^{-3} \Rightarrow 2.2 \times 10^{-4}$

^a⇒ means "calculated into"

^bPET + SiO_x + Ormocer[®]04a (= C5.5) + SiO_x

^cPET + ZnSn_xO_y + C5.5 + ZnSn_xO_y

^dPET + SiO_x + C5.5 + SiO_x + adhesive 2 (= A6.1) + SiO_x + C5.5 + SiO_x + PET

^ePET + ZnSn_xO_y + C5.5 + ZnSn_xO_y + adhesive 1 (= A5.10) + ZnSn_xO_y + C5.5 + ZnSn_xO_y + PET

^fPET + ZnSn_xO_y + C5.5 + ZnSn_xO_y + adhesive 2 (= A6.1) + ZnSn_xO_y + C5.5 + ZnSn_xO_y + PET

ingly improved intrinsic barrier properties improves the overall barrier performance of the encapsulation material for both multilayered and laminated structures: the WVTRs decrease by up to one to two orders of magnitude for both approaches.

Regarding first the multilayer stack materials only (materials A and B in Table 6.11), the exchange of the two thin inorganic barrier layers with two improved ones alone results in the mentioned decrease of the overall WVTR by one to two orders of magnitude. The materials A and B are basically of the same structure: a polymer film is coated with two thin inorganic barrier layers and one thin organic intermediate layer. Both use the same PET type "Melinex 401" ("P") as polymer substrate and the same intermediate layer of Ormocer[®]04a ("O"). Yet the two thin inorganic barrier layers are of very different intrinsic barrier properties: the SiO_x layer ("S") used in multilayer stack A has an effective permeability coefficient of approximately 2×10^{-18} mol/(m.Pa.s), which is already one of the best of the SiO_x barrier layer materials available on the market. Still, the ZnSn_xO_y layer ("Z") used in multilayer stack B has an even lower effective permeability coefficient of approximately 6×10^{-19} mol/(m.Pa.s). The comparison of the WVTR of materials A and B, measured by ACP test, shows a reduction of the overall WVTR by one order of magnitude: 3.3×10^{-3} g/(m² d) instead of 3.5×10^{-2} g/(m² d). The calcium tests show roughly the same difference, with the WVTR results of the *Konarka* test at ambient conditions, derived by calculation from the WVTR measured at higher temperature and humidity, fitting well to the results measured by directly by calcium test at ambient conditions. For material B, the WVTR results from the calciums tests span from highest 1.9×10^{-3} to lowest 6.0×10^{-5} g/(m² d). This range may result partially from the much smaller sample area of approximately 5 cm² that is analyzed by the calcium test in comparison to the

6 Results and Discussion: Barrier effects resulting from the combination of different layers

Table 6.12: Results regarding the transient barrier performance.

	ACP t_{nL} 23/50 [h]	Ca test (with precond.) t_{50} 23/50 [h]	Ca test (without preconditioning) t_{fail} 65/85 \Rightarrow 23/50 ^a [h]	OPV life test t_{fail} 85/85 \Rightarrow 23/50 ^a [h]
Multilayer stacks				
A	P+S+O+S ^b	56	540	-
B	P+Z+O+Z ^c	\gg 911	19500	178 \Rightarrow 4272
Laminates				
C	P+S+O+S//a2 ^d	271	800	292 \Rightarrow 7008
D	P+Z+O+Z//a1 ^e	\gg 193	3000	-
E	P+Z+O+Z//a2 ^f	\gg 1118	6500	1175 \Rightarrow 28200

^a \Rightarrow means "calculated into"

^bPET + SiO_x + Ormocer®04a (= C5.5) + SiO_x

^cPET + ZnSn_xO_y + C5.5 + ZnSn_xO_y

^dPET + SiO_x + C5.5 + SiO_x + adhesive 2 (= A6.1) + SiO_x + C5.5 + SiO_x + PET

^ePET + ZnSn_xO_y + C5.5 + ZnSn_xO_y + adhesive 1 (= A5.10) + ZnSn_xO_y + C5.5 + ZnSn_xO_y + PET

^fPET + ZnSn_xO_y + C5.5 + ZnSn_xO_y + adhesive 2 (= A6.1) + ZnSn_xO_y + C5.5 + ZnSn_xO_y + PET

ACP test. While the ACP test - which uses approximately 200 cm² as sample area - is virtually doing "an average over 40 calcium test results", the calcium test is more suited to capture the best possible WVTR, i.e. the potential, of a material. However, there is a general difference between the ACP and the calcium test results which is too large to result exclusively from material deviations over the sample area. A comparison of the measured time lags summarized in Table 6.12 helps to identify once again the time lag effect as the main reason for this difference. As in the previous chapter, the difference between the ACP test results and the calcium test results gets more pronounced the higher the time lag of the encapsulation material is: while material A has a time lag of 56 hours, the time lag of material B is more than 16 times longer.

Looking now at the measured WVTR of the laminated structures (materials C, D, E in Table 6.11), one does not find here the same time-lag-induced difference between ACP and calcium test - even though one should expect an even more pronounced time lag effect here due to many more layers in total. However, there is few gap (e.g. for material C) or nearly no gap at all (e.g. material E). The reason is the falsification of the calcium test results, because of side diffusion - which is neglectable for large area, multilayered samples, but becomes very large for small area, laminated samples. In face-to-face laminated materials, there will always be a relatively thick polymer substrate layer close to the detector of the WVTR measurement, i.e. either close to the ACP detector or adjacent to the calcium layer. Since the ACP test uses large samples for measurement, the percentage of side permeation is neglectable even for laminated samples and will not influence the resulting WVTR related to permeation orthogonal through all layers (see Chapter 4.4.4). The calcium test, however, uses very small sample areas. Therefore, side

diffusion plays an important role for this design of measurement. Samples that would allow a considerable high amount of side diffusion - e.g. face-to-face laminated samples - would then put out $WVTR^{Ca}$ results that contain a large additional part resulting from side diffusion. Hence, the $WVTR^{Ca}$ of the laminated samples in Table 6.11 are at the same time too high due to side diffusion and too low because of the time lag effect - which counterbalances to some extent, and which makes the gap to the according ACP results less pronounced. One indication working in favor for this theory, is the fact that the half-lifetimes “T50“ measured with the *Konarka* calcium test, correlate well to the time lags measured with the ACP test (Table 6.12): both indicate a very long instationary period of the water vapor permeation process for the laminated materials.

During this work, only material D could be tested in real OE device tests: in this case, an OPV module was encapsulated in material C from all sides and stored at 85°C and 85% RH. It survived 360 hours at these extreme conditions which would refer to a minimum lifetime at ambient conditions of approximately 1.5 years according to *Konarka*'s experience.

Hence,

- The time lag effect is a very important barrier effect, effective not only for the calcium test, but also in real life OE devices, and it should therefore be used when trying to develop OE encapsulation materials.
- The time lag of an OE encapsulation material can be increased by using thin inorganic and organic layers of high intrinsic barrier performance and by combining them using face-to-face lamination.
- For a targeted lifetime of 1.5 years at ambient conditions a time lag of 350 to 400 hours is required, which would refer to a required $WVTR^{Ca}$ of approximately $5 \times 10^{-4} \text{ g}/(\text{m}^2 \text{ d})$ measured by calcium test or to a required $WVTR$ of approximately 1×10^{-3} to $8 \times 10^{-4} \text{ g}/(\text{m}^2 \text{ d})$ measured by ACP test.
- When trying to understand the water vapor permeation mechanism through OE encapsulation materials, a method like the ACP test should always be used in parallel to the calcium test, i.e. a measurement design where (1) the permeated water vapor is transported away from the membrane so that always a constant concentration gradient is assured over the membrane, (2) the sensor is not chemically changed during the whole measurement period.
- When trying to screen potentially suited OE encapsulation materials, the calcium test is probably the best choice, as it correlates well and reflects all barrier effects that would be significant for the real device, too.

Yet, despite the ACP test and the calcium test are both very valuable for pre-screening, the final testing should always be verified by encapsulating the actual OE device. Especially for OLED encapsulation, additional effects may occur that are not captured neither by the ACP nor by the calcium test [147].

7 Results and Discussion: Importance of the barrier effects within the entire layer stack

7.1 Influence of the barrier level of the inorganic layer

In order to clarify to which extent an improvement of the intrinsic barrier performance of an inorganic barrier layer would influence the encapsulation material, six different structures ("a" to "f") were produced four times - giving four sets being called "S" to "Z3" (Table 7.1). The only difference between the four sets are the thin inorganic barrier layers. Set "S" uses thin SiO_x layers that were produced by *Alcan Packaging Services AG* via electron beam deposition. The sets "Z1", "Z2" and "Z3" use thin ZnSn_xO_y layers that were produced by *Fraunhofer FEP* via magnetron sputtering. From set "Z1" to set "Z3", the same deposition process was used, but continuously improved - even though the im-

Table 7.1: WVTR of encapsulation materials with varying inorganic qualities, measured by ACP test, at 23°C and 50% RH.

Structure, with "X" being:	WVTR in [g/(m ² d)]			
	S	Z1	Z2	Z3
Multilayer stacks				
a P + X ^a	0.09729	0.02503	0.02082	-
b P + X + OR ^b	0.06241	0.01099	-	0.00674
c P + X + OR + X ^c	0.03548	0.00658	0.00173	0.00348
Laminates				
d P + X // A6.1 ^d	0.03763	-	0.00157	-
e P + X + OR // A6.1 ^e	0.02207	0.00194	0.00090	0.00044
f P + X + OR + X // A6.1 ^f	0.00287	0.00050	0.00030	0.00043

^aPET + inorganic X

^bPET + inorganic X + Ormocer[®]04a

^cPET + inorganic X + Ormocer[®]04a + inorganic X

^dPET + inorganic X + adhesive A6.1 + inorganic X + PET

^ePET + inorganic X + Ormocer[®]04a + adhesive A6.1 + Ormocer[®]04a + inorganic X + PET

^fPET + in. X + Ormocer[®]04a + in. X + adhesive A6.1 + in. X + Ormocer[®]04a + in. X + PET

7 Results and Discussion: Importance of the barrier effects within the entire layer stack

Table 7.2: WVTR^{Ca} of encapsulation materials with varying inorganic qualities, measured by calcium test at 23°C and 50% RH.

Structure, with “X” being:	WVTR ^{Ca} , in [g/(m ² d)]			
	S2	Z1	Z2	Z3
Multilayer stacks				
a P + X ^a	≥ 10 ⁻³	≥ 10 ⁻³	-	-
b P + X + OR ^b	-	-	1 × 10 ⁻³	6.5 × 10 ⁻⁴
c P + X + OR + X ^c	-	2 × 10 ⁻³	-	8 × 10 ⁻⁵
Laminates				
d P + X // A6.1 ^d	1.5 × 10 ⁻²	1.8 × 10 ⁻³	-	-
e P + X + OR // A6.1 ^e	1 × 10 ⁻²	1 × 10 ⁻³	5 × 10 ⁻⁴	4 × 10 ⁻⁴
f P + X + OR + X // A6.1 ^f	6 × 10 ^{-4g}	8 × 10 ⁻⁴	-	2 × 10 ⁻⁴

^aPET + inorganic X

^bPET + inorganic X + Ormocer[®]04a

^cPET + inorganic X + Ormocer[®]04a + inorganic X

^dPET + inorganic X + adhesive A6.1 + inorganic X + PET

^ePET + inorganic X + Ormocer[®]04a + adhesive A6.1 + Ormocer[®]04a + inorganic X + PET

^fPET + in. X + Ormocer[®]04a + in. X + adhesive A6.1 + in. X + Ormocer[®]04a + in. X + PET

^gOnly one sample, no average.

provements were rather small compared to the general difference in barrier performance between the ZnSn_xO_y sets and the SiO_x sets.

The intrinsic barrier performance of the thin inorganic barrier layers used in the four sets, increases from S to Z3 - which can be seen when comparing the structure types (a) (Table 7.1). The more layers that are added to the multilayer stack - comparing structure types (a) to (c) - the more effectively an improved thin inorganic barrier layer reduces the overall transmission rates. Even minor improvements of the thin inorganic barrier layer of around 15%, e.g. from Z1 to Z2, lead to barrier improvements for the multilayer stack type (c) of over 70% (Table 7.1) - which is nearly a factor of improvement of four. For large differences in the barrier quality of the inorganic layer, the improvement of the multilayer stack gets over-proportionally more pronounced: e.g. the WVTR for structure type (c) improves by a factor of 10 when using thin inorganic barrier layers of type “Z2” instead of type “S” having an original factor of improvement of only approximately four. This indicates a time lag effect as demonstrated in Chapters 6.3 and 6.4.

Theoretically, when comparing laminated structures - like (d) to (f) - to their original half-structures - like (a) to (c) - their WVTR results should (when assuming steady state) be roughly the half of the WVTR of the half-structures. That this is not the case for the laminated structures (Table 7.1) is due to the time lag effect. For the same reason, the corresponding WVTR^{Ca} (Table 7.2) show an increasing gap from structures (a) to (f) towards the WVTR measured by ACP (Table 7.1) as explained in Chapter 6.4.

The factor by which the WVTR of the structures type (f) deviate from the theoretical half of the WVTR of the corresponding half-structures is for all sets between 3 and 6 (Table 7.1) - without any trend correlated to the intrinsic barrier performance of the (a)

structures. Hence the time lag effect is working similarly for all four sets, independent of the intrinsic barrier performance of the thin inorganic barrier layers. However, as the "starting point" is a different one, the final WVTR of the (f) structures is lowest for Z3 (Table 7.1).

During this work, an AlO_x layer was deposited by *Max Planck Institute (MPI) Halle* using atomic layer deposition (ALD). Its WVTR^{Ca} on top of the same PET substrate as used above (similar to structure (a)) was measured to be $(1 - 5) \times 10^{-4} \text{ g}/(\text{m}^2 \text{ d})$. Further experiments with structures of type (b) to (f) based on this inorganic barrier layer were not possible within this work due to a lack of material. Yet, taking into account the strong improvement of structures (c) or (f) when using "Z3" instead of "S" (seen in Tables 7.1, 7.2), the improvement for the same structures must be huge when starting with this ALD material. Concluding from the data in Table 7.2, a structure of four or more layers, i.e. containing two or more ALD- AlO_x layers, should already show a WVTR^{Ca} in the $10^{-5} \text{ g}/(\text{m}^2 \text{ d})$ regime and a structure of 6 or more layers, i.e. containing at least three AlO_x layers, should show a WVTR^{Ca} in the $10^{-6} \text{ g}/(\text{m}^2 \text{ d})$ regime. Even lower WVTR^{Ca} should be achievable by using ALD deposited thin inorganic barrier layers of still better barrier performance - like the single, 25 nm thick AlO_x layer that was reported to have shown a WVTR^{Ca} of $6 \times 10^{-6} \text{ g}/(\text{m}^2 \text{ d})$ (though for a small, batch processed sheet) [34]. Therefore, working on the improvement of the thin inorganic barrier layer to develop OE encapsulation material of very low WVTR or WVTR^{Ca} , respectively, is definitely the right way to go.

7.2 Influence of the barrier level of the organic layer

Aiming to clarify the same question for the thin organic barrier layers now, i.e. to which extent would an improvement of the intrinsic barrier performance of an organic barrier layer influence the overall barrier performance of the encapsulation material, similar trials were performed. As there generally exist two types of organic materials in an OE encapsulation material, i.e. lacquers and adhesives, two ranges of materials were evaluated separately.

First, materials were produced that consist all of the same base polymer, the same thin inorganic barrier layer and the same lamination adhesive, but differ in the type of lacquer materials. From lacquer C5.1 to C5.5 the intrinsic barrier performance against water vapor

Table 7.3: Barrier properties of the lacquers.

Lacquer	P_{wv} [mol/(m s Pa)]	S_{wv} at 50 % RH [mol/(m ³ Pa)]	D_{wv}^a at 50 % RH [m ² /s]	P_{O_2} [mol/(m s Pa)]
C5.1	3.8×10^{-14}	0.33	11.5×10^{-14}	5.4×10^{-18}
C5.3	$2.0 \times 10^{-14}^b$	1.0 - 1.7 ^b	$(1.2 - 2.0) \times 10^{-14}$	2.8×10^{-18}
C5.5	1.6×10^{-13}	1.28	1.0×10^{-14}	9.8×10^{-19}

^aCalculated from P_{wv} and S_{wv} using Equ. (3.7).

^bValues taken from [19], where the sorption coefficient was measured with a different method having less accuracy (therefore this greater range).

7 Results and Discussion: Importance of the barrier effects within the entire layer stack

Table 7.4: WVTR of encapsulation materials with varying organic qualities, at 23°C and 50% RH.

Structure	WVTR, by ACP test [g/(m ² d)]	WVTR, by calcium test [g/(m ² d)]
Multilayer stacks		
P + S + C5.1 ^a	0.06805	-
P + S + C5.5 ^b	0.06242	-
P + S + C5.3 ^c	0.05076	-
P + S + C5.1 + C5.3 ^d	0.05769	-
P + S + C5.3 + C5.1 ^e	0.04297	-
Laminates		
P + S + C5.1 // A6.2 ^f	0.02617	(3 – 5) × 10 ⁻³
P + S + C5.3 // A6.2 ^g	0.01053	2 × 10 ⁻³
P + S + C5.1 + C5.3 // A6.2 ^h	0.01430	1 × 10 ⁻³
P + S + C5.3 + C5.1 // A6.2 ⁱ	0.00690	8 × 10 ⁻⁴

^aPET + SiO_x + coating C5.1

^bPET + SiO_x + coating C5.5

^cPET + SiO_x + coating C5.3

^dPET + SiO_x + coating C5.1 + coating C5.3

^ePET + SiO_x + coating C5.3 + coating C5.1

^fPET + SiO_x + coating C5.1 + adhesive A6.2 + coating C5.1 + SiO_x + PET

^gPET + SiO_x + coating C5.3 + adhesive A6.2 + coating C5.3 + SiO_x + PET

^hPET + SiO_x + coat. C5.1 + coat. C5.3 + adhesive A6.2 + coat. C5.3 + coat. C5.1 + SiO_x + PET

ⁱPET + SiO_x + coat. C5.3 + coat. C5.1 + adhesive A6.2 + coat. C5.1 + coat. C5.3 + SiO_x + PET

is improving: the permeability coefficients towards water vapor P_{wv} decrease (Table 7.3). When looking at the diffusion coefficient against water vapor D_{wv} , it becomes clear that this difference in intrinsic water vapor barrier probably results from an increase in network density from lacquer C5.1 over lacquer C5.3 to lacquer C5.5: the diffusion coefficients against water vapor decrease accordingly. This conclusion is affirmed by the decrease of the permeability coefficients towards oxygen P_{O_2} , which is decreasing accordingly, too. Using these three lacquers, several encapsulation materials were produced and their WVTR were measured using the ACP test and, if possible, the calcium test, too (Table 7.4).

The WVTR results of the multilayer stacks type [PET + SiO_x + coating] do not correlate entirely to the intrinsic barrier properties of the coating materials: the WVTRs decrease from lacquer C5.1 to lacquer C5.5 to lacquer C5.3. In Chapter 6.1 it was demonstrated that coating materials may show such a good synergistic barrier effect on top of a thin inorganic barrier coating that it out-performs their less pronounced intrinsic barrier performance, and a good synergistic barrier effect was observed for lacquer C5.5. Due to the similarities of the lacquers C5.3 and C5.5 in their chemical basis, it is to be expected that both show a good synergistic barrier effect on top of the thin inorganic barrier layer

Table 7.5: Barrier properties of the adhesives.

Adhesive	P_{wv} [mol/(m s Pa)]	S_{wv} at 50 % RH [mol/(m ³ Pa)]	D_{wv} ^a at 50 % RH [m ² /s]	P_{O_2} [mol/(m s Pa)]
A6.1	1.2×10^{-12}	0.06	2×10^{-11}	1.2×10^{-15}
A5.3	1.2×10^{-12}	0.59	2×10^{-12}	7.0×10^{-17}
A5.4	9.1×10^{-14}	0.26	3.5×10^{-13}	1.9×10^{-18}

^aCalculated from P_{wv} and S_{wv} using Equ. (3.7).

used here (SiO_x). Concluding from the first three results in Table 7.4, it seems as if the synergistic barrier effect is more pronounced for lacquer C5.3 than lacquer C5.5.

The next two multilayer stack materials emphasize this theory: if there was no synergistic barrier effect, the structure [PET + SiO_x + coating C5.1 + coating C5.3] would have exactly the same WVTR as the structure [PET + SiO_x + coating C5.3 + coating C5.1] - yet, it does not (Table 7.4).

Then, these multilayer stack structures were laminated face-to-face using for all of them the same adhesive A6.2. This adhesive was chosen because it has only a medium water vapor barrier ($P_{wv} \gg 1.2 \times 10^{-13}$ mol/(m s Pa)) in order not to overlap the effects resulting from the lacquer layers. All laminated structures show WVTR less than the half of their original halves, hence, are influenced by the time lag effect. The lower the WVTR of the combination [PET + SiO_x + coating] was before, the better the WVTR of the laminate - and additionally over-proportionally better due to the time lag effect, which can be seen even more when looking at the calcium test results (Table 7.4).

Hence, taking an organic material with improved intrinsic barrier properties is useful to reduce the final transmission rate of the encapsulation material, especially when it generates a high synergistic barrier effect on top of the thin inorganic barrier layer. Therefore, even the order in which several organic layers are stacked on top of a thin inorganic barrier layer is of importance. However, the improvement gained by optimising the organic barrier layer(s) is small compared to the improvement gained by the optimization of the thin inorganic barrier layers: the WVTR of the structure [PET + SiO_x + coating + adhesive A6.2 + coating + SiO_x + PET] gets reduced only by a factor of approximately two when using C5.3 instead C5.5 (from 0.02207 to 0.01053 g/(m² d), Tables 7.1, 7.4), while the WVTR of the same structure gets reduced by a factor of 11 when replacing the SiO_x by a non-optimized ZnSn_xO_y (from 0.02207 to 0.00194 g/(m² d), Table 7.1). Using an optimized ZnSn_xO_y would lead to an improvement factor of 50 (from 0.02207 to 0.00044 g/(m² d), Table 7.1).

Now, to study to which extent an improvement of the intrinsic barrier performance of an adhesive would influence the overall barrier performance of the encapsulation material, eight different structures were produced three times to give three sets called "A6.1", "A5.3" and "A5.4" (Tables 7.6, 7.7). The difference between the three sets is - as the names indicate - the adhesive. These three adhesives were chosen, because of their increasing intrinsic barrier performance against water vapor and oxygen: the corresponding diffusion coefficients decrease by orders of magnitude (Table 7.5).

When using these adhesives in laminated structures, the overall WVTR decreases with

7 Results and Discussion: Importance of the barrier effects within the entire layer stack

Table 7.6: WVTR of encapsulation materials with varying adhesive qualities, measured with ACP test, at 23°C and 50% RH.

Structure, with “X” being:	WVTR, measured by ACP, in [g/(m ² d)]		
	A6.1	A5.3	A5.4
P + S // X ^a	0.03768	0.03501	0.00333
P + S + C5.5 // X ^b	0.02207	0.01600	0.00947
P + S + C5.3 // X ^c	-	0.00631	0.00172
P + S + C5.5 + S // X ^d	0.00287	-	0.00033
P + Z1 // X ^e	0.00157	0.00970	0.00098
P + Z1 + C5.5 // X ^f	0.00097	0.00101	0.00121
P + Z2 + C5.5 // X ^g	0.00090	-	0.00042
P + Z1 + C5.5 + Z1 // X ^h	0.00050	-	0.00032

^aPET + SiO_x + adhesive X + SiO_x + PET

^bPET + SiO_x + coating C5.5 + adhesive X + coating C5.5 + SiO_x + PET

^cPET + SiO_x + coating C5.3 + adhesive X + coating C5.3 + SiO_x + PET

^dPET + SiO_x + coating C5.5 + SiO_x + adhesive X + SiO_x + coating C5.5 + SiO_x + PET

^ePET + ZnSn_xO_y + adhesive X + ZnSn_xO_y + PET

^fPET + ZnSn_xO_y + coating C5.5 + adhesive X + coating C5.5 + ZnSn_xO_y + PET

^gPET + ZnSn_xO_y + coating C5.5 + adhesive X + coating C5.5 + ZnSn_xO_y + PET

^hPET + ZnSn_xO_y + coat. C5.5 + ZnSn_xO_y + adhesive X + ZnSn_xO_y + coat. C5.5 + ZnSn_xO_y + PET

Table 7.7: WVTR^{Ca} of encapsulation materials with varying adhesive qualities, measured with calcium test, at 23°C and 50% RH.

Structure, with “X” being:	WVTR, Ca Test 23/50 [g/(m ² d)]	
	A6.1	A5.4
P + S // X ^a	1.5 × 10 ⁻²	5 × 10 ⁻⁴
P + S + C5.5 // X ^b	1 × 10 ⁻²	1.5 × 10 ⁻³
P + S + C5.5 + S // X ^c	1 × 10 ⁻³	6 × 10 ⁻⁴ ^d
P + Z1 // X ^e	1.8 × 10 ⁻³	1 × 10 ⁻³ ^d
P + Z1 + C5.5 // X ^f	1 × 10 ⁻³	1 × 10 ⁻⁴

^aPET + SiO_x + adhesive X + SiO_x + PET

^bPET + SiO_x + coating C5.5 + adhesive X + coating C5.5 + SiO_x + PET

^cPET + SiO_x + coat. C5.5 + SiO_x + adh. X + SiO_x + coat. C5.5 + SiO_x + PET

^dOnly one sample, no average.

^ePET + ZnSn_xO_y + adhesive X + ZnSn_xO_y + PET

^fPET + ZnSn_xO_y + coating C5.5 + adhesive X + coating C5.5 + ZnSn_xO_y + PET

decreasing intrinsic transmission of the adhesives - no matter how many layers in total or whether the structures contain SiO_x or ZnSn_xO_y as thin inorganic barrier layers, and both for ACP and calcium test measurements (Tables 7.6, 7.7). Again, as seen in the previous chapters, the effect is more pronounced in the calcium test results than in the ACP test results - due to the time lag effect. Compared to the optimization of the organic barrier

layer, the optimization of the adhesive can be less, similarly or more effective, depending on the combination of materials:

- Example 1: When starting from a structure containing a medium barrier adhesive like A6.2, the use of an improved barrier adhesive like A5.4 would lead to significant improvements far above those of an improved organic coating: the WVTR of the structure [PET + SiO_x + coating C5.3 // adhesive A5.4] would then be 0.00172 g/(m² d) (Table 7.6) instead of 0.01053 g/(m² d) (Table 7.4) for the structure [PET + SiO_x + coating C5.3 // adhesive A6.2]. Hence, for this combination of materials, the optimization of the adhesive outperforms the optimization of organic coating material.
- Example 2: When starting with an already very much improved barrier adhesive (i.e. adhesive A5.3), the use of a “half-structure” material with an improved organic top coat, namely [PET + SiO_x + coating C5.3], having a WVTR of 0.05076 g/(m² d) (Table 7.4), instead of [PET + SiO_x + coating C5.5], having a WVTR of 0.06242 g/(m² d) (Table 7.4), leads to a WVTR of the laminated structure [PET + SiO_x + coating C5.3 // adhesive A5.3] of 0.00631 g/(m² d) instead of 0.01600 g/(m² d) for the laminated structure [PET + SiO_x + coating C5.5 // adhesive A5.3] (Table 7.6). Using a different adhesive, for example adhesive A5.4, to laminate the original structure would only lead to a WVTR of the laminated structure [PET + SiO_x + coating C5.5 // adhesive A5.4] of 0.00974 g/(m² d) (Table 7.6). Hence, for this combination of materials, the optimization of the lacquer had the more important effect (because 0.00631 g/(m² d) as WVTR is better than 0.00947 g/(m² d)).

Even though improvements of the WVTR higher than one order of magnitude are possible by using optimized barrier adhesives (see example 1), the effect of optimized adhesives is easily out-performed by the use of optimized thin inorganic barrier layers: The WVTR of the laminated structure [PET + SiO_x + coating C5.5 // adhesive X] decreases only from 0.02207 to 0.00947 g/(m² d) when using adhesive A5.4 instead of A6.1 (Table 7.6), while the WVTR of the same structure [PET + inorganic X + coating C5.5 // adhesive A6.1] gets improved from 0.02207 to 0.00090 g/(m² d) when using good ZnSnO_x instead of SiO_x layers (Table 7.6). Still, when using additionally an improved barrier adhesive (like A5.4), the WVTR would decrease a little further to 0.00042 g/(m² d) (Table 7.6).

Hence, from all layers that play a role for the overall barrier performance of the encapsulation material, the optimization of the thin inorganic barrier layers shows the greatest effect - largely laying ahead the (roughly equal) improvement effects resulting from the optimization of the lacquers and the adhesives, respectively. Still, despite the optimization of the thin inorganic barrier layers should be first priority, the optimization of the organic barrier layers will still be of use, as their impact on the overall transmission rates is - though of minor size - not negligible.

7.3 Structures with a high number of layers

Taking into account the conclusions from Chapter 7.2, one strategy could be to only improve the thin inorganic barrier layers and combine as many as possible of them, without

7 Results and Discussion: Importance of the barrier effects within the entire layer stack

Table 7.8: Structures with a high number of layers, sorted according their number of thin inorganic barrier layers included. All WVTR values are given at 23°C and 50% RH.

Structure	i^a / t^b	WVTR ^{ACP} [g/(m ² d)]	WVTR ^{Ca} [g/(m ² d)]
α (P + S + C5.1 + C5.3 // A6.2) // A5.3	4 / 19	-	1×10^{-3}
β (P + S + C5.1 + C5.3 // A6.2) // A5.4	4 / 19	-	8×10^{-4}
γ (P + S + C5.3 + C5.1 // A6.2) // A5.3	4 / 19	0.00227	$1 \times 10^{-3}{}^c$
δ (P + S + C5.3 + C5.1 // A6.2) // A5.4	4 / 19	0.00191	5×10^{-4}
ε P + 5 (A2 + PAC) ^d	5 / 11	0.00241	2×10^{-5}
ζ P + A1 + OR + A1 + OR + T // A5.3	6 / 13	0.00102	-
η P + A1 + OR + A1 + OR + T // A5.4	6 / 13	0.00091	-

^a i ... number of inorganic layers included

^b t ... total number of layers

^cOnly one sample, no average.

^dBarix FEG 200 structure of Vitex Systems.

caring much for any of the organic layers. The assumption laying behind this argumentation is, that for a high number of layers, the organic layers would anyway no longer have a significant effect on the overall WVTR. Whether this is true will be studied by evaluating encapsulation materials that were produced with a high total number of layers (Table 7.8).

Comparing the WVTR^{Ca} results of structures α and β shows that the choice of an improved adhesive still has a significant (though small) influence on the water vapor transmission, despite only one out of 19 layers being changed: the WVTR^{Ca} is reduced from 1×10^{-3} to 8×10^{-4} g/(m² d) (Table 7.8).

The WVTR^{Ca} of the same 19 layers structure is even reduced when changing the order of two of the organic coatings: just the increase in synergistic effect from structure β to structure δ reduces the WVTR^{Ca} from 8×10^{-4} to 5×10^{-4} g/(m² d) (Table 7.8). For six thin inorganic barrier layers and 13 layers in total, the use of a better barrier adhesive (A5.4 instead of A5.3) decreases the WVTR from 0.00102 to 0.00091 g/(m² d) (Table 7.8) - which is a lot at this low level and which would probably give a WVTR^{Ca} of somewhere in the 10^{-5} g/(m² d) regime. Hence, despite this high number of layers, the optimization of the thin organic barrier layers is still useful.

However, the integration of additional thin inorganic barrier layers (e.g. structures ε , ζ compared to structure γ) seems to have a much higher effect on the improvement of the water vapor barrier: materials with a much smaller total number of layers show a much reduced WVTR just because of the higher number thin inorganic barrier layers included (Table 7.8). Therefore, even for large amounts of layers, the major barrier impact is still resulting from the optimization / addition of a thin inorganic barrier layer.

8 Conclusions

Most importantly, an OE encapsulation material should block water vapor, since this is the one of the three environmental substances - water vapor, oxygen and nitrogen - that would degrade fastest the sensitive calcium parts of OE devices. This is a challenging task as it is water vapor, too, that permeates much faster than the two others.

During this work, it was found that the ratio between the intrinsic permeability against water vapor compared to the intrinsic permeability against oxygen of roughly 10,000 to 1 applies not only for the polymer substrates, but as well for thin inorganic and organic barrier layers. Significant exceptions from that ratio are rare and they occur only for highly non-polar organic materials (polyolefin type) or very polar organic materials (PVOH type). Due to this general permeability rule, it is not possible to improve the water vapor barrier alone by adding non-polar functional groups to the material to such an extent that it would be sufficient to create effective OE encapsulation materials. Improvements of the intrinsic water vapor barrier of materials always have to happen via structural changes of the materials, i.e. via the increase of the crosslink density of the organic network (for organic materials) or via the reduction of the amount of pores and nanopores in the thin inorganic barrier layers (for inorganic materials).

Basically, there is a certain physico-economical limit of structural improvements, both for the organic and the inorganic barrier materials, that would make it impossible to develop very water vapor tight encapsulation materials - if there was only the possibility to stack barrier materials on top of each other to sum up the intrinsic barrier properties. However, there are more barrier effects resulting from the combination of layers - some of them so important that the target of developing (cost-effective) encapsulation materials, enabling OE devices having a lifetime of several years, is achievable.

It was found during this work that the most important barrier effect concerning the protection of OE devices against water vapor is the time lag effect. Thanks to this effect, the instationary part of the water vapor permeation process can be extended by orders of magnitude - so long that finally the water vapor permeation process cannot arrive in steady state at its final (higher) absolute WVTR any more, because the calcium layers are inhibited before and block further (fast) increase of permeation. This inhibition virtually increases the instationary period even more and holds the water vapor permeation at low level for a long time. The final absolute WVTR value becomes unimportant, because the lifetime of the OE device would happen during this instationary part of the water vapor permeation process. First priority should therefore be to maximize the time lag effect.

In value largely behind the time lag effect, but still existent to a significant extent, is the synergistic barrier effect. Here, for this work, this name represents the sum of all phenomena that lead to a surplus of barrier improvement when coating an organic barrier material on top of a thin inorganic barrier layer - "surplus" regarding the expected

transmission rates that are theoretically calculated when just adding the intrinsic barrier performance of the thin organic layer to the one of the thin inorganic layer. The synergistic barrier effect was found to be more pronounced for water vapor permeation than for oxygen permeation. Two phenomena were mainly identified to possibly be the factors behind this effect: the (partial) filling of the larger (but still micro scale) pores of the thin inorganic barrier layers and - more important for the water vapor barrier - the (partial) filling of the nanopores of the inorganic bulk. The assumed covalent bonding of the organic coating material to the surface of the thin inorganic barrier layer was found to possibly play a minor or no role for this effect.

The last theoretically expected barrier effect, the tortuous path effect, was found to not occur in practice. There are two possible explanations of this result: either this effect does not exist in reality or is entirely suppressed by the unavoidable mechanical (small) damage of the thin inorganic barrier layers that happens during the transport of the multilayered encapsulation material through the machine.

It was found that the time lag effect could be increased effectively by using many improved thin inorganic barrier layers. Some additional improvement of the time lag effect can also be gained by choosing improved organic barrier materials. Especially useful are such organic barrier materials that would create a high synergistic barrier effect on top of the respective inorganic layer. The improvements comparing the use of better lacquers or of better lamination adhesives are either similar or in favor of one of the two, i.e. there is no clear trend, because it depends to a great extent on the combination of layers in total in one encapsulation material.

Yet all improvements gained by optimized organic layers - even counting maximized synergistic barrier effects for it - are always much lower than improvements gained by improved thin inorganic barrier layers. In general, very small improvements of the thin inorganic barrier layers (e.g. 15%) can lead to high improvements of the final barrier performance of the multilayered encapsulation material (e.g. by a factor of $\gg 10$). Optimization of the organic coating materials achieve much lower improvements. Optimization of the organic layers lead, for the structures evaluated in this work, to improvements of the final barrier performance for a factor of up to five. The small improvements achieved for the intrinsic barrier performance of organic coating material by optimizing their curing parameters from "good cure" to "very good cure" were not even detectable in the final barrier performance of the multilayered encapsulation material. Since the barrier improvement effect of very well cured organic layers compared to normally cured layers is not detectable for the completed multilayer structure, the Raman method, developed during this work for the optimization of the curing of organic coating materials, is not useful (too much effort for little to no benefit).

Hence, if one had to choose between the improvement of the thin inorganic barrier layers and the optimization of the organic materials, the first strategy should be preferred, because it would lead much earlier to the desired results. Still, some small barrier improvement could even be gained for structures having a high number of (inorganic) layers by optimization of the organic barrier materials - which was shown for structures having up to 19 layers in total.

A very effective increase of the time lag effect can be achieved when creating structures with a high number of layers (e.g. 9 layers or more) by preparing structures of a lower number of layers in total (e.g. four layers) and doubling it by face-to-face lamina-

tion - at least as long as side diffusion of water vapor does not play a role, like for large area or side protected OE products. By face-to-face lamination, a high amount of barrier layers is stacked in the middle of the laminate structure. It would have the same barrier performance as one side multilayered structures, but have the advantage to protect the sensitive barrier layers from mechanical, chemical or environmental impact. Additionally, the layers are situated on the neutral axis of the encapsulation material and would as such be protected from tension or compression strains that would occur during bending. This is especially important as the OE encapsulation materials would always have to withstand bending - if not during the later use of the OE product, bending will happen in any case during the transport in roll-to-roll processing machines.

Since the tortuous path effect is of no importance (and given side diffusion neither) it is not necessary to use very thin organic layers of below 1 μm thickness. On the contrary, the thinner the organic intermediate layers, the less decoupled the thin inorganic layers are from each other - in terms of creating smooth, close inorganic layers (no shadowing of the previous one) as well as with respect to mechanical sensitivity. For roll-to-roll processing machines that handle the web very delicately, e.g. the sensitive coated side never touches a transport or winding roll, the minimum thickness should not go below 1 μm . For more industrial like, "rougner" machines, the minimum thickness should be several micrometers at least.

Further protection of the barrier performance of the thin inorganic barrier layers is achieved when avoiding high shrinkage of the polymer substrate, e.g. during steps of thermal curing of the subsequent layers. It was found that the previously reported 1% for the maximum shrinkage a thin inorganic barrier could withstand without a reduction in barrier performance, was too high. Maximum shrinkage should be the half of it or even lower: less than 0.3% would be best. This can be achieved by reducing the temperatures and the time spans during which the temperatures are applied, by increasing (a little) the thicknesses of the polymer substrate and the inorganic barrier layer and by choosing inorganic barrier layers of low intrinsic stiffness (i.e. low E modulus).

Furthermore, both the organic and the inorganic barrier layers have to be screened and selected according to their intrinsic barrier performance as well as according to their mechanical, chemical, UV and climate stability - which can be opposing criteria. A compromise has to be selected. Yet, there is another constraint: all these criteria are not only to be evaluated for each of the materials independently from the others, but also in combination, because it can happen that a quite stable organic coating material is not stable under climate any more when in combination with a thin inorganic barrier layer. Vice versa, an organic material can trigger degradation of the inorganic material which would otherwise be stable enough. Bond strength, too, is a property where the bonded substrates and the adhesive have to be fitted to each other - in terms of mechanical properties (like flexibility and cohesive strength) as well in terms of surface related characteristics (like wetting behavior). The synergistic barrier effect, too, is highest for best "interface building properties" of the organic coating material onto the thin inorganic barrier layer, instead of for the best intrinsic water vapor barrier.

Hence, for the development of OE encapsulation material, it is not sufficient to search exclusively for the ultimate coating materials of lowest possible intrinsic water vapor barrier. It is the match of the materials that has such a significant influence that in some cases - e.g. for the synergistic barrier effect, the bond strength or the climate stability -

a good match of materials can even outperform the barrier improvement gained by best intrinsic barrier against water vapor.

Since a lot of combinations would have to be tested, the experimental effort would be high. Theoretical methods can help to decrease it. Though - according to the results of this work - the absolute data for the time lags cannot be calculated correctly by FEA based calculations, the trend is predicted correctly and the absolute WVTR are correct. Putting a method like the ACP test - which purely monitors the water vapor permeation process - next to the calcium test - which is affected at the same time by the water vapor permeation process and the reaction kinetics of the calcium - helps to gain a basic understanding about water vapor permeation and the degradation of very thin calcium layers. Yet, for the actual suitability screening of encapsulation materials, tests with the actual OE devices are essential.

From the engineering point of view, there is one further (non-scientific) criterion which is important for the selection and combination of barrier materials to create the final encapsulation material: the costs. From the experience gained during this work, it is not true - as assumed in the community at the beginning of this work - that a low cost encapsulation material of very high barrier performance could be fabricated by stacking "millions" of low cost, "very low performing" coating materials on top of each other. First, it would not work from the point of view of technical feasibility and, second, it would not work either from the costs perspective. To achieve a certain low level of WVTR, one sooner or later has to switch to the next better performing inorganic barrier layer and the structures and processes based on it - accepting the increasing costs.

Therefore, not at least from taking this last point into account, there is no ultimate encapsulation material. It is a question of finding the balance between, on the one hand, how much of barrier improvement one would gain from the use of (a) better material(s) or process(es) and, on the other hand, the additional in costs one would have to take into account for that (these) material(s) or process(es).

For the encapsulation of OPV, the best materials produced during this work, would work well. For a targeted lifetime of the OPV module of 1.5 years at ambient conditions a time lag of 350 to 400 hours is required, which would refer to a required WVTR^{Ca} of approximately $5 \times 10^{-4} \text{ g}/(\text{m}^2 \text{ d})$ measured by calcium test or to a required WVTR of approximately 1×10^{-3} to $8 \times 10^{-4} \text{ g}/(\text{m}^2 \text{ d})$ measured by ACP test. This was achieved by using high quality, climate and UV stable inorganic layers (sputtered ZnSn_xO_y), relatively climate and UV stable organic coatings of good synergistic barrier effect on top of it (C5.5) and a climate and UV stable adhesive of high intrinsic water vapor barrier and good bond strength on top of the inorganic barrier layer (A5.10).

Nevertheless, improvement is still possible for the roll-to-roll strategy: during this work, it was demonstrated that roll-to-roll ALD deposited thin inorganic barrier layers do have the potential to create roll-to-roll produced OE encapsulation materials showing a WVTR^{Ca} in the $10^{-6} \text{ g}/(\text{m}^2 \text{ d})$ or even $10^{-7} \text{ g}/(\text{m}^2 \text{ d})$ regime. Multilayered encapsulation material based on ALD coated thin inorganic barrier layers would be a promising way towards further increased overall barrier performance.

9 Outlook

Based on the experience gained during this work and based on the current status of knowledge regarding the fabrication of OE encapsulation materials (as of 2011), it can be said that the roll-to-roll production of encapsulation material of transmission rates down to the low 10^{-4} g/(m² d) / high 10^{-5} g/(m² d) regime should not be a problem any more. Just one characteristic of this type of OE encapsulation material was not evaluated sufficiently up to now: the mechanical stability towards bending during the use of the final application. So far, there is no quantification of this property. It is of great interest to find a value that gives an idea about how much the gas barrier would decrease after how many cycles of bending at which frequency around a roll of which radius. Work is in progress to install test methods and define test parameters [148, 149, 150, 151, 152].

However, while the roll-to-roll strategy works well for OE products with a medium level of requirements, like OPV modules with lifetimes shorter than approximately 5 years, the way towards very high protection of OE devices against water vapor, as needed for OLED displays, will have to use another strategy. The roll-to-roll strategy is limited in its performance when it comes to achieving very low WVTR^{Ca} very homogeneously over a large area, i.e. high requirements regarding spot defects.

In this case, mainly two promising approaches are under evaluation currently. First, it could be worked with thin film encapsulation directly on top of the OE device. In this field, too, much improvement was achieved during the same time while this work was ongoing: the best barrier performance of thin film encapsulation stacks is now at 10^{-7} g/(m² d) regime (Fig. 9.1). The second strategy is the development of a layer material (and the according roll-to-roll coating processes) that would integrate active electronic and gas barrier properties in one, like when using graphene as a layer material. Both approaches are already delivering promising results [153, 154].

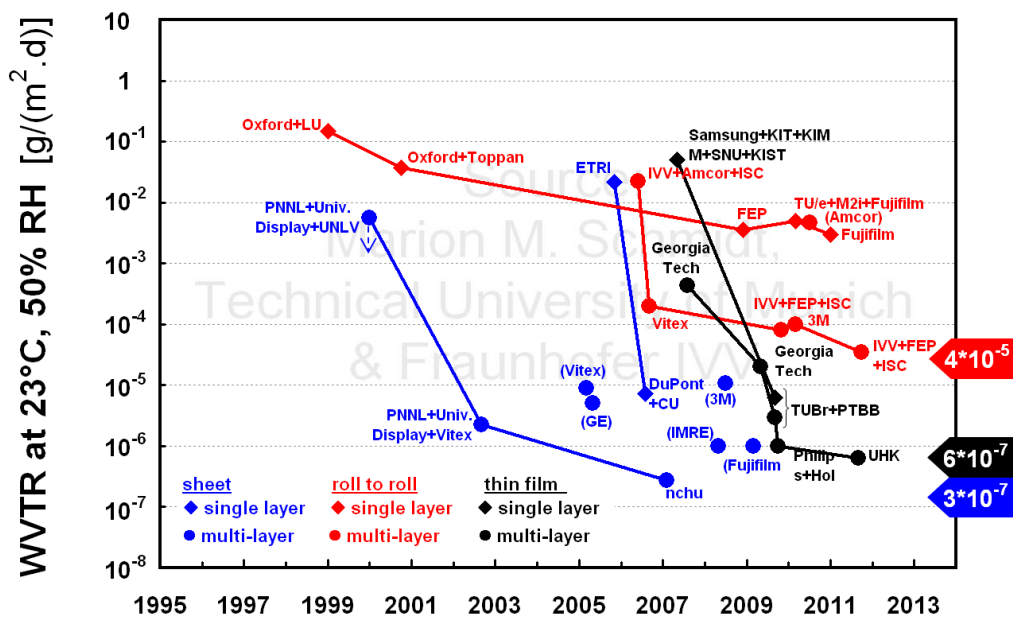


Figure 9.1: Best reported WVTR over time for each encapsulation strategy until now (2011) [26, 25, 14, 30, 31, 32, 33, 34, 35, 36, 37, 38, 39, 68, 69, 70, 71, 72, 73, 15, 74]. (Some WVTR results are included in this diagram despite the fact that they were no improvement over previous achievements, because they belong to important research groups in the research field of OE encapsulation.)

Appendices

A Additional experimental results

A1. Relation between curing quality of organic coatings and their barrier performance on the example of Ormocer[®] coating materials

Influence of the curing quality of organic coatings on their barrier performance

Since for some of the evaluated organic coating materials it was mentioned that a lower curing quality would lead to significant loss of barrier performance of the multilayered encapsulation material [155], it is necessary to study this effect quantitatively. Because of the network-structure-related permeation nature of the oxygen (Chapter 2.1) it is more favorable to study the oxygen than the water vapor barrier performance in comparison to the curing parameters. Assuming that varying curing parameters are correlated to varying structural, network-density-dependant barrier properties of the organic coatings, this effect should be seen more clearly for oxygen - without any other interfering effect that could result from a permeant with higher interaction like water vapor (Chapter 2.1).

For the experimental variation of the curing parameters and their correlation to the intrinsic oxygen barrier properties, Ormocer[®] 04a (coating material C5.5) and Ormocer[®] 08 (coating material C5.6) were chosen. These two lacquers both show a very good oxygen barrier performance (Section 5.3), even in very thin layers. Therefore, if coated on top on a very transmittive substrate like an ETFE film, one should be able to capture differences in the intrinsic oxygen barrier performance of the organic layer even though it is up to 200 times thinner than the substrate. Furthermore, these two lacquers are entirely thermal curing materials. i.e. there is only one parameter to be controlled: the input of thermal energy into the coating during the curing process.

Control of curing quality by Raman spectroscopy

To be able to quantify the curing quality of thin, roll-to-roll coated layers of Ormocer[®] lacquers as a function of the curing conditions, a Raman method was developed by the author. For the quantification of intensity peaks in Raman spectroscopy, the fluctuations of the basic intensity of the laser beam had to be taken into account, i.e. the laser intensity had to be quantified before each measurement. For this, the rough side of a silicon wafer was taken as calibration material. This has several advantages:

- The rough side of a silicon wafer shows a typical "packed" structure at the surface which is easy to focus in light microscopy (Fig. A.1a). This helps to adjust the

A Additional experimental results

confocal spot of the Raman laser beam exactly at the surface if this is required - given that a device like the alpha500 is used which contains light microscopy and Raman spectroscopy in one head.

- The perfectly crystalline structure of the silicon wafer results in one single and very well pronounced intensity peak in Raman spectroscopy (Fig. A.2a). Therefore, even very small fluctuations of the laser beam intensity can be captured.
- Crystalline silicon alters very slowly under the laser beam compared to the polymeric calibration materials (e.g. a piece of PMMA) recommended from the device producer. And if so, the altered areas are distinguishable easily from the "good" parts of the wafer in light microscopy, because they are visible as small black dots (Fig. A.1b).

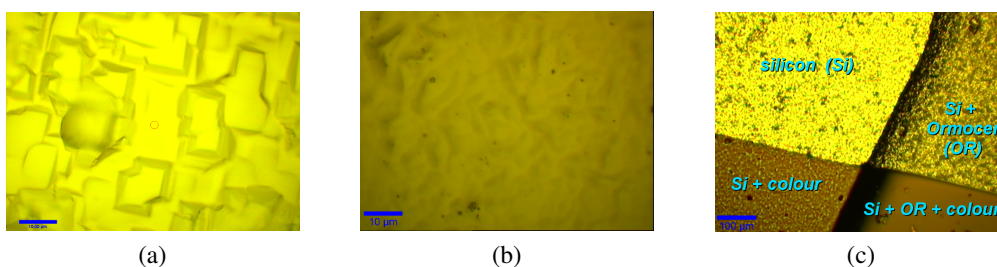
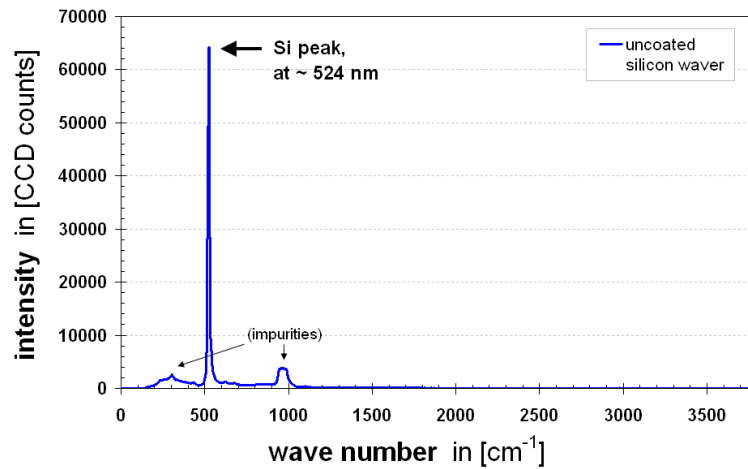


Figure A.1: Light microscopic pictures of the surfaces of an intact silicon wafer (a), of one altered by a laser beam (b) and of one coated with Ormocer[®] and marked with a coloured pen (c).

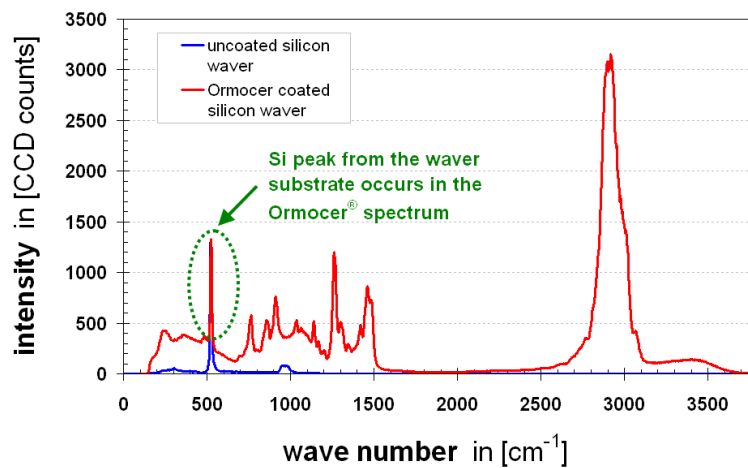
When trying to evaluate the curing quality of a thin, roll-to-roll coated organic layer, one has to take care of another difficulty: the Raman spectrum of the polymer substrate may superimpose the important peaks of the thin organic coating. In the case of Ormocer[®] lacquers, which additionally have a very weak (low intensity) spectrum, no polymer substrate exists that does not cover the important peaks of the Ormocer[®] layer.

Therefore, during the roll-to-roll coating trials, a thin and small piece of silicon wafer was fixed on the substrate. At the application unit, both the polymer film and the small piece of Silicon wafer were roll-to-roll coated with Ormocer[®] and dried under same conditions in the curing sections of the pilot plant. The coated polymer substrates were evaluated with respect to barrier performance and the small pieces of silicon wafer could be analysed in Raman spectroscopy.

As the peak of the silicon spectrum is very narrow (Fig. A.2a), it doesn't cover much of the Ormocer[®] spectrum. Even better, the intense peak of the silicon wafer even appears out of the combined spectrum when the Ormocer[®] coated silicon wafer is measured in the upper part of the Ormocer[®] layer (Fig. A.2b) and can therefore be used as calibration scale. This calibration is essential for comparisons between the Raman spectra of the different samples of Ormocer[®] coated silicon wafer - for two reasons. First, one has to take care of the daily intensity fluctuations of the laser beam source that dampen or amplify the whole recorded Raman spectrum and would therefore - if not calibrated - otherwise make comparisons impossible between measurements taken on different days.



(a)



(b)

Figure A.2: Raman spectra of the silicon wafer used for calibration (a) and coated with Ormocer[®] (b).

Second, not knowing whether the entire Raman spectrum of the Ormocer[®] layer changes with different curing statuses, one needs a point in the Raman spectrum that does not belong to the Ormocer[®] layer and that would definitely not change with varying curing conditions. This is the case for the silicon peak, as the silicon wafer (and therefore its spectrum) is not affected by the conditions that are typical for wet chemical coating.

Calculation of the thermal energy introduced in the laboratory oven

The input of thermal energy into the organic layer depends on two technological parameters: the curing temperature and the curing period - as long as one compares the same process of heat transfer. Yet, for this work, the curing procedures in the laboratory were different from the pilot plant: the first one uses an oven without active movement of the air, i.e. natural convective flow of heat, while the second one uses a drying channel that is equipped with a pump which circulates actively the hot air, i.e. forced convective flow

of heat. Therefore, the comparisons between barrier performance and curing parameters in the following diagrams will be made based on the thermal energy introduced into the organic layer during curing.

The thermal energy introduced into the organic layer can be described using the heat transfer law of Newton:

$$E_{in} = \alpha \Delta \vartheta \Delta t \quad (\text{A.1})$$

with α being the coefficient of heat transfer between the air and the coating, $\Delta \vartheta$ being the temperature difference between air and coating and Δt being the time span from beginning to end of the curing step. For natural convective heat flow, the coefficient of heat transfer is calculated:

$$\alpha = \frac{\lambda Nu}{L} \quad (\text{A.2})$$

with λ being the coefficient of heat thermal conduction of dry air at ambient pressure (0.1 MPa), Nu being the coefficient of Nusselt describing the flow of the air close to the organic layer and L being the so-called "characteristic dimension" of the setup. For setups that are classified as "horizontal plate", the width of the plane is the characteristic dimension. For natural thermal convection at a horizontal plate, the coefficient of Nusselt is calculated:

$$Nu = (0.011 Ra^{\frac{1}{3}} + Ra^{0.1}) K_T \quad (\text{A.3})$$

For gases, the correction factor K_T is not required, i.e. it is equal to one. The coefficient of Rayleigh is derived from the isobaric coefficient of volumetric expansion β , the gravimetric acceleration constant g , the characteristic dimension L , the temperature difference ΔT , the coefficient of heat conduction a and the kinematic viscosity ν :

$$Ra = \frac{\beta g L^3 \Delta \vartheta}{a \nu} \quad (\text{A.4})$$

with a being derived from coefficient of heat thermal conduction of dry air λ , the density of the air ϱ and the specific heat capacity of the air c_p (all for ambient pressure and the individual temperature applied in the oven):

$$a = \frac{\lambda}{\varrho c_p} \quad (\text{A.5})$$

Calculation of the thermal energy introduced in the pilot plant

Again, the thermal energy introduced into the organic layer can be described using the heat transfer law of Newton with, in this case, the curing period being determined by the web speed v_{web} and the length of the drying tunnel l_{dryer} :

$$E_{in} = \alpha \Delta T \Delta t = \alpha \Delta \vartheta \frac{l_{dryer}}{v_{web}} \quad (\text{A.6})$$

with α being again:

$$\alpha = \frac{\lambda Nu}{L} \quad (\text{A.7})$$

The coefficient of Nusselt is calculated differently for forced convective heat flow by means of air that flows turbulently and in a setup that is classified "lengthwise to a plate":

$$Nu = 0.037 Re^{0.8} Pr^{0.43} K_T \quad (A.8)$$

with the correction factor K_T again being equal to one and the coefficient of Prandtl Pr being derived from the dynamic viscosity η , the specific heat capacity of the air c_p and the coefficient of heat thermal conduction of dry air λ (all for ambient pressure and the individual temperature applied in the drying tunnel):

$$Pr = \frac{\eta c_p}{\lambda} \quad (A.9)$$

The coefficient of Reynolds Re is calculated from the speed of the air ω , the characteristic dimension L and the kinematic viscosity ν :

$$Re = \frac{\omega L}{\nu} \quad (A.10)$$

For this turbulent air flow lengthwise against a plate, the length (of the drying section) is the characteristic dimension.

Results

In parallel to the oxygen barrier evaluation of the EFTE films coated with Ormocer[®] 04a or Ormocer[®] 08 at different curing conditions, Raman spectroscopy was performed on these top coats. The focus was to evaluate to which extent the characteristic chemical groups of the liquid lacquers were integrated correctly into the final network of the solid Ormocer[®] layer that is created during the curing process. This is feasible as the two chosen Ormocer[®] lacquers consist of very few ingredients that even show structural similarities which further reduces the number of functional groups that could act as indicators for the creation of the final network.

The sol of the Ormocer[®] 08 is created using tetramethyl orthosilicate (TMOS), 3-glycide oxypropoyl trimethoxy silane (GLYMO) and two metal alcoxides, zirconium-n-propoxide and aluminum-sec-butoxide, both complexated with tri ethanole amine. After the hydrolysis of the sol, large parts of the solvents are replaced under cooling by hydrogen chloride solution. The curing with heat should lead to a removal of the alcohol groups of the silane and of the silicate and to their bonding to each other and to the remaining "core" of the metal alcoxides (to the Me-O-...). Furthermore, the epoxy ring of the GLYMO should open and also connect to itself or to the other educts. Such completed reactions towards a dense, final network should be accompanied by the disappearance of the epoxy rings and of the alcohol groups from the Raman spectrum. (As the Si-O-C or Si-O-Si bonds are not taking up much energy for molecular movements, their increase after curing cannot be studied distinctively in Raman spectroscopy.)

The sol of the Ormocer[®] 04a is created by using only 3-glycide oxypropoyl trimethoxy silane (GLYMO), distilled water and one metal alcoxide, aluminum-sec-butoxide, this time complexated with ethyl acetoacetate (EAA). As for the Ormocer[®] 08, the hydrolysis happens at room temperature. Again, the curing with heat should lead to a removal of the alcohol groups of the silane, to the opening of the epoxy ring of the GLYMO

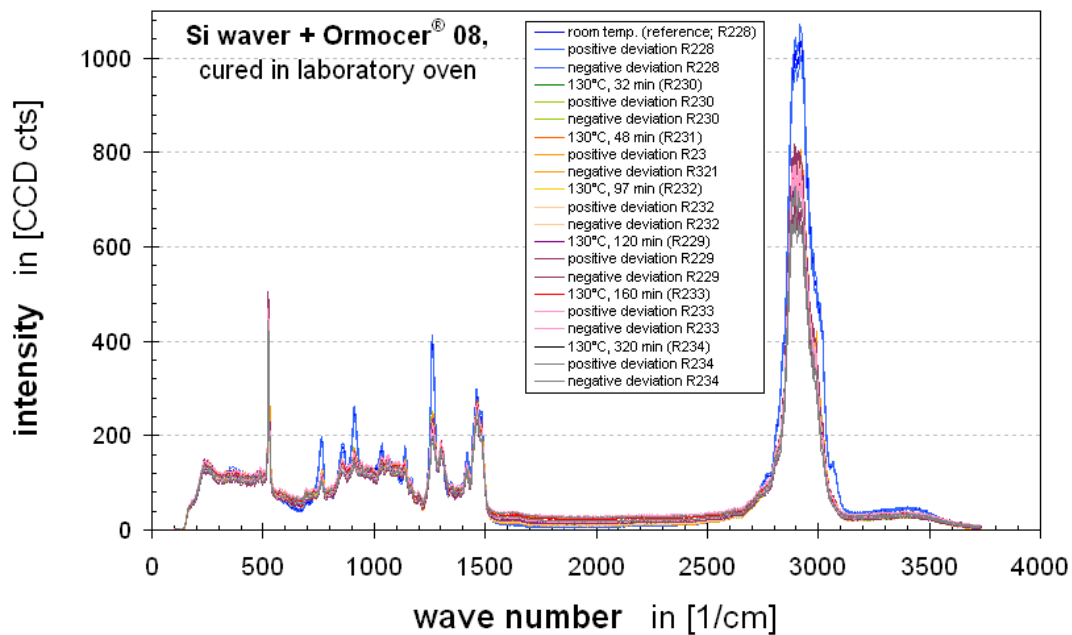


Figure A.3: Exemplary display of the curves of the standard deviations in comparison to the differences in the curves of the averages resulting from varying curing conditions.

and to the bonding of all parts to each other and to the remaining "core" of the aluminum-sec-butoxide (to the Al-O-...). Again, completed reactions towards a dense, final network should be accompanied by the disappearance of the epoxy rings and of the alcohol groups.

In order to ensure that variations of the Raman spectrum are resulting from the curing parameters and not from variations within the Ormocer[®] layer, 80 spectra were recorded for each sample, all over the area of the respective specimen. This reduced the standard deviations so much (to between 0.3 and 1.5%) that they are hardly visible if displayed together with the curve of the averages (see example in Fig. A.3). Therefore, in all following Raman diagrams, the standard deviation curves will be omitted.

Even though the sols are stored or transported under cooled conditions (at $-20\text{ }^{\circ}\text{C}$), the complexing agents for the metal alcoxides are necessary to avoid too early gelation of the lacquers. While the complexing agents are on the one hand helpful to increase the stability of the sol, on the other hand they decelerate strongly the reaction speed during the final curing step. High temperatures of curing, i.e. "as much above room temperature as possible", are recommended to complete the reactions correctly and within reasonable time [155]. For the trials of this work, temperatures between $60\text{ }^{\circ}\text{C}$ and $140\text{ }^{\circ}\text{C}$ were tested, as well as curing periods between 0.1 seconds (for pilot plant) and 7 hours (for laboratory oven).

From all trials, the lowest oxygen transmission rates are achieved with Ormocer[®] 08 layers, cured in the laboratory oven at high temperatures, i.e. $120\text{ }^{\circ}\text{C}$, and for several hours, minimum 2 hours (Fig. A.6a). This fits very well the general recommendation from the chemical developers of these lacquers (who only had the ability to test them at laboratory conditions) to cure Ormocer[®] coatings at $130\text{ }^{\circ}\text{C}$ for 2.5 hours. It furthermore correlates

very well with the best decrease of all samples of the epoxy ring vibrations in the Raman spectrum, which are: the deformation mode of the epoxy ring at ca. 765/cm, the vibration mode of the epoxy ring at ca. 910/cm (both according to [156]) and the "breathing" mode of the epoxy ring at ca. 1265/cm (according to [157]) (Fig. A.6b, , marked in green). The vibrations of the alcohol groups also diminish most of all trials: the asymmetric and symmetric bending vibrations of the -CH_x groups at ca. 860/cm, 1030/cm, 1120-1140/cm, 1420/cm, 1465/cm, 1480/cm (according to [158]) and the asymmetric and symmetric stretching vibrations of the -CH_x groups between 2850/cm and 3100/cm (according to [159]) (Fig. A.6b, A.6c, A.6d and A.6e, marked in blue).

Taking the same curing parameters, but using the pilot plant, delivers a completely different result: The higher the introduced thermal energy, the worse the intrinsic oxygen barrier of the layer. The Raman spectra (in Fig. A.7) show the reason: the peaks of the alcohol groups (in blue) diminished nearly as good as in Fig. A.6, but the peaks of the epoxy group (in green) barely decreased. This seems to indicate a "shock drying" of the Ormocer[®] layer, where the silicates and the silanes connect so fast due to the thermally induced "extraction" of the alcohol groups that the epoxy group could barely catch free reactive endings. The organic chain of the GLYMO (that contains the epoxy ring) can no longer act as "covalently bonded flexibilizer" (see Fig. A.4), but widens the network requiring empty volume to "lay there" without being covalently bonded to the network. These may be the two reasons for the reduced intrinsic oxygen barrier: organic chains laying unbonded within the network, widening it and making it more open to oxygen permeation, and the increased brittleness of the Ormocer[®] layer missing the "covalently bonded flexibilizer".

In contrary to the results for Ormocer[®] 08, there is no clear correlation between the oxygen transmission rates and the curing parameters for Ormocer[®] 04a (Fig. A.8, A.9). The Raman spectra show low epoxy peaks (Fig. A.8b, A.8d, A.9b, A.9d, marked in green) which indicate well-opened epoxy rings, comparable to Fig. A.6, while the peaks of the -CH_x groups are not accordingly well reduced (Fig. A.8b, A.8d, A.9b, A.9d, marked in

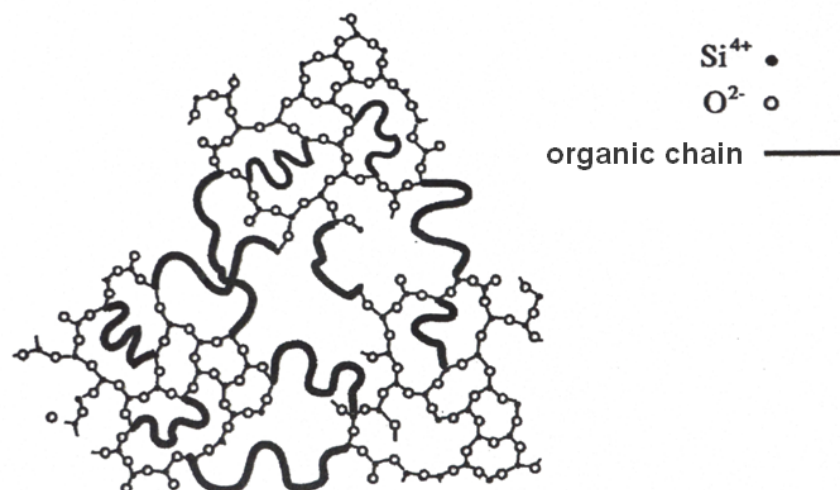


Figure A.4: Schematic picture of how organic and inorganic parts are chemically cross-linked within the the Ormocer[®] network.

red). Furthermore, additional Raman peaks are visible that are assigned to groups that should not occur for a sol with well completed hydrolysis: like the vibrations of methoxy silyl groups at ca. 600/cm, the oscillations of the C=C double bonds at ca. 1640/cm or the oscillations of the C=O double bonds at ca. 1740/cm (all according to [158]) (Fig. A.8b, A.8d, A.9b, A.9d, marked in red). As these indications of (partially) insufficient hydrolysis occur in all Raman spectra of theOrmocer® 04a samples, it may explain the high deviations in the OTR and the generally worse barrier performance.

Comparing both the OTR and the Raman results of the two lacquers, it becomes obvious that a prediction of the barrier properties based on the Raman evaluations may work well, but only when taking all information of the spectrum into consideration. This means a high level of knowledge of the Raman spectra as well as of the barrier properties of the respective organic coating material would be required to enable an automatic tool.

From all trials performed, a maximum difference in the OTR for the two layer system (ETFE film + Ormocer® layer) of 28 to 322 cm³(STP)/(m² d bar) between good curing quality and very bad (nearly uncured) quality (Fig. A.7a) could be found as well as a more typical difference in the OTR of 26 to 153 cm³(STP)/(m² d bar) between good curing quality and less good quality (Fig. A.7a). These data can be used to assess theoretically the usefulness of extensive optimization activities concerning the curing conditions. Using Equ. (3.11), knowing that the same ETFE substrate was used and that the Ormocer® layer was coated with the same layer thickness, gives the following equation:

$$\frac{P_{\text{organic,bad curing}}}{P_{\text{organic,good curing}}} = \frac{\frac{1}{T_{2L, \text{good curing}}} - \frac{1}{T_{\text{polymer}}}}{\frac{1}{T_{2L, \text{bad curing}}} - \frac{1}{T_{\text{polymer}}}} \quad (\text{A.11})$$

For the typical situation (26 to 153 cm³(STP)/(m² d bar)), this reveals a difference in the permeability coefficients for oxygen of 1: 9.7 which is nearly an order of magnitude of improvement. For the extreme example (28 to 322 cm³(STP)/(m² d bar)), the improvement of the permeability coefficient for oxygen goes up to 1 : 132 which is more than two orders of magnitude of improvement.

Concerning the overall oxygen barrier performance of a multilayered encapsulation material, this improvement can directly be transferred to the overall oxygen barrier performance - since oxygen is assumed to permeate through the pores only that are now covered with a much better organic material.

However, for water vapor - which is assumed to permeate through the bulk as well as through the pores - there is no such “bottleneck effect” and the two permeability coefficients (of the organic and inorganic layer) are working in kind of a serial connection. In fact, there are two serial connections in parallel: the first one: inorganic bulk and organic layer and the second one: pore and organic layer (for more details, see Chapter 3.1.8). Therefore it cannot be stated generally whether an improved permeability coefficient of the organic layer will affect the barrier performance of the entire encapsulation material, but the barrier performance of the bulk of thin inorganic barrier layer and the geometry and distribution of its pores have to be taken into account.

Fig. A.5 shows the water vapor transmission rate (WVTR) of a two layer structure, consisting of one thin inorganic barrier layer - containing pores of typical average pore size and average pore distance - and one organic layer on top. This structure can in fact stand for the three layer structure, since the polymeric carrier substrate does not contribute

significantly to the barrier performance of the entire structure. (For the simplification of the calculation, it was neglected.) Along the x-axis, the intrinsic barrier performance of the organic top coat against water vapor is varied by changing its permeability coefficient: the lower the permeability coefficient, the more to the left. The intrinsic barrier performance of the thin inorganic barrier layer is varied by changing the permeability coefficient of its bulk, while the geometry and the distribution of the pores is kept constant: the lower the permeability coefficient of the inorganic bulk, the lower the entire curve (from the dark green one to the red one).

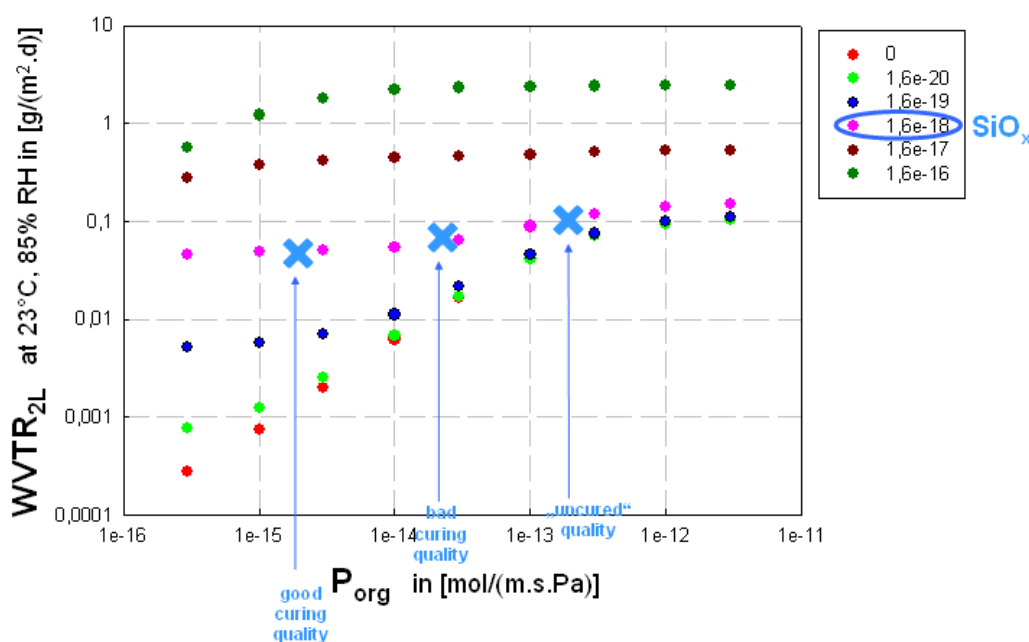


Figure A.5: Water vapor transmission rate of the two layer system for varying permeability coefficients of the organic top coat, in dependence of the permeability coefficient of the inorganic bulk (assuming pores with an average diameter of 170 nm and an average distance of 29 μm) (Fig. modified from [14]).

Now, to see whether an improved permeability coefficient of the organic layer will effect the barrier performance of the two (resp. three) layer structure, one has to follow the curve that follows the barrier performance of the thin inorganic barrier layer used. The typical SiO_x layer used during this work has a typical, average permeability coefficient for water vapor of 1.6×10^{-18} mol/(m·s·Pa) (which is the pink curve). Following this curve, it becomes clear that even an increase of the permeability coefficient of the organic top coat by over two orders of magnitudes would only lead to a reduction of the WVTR of the two (resp. three) layer structure by approximately a factor of 2 (marked by blue crosses in Fig. A.5). Hence, for the multilayered encapsulation materials based on this thin inorganic barrier layer, extensive optimization activities regarding the curing quality of the thin organic barrier layer would not be of use. (Of course, a proper minimum of curing quality should be kept.)

Yet, from a global point of view, there would be one exception: in case the permeability coefficient of the thin inorganic barrier layer could significantly be improved towards

a lower intrinsic permeability, e.g. by one order of magnitude (which would be the dark blue curve in Fig. A.5), the reduction of the permeability coefficient of the organic barrier layer against water vapor by over two orders of magnitude would reduce the WVTR of the two (resp. three) layer structure by nearly one order of magnitude. Plus the additional barrier performance that results from the improvement of the thin inorganic layer itself anyway, because in reality, the bulk of the inorganic barrier layer does not improve independently of the pores - the pores would be reduced in size, too (which is not reflected by the calculations on which Fig. A.5 is based).

Hence, for the target of creating an OE encapsulation material showing a very low WVTR, if one has to choose between the optimization activities of the thin inorganic or the thin organic barrier layers (e.g. for capacity reasons), the first one would be of much greater use and should therefore be focused on.

A Additional experimental results

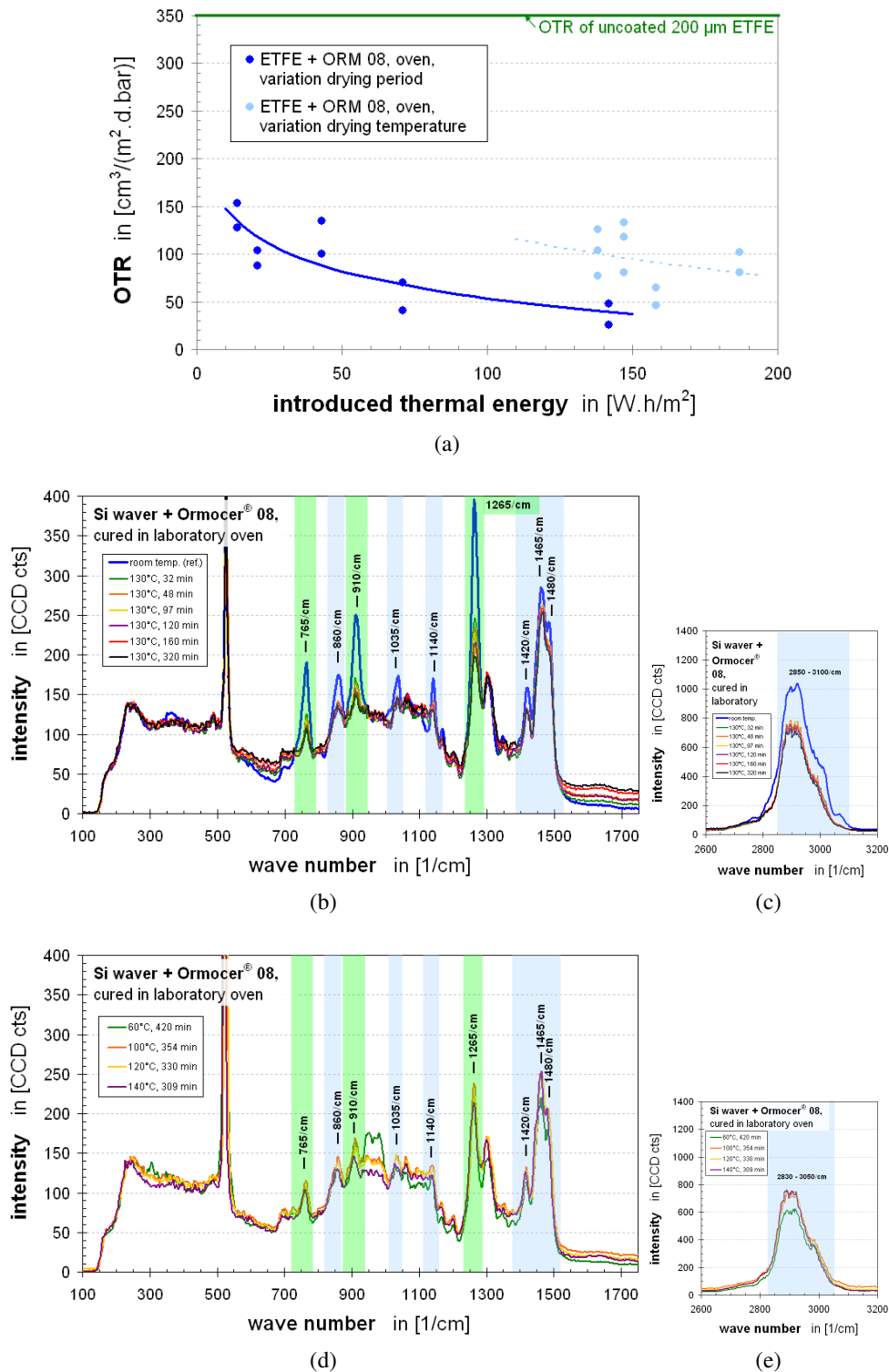


Figure A.6: Transmission rates and Raman spectra of a thin Ormocer® 08 layer cured on top of a 200 μm ETFE film in a laboratory oven, as a function of drying period (b), (c) or drying temperature (d), (e), respectively.

A Additional experimental results

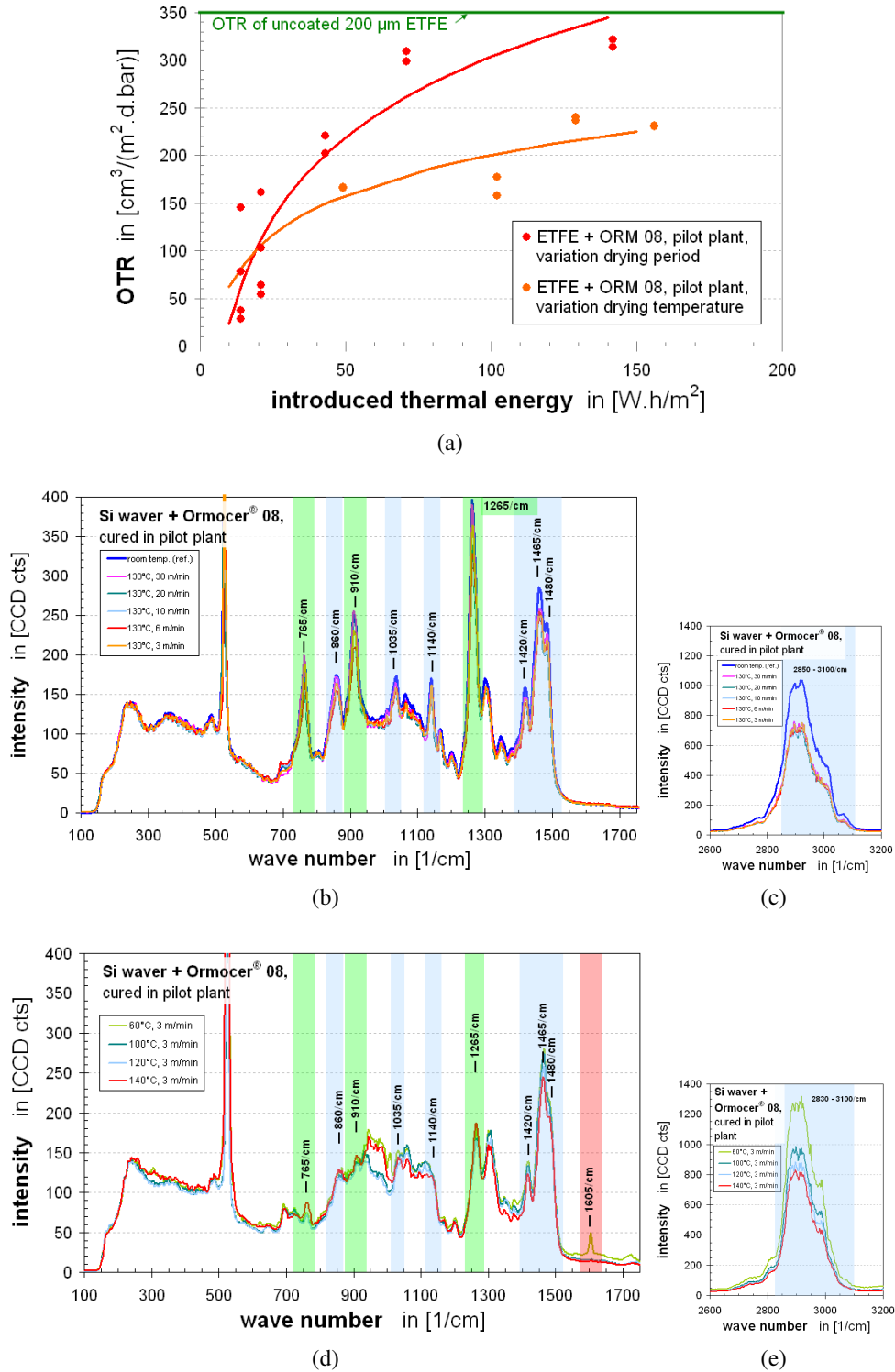


Figure A.7: Transmission rates and Raman spectra of a thin Ormocer® 08 layer cured on top of a 200 μm ETFE film in the pilot plant, as a function of drying period (b), (c) or drying temperature (d), (e), respectively.

A Additional experimental results

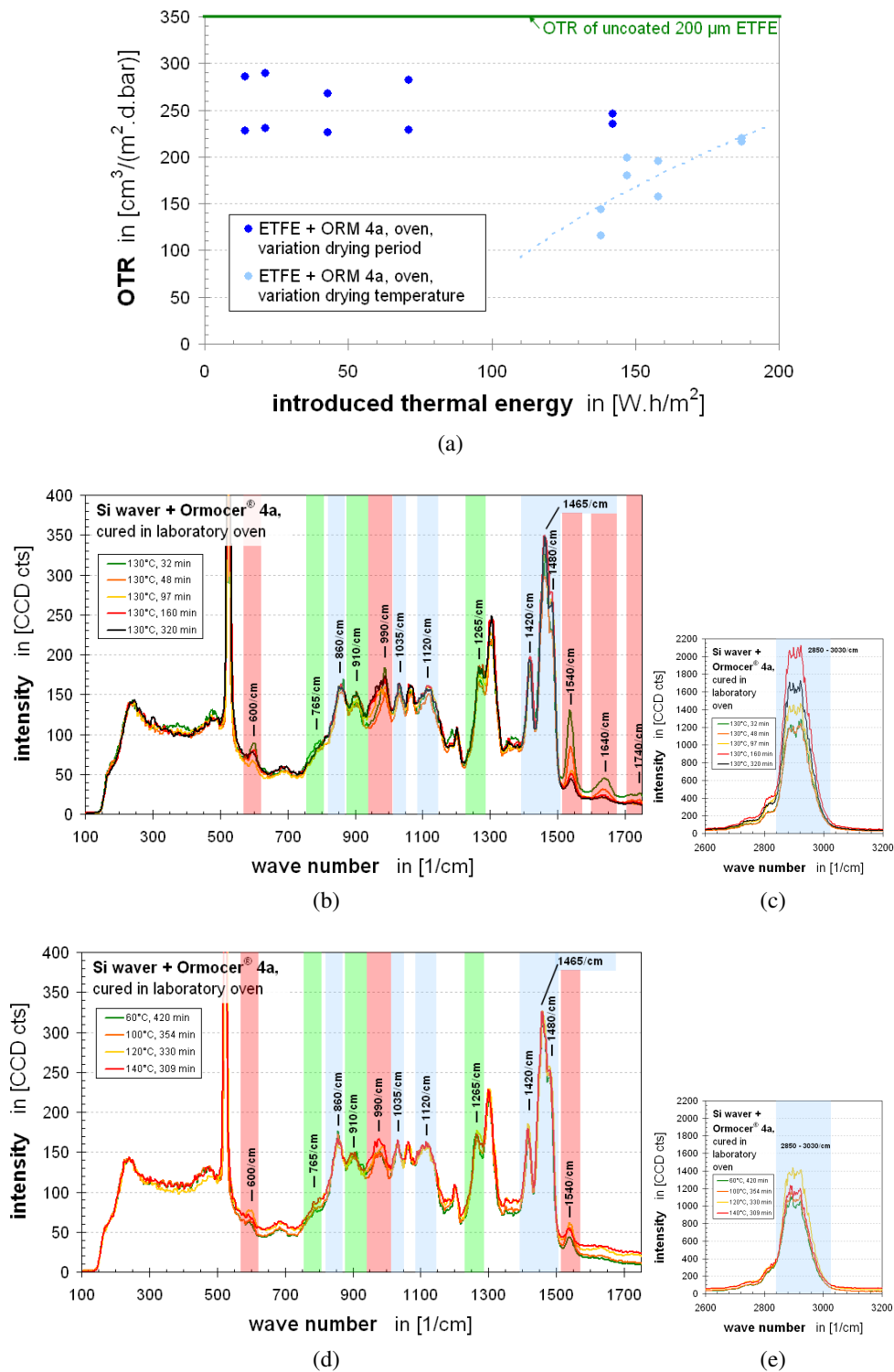


Figure A.8: Transmission rates and Raman spectra of a thin ORMOCER® 04a layer cured on top of a 200 μm ETFE film in a laboratory oven, as a function of drying period (b), (c) or drying temperature (d), (e), respectively.

A Additional experimental results

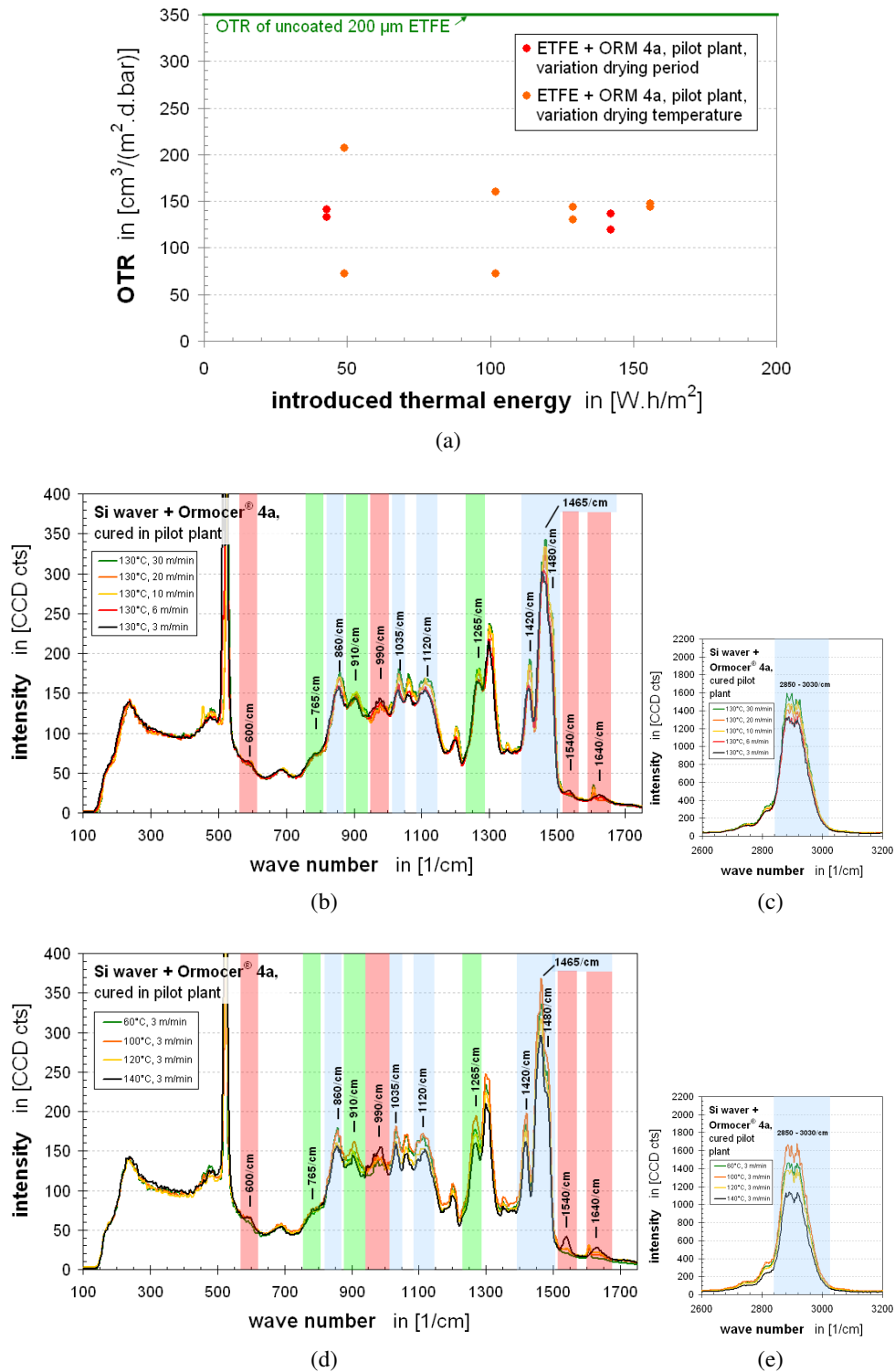


Figure A.9: Transmission rates and Raman spectra of a thin Ormocer® 04a layer cured on top of a 200 μm ETFE film in a laboratory oven, as a function of drying period (b), (c) or drying temperature (d), (e), respectively.

A2. Relation between barrier performance and adhesive / cohesive strength

Background and experimental setup

In Chapter 6.1 and 7 it was already shown that when choosing an organic coating material it is not only its intrinsic barrier performance that counts due to the synergistic barrier effects between the thin inorganic and organic layers. In case of the adhesive choice, one further criterion has to be taken into consideration: its bond strength on top of the respective materials.

In order to study the relation between barrier performance and the bond strength of laminates, several versions of the structure type [PET + inorganic X + adhesive A + inorganic X + PET] were designed - varying the type of inorganic layer (X) and the type of adhesive (A).

Three adhesives were used, differing in intrinsic barrier performance and mechanical properties. From adhesive a1 over a2 to a3, their intrinsic barriers against water vapor and oxygen are increasing - to be seen in decreasing permeability coefficients (Table A.1).

Table A.1: Barrier related properties of the adhesives.

adhesive A =	permeability coefficient towards water vapor in [mol/(m.s.Pa)]	permeability coefficient towards oxygen in [mol/(m.s.Pa)]	water uptake [%]
a1 ^a	110×10^{-14}	60×10^{-18}	2.80
a2 ^b	20×10^{-14}	9×10^{-18}	2.17
a3 ^c	9×10^{-14}	1.5×10^{-18}	0.77

^aadhesive A5.3

^badhesive A5.5

^cadhesive A5.4

Table A.2: Mechanical properties of the adhesives.

adhesive A =	E' modulus at 23°C (second run) in [MPa]	Tg (second run) in [°C]	tensile stress at break in [MPa]	tensile strain at break in [%]
a1 ^a	988	32.5	5.0 ± 0.4	55 ± 3
a2 ^b	3658	96.2	14 ± 1	47 ± 1
a3 ^c	6291	177	34 ± 5	0.8 ± 0.1

^aadhesive A5.3

^badhesive A5.5

^cadhesive A5.4

The water uptake of the adhesives - which indicates their sorption capacities - decreases from a1 to a3, too (Table A.1). The capacity of a material to absorb water

molecules (or any permeant in general) is for these three adhesives mostly linked to the crosslink density of their chemical network, because their mechanical properties are varying accordingly: from adhesive a1 to a3 their stiffness and cohesive strength (i.e. E' modulus and tensile stress at break) increase and their flexibility (i.e. tensile strain at break) decreases (Table A.2).

Results

The laminate bond strength was measured 10 times per sample. From the samples, stripes of 200 mm by 15 mm were cut and conditioned for 24 hours at 23 °C and 50% RH. Per sample, 10 stripes were measured to derive an average, using a “Universalprüfmaschine Schenck-Trebel Typ RM 50“ from *Bischoff Prüftechnik GmbH*. Before the measurement, at one end of the stripe the “two halves” of the material were split manually till approximately 40 mm in length. The unchanged end and one “half” of the split end were fixed in the clamps, leaving a test length at start between the clamps of 50 mm. Test speed was 50 mm/min and the angle between the two split “halves“ (non-fixed and fixed) was kept at 90°. Per sample, five stripes were tested.

Matching with their intrinsic barrier against water vapor, the WVTR of the laminates follow the trend: the WVTR are decreasing for the laminates containing a1 over a2 to a3 - for SiO_x based structures as well as for Zn_xSnO_y based structures (Tables A.3, A.4) as well as for different lamination processes (Table A.3).

The laminate bond strength was found to be not so obviously linked to the intrinsic cohesive strength of the adhesives. The highest bond strength is shown by adhesive a1 which has not the highest cohesive strength but the highest flexibility. This indicates a substrate that does not support very strong adhesion. For situations of weak adhesion to the substrate, a very flexible adhesive is advantageous: mechanical shear or peel stress applied to the bond area would be transformed much longer into deformation energy before it actually breaks the adhesive itself, due to its weaker cohesive strength (Fig.

Table A.3: WVTR and bond strength of laminates of the structure [PET + SiO_x + adhesive A + SiO_x + PET].

adhesive A =	thickness of adhesive layer in [μm]	WVTR 23/100 ^a [g/(m ² d)]	bond strength [N/15 mm]
Thick adhesive layers (bench lamination)			
a1	40 ±1	0.070	3.6 ±0.7
a2	26 ±1	-	0.09 ±0.01
a3	66 ±2	0.007	0.5 ±0.1
Thin adhesive layers (pilot plant lamination)			
a1	4.0 ±0.3	0.059	1.3 ±0.2
a3	10 ±1	0.009	very weak ^b

^aMeasured with ACP test at at 23°C and 100% relative humidity.

^bNot measurable.

Table A.4: WVTR and bond strength of laminates of the structure [PET + ZnSn_xO_y + adhesive A + ZnSn_xO_y + PET] - all fabricated using bench lamination.

adhesive A =	thickness of adhesive layer in [μm]	WVTR 23/100 ^a [g/(m ² d)]	bond strength [N/15 mm]
a1	40 ±1	0.004	5.3 ±0.8
a3	62 ±3	0.002	very weak ^b

^aMeasured with ACP test at at 23°C and 100% realive humidity.

^bNot measurable.

A.10a). This failure type was observed only for the flexiblest of the three adhesives, adhesive a1, and only when applied in thick layers. Furthermore, the longer the two halves of the laminated encapsulation material are still bonded (i.e. the more of adhesive is still "absorbing" peel stress), the larger is the effective bond area or bond volume (Fig. A.11a, A.11b).

A stiffer adhesive with higher cohesive strength would not deform so much (and this way absorb energy) but pass the stress nearly unreduced into the interfaces between adhesive and substrates. Since, for a stronger adhesive, the adhesion on the substrate is the weaker point, it would fail first before the adhesive could break - either completely on one side of the laminate (Fig. A.10b) or alternating randomly between the two sides. This failure type was seen for all other laminates of Tables A.3 and A.4 - even for the laminate using a thin layer of adhesive a1. The reason is that a thin adhesive layer passes the mechanical stress earlier to the interfaces between adhesive and substrates than a thicker one, because it just does not provide enough material able to absorb energy.

Yet, comparing the more flexible adhesive a2 with the stronger adhesive a3 on the same SiO_x surface, does not follow the same trend: the laminate with a2 still shows much weaker bond strength: 0.09 instead of 0.5 N/15 mm (Table A.3). Since the bond strength of a laminate is not only resulting alone from the adhesive properties, but also from the surfaces to be bonded, it helps to take a closer look at the surface of the inorganic layers on

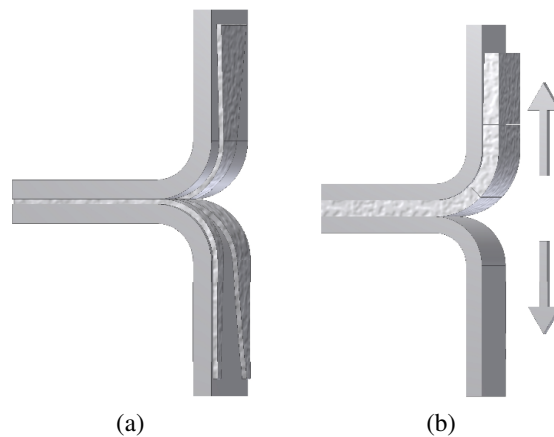


Figure A.10: Schematic pictures of failure types of laminated samples under peel stress.

A Additional experimental results

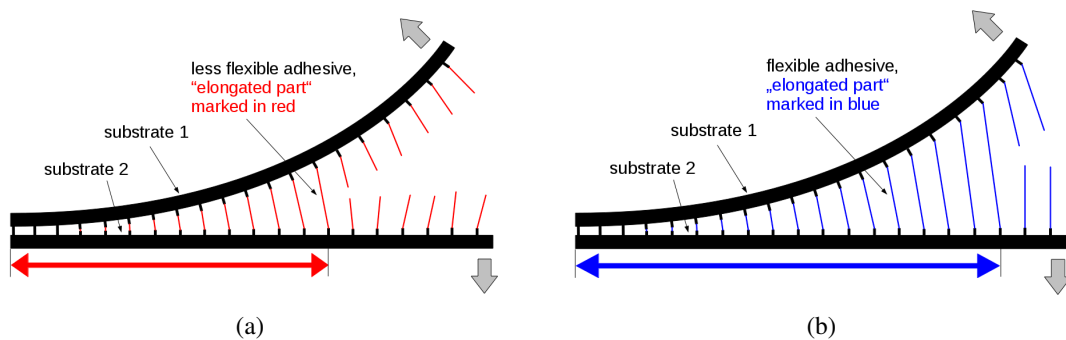


Figure A.11: Schematic pictures of the influence of the intrinsic flexibility of the adhesive on the effective bond area.

top. The SiO_x layers have a total surface energy of 39 mN/m and the ZnSn_xO_y layers of 35 mN/m. This is sufficient to ensure a good wetting for adhesives a1 and a3, having surface tensions of 31 and 30 mN/m, respectively, but is insufficient for adhesive a2 having a surface tension of 45 mN/m. Since wettability is an essential minimum criterion for bond strength, the surface energy of the substrate has to be higher than the surface tension of the liquid adhesive, otherwise the wetting of the adhesive on top of the substrate would be incomplete and lead to a reduced bond area. The smaller the bond area, the smaller the bond strength that can be achieved. Hence, to achieve good bond strength with adhesive a2, the substrate needs to have a surface energy greater than 45 mN/m.

By adjustments in the production process of the SiO_x coatings, the polar part of their surface energy can be increased. In doing so, a material called $\text{SiO}_x^{\text{HSE}}$ (SiO_x of higher surface energy) was fabricated, having a total surface energy of 53 mN/m. The disperse part of the surface energy was in fact similar to the original SiO_x layers (30 and 31 mN/m, respectively) but the polar part was tripled: 23 instead of 8 mN/m.

The face-to-face lamination of this $\text{PET}+\text{SiO}_x^{\text{HSE}}$ material with adhesive a2 resulted in a laminate material showing a bond strength higher than the cohesive strength of the

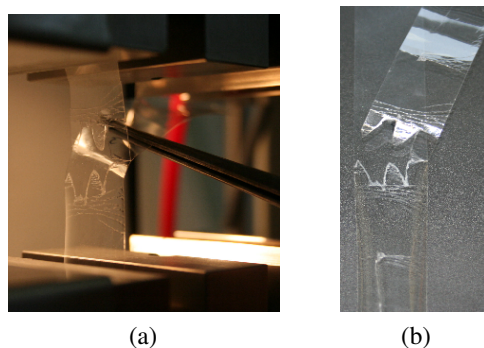


Figure A.12: No quantitative bond strength value can be measured if the encapsulation material (i.e. mainly the PET substrate) breaks before bond failure: pictures of such a broken sample in the test machine (a) and after taking it out (b).

Table A.5: WVTR and bond strength of the structure [PET + SnO_x^{HSE} + adhesive A + SiO_x^{HSE} + PET] laminated with adhesive a2 by bench lamination.

adhesive A =	thickness of adhesive layer in [μm]	WVTR 23/100 ^a [g/(m ² d)]	bond strength [N/15 mm]
a2	25 ±1	0.008	Very strong bond strength - could not be measured (rupture of encapsulation material).

^aMeasured with ACP test at at 23°C and 100% relative humidity.

PET carrier substrate: when trying to measure the laminate bond strength of this structure, the PET film broke before the bond area failed (Table A.5, Fig. A.12).

The WVTR of the so laminated material is with 0.008 g/(m² d) very close to the WVTR of the SiO_x material laminated with adhesive a3 of 0.007 g/(m² d) (Tables A.5, A.3) - closer than what one would expect from the difference in their permeability coefficients towards water vapor.

This seems to indicate that the improvement of the interfacial layer between the barrier adhesive and the thin inorganic barrier layer does not only improve the adhesive strength between these two layers and therefore the bond strength of the laminate, but also reduce the overall WVTR of the laminate - which fits the conclusion of Chapter 6.1 regarding the good “interface building properties” of organic materials on top of thin inorganic barrier layers. Hence, the barrier adhesive should not be chosen purely according to its intrinsic barrier properties and mechanical strength and flexibility, but also to be matching the surface of the substrate. Or - in reverse conclusion - the barrier material should, if possible, be fitted to the requirements of the adhesive of choice.

A3. Relation between barrier performance and climate stability on the examples of some selected organic and inorganic barrier materials

Background and experimental setup

One further criterion for the selection of barrier materials - besides their intrinsic barrier performance and their match with each other to maximize additional barrier effects - is their stability against the environmental conditions during the use of the final, encapsulated OE product.

For the climate and UV simulation, three different tests were used: the damp heat test, the outdoor test and the UV test (Table A.6). With respect to the development of longtime UV and climate stable encapsulation materials, the simulated exposure periods of this work would be too short for many applications. The six months are more meant as a first development step, adequate for the development of low cost OE products with short intended lifetimes (“gadgets”) or OE products with mainly indoor use (like solar bags). For more complex consumer products, the targeted lifetimes would be 3 years (e.g. mobile phones) up to 10 years (e.g. TV screens). Building integrated applications (e.g. OPV products on facades and roofs) would require the highest minimum lifetimes of at least 20 to 30 years, better up to 50 years [16].

For the damp heat test, five sheets of each sample were fixed in the inner of a desiccator (Fig. A.13a) filled with a saturated solution of sodium sulfate (Na_2SO_4). The desiccator is stored in a climate chamber at 65 °C for 1000 hours. At this temperature, the saturated solution of sodium sulfate keeps a constant relative humidity of 90% in the inner of the

Table A.6: Test conditions of the UV and climate stability tests used in this work.

test	temperature	relative humidity (RH)	irradiance	duration
climate stability	38 °C	90 %	-	1000 h
	65 °C	65 %	-	1000 h
	85 °C	85 %	-	1000 h
UV stability	35 °C	0 %	750 W/m ² ≅ 0.75 ”sun“ ^b	381 h ^a
outdoor stability	middle europe	middle europe	middle europe ≈ 2059 MJ/(m ² a) ^c	6 months

^aThe UV dose was chosen to simulate 6 months at middle european climate (381 hours at 750 W/m² is the equivalent 6 months at 2059 MJ/(m² a).

^bThe expression ”1 sun“ is a casual term of the OPV community rooted in the solar constant E_0 which is the amount of incoming solar electromagnetic radiation per unit area at the mean distance from the sun to the earth. Yet, while $E_0 = 1367 \text{ W/m}^2$, ”1 sun“ = 1000 W/m² for simplification of the test procedures.

^cThis average irradiation was the result of longtime measurements at different places in middle europe performed by the ATLAS company [160].

desiccator. This construction was made to be able to test at both high temperature and humidity without having the appropriate climate chamber at hand.



Figure A.13: Simulation of climate stress by (a) damp heat test and (b) outdoor test.

For the outdoor test, the samples were cut into rectangles having an area of approximately 210 mm by 297 mm (size "A4") and fixed in a specially designed frame (Fig. A.13b) that could be fixed at the outer walls of the *Fraunhofer IVV* building. There, the samples were exposed to radiation from the sun as well to the environmental conditions without barriers for 6 months during the summer period.

The UV test was done using a Suntest XLS + from *Atlas Material Testing Technology GmbH*. For all samples, the maximum dose of 750 W/m² was applied for 381 hours at 35 °C and 0% RH.

Pre-tests

To be able to measure the climate and UV stability of thin organic and inorganic barrier layers, base substrates had to be selected which withstood themselves the test conditions. In case of the stability towards 1000 hours at 65 °C and 90% relative humidity, all three

Table A.7: Climate stability of three transparent polymer films suitable for climate stability tests (marked in green).

Polymer film	yellowing Δb^* ^a	OTR 23/50 [cm ³ (STP)/(m ² d bar)]	WVTR 23/85 [g/(m ² d)]
ETFE (200µm)	O ^b T ^c 0	329 ± 22 359; 337	0.74 ± 0.04 0.98; 0.71
PET (50µm)	O T 0	26 ± 2 27.5; 20.0	4.8 ± 0.9 4.3
PET + SiO _x (ca. 50µm)	O T 0	93 ± 17 3.9; 4.0	0.74 0.74; 0.68

^a Δb^* ... Relative increase of the yellow part b^* of the colour of the polymer foil between before and after treatment, measured according the CIE colour system.

^bO ... Original film.

^cT ... Treated for 1000 hours at 65 °C, 90 % RH.

A Additional experimental results

Table A.8: UV stability of one transparent polymer film suitable for UV stability tests (marked in green) and one unsuitable one.

Polymer film	yellowing $\Delta b^*{}^a$	
ETFE (200 μ m)	O ^b	
	T ^c	0
PET (50 μ m)	O	
	T	+ 1

^a Δb^* ... Relative increase of the yellow part b^* of the colour of the polymer foil between before and after treatment, measured according the CIE colour system.

^bO ... Original film.

^cT ... Treated for 381 hours at 100% UV, 35 °C, 0 % RH.

tested base substrates, namely PET films, ETFE films and SiO_x coated PET films, were found to be stable (Table A.7). In case of the stability towards 381 hours at 100% UV at 35°C and 0% relative humidity, only ETFE films were found to be stable enough to act as base material (Table A.8).

Results

On the (stable) test substrates, three organic coating materials of different barrier performance (Table A.9) were applied and tested with respect to their climate or UV stability. The results (Tables A.10, A.11) show that a selection of the organic coating material

Table A.9: Typical permeability coefficients of three organic coating materials (permeability coefficients from Chapter 5.3).

Coating	P_{O_2} [mol/(m s Pa)]	P_{H_2O} [mol/(m s Pa)]
C5.5	9.8×10^{-19}	1.6×10^{-13}
C5.6	1.2×10^{-18}	2.1×10^{-14}
C5.9	1.5×10^{-18}	1.7×10^{-14}

purely according its barrier properties would lead to a high performing, but unstable encapsulation material: the organic coating materials C5.6 and C5.9 would both have better intrinsic water vapor barrier than the organic coating material C5.5, but they are not stable enough. The organic coating material C5.9 is simply not UV stable at all: strong yellowing occurs, not acceptable for OE applications. The organic coating material C5.6 is not climate stable if coated on a thin inorganic barrier layer: already after some hours first spots occur that look like “snow crystals”, because interaction between the SiO_x and the organic layer leads to breakage of the organic layer into many small pieces with no adhesion left to the layer underneath - a soft finger touch already wipes these parts away. After 1000 hours of measurement the whole sample is degraded the same way (Fig. A.14). Therefore, despite the organic coating material C5.5 having the worst intrinsic water va-

por barrier of the three organic coating material, it will be the one that has to be selected out of these three for the reason that it the only one that fulfills all stability criteria.

Table A.10: Climate stability of the three organic coating materials when applied as top coat on top of polymer films or inorganically coated polymer films.

Coated samples		yellowing Δb^* ^a	OTR 23/50 [cm ³ (STP)/(m ² d bar)]	WVTR 23/85 [g/(m ² d)]
PET + C5.5	O ^b	0	15.7 20.2	4.0 4.8
	T ^c	0	22.8 21.2	4.1 4.1
PET + SiO _x + C5.5	O	0	0.05 0.09	0.04 0.04
	T	0	0.14 0.04 0.09	0.14 0.38
PET + C5.6	O	0	16.5 13.4	5.0 4.7
	T	0	23.6 22.2	5.2 4.6
PET + SiO _x + C5.6	O	0	0.01 0.01	0.3 0.02
	T	0	Samples destroyed (see Fig. A.14).	
ETFE + C5.9	O	0	136 154 121 113	0.63 0.64 0.74
	T	0	246 265 287	0.65 0.95 1.27
PET + C5.9	O	0	19.0 16.1	4.4 4.5
	T	0	21.1 22.3	4.4 4.3
PET + SiO _x + C5.9	O	0	0.02 < 0.01	0.07 0.02
	T	0	0.10 0.25	0.67 0.22

^a Δb^* ... Relative increase of the yellow part b^* of the colour of the polymer foil between before and after treatment, measured according the CIE colour system.

^bO ... Original film.

^cT ... Treated for 1000 hours at 65 °C,90 % RH.

Table A.11: UV stability of the three organic coating materials when applied as top coat on top of uncoated polymer films.

Polymer film		yellowing Δb^* ^a
ETFE + C5.5	O ^b	
	T ^c	0
ETFE + C5.6	O	
	T	0
ETFE + C5.9	O	
	T	+ 10

^a Δb^* ... Relative increase of the yellow part b^* of the colour of the polymer foil between before and after treatment, measured according the CIE colour system.

^bO ... Original film.

^cT ... Treated for 381 hours at 100% UV, 35 °C,0 % RH.

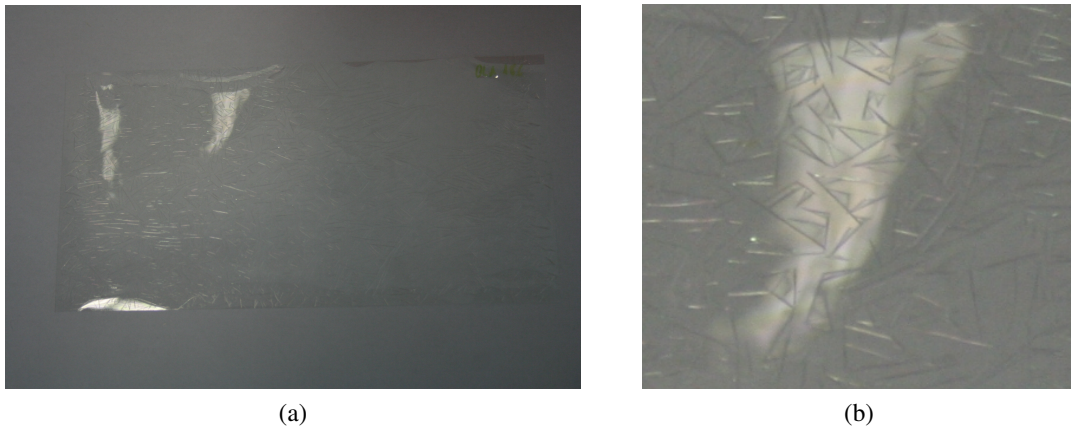


Figure A.14: Sample of the structure [PET + SiO_x + C5.6] after the climate test (1000 hours at 65°C and 09% RH). Figure (b) is a zoom into figure (a).

B Additional calculated results

B1. Time lag calculation for homogeneous multilayered materials

Using the analogy of the gas permeation process to the flow of electrical current [18], the calculation of the time lag can be extended to many layers. For this, the number n of layers will be regarded as the serial connection of n membranes. To be able to connect one membrane mathematically to the next one, both the characteristics of the incoming flux, i.e. J_1 , Q_1 and $t_{1L,J1}$, as well as of the outgoing flux, i.e. J_2 , Q_2 and $t_{1L,J2}$, have to be calculated. The relations of all these quantities to each other are visualized in Fig. B.1.

In Chapter 3.1, the calculation of the time lag t_{1L} of a monolayer membrane, based on the outgoing flux $-J_2$, was already demonstrated. The same can be done for flux J_1 or, in general, for both fluxes. The time lags are such defined as:

$$y_i(t = t_{L,J_i}) = 0 \quad (\text{B.1})$$

with the asymptotes being

$$y_i = \lim_{t \rightarrow +\infty} Q_i(t) \quad (\text{B.2})$$

The cumulated volumes $Q_i(t)$ are

$$Q_i(t) = \int_0^{+\infty} J_i(\tau) d\tau \quad (\text{B.3})$$

Applying Fick's first law for diffusion [161] to the fluxes $J_i(x, t)$, which are perpendicular to the area of permeation A , leads to:

$$J_i(x, t) = -D \frac{\partial c(x, t)}{\partial x} \quad (\text{B.4})$$

With the concentrations being

$$\begin{aligned} c(x, t) = & c_A + (c_B - c_A) \frac{x}{d} + \frac{2}{\pi} \sum_{n=1}^{\infty} \left[\frac{c_B \cos(n\pi) - c_A}{n} \sin\left(\pi x \frac{n}{d}\right) e^{-\frac{Dn^2 t}{d^2}} \right] \\ & + \frac{4c_0}{\pi} \sum_{m=1}^{\infty} \left[\frac{1}{2m+1} \sin\left(\pi x \frac{2m+1}{d}\right) e^{-\frac{D(2m+1)^2 t}{d^2}} \right] \end{aligned} \quad (\text{B.5})$$

B Additional calculated results

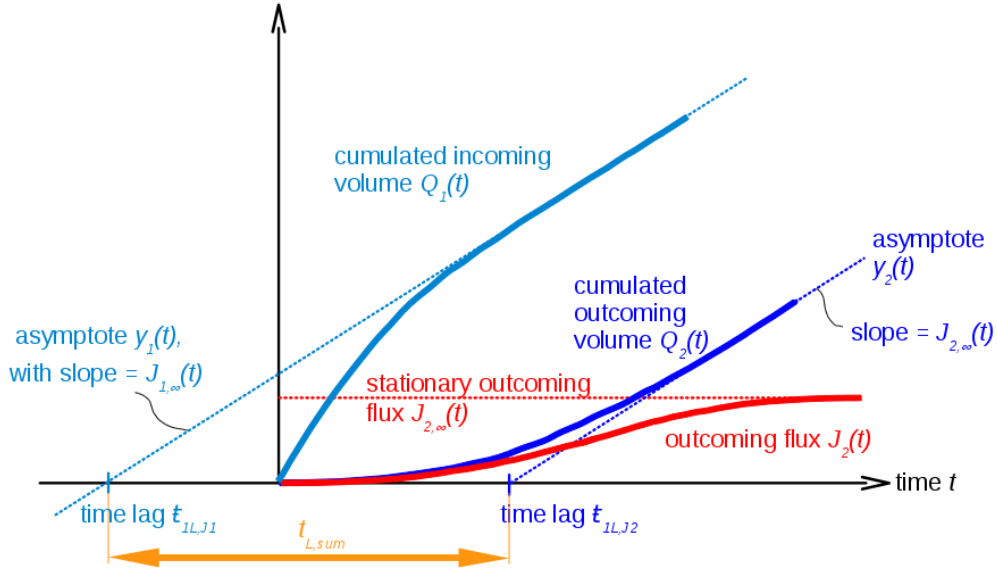


Figure B.1: Both fluxes and cumulated fluxes as a function of time, schematic, following [18].

the changes of the concentration $\frac{\partial c}{\partial x}$ are

$$\begin{aligned} \frac{\partial c(x, t)}{\partial x} &= \frac{c_B - c_A}{d} + \frac{2}{d} \sum_{n=1}^{\infty} \left[(c_B \cos(n\pi) - c_A) \cos\left(\pi x \frac{n}{d}\right) e^{-\frac{Dn^2 t}{d^2}} \right] \\ &+ \frac{8c_0}{d} \sum_{m=1}^{\infty} \left[\cos\left(\pi x \frac{2m+1}{d}\right) e^{-\frac{D(2m+1)^2 t}{d^2}} \right] \end{aligned} \quad (\text{B.6})$$

As the concentration in the membrane is zero at $t = 0$ the last part of Eq. (B.6) gets eliminated:

$$\frac{\partial c(x, t)}{\partial x} = \frac{c_B - c_A}{d} + \frac{2}{d} \sum_{n=1}^{\infty} \left[(c_B \cos(n\pi) - c_A) \cos\left(\frac{n\pi x}{d}\right) e^{-\frac{Dn^2 t}{d^2}} \right] \quad (\text{B.7})$$

Combining Eqs. (B.3), (B.4) and (B.7) gives $J_1(t)$ at $x = 0$ and $J_2(t)$ at $x = d$:

$$\begin{aligned} J_1(0) &= -D \frac{\partial c}{\partial x} \Big|_{x=0} \\ &= \frac{D}{d} (c_A - c_B) - \frac{2c_B D}{d} \sum_{n=1}^{\infty} \left[(-1)^n e^{-\frac{Dn^2 t}{d^2}} \right] + \frac{2c_A D}{d} \sum_{n=1}^{\infty} \left[e^{-\frac{Dn^2 t}{d^2}} \right] \end{aligned} \quad (\text{B.8})$$

$$\begin{aligned} J_2(0) &= -D \frac{\partial c}{\partial x} \Big|_{x=d} \\ &= \frac{D}{d} (c_A - c_B) - \frac{2c_B D}{d} \sum_{n=1}^{\infty} \left[e^{-\frac{Dn^2 t}{d^2}} \right] + \frac{2c_A D}{d} \sum_{n=1}^{\infty} \left[(-1)^n e^{-\frac{Dn^2 t}{d^2}} \right] \end{aligned} \quad (\text{B.9})$$

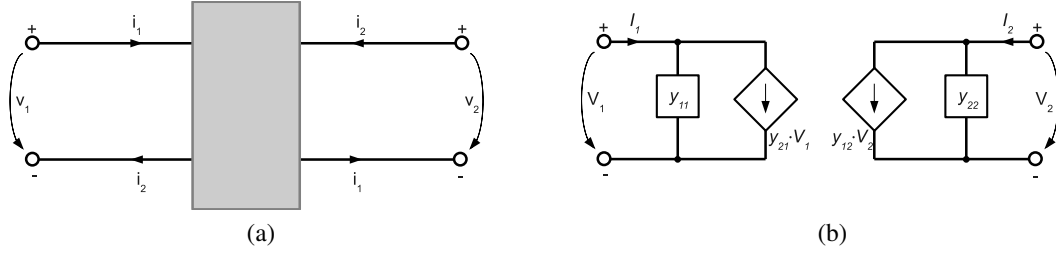


Figure B.2: Schematic of (a) a two-port and (b) its equivalent circuit in terms of the short-circuit admittance parameters [75].

and thus the following cumulated fluxes:

$$Q_1(t) = \frac{D}{d}(c_A - c_B)t + \frac{2c_B d}{\pi^2} \sum_{n=1}^{\infty} \left[\frac{(-1)^n}{n} e^{-\frac{D\pi^2 n^2}{d^2}} \right] - \frac{2c_A d}{\pi^2} \sum_{n=1}^{\infty} \left[\frac{1}{n^2} e^{-\frac{D\pi^2 n^2}{d^2}} \right] + \frac{d}{6}(2c_A + c_B) \quad (\text{B.10})$$

$$Q_2(t) = \frac{D}{d}(c_A - c_B)t + \frac{2c_B d}{\pi^2} \sum_{n=1}^{\infty} \left[\frac{1}{n^2} e^{-\frac{D\pi^2 n^2}{d^2}} \right] - \frac{2c_A d}{\pi^2} \sum_{n=1}^{\infty} \left[\frac{(-1)^2}{n^2} e^{-\frac{D\pi^2 n^2}{d^2}} \right] + \frac{d}{6}(c_A - 2c_B) \quad (\text{B.11})$$

The according asymptotes are

$$y_1 = \frac{D}{d}(c_A - c_B)t + \frac{d}{6}(2c_A + c_B) \quad (\text{B.12})$$

$$y_2 = \frac{D}{d}(c_A - c_B)t - \frac{d}{6}(c_A - 2c_B) \quad (\text{B.13})$$

Hence, for $c_B = 0$, the time lags for each flux t_{L,J_i} and the accumulated time lag $t_{L,sum}$ are:

$$t_{L,J_1} = -\frac{d^2}{3D} \quad (\text{B.14})$$

$$t_{L,J_2} = \frac{d^2}{6D} \quad (\text{B.15})$$

$$t_{L,sum} = t_{L,J_2} - t_{L,J_1} = \frac{d^2}{2D} \quad (\text{B.16})$$

For the establishment of the serial connection, the transport of a permeant through one monolayer membrane will be mathematically described as the transport of electrical current through a network with two pairs of terminals, a so-called two-port network (Fig. B.2a). Likewise the transport of a permeant through a multi-laminate membrane can be described as the transport of electrical current through a coupling of several two-port

B Additional calculated results

networks [162, 18, 163]. This coupling is done using a Laplace transformation method that simplifies the problem for the constraints of the present study (slab membrane and linear and time-independent diffusion processes) [18].

Basically, the two-port networks are coupled via their transmittance matrices into an overall transmittance matrix of the multilaminate membrane T_{all}

$$T_{all} = T_1 T_2 \dots \quad (B.17)$$

and the time lag of this membrane is calculated from parts of the overall transmittance matrix and its first derivative.

$$\theta_n = t_{L,J_2,all} = \frac{T'_{all,12}}{T_{all,12}} \quad (B.18)$$

To get to the transmittance matrix of one layer of the membrane, one has to describe the admittance matrix first [18]. The admittance matrix can then be transformed, for a two-port network of linear time-invariant elements and when only the zero-state response is sought, into the transmittance matrix with the help of exchange tables like in [75]. Originally, the short-circuit admittance matrix of a two-port network originally relates the Laplace transforms of the port-currents $I_i(s)$ to the port-voltages $V_i(s)$. For the layer of the membrane, the corresponding term to the electrical current $I_i(s)$ is the flux $J_i(s)$, to the electrical voltage $V_i(s)$ it is the partial pressure $P_{M,i}(s)$ of the permeating matter (Fig. B.2a). Therefore, the membrane related equation is

$$J(s) = Y(s)P_M(s) \quad (B.19)$$

where the admittance matrix $Y(s)$ is

$$Y(s) = \begin{bmatrix} Y_{11}(s) & Y_{12}(s) \\ Y_{21}(s) & Y_{22}(s) \end{bmatrix} \quad (B.20)$$

The short-circuit admittance parameters $Y_{ij}(s)$ can be interpreted as forward and reverse transfer admittance under the condition that always the respective port is short-circuited (Fig. B.2b).

$$Y(s) = \begin{bmatrix} \left. \frac{J_1(s)}{P_{M,1}(s)} \right|_{P_{M,2}=0} & \left. \frac{J_1(s)}{P_{M,2}(s)} \right|_{P_{M,1}=0} \\ \left. \frac{J_2(s)}{P_{M,1}(s)} \right|_{P_{M,2}=0} & \left. \frac{J_2(s)}{P_{M,2}(s)} \right|_{P_{M,1}=0} \end{bmatrix} \quad (B.21)$$

For the steady state, i.e. for $t \rightarrow \infty$ or $s = 0$, the admittance parameters shall be denoted as Y_{ij} and the admittance matrix becomes

$$\begin{aligned} Y(0) &= \begin{bmatrix} Y_{11} & Y_{12} \\ Y_{21} & Y_{22} \end{bmatrix} \\ &= \begin{bmatrix} \frac{J_{1,ss}}{P_{M,A}} & \frac{J_{1,ss}}{P_{M,B}} \\ \frac{J_{2,ss}}{P_{M,A}} & \frac{J_{2,ss}}{P_{M,B}} \end{bmatrix} \end{aligned} \quad (B.22)$$

Using Eq. (3.7) and introducing P^* , δ and ϵ as

$$P^* = P \frac{A(1 + \epsilon)}{d} = -\frac{J_{2,ss}}{P_{M,A}} \quad (B.23)$$

$$\delta = -\frac{J_{2,ss}}{J_{1,ss}} \quad (\text{B.24})$$

$$\epsilon = -\frac{P_{M,B}}{P_{M,A}} \quad (\text{B.25})$$

and using the reciprocity relation $Y_{12} = Y_{21}$ [75] for unbiased, passive membranes, the admittance matrix for steady state becomes

$$Y(0) = \begin{bmatrix} \frac{P^*}{\delta} & -P^* \\ -P^* & \frac{P^*}{\epsilon} \end{bmatrix} \quad (\text{B.26})$$

The first derivative of the admittance matrix at steady state is

$$\begin{aligned} Y'(0) &= \begin{bmatrix} Y'_{11} & Y'_{12} \\ Y'_{21} & Y'_{22} \end{bmatrix} \\ &= \begin{bmatrix} \lim_{s \rightarrow 0} \left(s \frac{d}{ds} \left(\frac{J_1(s)}{P_1(s)} \right) \right) & \lim_{s \rightarrow 0} \left(s \frac{d}{ds} \left(\frac{J_1(s)}{P_2(s)} \right) \right) \\ \lim_{s \rightarrow 0} \left(s \frac{d}{ds} \left(\frac{J_2(s)}{P_1(s)} \right) \right) & \lim_{s \rightarrow 0} \left(s \frac{d}{ds} \left(\frac{J_2(s)}{P_2(s)} \right) \right) \end{bmatrix} \end{aligned} \quad (\text{B.27})$$

It was shown in [163] that the following relation is true for permeation processes with the permeability coefficient being independent of both time and concentration.

$$t_{L,J_i} = -\lim_{s \rightarrow 0} \left(\frac{d}{ds} \left(\frac{s J_i(s)}{J_{i,ss}} \right) \right) \quad (\text{B.28})$$

Using Eq. (B.28) and the reciprocity relation $Y'_{12} = Y'_{21}$ gives

$$Y'(0) = \begin{bmatrix} -\frac{P^* t_{L,J_1}}{\delta} & P^* t_{L,J_2} \\ P^* t_{L,J_2} & -\frac{P^* t_{L,J_2,rev}}{\epsilon} \end{bmatrix} \quad (\text{B.29})$$

Using conversion relations [75] leads from the admittance matrix and its first derivative to the transmittance matrix and its first derivative (all at $s = 0$).

$$\begin{aligned} T(0) &= \begin{bmatrix} T_{11} & T_{12} \\ T_{21} & T_{22} \end{bmatrix} \\ &= \begin{bmatrix} -\frac{Y_{22}}{Y_{21}} & -\frac{1}{Y_{21}} \\ -\frac{Y_{11}Y_{22}}{Y_{21}} + Y_{12} & -\frac{Y_{11}}{Y_{21}} \end{bmatrix} \\ &= \begin{bmatrix} \frac{1}{\delta} & \frac{1}{P^*} \\ P^* \left(\frac{1}{\delta\epsilon} - 1 \right) & \frac{1}{\delta} \end{bmatrix} \end{aligned} \quad (\text{B.30})$$

and

$$\begin{aligned} T'(0) &= \begin{bmatrix} T'_{11} & T'_{12} \\ T'_{21} & T'_{22} \end{bmatrix} \\ &= \begin{bmatrix} \frac{d}{ds} \left(-\frac{Y_{22}}{Y_{21}} \right) & \frac{d}{ds} \left(-\frac{1}{Y_{21}} \right) \\ \frac{d}{ds} \left(-\frac{Y_{11}Y_{22}}{Y_{21}} + Y_{12} \right) & \frac{d}{ds} \left(-\frac{Y_{11}}{Y_{21}} \right) \end{bmatrix} \\ &= \begin{bmatrix} \frac{Y_{22}Y'_{21} - Y'_{22}Y_{21}}{Y_{21}^2} & \frac{Y'_{21}}{Y_{21}^2} \\ \dots & \frac{Y_{11}Y'_{21} - Y'_{11}Y_{21}}{Y_{21}^2} \end{bmatrix} \\ &= \begin{bmatrix} \frac{t_{L,J_2,sum}}{\epsilon} & \frac{t_{L,J_2}}{P^*} \\ \dots & \frac{t_{L,sum}}{\delta} \end{bmatrix} \end{aligned} \quad (\text{B.31})$$

B Additional calculated results

As the third (lower left) parameter of the first derivative of the transmittance matrix T'_{21} is too space consuming, but not important for further mathematical manipulation, it is not presented in Eq. (B.31).

Comparing the second (upper right) parameters of the matrices $T(0)$ and $T'(0)$ of Eqs. (B.30) and (B.31) reveals a relation for the time lag of one layer of the membrane.

$$t_{L,J_2} = \frac{T'_{12}}{T_{12}} \quad (\text{B.32})$$

Extending this relation to the whole membrane consisting of n layers leads to Eq. (B.18).

For any number of layers the time lag can now be determined by calculating first the overall transmittance matrix and its first derivative and then replacing all $t_{L,J_2,i}$, $t_{L,sum,i}$ and $t_{L,sum,rev,i}$ by the help of Eqs. (B.14), (B.15) and (B.16). Hence, the overall time lag θ_n of the whole membrane with n layers can always be expressed as a function of the solubility coefficient S_i , the diffusion coefficient D_i and the layer thickness d_i of each of the layers.

For example, for a two-layer membrane ($n = 2$) the second parameters of the transmittance matrix and of its first derivative (both at $s = 0$) become

$$T_{all,12} = \frac{1}{\epsilon_1 P_2^*} + \frac{1}{P_1^* \delta_2} \quad (\text{B.33})$$

$$T'_{all,12} = \frac{\delta_2}{P_2^*} (t_{L,J_2,2} + t_{L,rev,1}) + \frac{\epsilon_1}{P_1^*} (t_{L,sum,2} + t_{L,J_2,1}) \quad (\text{B.34})$$

With Eqs. (B.14), (B.15) and (B.16) and identical areas of permeation ($A_1 = A_2 = A$) the time lag for a two-layer membrane can be expressed as

$$\theta_2 = \frac{\frac{d_1}{S_1 D_1} \left(\frac{d_2^2}{2D_2} + \frac{d_1^2}{6D_1} \right) + \frac{d_2}{S_2 D_2} \left(\frac{d_1^2}{2D_1} + \frac{d_2^2}{6D_2} \right)}{\frac{d_1}{S_1 D_1} + \frac{d_2}{S_2 D_2}} \quad (\text{B.35})$$

The repetition of this method for an increasing number of layers (as demonstrated in Table B.1) reveals the following relation for the time lag θ_n of a multilaminar membrane consisting of n layers:

$$\begin{aligned} \theta_n = & \frac{1}{\sum_{i=1}^n \left[\frac{d_i}{S_i D_i} \right]} \left(\sum_{i=1}^n \left[\frac{d_i}{S_i D_i} \left(\sum_{j=1}^n \left[\frac{d_j^2}{2D_j} \right] - \frac{d_i^2}{3D_i} \right) \right] \right. \\ & \left. + \sum_{k=2}^{n-1} \left[d_k S_k \left(\sum_{l=1}^{k-1} \left[\frac{d_l}{S_l D_l} \sum_{m=k+1}^n \left[\frac{d_m}{S_m D_m} \right] \right) \right] \right]_{n>2} \right) \end{aligned} \quad (\text{B.36})$$

Note that for $n \leq 2$ the second line of Eq. (B.36) gets eliminated.

The expressions for two and three layers are in agreement with [119] and [18]. All together, all the expressions derived for two, three and n layers by the author (Table B.1) and the ones derived in [119] and [18] would be in agreement with [76], if the number “2” would be deleted in the last denominator of Equ.(17) (Fig. B.3) which is probably just a printing error.

Table B.1: Overview of the equations for permeability and time lag for n layers.

Number of layers n	Calculation of overall $J_{2,ss,n}$	Calculation of overall lag time θ_n
1	$\frac{D_1 S_1}{d_1}$	$\frac{d_1^2}{6D_1}$
2	$\frac{1}{\frac{d_1}{D_1 S_1} + \frac{d_2}{D_2 S_2}}$	$\frac{1}{\left[\frac{d_1}{S_1 D_1} \left(\frac{d_1^2}{6D_1} + \frac{d_2^2}{2D_2} \right) + \frac{d_2}{S_2 D_2} \left(\frac{d_1^2}{2D_1} + \frac{d_2^2}{6D_2} \right) \right]}$
3	$\frac{1}{\frac{d_1}{D_1 S_1} + \frac{d_2}{D_2 S_2} + \frac{d_3}{D_3 S_3}}$	$\frac{1}{\frac{d_1}{S_1 D_1} + \frac{d_2}{S_2 D_2} + \frac{d_3}{S_3 D_3}} \left[\frac{d_1}{S_1 D_1} \left(\frac{d_1^2}{6D_1} + \frac{d_2^2}{2D_2} + \frac{d_3^2}{2D_3} \right) + \frac{d_2}{S_2 D_2} \left(\frac{d_1^2}{2D_1} + \frac{d_2^2}{6D_2} + \frac{d_3^2}{2D_3} \right) + \frac{d_3}{S_3 D_3} \left(\frac{d_1^2}{2D_1} + \frac{d_2^2}{2D_2} + \frac{d_3^2}{6D_3} \right) + \frac{d_1 d_2 d_3 S_2}{S_1 S_3 D_1 D_3} \right]$
4	$\frac{1}{\frac{d_1}{D_1 S_1} + \frac{d_2}{D_2 S_2} + \frac{d_3}{D_3 S_3} + \frac{d_4}{D_4 S_4}}$	$\frac{1}{\frac{d_1}{S_1 D_1} + \frac{d_2}{S_2 D_2} + \frac{d_3}{S_3 D_3} + \frac{d_4}{S_4 D_4}} \left[\frac{d_1}{S_1 D_1} \left(\frac{d_1^2}{6D_1} + \frac{d_2^2}{2D_2} + \frac{d_3^2}{2D_3} + \frac{d_4^2}{2D_4} \right) + \frac{d_2}{S_2 D_2} \left(\frac{d_1^2}{2D_1} + \frac{d_2^2}{6D_2} + \frac{d_3^2}{2D_3} + \frac{d_4^2}{2D_4} \right) + \frac{d_3}{S_3 D_3} \left(\frac{d_1^2}{2D_1} + \frac{d_2^2}{2D_2} + \frac{d_3^2}{6D_3} + \frac{d_4^2}{2D_4} \right) + \frac{d_4}{S_4 D_4} \left(\frac{d_1^2}{2D_1} + \frac{d_2^2}{2D_2} + \frac{d_3^2}{2D_3} + \frac{d_4^2}{6D_4} \right) + \frac{d_1 d_2 d_3 S_2}{S_1 S_3 D_1 D_3} + \frac{d_1 d_2 d_3 S_4}{S_1 S_4 D_1 D_4} + \frac{d_1 d_2 d_3 d_4 S_3}{S_1 S_3 D_1 D_3} + \frac{d_1 d_2 d_3 d_4 S_4}{S_1 S_4 D_1 D_4} + \frac{d_1 d_2 d_3 d_4 S_5}{S_1 S_3 D_1 D_3} + \frac{d_1 d_2 d_3 d_4 S_5}{S_1 S_4 D_1 D_4} \right]$
5	$\frac{1}{\frac{d_1}{D_1 S_1} + \frac{d_2}{D_2 S_2} + \frac{d_3}{D_3 S_3} + \frac{d_4}{D_4 S_4} + \frac{d_5}{D_5 S_5}}$	$\frac{1}{\frac{d_1}{S_1 D_1} + \frac{d_2}{S_2 D_2} + \frac{d_3}{S_3 D_3} + \frac{d_4}{S_4 D_4} + \frac{d_5}{S_5 D_5}} \left[\frac{d_1}{S_1 D_1} \left(\frac{d_1^2}{6D_1} + \frac{d_2^2}{2D_2} + \frac{d_3^2}{2D_3} + \frac{d_4^2}{2D_4} + \frac{d_5^2}{2D_5} \right) + \frac{d_2}{S_2 D_2} \left(\frac{d_1^2}{2D_1} + \frac{d_2^2}{6D_2} + \frac{d_3^2}{2D_3} + \frac{d_4^2}{2D_4} + \frac{d_5^2}{2D_5} \right) + \frac{d_3}{S_3 D_3} \left(\frac{d_1^2}{2D_1} + \frac{d_2^2}{2D_2} + \frac{d_3^2}{6D_3} + \frac{d_4^2}{2D_4} + \frac{d_5^2}{2D_5} \right) + \frac{d_4}{S_4 D_4} \left(\frac{d_1^2}{2D_1} + \frac{d_2^2}{2D_2} + \frac{d_3^2}{2D_3} + \frac{d_4^2}{6D_4} + \frac{d_5^2}{2D_5} \right) + \frac{d_5}{S_5 D_5} \left(\frac{d_1^2}{2D_1} + \frac{d_2^2}{2D_2} + \frac{d_3^2}{2D_3} + \frac{d_4^2}{2D_4} + \frac{d_5^2}{6D_5} \right) + \frac{d_1 d_2 d_3 S_2}{S_1 S_3 D_1 D_3} + \frac{d_1 d_2 d_3 S_4}{S_1 S_4 D_1 D_4} + \frac{d_1 d_2 d_3 S_5}{S_1 S_3 D_1 D_3} + \frac{d_1 d_2 d_3 S_5}{S_1 S_4 D_1 D_4} + \frac{d_1 d_2 d_3 d_4 S_3}{S_1 S_3 D_1 D_3} + \frac{d_1 d_2 d_3 d_4 S_4}{S_1 S_4 D_1 D_4} + \frac{d_1 d_2 d_3 d_4 S_5}{S_1 S_3 D_1 D_3} + \frac{d_1 d_2 d_3 d_4 S_5}{S_1 S_4 D_1 D_4} \right]$
...
n	$\frac{1}{\sum_{i=1}^n \left[\frac{d_i}{D_i S_i} \right]}$	$\frac{1}{\sum_{i=1}^n \left[\frac{d_i}{S_i D_i} \left(\sum_{j=1}^n \left[\frac{d_j^2}{2D_j} \right] - \frac{d_i^2}{3D_i} \right) \right]} + \sum_{k=2}^{n-1} \left[d_k S_k \left(\sum_{l=1}^{k-1} \left[\frac{d_l}{S_l D_l} \right] \sum_{m=k+1}^n \left[\frac{d_m}{S_m D_m} \right] \right) \right]_{n>2}$

B Additional calculated results


$$\begin{aligned}
 L^{\text{slab}} = & \left[\sum_{i=1}^n \left\{ \frac{l_i}{D_i} \prod_{j=0}^{i-1} k_j \right\} \right]^{-1} \left[\sum_{i=1}^n \left\{ \frac{\alpha_i l_i^2}{D_i} \prod_{j=0}^{i-1} k_j \right\} - \frac{\alpha_i l_i^3}{D_i^2} \prod_{j=0}^{i-1} k_j \right] \\
 & + \sum_{i=1}^n \left\{ \frac{l_i}{D_i} \left(\prod_{j=0}^{i-1} k_j \right) \sum_{\beta=i+1}^n \left[\alpha_\beta \left\{ \frac{l_\beta}{\prod_{j=0}^{\beta-1} k_j} \prod_{j=0}^{\beta-1} \left[\frac{l_\beta}{D_\beta} \prod_{j=0}^{\beta-1} k_j \right] - \frac{l_\beta^2}{D_\beta} \right\} \right] \right\} \right] \quad (17)
 \end{aligned}$$


Figure B.3: If the indicated number in the denominator would be deleted, all previously cited expressions for time lag calculations and the ones derived by the author would be in agreement with this expression, too (equation taken as a picture from [76] and modified).

C Cost assessment

The maximum overall costs of a targeted OE product have to be at the same level or below the current costs of the existing competitive products of the inorganic based electronics market. The target costs for the OE encapsulation material have to be derived from this value.

OPV modules shall be taken as a numeric example. As they have to compete with the existing PV concepts, they should cost less than 1.7 €/Wp (Table C.1). For the roughly 1 kW/m² of solar power that arrive at the earth, OPV products could, at the current efficiencies, use 30 to 80 Wp/m². Hence, the maximum costs per power of 1.7 €/Wp correspond to maximum 50 to 130 €/m². In case the OPV modules have to be renewed more often than the inorganic panels, this would decrease the maximum costs further by the factor of additional changes. Taking the typical cost structure of packed goods as an indicator (i.e. not more than 10 % of the total costs of a product should be allocated to the packaging material [164]) the total costs of the encapsulation material of an OPV product should not exceed 5 to 13 €/m²[15].

The costs of the encapsulation material are mainly driven by the production costs of its barrier layers, the targeted maximum costs determine the selection of the barrier materials and their coating processes. Especially the process costs of the inorganic coating steps are contributing: though the better the barrier performance of an inorganic barrier layer gets with increasing complexity of its coating process, the more expensive (because slower) its production gets, too.

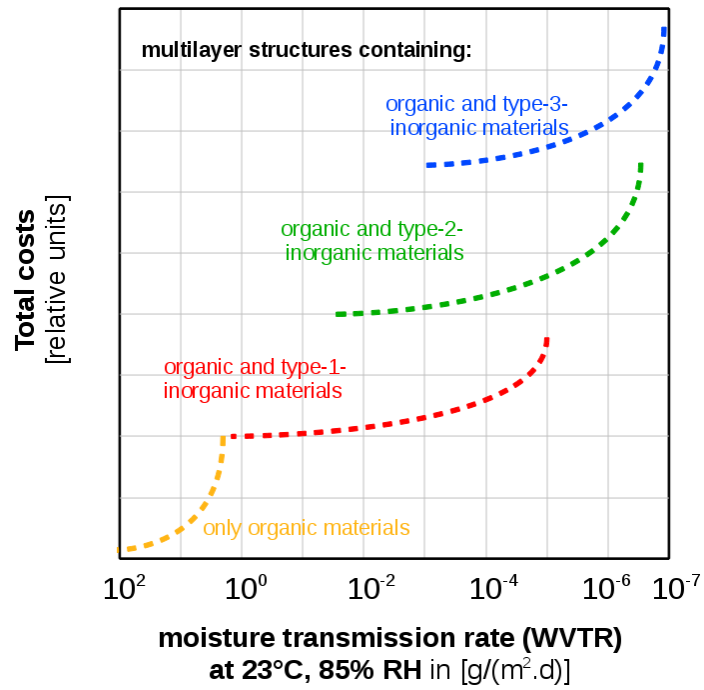
Generally, at the same level of process optimization, the barrier performance of the same inorganic barrier layer increases when changing from thermal evaporation to electron beam evaporation to magnetron sputtering to chemical vacuum deposition (CVD) to atomic layer deposition (ALD). Its production costs increase accordingly.

At the beginning of this work, the exact relationship between the total costs of an en-

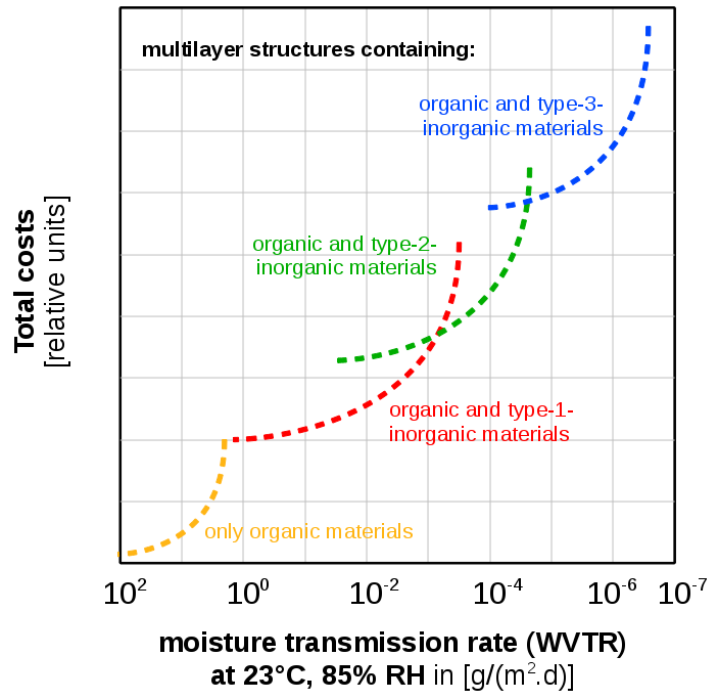
Table C.1: Photovoltaics market: efficiencies and costs from 2010 [85].

Photovoltaics concept	Efficiency [%]	Costs [€/Wp ^a]
1 polycrystalline Si	~ 14	} 2.0-2.5
2 monocrystalline Si	~ 14	
3 thin film PV	~ 7-11	<u>1.7</u> - 2.3
4 1-3 with back grid	~ 18	+ 30%

^aWp stands for "Wattpeak", i.e. for the power produced at the optimum wavelength of the light spectrum.



(a)



(b)

Figure C.1: Relationship of total costs of the encapsulation material versus its barrier performance: (a) as assumed in the community in 2008, (b) as found as a result of this work.

capsulation material and its barrier performance was not known. It was assumed in the community to be as sketched in Fig. C.1a. This means, in 2008, the choice of the inorganic coating steps of an encapsulation material was based on the following assumptions which actually were not proven:

- Assumption 1: The overall barrier performance of the encapsulation material is dominated by the barrier performance of the thin inorganic barrier layer.
- Assumption 2: The barrier performance of thin inorganic barrier layers produced with increasingly complex (better) coating processes overlaps a lot, so that there is plenty of choice of coating processes for the same targeted level of WVTR.
- Assumption 3: The differences in production costs between one coating method and the next more complex (better) one are huge (without overlap).

For this work, many types of OE encapsulation materials were produced: varying the barrier materials themselves, the number and the order of the barrier layers, their coating processes and the design type of the OE encapsulation material in general (multilayer stacking versus lamination). The WVTR results (measured by ACP) from all these materials were used to create Fig. C.1b. The costs were calculated assuming large scale industrial processes and realistic production costs (the author has consulted several companies producing coating machines, equipment, coating materials or converting coating materials under the constraint of a confidentiality agreement). Although the diagram does not disclose the sample structures in detail nor the absolute costs per square meter, all samples containing the same type of thin inorganic barrier layer are indicated (by giving them the same colour); and the ratios of the costs are realistic. This way, the following conclusions can be drawn:

- Assumption 1 is true: the overall barrier performance as well as the costs of an encapsulation material are dominated by the thin inorganic barrier layer(s).
- Assumption 2 is not true. In order to achieve the same overall WVTR with a “lower-performing“ inorganic type, one has to stack so many thin inorganic layers or to add more costly organic materials or to take more costly measures during the production process for compensation that the total costs increase quickly to the level of materials containing “better-performing“ inorganic layers. Furthermore, there is not that much overlap in barrier performance as what was assumed. Therefore, if one wants to go beyond a certain level of WVTR, at one point the next “better-performing“ inorganic layer(s) has (have) to be used - even in the case the overall costs would not play any role. Hence, it is not true that the same targeted level of WVTR could be produced by plenty of different ways of production or that one would have a great choice of materials types.
- Assumption 3 is not true either. It is not correct that a low cost encapsulation material of very high barrier performance could be fabricated by stacking “millions“ of low cost “very low-performing“ coating materials on top of each other - this neither works from the point of view of technical feasibility, nor from the costs point of view.

Looking at the development of OE encapsulation material from a purely scientific point of view, there is just one focus: to gain understanding of the barrier mechanisms and to use this knowledge to design OE encapsulation material with the best possible barrier performance - irregardless of the increasing costs. However, from the engineering point of view (i.e. with the focus of developing a sellable product), the results of this work and the conclusions drawn from it show that there are two focal points that have to be balanced:

- (a) How much improvement of barrier performance would be gained by using an alternative (better) material or process.
- (b) How much more in costs one would have to take into account for this alternative (better) material or process.

D Further explanation on the best barrier materials of this work

D1. Original question and answer (in German)

Diese Erklärung wurde per Email an die drei Haupt-Gutachter versandt am 22.09.2013 als Antwort auf eine Frage von Prof. Briesen:

”Sehr geehrte Prof. Langowski und Majschak,

Prof. Briesen hatte eine Frage zu meiner Arbeit, deren Antwort eventuell auch für Sie interessant sein kann. Daher möchte ich sie die Antwort ebenfalls gern wissen lassen.

Frage war: Wieso taucht der Bestwert von 4×10^{-5} g/(m² d) aus dem Diagramm auf Seite 142 (Fig. 9.1) nirgendwo sonst in der Arbeit auf? Wieso wird stattdessen die reale OPV-Zelle in einem Material mit einem Wert von nur 5×10^{-4} g/(m² d) final getestet (Seiten 124-127 und conclusions)?

(ausführliche) Antwort:

Das Diagramm hatte ich bereits 2009 erstellt, weil ich damals das erste Mal einen Bestwert erreichen konnte, der unter dem bisher Erreichten lag. Der Bestwert war 8.0×10^{-5} g/(m² d) im Calcium-Spiegel-Test für ein Material, das in meiner Buchführung den Code OLA374 trägt (meine Fraunhofer-Kollegen könnten anhand dieser Codes alles nachvollziehen, ich habe eine ausführliche Übergabe über meine verschiedenen Datenbanken gemacht). Nach der Beschichtung der obersten ZnSn_xO_y-Schicht am Fraunhofer FEP ist es am 13.9.2009 bei mir eingetroffen. Es ist der Bestwert aus 9 Messungen. Das Diagramm enthält nur Bestwerte, keine Mittelwerte, weil der internationale Vergleich von Erfolgen auf diesem Gebiet anhand von Bestwerten erfolgt. In der Arbeit verwende ich Mittelwerte aus Einzelmessungen, die an mehreren Stellen des Rollenmaterials gemessen wurden, weil ich das für eine zuverlässigere Aussage halte, da so die Homogenität des Materials quer zur Rolle und entlang der Lauflänge, sprich die Konstanz des Rolle-zu-Rolle-Produktionsprozesses, mit beachtet wird. Der Mittelwert von OLA374 ist 6.0×10^{-5} g/(m² d) und taucht in der Arbeit z.B. auf Seite 125 in Tabelle 6.11 als Material "B", erste Zeile, auf.

Die dazugehörige face-to-face-Kaschierung mit Klebstoff A6.1 ist OLA402 (hergestellt

am 10.11.2009) mit einem Mittelwert im Calcium-Spiegel-Test von 2.0×10^{-4} g/(m² d). Die (Mittelwert-)Ergebnisse dieses Materials tauchen z.B. in den Tabellen 6.11 und 6.12 auf den Seiten 125 und 126 als Material "E" auf. (Warum das kaschierte Material zwar eine größere Barrierewirkung hat, aber trotzdem im Calcium-Spiegel-Test einen schlechteren Mittelwert zeigt als sein "Hälftenmaterial" wird in der Arbeit erklärt.)

Diese beiden Materialien wurden aufgebraucht durch vor allem zahlreiche Durchlässigkeitstests, auch bei verschiedenen Projektpartnern, mit dem Ziel, zu überprüfen, ob diese Materialien tatsächlich so gut wären. Die hohe Barrierewirkung von beiden Materialien wurde schließlich von allen Seiten bestätigt und Konarka zeigte sich interessiert, es an richtigen OPV-Zellen zu testen.

Das Material OLA 374 wurde bis Juli 2010 als OLA522 reproduziert, mit einem Mittelwert von 8.0×10^{-4} g/(m² d) und einem Bestwert aus 9 Einzelmessungen von 3.5×10^{-5} g/(m² d). Die (Mittelwert-)Ergebnisse dieses Materials tauchen in den Tabellen 6.11 und 6.12 als Material "B", zweite Zeile, auf. Zu diesem Zeitpunkt änderte ich den Bestwert im Diagramm 9.1 auf 4×10^{-5} g/(m² d).

Während der Reproduktion von OLA374, also der Herstellung von OLA 522, wurden die Klimabelastungstests an OLA374 und OLA402 (neben weiteren Materialien) fertig. Dabei zeigte sich, dass kleinste Mengen an unabhäufigen Komponenten des Klebstoffs A6.1 bzw. Nachreaktionsprodukte derer, die bei Materialien mit niedrigerer Sperrwirkung noch im Nachgang aus der Mitte der Kaschierung nach draußen ausgasen, bei einem Material mit so hoher Sperrwirkung "stecken bleiben". Im Klimatest, beschleunigt durch die hohe Temperatur, reagieren diese Bestandteile dann mit den in den Verbund permeierenden oder bereits enthaltenen kleinsten Mengen an Feuchte ab und bildet kleine, aber für gute Augen sichtbare, gleichmäßig über die gesamte Klebfläche verteilte Gasbläschen (A6.2 ist ein PUR-basierter Klebstoff, bei dem nicht verbrauchte Isocyanatkomponenten mit Wasser zu Kohlendioxid abreagieren würden).

Daher wurden dann Anfang September 2010 aus OLA522 nicht nur das face-to-face-kaschierte Pendant mit Klebstoff A6.1 hergestellt (OLA623 und OLA678), sondern auch Verbundmaterialien mit den Klebstoffen A5.1, A5.2, A5.4, A5.5, A5.8, A5.9, A5.10 und A6.2 (OLA610, OLA611, OLA612, OLA617, OLA634, OLA635, OLA636, OLA677). Ziel war es, einen Klebstoff zu finden, der eine so gute Haftfestigkeit auf OLA522 und optische Qualität (hohe Transparenz und "Makellosigkeit") zeigt wie A6.1 und gleichzeitig diese Eigenschaften auch trotz Klimabelastung (1000 Stunden bei 65°C und 90% r.F.) behält. Im Dezember 2010 war klar, dass von allen getesteten Klebstoffen A5.10 diese Forderungen am besten erfüllt und so wurde von da an nur noch mit dem entsprechenden face-to-face-kaschierten Material OLA617 weitergearbeitet. Die (Mittelwert-)Ergebnisse von OLA617 tauchen in den Tabellen 6.11 und 6.12 als Material "D" auf.

Bei Konarka wurde aus Kapazitätsgründen daher im Anschluss ausschließlich das aus Anwendungssicht interessantere Material OLA 617 an einer realen OPV getestet und nicht ein Material, das zwar bessere Sperrwirkung zeigt, aber nicht klimastabil und damit nicht für die Anwendung geeignet ist. Daher basiert meine Argumentation eines im

Rolle-zu-Rolle-Prozess produzierbaren und in einer realen OPV-Anwendung tauglichen Barrierematerials und die entsprechende Korrelation ACP-Ergebnis - Calcium-Spiegel-Test-Ergebnis - Lebensdauer reale OPV (Seite 127 und conclusions) in der Arbeit auf OLA617 (Mittelwert-Ergebnisse).

Bis 5.4.2011 wurden OLA374 bzw. OLA522 erneut reproduziert als OLA758. Bestwert aus 15 Einzelmessungen von OLA758 war $3.7 \times 10^{-5} \text{ g}/(\text{m}^2 \text{ d})$ im Calcium-Spiegel-Test, das Diagramm blieb damit korrekt bei Bestwert $4 \times 10^{-5} \text{ g}/(\text{m}^2 \text{ d})$. Ab da endet meine Buchführung, weil ich mich zu diesem Zeitpunkt komplett aus der Projektarbeit am Fraunhofer zurückgezogen habe (Übergabe der Projektarbeit an meine Kollegen war Januar bis März 2011). Das muss nicht bedeuten, dass danach keine Kaschierungen mehr erfolgt oder noch bessere Werte entstanden sind, aber ich habe keine Informationen darüber und es würde ohnehin nicht zu meiner Arbeit gehören.

Die Ergebnisse zur Klimastabilität von den Verbunden mit OLA 522 und verschiedenen Klebstoffen (siehe oben) sind in der Arbeit nicht erwähnt, um den Fokus der Arbeit nicht zu stark abzulenken.

Vielen Dank und
Viele Grüße,
Marion Schmidt“

D2. English translation

This explanation was sent via email to the three main reviewers on 22nd September 2013 to answer a question from Prof. Briesen:

Dear Prof. Langowski and Majschak,

Prof. Briesen had a question concerning my work. Because the answer to this question could be of interest to you as well, I would like to forward it to you.

The question was: Why does the very best WVTR value of $4 \times 10^{-5} \text{ g}/(\text{m}^2 \text{ d})$ only appear in the diagram on page 142 (Fig. 9.1) and nowhere else in my written work? Why was the real OPV tested encapsulated in a material with a WVTR of only $5 \times 10^{-4} \text{ g}/(\text{m}^2 \text{ d})$ instead (pages 124-127 and conclusions)?

(detailed) answer:

I had created the diagram in 2009 for the first time, because it was then that I managed to fabricate for the first time a material having a top WVTR that was better than all previously achieved top WVTR results. The best WVTR value achieved was $8.0 \times 10^{-5} \text{ g}/(\text{m}^2 \text{ d})$ by Calcium test für a material named OLA374 in my data bases (my colleagues from Fraunhofer could do a complete reconstruction of all events using these codes; I did an extensive transfer of knowledge concerning all my data bases). After having got the

top ZnSn_xO_y coating at Fraunhofer FEP I received it on 13th of September 2009. The mentioned WVTR is the best value out of 9 measurements. The diagram contains only best WVTR values, not average WVTR values, because the comparison of achievements on this topic within the international community is typically done on best values. In this written work I only used WVTR values that are averages of several measurements done on different parts of the material rolls, because I believe this to give more reliable conclusions, because it takes into account the (in)homogeneity of the encapsulation material across the roll width and along the length of the roll, i.e. the (in)homogeneity of the roll-to-roll fabrication process. The average WVTR of OLA374 is $6.0 \times 10^{-5} \text{ g}/(\text{m}^2 \text{ d})$ which appears in this written work for example on page 125 in Table 6.11 as material "B", first line.

The according face-to-face laminated material with adhesive A6.1 is OLA402 (fabricated on 10th November 2009) had an average WVTR in Calcium test of $2.0 \times 10^{-4} \text{ g}/(\text{m}^2 \text{ d})$. This (average) result appears for example in Tables 6.11 and 6.12 on pages 125 and 126 as material "E". (It is explained in this work why the laminated material - despite showing a worse average WVTR value in the Calcium test - has a better barrier performance than its "half material".)

Both materials (OLA374 and OLA402) were consumed mainly because of numerous transmission rate measurements, at project partners as well, focussing on verifying whether these materials were indeed having such a very good barrier performance. The high barrier performance of both materials was finally approved from all partners and Konarka showed interest in testing these materials on real OPV cells.

The material OLA374 was reproduced until July 2010 and named OLA522. Its average WVTR was $8.0 \times 10^{-4} \text{ g}/(\text{m}^2 \text{ d})$, its best value out of 9 measurements was $3.5 \times 10^{-5} \text{ g}/(\text{m}^2 \text{ d})$. The average WVTR value appears in Tables 6.11 and 6.12 as material "B", second line. By then I changed the best value in diagram 9.1 to $4 \times 10^{-5} \text{ g}/(\text{m}^2 \text{ d})$.

During the reproduction of OLA374, i.e. during the fabrication of OLA 522, the climate tests on OLA374 and OLA402 (and on many more materials) were finished. It was found that very small amounts of unused components of adhesive A6.1 or reaction products resulting from the post-curing of these unused components, respectively, permeate from the inner of the laminated material to the outside for encapsulation materials with low barrier performance but are kept "locked" in the inner for encapsulation materials of very high barrier performance. During the climate test, accelerated because of the elevated temperatures, these unused components reacted with humidity already contained or afterwards permeating into the laminated material and caused small gas bubbles, visible by naked eye and homogeneously distributed over the entire laminated area (A6.2 is a PUR based adhesive; unused isocyanate components of polyurethanes would react with water to carbon dioxide).

For this reason, at beginning of September 2010, OLA522 was not only used to fabricate face-to-face laminated materials with adhesive A6.1 (OLA623 and OLA678) but also with adhesives A5.1, A5.2, A5.4, A5.5, A5.8, A5.9, A5.10 and A6.2 (OLA610,

OLA611, OLA612, OLA617, OLA634, OLA635, OLA636, OLA677). The screening was done to find an adhesive that would show a similarly good bond strength on OLA522 and optical quality (high transparency and "spotlessness") as A6.1 but at the same time maintain these properties even under climate stress (1000 hours at 65°C and 90% r.F.). In December 2010, adhesive A5.10 was found to fulfil these requirements best of all tested adhesives. From then on all tests were only done on the according face-to-face laminated material (OLA522 laminated with A5.10) named OLA617. The (average) WVTR result of OLA617 appears in Tables 6.11 and 6.12 as material "D".

At Konarka only one material could be tested on a real OPV because of capacity reasons. Hence, only the more stable material OLA617 was tested and not a material that had better barrier performance but would not be implementable in the final application because of insufficient climate stability. Therefore my reasoning is based on on these results of a roll-to-roll producible, climate stable encapsulation material suitable for OPV encapsulation (OLA617) and on the correlation of its (average) WVTR results (ACP and Calcium test) to the lifetime of a real OPV encapsulated into it (page 127 and conclusions).

Until 5th April 2011, OLA374 (or OLA522, respectively) was reproduced and named OLA758. The best WVTR value out of 15 measurements of this material was 3.7×10^{-5} g/(m² d) in the Calcium test. With this result the diagram stayed correct indicating a top WVTR result of 4×10^{-5} g/(m² d). I have no more information on that as, from this time on, I stopped keeping track of the encapsulation materials fabricated at Fraunhofer IVV because I withdrew from project work (I had transferred my project work to my Fraunhofer colleagues between January and March 2011). This doesn't mean that no further encapsulation materials were produced having better WVTR results, just that it would anyway not be part of my own PhD work.

The results about the climate stability of the laminated materials consisting of OLA522 and diverse adhesives were not included in this written work to avoid blurring its focus.

Thank you very much and
Best regards,
Marion Schmidt

Bibliography

Bibliography

- [1] *The Nobel Prize in Chemistry, 2000: Conductive polymers*. The Royal Swedish Academy of Sciences, 2000.
- [2] Pioneer: „Company history.“ Internet: <http://www.pioneer.eu/uk/content/company/company/history.html> [Feb. 11, 2011] .
- [3] Kodak: „Easyshare ls633.“ Internet: http://www.oled-info.com/digital_cameras/kodak_easyshare_ls633 [Feb. 11, 2011)].
- [4] BenQ-Siemens: „S88.“ Internet: http://www.oled-info.com/mobile_phones/benq_siemens_s88 [Feb. 11, 2011].
- [5] Konarka: „OPV products.“ Internet: http://www2.epia.org/New2009/Members_2009_fiche.asp?id=68 [Feb. 11, 2011)].
- [6] OLED info: „Osram lighting tile.“ Internet: http://www.oled-info.com/oled_lighting_products/osram_lighting_tile [Feb. 11, 2011].
- [7] knol: „Sony first commercial OLED TV.“ Internet: <http://knol.google.com/k/erich-strasser/oled/3eonl454tkub0/2#> [Feb. 11, 2011].
- [8] Shiny Plastics: „Flexible transparent oled from universal display corporation.“ Internet: <http://www.shinyplastic.com/archives/05-21-2008-military-and-weapons-4-flexible-transparent-oled-from-universal-/display-and-lg.php> [Feb. 11, 2011].
- [9] treehugger: „Konarka technologies keeps the us army in solar power.“ Internet: http://www.treehugger.com/files/2005/05/konarka_technol.php [Feb. 11, 2011].
- [10] OLED displays: „OLED lighting from GE global research.“ Internet: <http://www.oled-display.net/great-oled-lighting-video-from-ge-global-research> [Feb. 11, 2011].
- [11] Nokia: „The morph concept.“ Internet: <http://research.nokia.com/morph> [Feb. 11, 2011)].
- [12] S. Wong, Ed. *Flexible Electronics*. Springer Science and Business Media, 2009.
- [13] M.-C. Choi, Y. Kim and C.-S. Ha. “Polymers for flexible displays: From material selection to device applications,” *Progress in Polymer Science*, vol. 33, p. 581630, 2008.
- [14] “Ultra-high barrier films for r2r encapsulation of flexible electronics,” European Commission, Research Directorate, FP6, STREP project: FLEXONICS, Tech. Rep., 2006-2009.
- [15] “Development and integration of processes & technologies for the production of organic low-cost & large-area flexible electronics,” European Commission, Research Directorate, FP7, ICT, STREP project: OLATRONICS, Tech. Rep., 2008-2011.
- [16] “Development of nanotechnology-based high performance opaque & transparent insulation systems and biocide formulations for energy efficient buildings,” European Commission, Research Directorate, FP7, NMP-ICT, project NANOINSULATE, Tech. Rep., 2011-2014.

- [17] M. Schmidt. "Systematische Untersuchung der Einflüsse von Lacken auf Papier- und Kartoneigenschaften," M.Eng. thesis, Technische Universität Dresden, Fakultät für Maschinenwesen, Institut für Verarbeitungsmaschinen, Landmaschinen und Verarbeitungstechnik, Germany, 2005.
- [18] R.A. Siegel. "Algebraic, differential and integral relations for membranes in series and other multilaminar media: Permeabilities, solute consumption, lag times and mean first passage times," *Journal of Physical Chemistry*, vol. 95, pp. 2556–2565, 1991.
- [19] K. Vasko. "Schichtsysteme für Verpackungsfolien mit hohen Barriereigenschaften." Ph.D. thesis, Technische Universität München, Wissenschaftszentrum Weihenstephan für Ernährung, Landnutzung und Umwelt, Lehrstuhl für Lebensmittelverpackungstechnik, Germany, 2006.
- [20] H.-C. Langowski. "Flexible barrier materials for technical applications," in *Proc. SVC 46th Annual Technical Conference*, 2003, pp. 561-565.
- [21] A.S. da Silva Sobrinho, G. Czeremuszkina, M. Latreche, G. Dennler and M.R. Wertheimer. "A study of defects in ultra-thin transparent coatings on polymers," *Surface and Coatings Technology*, vol. 116/119, pp. 1204–1210, 1999.
- [22] M. Creatore, V.I.T.A. Lohmann, M.A. Blauw and M.C.M. van de Sanden. "Flexible organic electronics: The role of plasma deposition multilayer permeation barrier technology," in *Proc. SVC 49th Annual Technical Conference*, 2006, pp. 143–146.
- [23] H. Utz. "Barriereigenschaften aluminiumbedampfter Kunststoffolien," Ph.D. Thesis, Fakultät Brauwesen, Lebensmitteltechnologie und Milchwissenschaften der Technischen Universität München, Germany, 1995.
- [24] J. Fahlteich. "Permeation barrier properties of oxide layers on polymer film deposited by pulsed magnetron sputtering," in *Proc. SVC 50th Annual Technical Conference*, 2007, pp. 723–727.
- [25] B.M. Henry, A.G. Erlat, A. McGuigana, C.R.M. Grovenor, G.A.D. Briggs, Y. Tsukahara, T. Miyamoto, N. Noguchi and T. Nijima. "Characterization of transparent aluminium oxide and indium tin oxide layers on polymer substrates," *Thin Solid Films*, vol. 382, pp. 194-201, Feb. 2001.
- [26] A.G. Erlat, B.M. Henry, J.J. Ingram, D.B. Mountain, A. McGuigan, R.P. Howson, C.R.M. Grovenor, G.A.D. Briggs and Y. Tsukahara. "Characterisation of aluminium oxynitride gas barrier films," *Thin Solid Films*, vol. 388, pp. 78–86, June 2001.
- [27] E.H.H. Jamison and A.H. Windle. "Structure and oxygen-barrier properties of metallized polymer film," *Journal of Materials Science*, vol. 18, pp. 64–80, 1983.
- [28] M. Hanika. "Zur Permeation durch aluminiumbedampfte Polypropylen- und Polyethylen-terephthalatfolien," Ph.D. thesis, Technische Universität München, Lehrstuhl für Feststoff und Grenzflächenverfahrenstechnik, Germany, 2003.
- [29] A.P. Roberts, B.M. Henry, A.P. Sutton, C.R.M. Grovenor, G.A.D. Briggs, T. Miyamoto, M. Kano, Y. Tsukahara and M. Yanaka. "Gas permeation in silicon-oxide/polymer (SiO_x/PET) barrier films: role of the oxide lattice, nano-defects and macro-defects," *Journal of Membrane Science*, vol. 208, pp. 75–88, 2002.

Bibliography

- [30] L. Moro, N.M. Rutherford, R.J. Visser, J.A. Hauch, C. Klepek, P. Denk, P. Schilinsky and C.J. Brabec. "Barix multilayer barrier technology for organic solar cells," in *Proc. SPIE 6334*, 2006.
- [31] H.-K. Kim, S.-W. Kim, D.-G. Kim, J.-W. Kang, M.S. Kim and W.J. Cho. "Thin film passivation of organic light emitting diodes by inductively coupled plasma chemical vapor deposition," *Thin Solid Films*, vol. 515, no. 11, pp. 4758–4762, April 2007.
- [32] N. Kim, S. Yo and W. Potscavage, "Fabrication and characterisation of SiO_x/parylene and SiN_x/parylene thin film encapsulation layers," in *Proc. ASME 2007 InterPACK Conference Vancouver*, 2007, pp. 933–938.
- [33] S.-H. K. Park, J. Oh, C.-S. Hwang, J.-I. Lee, Y.S. Yong, H.Y. Chu and K.-Y. Kang. "Ultra thin film encapsulation of organic light emitting diode on a plastic substrate," *ETRI Journal*, vol. 27, no. 5, pp. 545–550, Oct. 2005.
- [34] P. F. Carcia, R.S. McLean, M.H. Reilly, M.D. Groner and S.M. George. "Ca test of Al₂O₃ gas diffusion barriers grown by atomic layer deposition on polymers," *Applied Physics Letters*, vol. 89, pp. 1–3, 2006.
- [35] P.E. Burrows, G.L. Graff, M.E. Gross, P.M. Martin, M. Hall, E. Mast, C. Bonham, W. Bennett, L. Michalski, M. Weaver, J.J. Brown, D. Fogarty and L.S. Sapochak. "Gas permeation and lifetime tests on polymer-based barrier coatings," *SPIE Annual Meeting*, Invited Paper, pp. 1–9, 2000.
- [36] M.S. Weaver, L.A. Michalski, K. Rajan, M.A. Rothman, J.A. Silvernail, J.J. Brown, P.E. Burrows, G.L. Graff, M.E. Gross, P.M. Martin, M. Hall, E. Mast, C. Bonham, W. Bennett and M. Zurnhoff. "Organic light-emitting devices with extended operating lifetimes on plastic substrates," *Applied Physics Letters*, vol. 81, no. 16, pp. 2929–2931, 2002.
- [37] T.-N. Chen, D.-S. Wu, C.-C. Wu, C.-C. Chiang, Y.-P. Chen and R.-H. Horng. "Improvements of permeation barrier coatings using encapsulated parylene interlayers for flexible electronic applications," *Plasma Processes and Polymers*, vol. 4, pp. 180–185, 2007.
- [38] N. Rutherford, "Flexible displays - A Low Cost Substrate / Encapsulation Packaging Solution," in *Proc. Flexible Displays & Microelectronics Conference*, 2005.
- [39] M. Yan, "Ultra-high barrier plastic," GE Global Research, Tech. Rep., September 2008.
- [40] K.-H. Haas, S. Amberg-Schwab, K. Rose and G. Schottner, "Functionalized coatings based on inorganicorganic polymers (ORMOCER's) and their combination with vapor deposited inorganic thin films," *Surface and Coatings Technology*, vol. 111, pp. 72–79, 1999.
- [41] G. L. Graff, R. E. Williford and P. E. Burrows. "Mechanisms of water vapor permeation through multilayer barrier films: Lag time versus equilibrium permeation," *Journal of Applied Physics*, vol. 96, pp. 1840–1849, 2004.
- [42] O. Miesbauer, M. Schmidt and H.-C. Langowski, "Stofftransport durch Schichtsysteme aus polymeren und dünnen anorganischen Schichten (mass transport through layer systems consisting of polymers and thin inorganic layers)," *Vakuum in Forschung und Praxis*, vol. 20, no. 6, pp. 32–40, 2008.

Bibliography

- [43] Alcan Packaging Services AG: Alcan packaging - technology 2007. Internet: http://ceramis.com/en/technologie_forschungsanlage.shtml [Oct. 16, 2011].
- [44] Fraunhofer IVV: Lackier- und Kaschieranlage. Internet: http://www.ivv.fraunhofer.de/load.html?/mainframes/germany/business/gf2_lackier_kaschier.html [Oct. 17, 2011].
- [45] G.G. Nisato. „Minutes of the oe-a working group encapsulation,” Organic Electronics Association (oe-a), Congress Center, Messe Frankfurt, Frankfurt, Germany, Tech. Rep., May 2010.
- [46] M.M. Schmidt, C. Boeffel, E. Kucukpinar, K. Noller and H.-C. Langowski. “Systematic study of steady state and transient moisture permeation through encapsulation materials for flexible organic electronic devices,” in *Proc. Plastic Electronics*, 2010.
- [47] C. Boeffel. “Voruntersuchungen und Auswertung der Calciumspiegel des round robin tests,” in *Proc. Meeting of the oe-a encapsulation group*, Dublin, Ireland, Sept. 2011.
- [48] O. Kahle: „Verkapselung von OLEDs. Fraunhofer PYCO.“ Internet: http://www.pyco.fraunhofer.de/EN/FuE/Methodenentwicklung/Verkapselung/Verkapselung_Grossbild.jsp, March 2008 [Oct. 17, 2011].
- [49] “Permatran-w model 3/33 plus. The standard for water vapor transmission rate testing of flat films and finished packages,” MOCON Minneapolis, Minnesota, USA, Tech. Rep., Jan. 2010.
- [50] labthink: „Discussion of the desiccant method and water method from the development trend of water permeability test.“ Internet: <http://www.google.com/imgres?um=1&hl=de&client=ubuntu&sa=N&channel=fs&biw=1255&bih=579&tbn=isch&tbnid=zD66vsAU2C5vuM:&imgrefurl=http://service.labthink.cn/en/article-Permeation-info-11011863.html&docid=VuUzj1WS1lfnrM&imgurl=http://upload.labthink.cn/Pictures/2011/Origin/tu7.jpg&w=283&h=135&ei=G8KcTo38JIKB4gSr5YWzCQ&zoom=1&iact=rc&dur=373&sig=101494463585051774153&page=2&tbnh=107&tbnw=225&start=21&ndsp=10&ved=1t:429,r:1,s:21&tx=95&ty=41> [Oct. 18, 2011].
- [51] M. Foellmer. “Entwicklung eines mehrlagigen Beschichtungssystems für Papier / Pappe / Karton aus nachwachsenden Rohstoffen,” M.Eng. thesis, Fachhochschule Stuttgart Hochschule der Medien, Germany, 2011.
- [52] BYK Additives and Instruments: „Permeabilitätsbecher.“ Internet: <http://www.byk.com/de/instrumente/physikalische-testgeraete/permeabilitaetsbecher/permeabilitaets-becher.html> [Oct. 18, 2011].
- [53] rycobel group: „Vapometer.“ Internet: http://www.rycobel.de/produkte_de/748.detail.html?kategorie=406&sprache_kuerzel=de, 2001 [Oct. 18, 2011].
- [54] M. Tscherner. “Opto-chemical method for ultra-low oxygen transmission rate measurement,” in *Proc. IEEE SENSORS 2009 Conference*, pp. 1660–1665, 2009.
- [55] wikipedia: „Contact angle.“ Internet: http://en.wikipedia.org/wiki/Contact_angle [Oct. 23, 2011].
- [56] E. Kopczynska and G.W. Ehrenstein. „Sonderdrucke: Oberflächenspannung von Kunststoffen - Messmethoden am LKT.“ Friedrich-Alexander-Universität Erlangen-

- Nürnberg, Lehrstuhl für Kunststofftechnik, Germany, 2011.
- [57] G.F. Sykes and A.K. St. Clair. "The effect of molecular structure on the gas transmission rates of aromatic polyimides," *Journal of Applied Polymer Science*, vol. 32, pp. 3725–3735, 1986.
- [58] Dow Chemical - Plastics Global: "Saran PVDC resins & films and the environment," Tech. Rep. No. 190-00500-0305 SMG, March 2005.
- [59] S. Pauly. „Permeability and diffusion data,“ in *Polymer Handbook*, 4th ed., J. Brandrup, E.H. Immergut and E.A. Grulke, Eds., John Wiley & Sons, 1999, pp. VI / 543 – VI / 569.
- [60] C. Bonten, "Biokunststoffe für Multilayer-Verpackungen," FKUR Kunststoffe, Tech. Rep., Nov. 2008.
- [61] K.-H. Michel. "Kuraray ExcevalTM." Internet: <http://www.kuraray-am.com/pvoh-pvb/exceval.php> [Oct. 25, 2011].
- [62] „EVAL Europe NV: Vorstellung der EVAL Harze,“ Zwijndrecht (Antwerp), Belgium, Tech. Rep., 2011.
- [63] M. Schmidt. "Einfluss der Trocknungsbedingungen auf die Eigenschaften lackierter Folien," B.Eng. thesis, Technische Universität Dresden, Fakultät für Maschinenwesen, Institut für Verarbeitungsmaschinen, Landmaschinen und Verarbeitungstechnik, Germany, 2004.
- [64] FEICA: "The FEICA-ASC adhesives & sealants classification manual," Tech. Rep. 2008.
- [65] D.E. Packham, Ed., *Handbook of Adhesion*, 2nd ed., John Wiley & Sons, 2005.
- [66] The Adhesive and Sealant Council, Inc. (ASC). Internet: <http://www.adhesives.org> [Aug. 10, 2010].
- [67] J. Affinito and D. Hilliard. "A new class of ultra-barrier materials," in *Proc. SVC 47th Annual Technical Conference*, 2004, pp. 563–593.
- [68] J. Meyer, D. Schneidenbach, T. Winkler, S. Hamwi, T. Weimann, P. Hinze, S. Ammermann, H.-H. Johannes, T. Riedl and W. Kowalsky. "Reliable thin film encapsulation for organic light emitting diodes grown by low-temperature atomic layer deposition," *Applied Physics Letters*, vol. 94, no. 233305, 2009.
- [69] D. Karnakis, "Mechanistic aspects of selective laser patterning of multilayered thin-film structures in OLED fabrication," in *Proc. LOPE-C 10*, 2010.
- [70] F.L. Wong, M.K. Fung, C.Y. Ng, A. Ng, I. Bello, S.T. Lee and C.S. Lee. "Co-sputtered oxide thin film encapsulated organic electronic devices with prolonged lifetime," *Thin Solid Films*, vol. 520, no. 3, pp. 1131–1135, 2011.
- [71] J. Fahlteich, M. Fahland, W. Schönberger and N. Schiller. "Permeation barrier properties of thin oxide films on flexible polymer substrates," *Thin Solid Films*, vol. 517, no. 10, pp. 3075–3080, 2009.

- [72] P.A. Premkumar, S.A. Starostin, M. Creatore, H. de Vries, R.M.J. Paffen, P.M. Koenraad and M.C.M. van de Sanden. "Smooth and Self-Similar SiO₂-like Films on Polymers Synthesized in Roll-to-Roll Atmospheric Pressure-PECVD for Gas Diffusion Barrier Applications," *Plasma Processes and Polymers*, vol. 7, no. 8, pp. 635–639, 2010.
- [73] T. Fujinami and M. Hasegawa. "Film deposition method, film deposition apparatus, and gas barrier film," U.S. Patent US 2010/0304155 A1, May 28, 2010.
- [74] F. McCormick. "Barrier films and adhesives for display applications," in *Proc. CCR OLED Workshop University of Minnesota*, 2011.
- [75] C.A. Desoer and E.S. Kuh. „Chapter 17: Two Ports“ in *Basic circuit theory*, 2nd ed., C.A. Desoer and E.S. Kuh, Eds., Singapore: McGraw-Hill International Book Company, 1969, pp. 711-759.
- [76] R. Ash, R.M. Barrer and D.G. Palmer. "Diffusion in multiple laminates," *British Journal of Applied Physics*, vol. 16, pp. 873–884, 1965.
- [77] M. Ciesinski. "Flexible electronics: Why the interest, where are the markets, what is next?" in *Proc. 3rd IS-FOE*, 2010.
- [78] J.-H. Jou. "OLED in Taiwan," in *Proc. 3rd IS-FOE*, 2010.
- [79] B. Carlowitz. *Kunststoff-Tabellen*, 4th ed., München Wien: Carl Hanser Verlag, 1995.
- [80] G.W. Ehrenstein. *Polymer-Werkstoffe*, 2nd ed., München Wien: Carl Hanser Verlag, 1999.
- [81] W. Weissbach. *Werkstoffkunde: Strukturen, Eigenschaften, Prüfung*, 17th ed., Wiesbaden: Vieweg + Teubner GWV Fachverlage GmbH, 2009.
- [82] Teijin DuPont Films Japan Limited: „Properties of various high performance films.“ Internet: http://www.tejindupontfilms.jp/english/product/hi_film.html [Oct. 25, 2011].
- [83] "DuPont™ Selar® PA3426 blends with Nylon 6," DuPont, Wilmington, Delaware, USA, Tech. Rep., 2005.
- [84] *EUWID Verpackung*, Gernsbach: Europäischer Wirtschaftsdienst GmbH, all vol. of the years 2008-2011.
- [85] Personal communication with several photovoltaic panel manufacturers during the *INTERSOLAR 2010*, München, 2010.
- [86] N.A. Vlasenko and L.A. Popov. "Study of the Electroluminescence of a Sublimed ZnS-Mn Phosphor," *Optics & Spectroscopy*, vol. 8, pp. 39–42, 1960.
- [87] C.W. Tang and S.A. VanSlyke. "Organic electroluminescent diodes," *Applied Physics Letters*, vol. 51, pp. 913–915, 1987.
- [88] W. Brütting, Ed., *Physics of Organic Semiconductors*. Weinheim: WILEY-VCH Verlag GmbH & Co. KGaA, 2005.

- [89] Nature online 2006: „High efficiency flat light source invented.“ Internet: <http://nanotechwire.com/news.asp?nid=3183> [July 29, 2010].
- [90] T.G. Krug, “Transparent barriers for food packaging,” in *Proc. SVC 33rd Annual Technical Conference*, 1990, pp. 163–169.
- [91] T.G. Krug, R. Ludwig and G. Steininger. “New transparent barrier coatings for food packaging,” *Papier + Kunststoff-Verarbeiter International*, pp. 26–34, 1992.
- [92] R. Kukla, R. Ludwig and J. Meinel, “Overview on modern vacuum web coating technology,” *Surface and Coatings Technology*, vol. 86-87, pp. 753–761, 1996.
- [93] M. Kiy, “Chips aus Plastik,” *Physik unserer Zeit*, vol. 1, pp. 27–31, 2003.
- [94] W. Demtröder. *Experimentalphysik I: Mechanik und Wärme*. 4th ed., Berlin Heidelberg New York: Springer-Verlag, 2008.
- [95] W. Demtröder. *Experimentalphysik III: Atome, Moleküle, Festkörper*. 4th ed., Berlin Heidelberg New York: Springer-Verlag, 2005.
- [96] R.E. Dickerson and I. Geis. *Chemie - eine lebendige und anschauliche Einführung*. 1st ed., Weinheim: Wiley-VCH Verlag GmbH & Co. KGaA, 1999.
- [97] VDI-Gesellschaft Verfahrenstechnik und Chemieingenieurwesen (GVC), Ed., *VDI Wärmeatlas*, 10th ed., Berlin Heidelberg New York: Springer-Verlag, 2006.
- [98] U. Hohm. “Dispersion of polarizability anisotropy of H₂, O₂, N₂O, CO₂, NH₃, C₂H₆ and cyclo-C₃H₆ and evaluation of isotropic and anisotropic dispersion-interaction energy coefficients,” *Chemical Physics*, vol. 179, pp. 533–541, 1994.
- [99] C. Kittel. *Einführung in die Festkörperphysik*, 14th ed., Oldenburg: Wissenschaftsverlag GmbH, 2006.
- [100] P. A. Christiansen and E.A. McCullough. “Numerical coupled Hartree-Fock parallel polarizabilities for FH and CO,” *Chemical Physics Letters*, vol. 51, no. 3, pp. 468–472, 1977.
- [101] J. Šesták, J.J. Mareš and P. Hubík, Eds. *Glassy, amorphous and nanocrystalline materials: Thermal physics, analysis, structure and properties*, vol. 8 of *Hot Topics in Thermal Analysis and Calorimetry*, 16th ed., J. Simon, Ed., Berlin Heidelberg New York: Springer Science and Business Media, 2011.
- [102] B. Lipsitt, “Performance Properties of Metallocene Polyethylene, EVA and Flexible PVC Films,” Labthink, Tech. Rep., 2006.
- [103] H. Yasuda and V. Stannet. “Permeation, Solution and Diffusion of Water in Some High Polymers,” *Journal of Polymer Science*, vol. 57, pp. 907–923, 1962.
- [104] J.Q. Shi and S. Durucan. “A bidisperse pore diffusion model for methane displacement desorption in coal by CO₂ injection,” *Fuel*, vol. 82, pp. 1219–1229, 2003.
- [105] K. Jousten, Ed. *Wutz Handbuch Vakuumtechnik: Theorie und Praxis*, 10th ed., Wies-

- baden: Friedr. Vieweg & Sohn Verlag | GWV Fachverlage GmbH, 2010.
- [106] D. A. Nissen. "The Low-Temperature Oxidation of Calcium by Water Vapor," *Oxidation of Metals*, vol. 11, pp. 241–261, 1977.
- [107] H. A. Daynes. "The Process of Diffusion through a Rubber Membrane," in *Proc. Royal Society of London / A*, vol. 1920, pp. 286–307, 1920.
- [108] C. Tang. "Lessons from OLED reliability," in *Proc. ISOS-1*, 2008.
- [109] D. Laird. "OPV Stability, Characterization and Standardization at Plextronics," in *Proc. ISOS-1*, 2008.
- [110] U. Bewersdorff-Sarlette, "Barriereanforderungen für die organische Photovoltaik auf flexiblen Substraten," in *Proc. 11. Wörlitzer Workshop*, 2010.
- [111] R. Gaudiana and D. Ginley. "Session Report Group A: Extrinsic degradation and packaging standards," in *Proc. ISOS-1*, 2008.
- [112] M. Koehl. "Reliability Testing of PV-Modules," in *Proc. Schott Solar*, 2006.
- [113] ISOS 1: „First international summit on organic photovoltaic stability: Summary.“ Internet: <http://isos-1.wikispaces.com/> [Sep. 25, 2011].
- [114] ISOS 2: „Second international summit on organic photovoltaic stability: Summary.“ Internet: <http://isos-2.wikispaces.com/> [Sep. 25, 2011].
- [115] VDMA: „Quality control and measurement. Organic Electronics Association.“ Internet: http://www.vdma.org/wps/portal/Home/en/Branchen/O/OEA/Projects_and_Initiatives/OEA_Projects_StK_20080429_Control_Mesurement?WCM_GLOBAL_CONTEXT=/vdma/Home/en/Branchen/O/OEA/Projects_and_Initiatives/OEA_Projects_StK_20080429_Control_Mesurement [Sep. 25, 2011].
- [116] M. Schmidt, N. Rodler, O. Miesbauer, M. Rojahn, T. Vogel, R. Dörfler, E. Kucukpinar and H.-C. Langowski. "Adhesion and Barrier Performance of Novel Barrier Adhesives used in Multilayered High-Barrier Laminates," *Journal of Adhesion Science and Technology*, vol. 26, no. 20-21, pp. 2405–2436, 2012.
- [117] Arthur Ruettgers and E. N. Vidal. "An Investigation Of The Permeability Of Mass Concrete With Particular Reference To Boulder Dam," in *Proc. American Concrete Institute*, vol. 31, no. 3, pp. 382–416, 1935.
- [118] J. Crank. *The Mathematics of Diffusion*, 2nd ed., Oxford: Oxford University Press, 1975.
- [119] J.A. Barrie, J.D. Levine, A.S. Michaels and P. Wong. "Diffusion and solution of gases in composite rubber membranes," *Transactions of the Faraday Society*, vol. 59, pp. 869–878, 1962.
- [120] W. Prins and J.J. Hermans. "Theory of permeation through metal coated polymer films," *Journal of Physical Chemistry*, vol. 63, pp. 716–719, 1959.
- [121] M. Yanaka, B.M. Henry, A.P. Roberts, C.R.M. Grovenor, G.A.D. Briggs, A.P. Sutton, T.

- Miyamoto, Y. Tsukahara, N. Takeda and R.J. Chater. "How cracks in SiO_x-coated polyester films affect gas permeation," *Thin Solid Films*, vol. 397, pp. 176–185, 2001.
- [122] M. Hanika, H.-C. Langowski and W. Peukert. "Simulation and Verification of Defect Dominated Permeation Mechanisms in Multiple Structures of Inorganic and Polymeric Barrier Layers," in *Proc. SVC 46th Annual Technical Conference*, 2003.
- [123] W.G. Perkins and D.R. Begeal. "Diffusion and Permeation of He, Ne, Ar, Kr and D₂ through silicon oxide thin films," *Journal of Chemical Physics*, vol. 54, no. 4, 1971.
- [124] D.L. Smith. *Thin-film deposition: principles & practice*. 1st ed., USA: McGraw-Hill Inc., 1995.
- [125] K. Wasa, M. Kitabatake and H. Adachi. *Thin Film Materials Technology: Sputtering of Compound Materials*. 1st ed., Norwich: William Andrew, Inc. & Heidelberg: Springer-Verlag GmbH & Co. KG, 2004.
- [126] D.A. Glocker and S.I. Shah, Eds. *Handbook of thin film process technology*, Bristol Philadelphia: Institute of Physics Publishing Ltd. (IOP), 1995.
- [127] D.G. Shaw and M.G. Langlois. „New High Speed Process for Vapor Depositing Acrylate Thin Films: An Update,“ in *Proc. SVC 36th Annual Technical Conference*, 1993, pp. 348-351.
- [128] J.D. Affinito, M.E. Gross, C.A. Coronado, G.L. Graff, I.N. Greenwell and P.M. Martin. "A new method for fabricating transparent barrier layers," *Thin Solid Films*, vol. 290-291, pp. 63–97, 1996.
- [129] J.D. Affinito, S. Eufinger, M.E. Gross, G.L. Graff and P.M. Martin. "PML/oxide/PML barrier layer performance differences arising from use of UV or electron beam polymerization of the PML layers," *Thin Solid Films*, vol. 308-309, p. 19-25, 1997.
- [130] L.E. Nielsen. "Models for the Permeability of Filled Polymer Systems," *Journal of Macromolecular Science: Part A - Chemistry*, vol. 1, no. 5, pp. 929–942, 1967.
- [131] R. Franz. "Permeation of Volatile Organic Compounds across Polymer Films - Part I: Development of a Sensitive Test Method Suitable for High-Barrier Packaging Films at Very Low Permeant Vapour Pressures," *Packaging Technology And Science*, vol. 6, pp. 91–102, 1993.
- [132] G. Nisato, P.C.P. Bouten, P.J. Slikkerveer, W.D. Bennet, G.L. Graff, N. Rutherford and L. Wiese. "Evaluating High Performance Diffusion Barriers: the Calcium Test," in *Proc. Asia Display / IDW '01*, 2001, pp. 1435-1438.
- [133] Discussion between the members of the oe-a encapsulation working group during the *Meeting of the oe-a encapsulation group*, Dublin, Ireland, Sept. 2011.
- [134] D.K. Owens and R.C. Wendt. "Estimation of the surface free energy of polymers," *Journal of Applied Polymer Science*, vol. 13, no. 8, pp. 1741–1747, 1969.
- [135] D.H. Kaelble. „Dispersion-Polar Surface Tension Properties of Organic Solids,“ *Journal of Adhesion*, vol. 66, no. 2, pp. 66-81, 1970.

- [136] T. Young. „An essay on the cohesion of fluids,“ *Philosophical Transactions of The Royal Society of London*, vol. 95, pp. 65-87, 1805.
- [137] P.S. Laplace. „Traité de mécanique céleste; supplément au livre X“, *Annales du Bureau des Longitudes, Gauthier-Villars, Paris*, vol. 4, 1805.
- [138] V. Jost and J. Sterr. “Characterization of crystallinity using Raman spectroscopy,” in *Proc. WITec focus innovations: Workshop Confocal Raman Imaging*, 2009.
- [139] Y. Leterrier, L. Boogh, J. Andersons and J.-A. E. Månson. “Adhesion of silicon oxide layers on poly(ethylene terephthalate). Part 1: Effect of substrate properties on coating’s fragmentation process,” *Journal of Polymer Science Part B: Polymer Physics*, vol. 35, no. 9, pp. 1449–1461, 1997.
- [140] D.G. Howells, B.M. Henry, Y. Leterrier, J.-A.E. Månson; J. Madocks and H.E. Assender. “Mechanical properties of SiO_x gas barrier coatings on polyester films,” *Surface Coatings and Technology*, vol. 202, no. 15, pp. 3529–3537, 2008.
- [141] “SABIC® LDPE shrink film,” Saudi Basic Industries Corporation (SABIC), Tech. Rep., 2011.
- [142] Personal communication with DuPont Teijin Films concerning the production of PET films of different gauge on the respective machines, 2008.
- [143] Y. Leterrier, J. Andersons, Y. Pitton and J.-A.E. Månson. “Adhesion of silicon oxide layers on poly(ethylene terephthalate). II: Effect of coating thickness on adhesive and cohesive strengths,” *Journal of Polymer Science Part B: Polymer Physics*, vol. 35, no. 9, pp. 1463–1472, 1997.
- [144] J. Fahlteich. “Vakuumtechnologien zur Herstellung von transparenten Hochbarrierefolien,” in *Proc. 11. Wörlitzer Workshop*, 2010.
- [145] N. Rodler. “Einfluss mechanischer Beanspruchung auf die Gas - und Wasserdampfdurchlässigkeit von Verbunden auf Basis transparenter, aufgedampfter Barrierschichten,” M.Eng. thesis, Fachhochschule Muenchen, Studiengang: Verfahrenstechnik Papier Kunststoff, Studienrichtung: Papier - und Kunststoffverarbeitung, Germany, 1996.
- [146] S. Amberg-Schwab. “Funktionelle Schichten auf Basis von ORMOCER®en und Methoden zur Qualitätssicherung,” Fraunhofer ISC, Tech. Rep., May 2006.
- [147] P. Van de Weijer and T. van Mol. “White paper on the characterisation of thin-film barrier layers for protection of organic light-emitting diodes (OLED),” Phillips Research and Holst Centre, Eindhoven, Netherlands (in cooperation with the European project FAST2LIGHT), Tech. Rep., 2009.
- [148] J. Lewis. “Material challenge for flexible organic devices,” *MaterialsToday*, vol. 9, pp. 38–45, 2006.
- [149] C.-J. Chiang, C. Winscom, S. Bull and A. Monkman. “Mechanical modeling of flexible OLED devices,” *Organic Electronics*, vol. 10, pp. 1268–1274, 2009.
- [150] M. Kanari, M. Kunitomo, T. Wakamatsu and I. Ihara. “Critical bending radius and electrical behaviors of organic field effect transistors under elastoplastic bending strain,” *Thin Solid Films*, vol. 518, pp. 2764–2768, 2010.

- [151] G.-H. Lee, J. Yun, S. Lee, Y. Jeong, J.-H. Jung and S.-H. Cho. "Investigation of brittle failure in transparent conductive oxide and permeation barrier oxide multilayers on flexible polymers," *Thin Solid Films*, vol. 518, pp. 3075–3080, 2010.
- [152] K. Cherenack, C. Zysset, T. Kinkeldei, N. Münzenrieder and G. Tröster. "Woven electronic fibers with sensing and display functions for smart textiles," *Advanced Materials*, vol. 22, pp. 5178–5182, 2010.
- [153] J. Meyer, H. Schmidt, W. Kowalsky, T. Riedl and A. Kahn. "The origin of low water vapor transmission rates through $\text{Al}_2\text{O}_3/\text{ZrO}_2$ nanolaminate gas-diffusion barriers grown by atomic layer deposition," *Applied Physics Letters*, vol. 96, pp. 243 308/1–243 308/3, 2010.
- [154] S. Bae, H. Kim, Y. Lee, X. Xu, J.-S. Park, Y. Zheng, J. Balakrishnan, T. Lei, H.R. Kim, Y.I. Song, Y.-J. Kim, K.S. Kim, B. Özyilmaz, J.-H. Ahn, B.H. Hong and S. Iijima. "Roll-to-roll production of 30-inch graphene films for transparent electrodes," *Nature Nanotechnology*, vol. 5, pp. 574–578, 2010.
- [155] S. Amberg-Schwab, H. Katschorek, U. Weber, M. Hoffmann and A. Burger. "Barrier properties of inorganic-organic polymers: Influence of starting compounds, curing conditions and storage on scaling up to industrial application," *Journal of Sol-Gel Science and Technology*, vol. 19, pp. 125–129, 2000.
- [156] K. Gigant. "Ramanspektroskopie hybridpolymerer Sol-Gel-Materialien: Vom Sol bis zur Schicht," Ph.D. thesis, Bayerische Julius-Maximilian-Universität Würzburg, Germany, 2005.
- [157] M. Gnyba, M. Keränen, M. Kozanecki and B.B. Kosmowski. "Raman investigation of hybrid polymer thin films," *Materials Science Poland*, vol. 23, no. 1, pp. 29–39, 2005.
- [158] M. Gnyba, M. Keränen, M. Kozanecki, R. Bogdanowicz, B.B. Kosmowski and P. Wroczyński. "Raman investigation of sol-gel-derived hybrid polymers for optoelectronics," *Opto-Electronics Review*, vol. 10, no. 2, pp. 29–39, 2003.
- [159] D. Lin-Vien, N.B. Colthup, W.G. Fately and J.G. Grasseli. *The handbook of infrared and Raman characteristic frequencies of organic molecules*. USA: Academic Press, 1991.
- [160] "Grundlagen der Bewitterung," Atlas Material Testing Technology, Tech. Rep., 2006.
- [161] A.E. Fick. "Über Diffusion," *Poggendorffs Annalen der Physik und Chemie*, vol. 170, no. 1, pp. 59–86, 1855.
- [162] J.C. Jaeger. *An Introduction to Applied Mathematics*, 1st ed., Oxford: Oxford University Press, 1951.
- [163] R.A. Siegel. "A Laplace transform technique for calculating diffusion time lags," *Journal Of Membrane Science*, vol. 26, pp. 251–262, 1986.
- [164] M. Schmidt. "Entwicklung eines kostengünstigen Verpackungskonzepts für Scheibenwischer," B.Eng. thesis, Technische Universität Dresden, Fakultät für Maschinenwesen, Institut für Verarbeitungsmaschinen, Landmaschinen und Verarbeitungstechnik, Germany, 2003.

Affidavit

I hereby declare that the dissertation titled

”High barrier materials for flexible and transparent encapsulation of organic electronics“

prepared under the guidance and supervision of

Univ.-Prof. Dr. H.-C. Langowski

at the Lehrstuhl für Lebensmittelverpackungstechnik and at the Fraunhofer Institute for Process Engineering and Packaging and submitted to the academic department of Wissenschaftszentrum für Ernährung, Landnutzung und Umwelt of the Technische Universität München is my own, original work undertaken in partial fulfillment of the requirements for the doctoral degree. I have made no use of sources, materials or assistance other than those specified pursuant to § 6 Abs. 5.

I have not submitted the dissertation, either in the present or a similar form, as part of another examination process.

I have not yet been awarded the desired doctoral degree nor have I failed the last possible attempt to obtain the desired degree in a previous doctorate program.

I am familiar with the Regulations for the Award of Doctoral Degrees of the Technische Universität München.

Munich, 10th May 2013

.....

Marion M. Schmidt

Publications

Book chapters

M. Rojahn, M. Schmidt, K. Kreul, "Adhesives for OPV packaging", in *Organic Photovoltaics*, 3rd ed., C. Brabec, Ed. John Wiley & Sons, to be published.

Peer reviewed articles

M. Schmidt, N. Rodler, O. Miesbauer, M. Rojahn, T. Vogel, R. Dörfler, E. Kucukpinar, H.-C. Langowski, "Adhesion and Barrier Performance of Novel Barrier Adhesives Used in Multilayered High-Barrier Laminates", *J. Adhes. Sci. Technol.*, vol. 26, no. 20-21, Special Issue: Adhesion Aspects in Packaging, pp. 2405-2436, 2012.

S. Logothetidis, A. Laskarakis, D. Georgiou, S. Amberg-Schwab, U. Weber, K. Noller, M. Schmidt, E. Küçükpinar-Niarchos, W. Lohwasser, "Ultra high barrier materials for encapsulation of flexible organic electronics", *Eur. Phys. J. - Appl. Phys.*, vol. 51, no. 03, art. 33203, pp. 1-5, 2010.

D. Georgiou, A. Laskarakis, S. Logothetidis, S. Amberg-Schwab, U. Weber, M. Schmidt, K. Noller, "Optical properties of hybrid polymers as barrier materials", *Appl. Surf. Sci.*, vol. 255, no. 18, pp. 8023-8029, 2009.

Articles, not peer reviewed

O. Miesbauer, M. Schmidt, H.-C. Langowski, "Stofftransport durch Schichtsysteme aus polymeren und dünnen anorganischen Schichten" (in German), *Vakuum in Forschung und Praxis*, vol. 20, pp. 32-40, 2008.

Presentations

M.M. Schmidt, C. Boeffel, E. Kucukpinar, K. Noller, H.-C. Langowski, "Systematic study of steady state and transient moisture permeation through encapsulation materials for flexible organic electronic devices", *Proc. Plastic Electronics*, Dresden, Germany, 2010.

O. Miesbauer, M. Schmidt, K. Noller, "Comparison and limitations of barrier measure-

Publications

ment methods for ultrabARRIER films“, *Proc. LOPE-C 2009*, Frankfurt, Germany, 2009, pp. 1-5.

M. Schmidt, O. Miesbauer, K. Müller, ”Beschichtungen für Barriereanwendungen“ (in German), *Proc. 16. Neues Dresdner Vakuumtechnisches Kolloquium - Beschichtung, Modifizierung und Charakterisierung von Polymeroberflächen*, Dresden, Germany, 2008, pp. 3-9.

M. Schmidt, „Nanoskalige Barrierschichten in der Ultrabarriereentwicklung“, *Proc. Thüringer Grenz- und Oberflächentage*, Jena, Germany, 2008, pp. 125-129.

Posters

O. Miesbauer, M. Schmidt, „Ultrabarrierrefolien zur Einkapselung flexibler elektronischer Bauelemente“, *Proc. Thüringer Grenz- und Oberflächentage*, Jena, Germany, 2008, p. 180.

Acknowledgements

The present work was prepared during the years 2008 to 2011 at the Fraunhofer Institute for Process Engineering and Packaging (Fraunhofer IVV). It was funded by the European Commission via several projects (FLEXONICS, OLAtronics, NanoInsulate, TRANSVIP, Sunflower) and by the Technische Universität München, for which I am very grateful.

I am sincerely thankful to my advisor, professor Langowski from the Technische Universität München, for the support and guidance he showed me throughout my dissertation writing. It certainly would not have been possible without his infectious enthusiasm and his helpful advice. I would also like to thank professors Briesen and Sommer from the Technische Universität München and professor Majschak from the Technische Universität Dresden for the useful criticisms and constructive recommendations on this dissertation.

I would like to express my great appreciation to Dr. Claudia Schönweitz, Dr. Klaus Noller and Dr. Cornelia Stramm from Fraunhofer IVV for confiding large European projects to me and for always encouraging me to think independently. Scientific assistance and advice provided by Dr. Kajetan Müller, Dr. Karol Vasko, Dr. Lucia Vaskova, Dr. Esra Küçükpinar-Niarchos, Oliver Miesbauer and Norbert Rodler from Fraunhofer IVV were greatly appreciated. I would like to single out Dr. Esra Küçükpinar-Niarchos and Oliver Miesbauer who have challenged and enriched my ideas on this research work. I owe sincere and earnest thanks to my colleagues Wolfgang Busch, Brigitte Seifert, Simone Drötboom, Alexandre Martins-Moreira and Georgina Bischur at Fraunhofer IVV for their committed help and their encouragement. I am no less obliged to many more colleagues at Fraunhofer IVV who supported me in a number of ways and cannot all be acknowledged by name.

I would like to show my gratitude to Dr. Christine Boeffel and Dr. Armin Wedel from Fraunhofer IAP, Dr. Giovanni Nisato from Centre Suisse d' Electronique et de Microtechnique (CSEM), Dr. Martin Tscherner from Technische Universität Graz, Dr. Jens Hauch from Konarka Technologies GmbH / Energie Campus Nürnberg, Prof. Dr. George Malliaras from Cornell University / Ecole Nationale Supérieure des Mines, Wolfgang Lohwasser from Amcor Flexibles Kreuzlingen AG, Gerhard Steiniger and Peter Sauer from Applied Materials GmbH & Co. KG, Dr. Rudolf Gensler, Hans-Dieter Feucht and Dr. Sandro Tedde from Siemens AG and Denis Cattelan from Horiba Jobin Yvon for the fruitful and encouraging scientific discussions. Dr. Adriana Szeghalmi from Max Planck Institute of Microstructure Physics Halle a.d. Saale deserves a special mention for her commitment in finding a way to cooperate on the development of ALD deposited thin inorganic barrier layers. I would like to offer my special thanks to Dr. Axel Gerstenberger from the Institute

Acknowledgements

for Computational Mechanics of the Technische Universität München for the implementation of the time lag calculations into the FEA program Baci and for his valuable and motivating support for this work.

Finally, I am truly indebted and thankful to Dr. Claudia Schönweitz and Kurt Becker who encouraged me and provided me great assistance in keeping my progress on schedule. It is also a great pleasure to thank Richard Doy for reviewing the manuscript. Last, but by no means least, I wish I to thank my family, especially my parents Margot and Konrad, and my friends for their support throughout my study. Most of all, I wish to express my immense thanks to Geoffrey Doy for being there for me during this work. I will forever be grateful to his selfless willingness to give his time and personal support so generously.

In theory, there is no difference between theory and practice.
In practice, there is a big difference.

Yogi Berra
(*American baseball player*)